ANKARA UNIVERSITY
FACULTY OF PHARMACY

ISOPS 13th International SYMPOSIUM ON PHARMACEUTICAL SCIENCES

Proceeding Book

JUNE 22-25, 2021
ANKARA, TURKEY

Ankara University Faculty of Pharmacy Publication No: 130

ANKARA UNIVERSITY
FACULTY OF PHARMACY

ISOPS 13th International SYMPOSIUM ON PHARMACEUTICAL SCIENCES

Proceeding Book

JUNE 22-25, 2021
ANKARA, TURKEY

Proceeding Book
Ankara University Faculty of Pharmacy Publication No:130
June 2021 Ankara, Turkey
ISBN: 978-605-136-536-7

Levent Karadeniz, Buğra Matbaacılık
Kazım Karabekir Caddesi Sütçüoğlu İşhanı N0:37/1 Altındağ/ANKARA
Tel: 0312 342 19 18
Sertifika No: 48845

Dear Participants and Guests,

I would like to express my sincere appreciation for the valuable contributions of all the participants of 13th International Symposium on Pharmaceutical Sciences (ISOPS). As we all know, the COVID-19 pandemic is still ongoing and the vaccination programmes are proceeding throughout the world. However, during 2021 we continue to face travel bans, governmental and contract restrictions in many countries. Therefore, the symposium was organized as a virtual event for the first time in its history.

ISOPS, initiated in 1989, has successfully brought international scientists, researchers, students together from pharmaceutical sciences and related areas. This symposium was organized biannually until 1997 and then every three years.

Ankara University, Faculty of Pharmacy is the first faculty of pharmacy in Turkey and was established in nineteen sixty (1960). Since the establishment, the institution rapidly progressed and now has very advanced scientific and physical infrastructure. Pharmaceutical science refers to a category of scientific fields and has followed important development processes, mainly in line with the developments in Biotechnology, Nanotechnology and Health Technologies, which are among the priority of the technology fields of today. While realizing the modern requirements, our Faculty has a 5-year undergraduate education programme since 2005 and besides Turkish; it provides an instruction programme in English language since 2015. Our faculty has 6689 graduates since its establishment and the current number of students is 1267. Present educational and scientific resources allow a total of 138 faculty members, 45 professors, 22 associate professors, 5 assistant professors, 51 research assistants in our faculty. Moreover, 66 administrative staff members and other personnel are working at different offices.

The mission of 13th International Symposium of Pharmaceutical Sciences was to perform a broad scientific perspective by the invitation of distinguished scientists having national / international reputation in their areas, so most recent advances were discussed interactively, and to empower the knowledge-based drug research development and multidisciplinary collaborations. It was our intention to make this symposium a memorable event.

This year, scientists from 24 countries registered to ISOPS-13. Our programme consisted of 40 plenary lectures, 212 oral and 200 poster presentations. Excellent research works were presented in different sessions. The speakers in the programme were uniquely placed in accordance to their area of expertise.

I would like to refer also to other initiatives that took place in our symposium. A workshop on “Employability of the Graduates of the Faculty of Pharmacy in Europe” was held with the contribution of Prof. Luciano Saso, Prof. Claire Anderson, Prof. Lilian M. Azzopardi, Prof. Sibel Süzen, Prof. İlkay Erdogan Orhan and Pharm. Nilhan Uzman. This workshop was interesting in terms of discussing the priorities and developments on this topic from local, regional and international respects.

On June 25, our panel on “University-industry-public sector cooperation in drug and vaccine development processes” was carried out by Prof. Dr. Asuman BOZKIR. The heads and *senior representatives of relevant institutions* including; Prof. Hasan Mandal, Assoc. Prof. Tolga Karakan, Pharm. Dr. Nihan Burul Bozkurt, Prof. Erhan Akdoğan, Assoc. Prof. Rabia Çakır Koç, Prof. Mayda Gürsel, Prof. Rana Sanyal, Prof. Hülya Ayar Kayalı, Dr. Süha Taşpolatoğlu, Dr. Hasan Ersin Zeytin, and Pharm. Dr. Ferhat Farşi were with us. This event has been a great platform to discuss the existing practices and requirements, and to propose solutions.

On behalf of the Organizing Committee, I would like to mention my gratitude to the President of Ankara University who gave full support for the Symposium Organization. ISOPS-13 was organized successfully, without any professional support, with the contribution of all our faculty members, especially our symposium secretary Assoc. Prof. Zerrin Sezgin-Bayındır. I congratulate the organizing committee and all the other committees with all my heart, as well as all academic and managing personnel because of their extensive work.

Prof. Dr. Asuman BOZKIR

Chair of ISOPS-13

Honory President of the Symposium

Prof. Dr. Necdet ÜNÜVAR

President of Ankara University

ORGANIZING COMMITTEE

Asuman BOZKIR (Chair)
Zerrin SEZGİN BAYINDIR (Secretariat)
Sinem ASLAN ERDEM
İlker ATEŞ
Zeynep ATEŞ ALAGÖZ
Filiz BAKAR ATEŞ
Meltem CEYLAN ÜNLÜSOY
Burcu DEVRİM
Gülnur EKŞİ BONA
Banu KAŞKATEPE
Gizem KAYKI MUTLU
Gülbin ÖZÇELİKAY
Bengi USLU
Özge ÜLKER

SOCIAL COMMITTEE

Muammer ÇALIKUŞU
Derya ÇİÇEK POLAT
Engin ER
Burçin ERGENE
Işıl ÖZAKÇA GÜNDÜZ
Mehmet Murat KIŞLA
Nuri ÖZMEN
Aysu SELÇUK
Tuğrul Mert SERİM
Aylin ÜSTÜNDAĞ
Müjde YÜCE ERYILMAZ

SCIENTIFIC COMMITTEE

Esin AKI YALÇIN (Turkey)
Fügen AKTAN (Turkey)
Raid ALANY (UK)
Nurten ALTANLAR (Turkey)
Claire ANDERSON (UK)
Asuman BOZKIR (Turkey)
Bezhan CHANKVETADZE (Georgia)
Jerka DUMIC (Croatia)
Francesco EPIFANO (Italy)
Ayşe Mine GENÇLER ÖZKAN (Turkey)
Alper GÖKBULUT (Turkey)
Ivan KOSALEC (Croatia)
Gustavo RIVAS (Argentina)
Luciano SASO (Italy)
Tanja SCHWERDTLE (Germany)
Sevgi ŞAR (Turkey)
Aylin ÜSTÜNDAĞ (Turkey)
Karel SMEJKAL (Czech Republic)

CONTENTS

OP001: DEVELOPMENT AND OPTIMIZATION OF SULPHAMETHOXAZOLE NANOSUSPENSION FORMULATIONS

[1]Ugur Kaplan, AB., [1]Cetin, M.

[1] Atatürk University, Department of Pharmaceutical Technology, Erzurum, Turkey, busra.ugur@atauni.edu.tr, melcetin@atauni.edu.tr

Introduction:

Sulfamethoxazole (SMX), a sulfonamide bacteriostatic antibiotic, is listed in BCS Class II (1-3). Nanosuspensions (NSs) can be defined as nano-sized colloidal dispersions of drug particles that are stabilized with surfactants and/or polymers (4). In this study, preliminary studies were carried out for the preparation of NS to increase the solubility and antimicrobial activity of SMX, and the effect of some process variables on NS was evaluated.

Materials and Methods:

SMX-NS were prepared with media milling technique. Firstly, SMX was added to surfactant (Pluronic F127) and polymer (PVP-K30) solution, and pre-mixed was applied first with Ultra-Turrax (15000 rpm, 10 min) and then with ultrasonic probe (55% power, 1 min). Zirconium oxide beads with a diameter of 0.3-0.4 mm were added to the suspension obtained after pre-mixing, and comminution was carried out on a magnetic stirrer.

A three-factor, three-level Box-Behnken design was used to evaluate the effect of polymer and surfactant concentration and stirring time on the critical quality properties (particle size, PDI, and zeta potential) of NS. Type of polymer and surfactant, milling media, SMX concentration, and stirring rate were kept the same for all experiments. The factors and levels used in the Box-Behnken design were shown in Table 1. A total fifteen experiments were designed by the software with three center points (Table 2). Each formulation was prepared three times and particle size, PDI and zeta potential values were determined and then the optimization was performed to minimize the particle size and PDI.

Table 1. Variables for the Box-Behnken design

Independent Variables	Design Level		
	Low	Middle	High
Stirring time (h)	12	18	24
Concentration of polymer	1%	1.5%	2%
Concentration of surfactant	1%	1.5%	2%

The mean particle size, PDI and zeta potential of the NS formulations were determined by Zetasizer Nano ZSP (Malvern Ins. Ltd, UK). Mastersizer Hydro 2000 MU (Malvern Ins. Ltd., UK) was used to determine the particle size of raw SMX.

The morphological characteristics of raw SMX and the optimized formulation (after lyophilization: -55°C, 0.021 mbar for 24 h; Martin Christ, Alpha 1-2 LD Plus) were examined by scanning electron microscope (SEM, Zeiss Sigma 300, Germany).

Results:

The particle size, PDI, and zeta potential values of SMX-NSs created with Box-Behnken design were given in Table 2. The $d_{50,}$ span, and zeta potential values of raw SMX were found to be 18.453±0.745 μm, 1.651±0.210 and 4.92±1.69 mV, respectively.

Table 2. The Box-Behnken design matrix and the mean particle size, PDI and zeta potential values of SMX-NSs (Mean±SD; n=9)

Formulation Code	Stirring time (h)	Concentration of surfactant (%)	Concentration of polymer (%)	Particle Size (nm)	PDI	Zeta Potential (mV)
F1	12	1	1.5	753.63±27.81	0.629±0.049	-4.96±0.33
F2	18	1	1	334.82±38.88	0.536±0.066	-7.61±0.98
F3	12	1.5	1	348.97±24.61	0.417±0.061	-5.48±1.45
F4	24	2	1.5	242.68±35.49	0.491±0.037	-11.65±0.84
F5	24	1	1.5	444.58±19.00	0.435±0.066	-3.12±0.58
F6	24	1.5	2	534.40±17.27	0.756±0.063	-3.83±0.50
F7	18	1.5	1.5	261.65±14.02	0.530±0.107	-10.61±2.58
F8	18	2	2	169.99±20.26	0.558±0.065	-15.71±2.07
F9	18	1	2	634.34±30.91	0.616±0.092	-8.89±0.54
F10	24	1.5	1	777.74±37.17	0.667±0.062	-1.90±0.61
F11	12	2	1.5	386.02±36.76	0.575±0.123	-9.29±1.04
F12	18	1.5	1.5	243.31±4.60	0.536±0.07	-13.72±2.69
F13	18	2	1	195.83±32.85	0.524±0.043	-3.61±0.87
F14	12	1.5	2	290.97±21.51	0.525±0.089	-2.44±0.52
F15	18	1.5	1.5	268.61±16.09	0.541±0.108	-10.82±1.22

The main effect and contour plots were created in order to evaluate the effects of the factors on the particle size and PDI (Figure 1). Consequently, the stirring time was determined as 15 hours, the surfactant concentration of 2%, and the polymer concentration of 1.4% for the optimum SMX-NS formulation. The mean particle size, PDI, and zeta potential values of this formulation were found to be 196.4±7.98 nm, 0.493±0.021 and - 8.17±1.09 mV, respectively. The SEM images of raw SMX and the optimized SMX-NS formulation were shown in Figure 2.

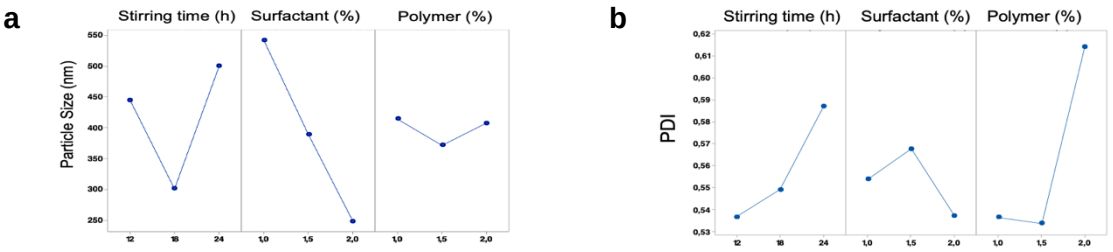

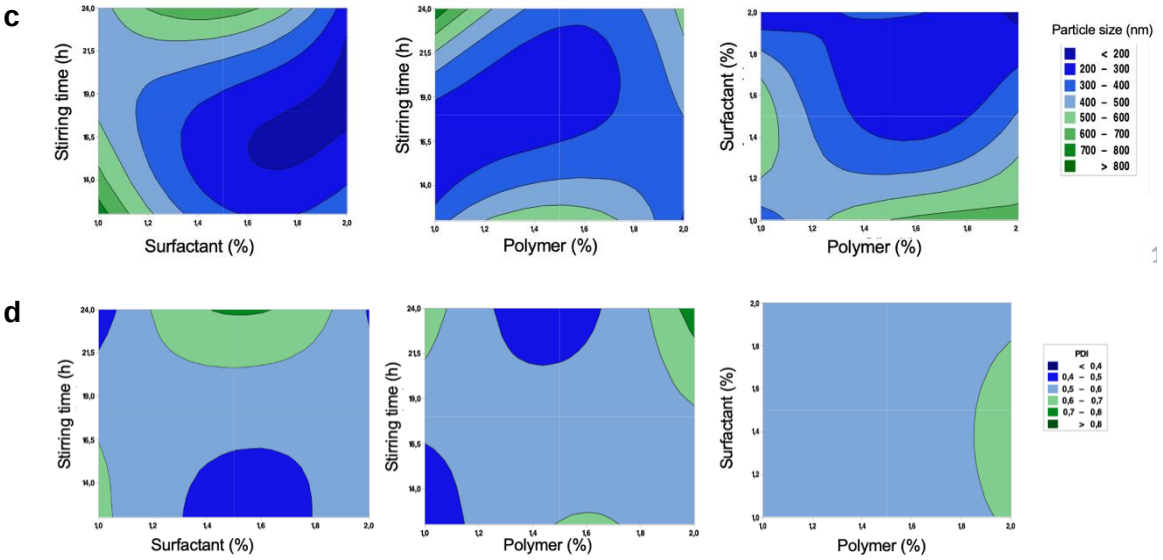

Figure 1. The main effect (a and b) and contour plots (c and d) of Box-Behnken design.

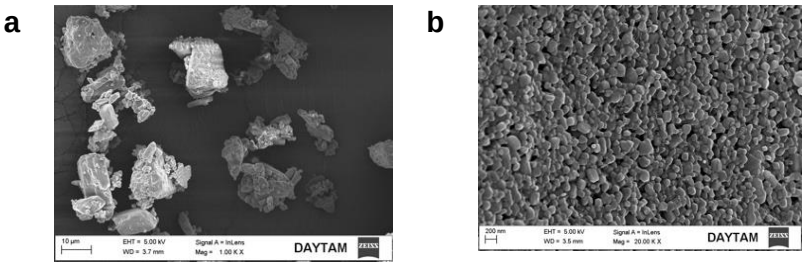

Figure 2. The SEM images of raw SMX (a) and the optimized SMX-NS formulation (b).

Conclusions:

This study demonstrated the effects of polymer and surfactant concentration and stirring time on the SMX-NS formulation using the Box Behnken design. Furthermore, the NS formulation may be useful to improve the solubility and antimicrobial activity of SMX.

Acknowledgement

This study was supported by Atatürk University, Scientific Research Foundation (Project No: THD-2020-8265)

References:

1. Gulay Z (2017). J Inf Dis-Special Topics, 10(1):6-19.
2. Sayar et al., (2008). FABAD J Pharm Sci, 33:87-94.
3. Kumar et al., (2020). J Drug Deliv Sci Tech, 55:101359.
4. Tehrani et al., (2019). Daru, 27(1):451-473.

OP002: STABILITY ENHANCEMENT OF S-ADENOSY-L-METHIONINE THROUGH NANOFORMULATION APPROACH

[1]Ergin, AD., [2]Sezgin-Bayındır, Z., [2]Yüksel, N.

[1]TrakyaUniversity. Department of Pharmaceutical Technology. Edirne, Turkey, adoganergin@trakya.edu.tr

[2] Ankara University. Department of Pharmaceutical Technology. Ankara. Turkey. zsezgin@pharmacy.ankara.edu.tr, nyuksel@harmacy.ankara.edu.tr

Introduction:

S-adenosyl-L-methionine (SAMe) is a universal methyl donor naturally present in all cells. SAMe is involved in many chemical reactions especially methylation. Although SAMe has a high potential for the treatment of different diseases, it has stability problems such as high chemical instability, diastereoisomerism, alkali sensitivity, oxidation and thermal degradation (1). In this study, SAMe was encapsulated in inulin and pectin nanoparticles to prevent its stability problems and characterization studies were conducted. These formulations were subjected to different storage conditions to evaluate the stability of SAMe.

Materials and Methods:

S-Adenosyl-L-methionine 1,4 butanedisulphonate (Carbosynth NA), pectin (55-70% esterified potassium salt. Sigma Aldrich) and inulin (Sigma Aldrich) were used in experiments. For encapsulation of SAMe, pectin and inulin nanoparticle formulations were prepared. Pectin nanoparticles were prepared by ionic gelation method. The aqueous solution of drug and crosslinking agent ($BaCl_2$) was added to pectin solution. After 30 min of stirring, nanoparticles were centrifuged at 13000 rpm for 10 min. The precipitate was washed 3 times. Inulin nanoparticles were prepared by desolvation method with ion pairing. EDC (1-Ethyl-3-(3-Dimethylaminopropyl) Carbodiimid) was chosen as crosslinking agent through the preliminary formulation studies. Afterwards, formulation optimization studies were conducted. According to the preparation method, the aqueous phase containing inulin and SAMe was added to organic phase including sodium lauryl sulfate (SLS) dissolved in formic acid and acetone, mixing at 700 rpm. SLS was used to form ion pair with SAMe. EDC was added to the obtained dispersion and organic solvent was allowed to evaporate under the fume hood by stirring for 4 hours. Obtained nanoparticles were centrifuged at 10˚C, 20000 g for 10 minutes.

In order to estimate the formulation stability, the prepared nanoparticles were kept in glass vials at 5±3˚C and 25±2˚C. At the end of certain stability test periods, (initial, 1st, 3rd and 6th months) samples were removed and characterized in terms of particle size, polydispersity index (PDI), zeta potential (ZP), drug loading (DL %) and encapsulation efficiency (EE %).

Results:

The most important stability problem of SAMe is chemical degradation. Therefore, drug concentration in nanoparticles was evaluated as a priority. As seen in the Table 1, drug amount decreased from 100 % to 0.9 % at the end of the 6th month at 25±2˚C. It was thought that hydrophilic crosslinker barium chloride may absorb moisture and make drug sensitive to the hydrolysis and oxidation. Then, the second stability studies were conducted using vacuumed

glass vials in order to prevent oxidation and hydrolysis risks. The reduction of drug amount was still there, but less. The size of the nanoparticles was highly preserved. While the negative zeta potential values of nanoparticles did not change significantly at 5±3˚C and 25°C in the first 3 months ($p>0.05$), a decrease was observed in the 6th month. This was attributed to the degradation products of SAMe.

Table 1. Stability results of SAMe in different nanoparticle formulations

	T=0	5±3˚C (1st Month)	5±3˚C (3rd Month)	5±3˚C (6th month)	25±2˚C (1st Month)	25±2˚C (3rd Month)	25±2˚C (6th month)
	Pectin nanoparticles						
EE %	41.34±1.61	24.35±0.41	12.52±0.17	2.42±0.11	6.34±0.6104	1.09±0.15	0.38±0.01
DL %	5.39±0.21	3.16±0.07	1.59±0.05	0.32±0.02	0.83±0.0764	0.14±0.08	0.05±0.01
S,S isomer %	60.85±0.09	57.23±0.13	57.24±1.16	54.04±0.77	51.57±0.4686	53.40±0.9779	60.80±5.66
R,S isomer %	39.15±0.09	42.77±0.13	42.76±1.16	45.96±0.77	48.43±0.4686	46.59±0.9779	39.20±5.66
Particle Size (nm) (n=6)	294.7±28.99	314.0±32.02	306.5±10.15	308.0±26.53	315.9±4.653	409.7±17.02	503.3±21.31
PDI	0.443±0.022	0.440±0.067	0.426±0.057	0.511±0.042	0.380±0.023	0.557±0.070	0.595±0.076
Zeta Potential (mV)(n=3)	-19.10±1.160	-20.6±0.8902	-19.6±0.52	-25.5±0.5	-14.7±3.02	-19.5±1.46	-23.7±0.38
	Pectin nanoparticles* (under the vacuum)						
EE %	33.64±3.07	29.12±2.54	12.44±0.69	6.24±0.444	15.40±1.53	11.49±0.69	3.06±0.35
DL %	4.38±0.40	3.80±0.33	1.62±0.09	0.815±0.06	2.01±0.20	1.50±0.09	0.40±0.04
S,S isomer %	49.68±1.24	47.71±0.82	45.22±1.19	40.75±1.35	47.96±0.68	46.52±1.49	42.10±0.78
R,S isomer %	50.30±2.22	52.29±0.82	54.78±0.71	59.75±1.35	52.04±0.68	53.48±1.49	57.90±0.78
Particle Size (nm) (n=6)	309.8±22.16	300.5±9.43	297.4±12.34	348.3 ±44.86	335.2±10.16	305.7±10.44	321.9±19.26
PDI	0.603±0.034	0.417±0.026	0.504±0.03	0.627±0.104	0.542±0.046	0.449±0.02	0.491±0.07
Zeta Potential (mV)(n=3)	-20.0±1.29	-20.9±1.95	-19.5±1.03	6.24±0.444	-20.3±0.35	-19.8±0.31	-6.78±0.885
	Drug Loading % Changes in Different Condition						
DL% (Mean)	100	58.42	29.51	14.61	15.21	2.6	0.9
DL% (Under vacuum) (Mean)	100	86.76	36.99	18.61	45.89	34.24	9.1
	Inulin Nanoparticles						
	T=0	5±3˚C (1st Month)	5±3˚C (3rd Month)	5±3˚C (6th month)	25±2˚C (1st Month)	25±2˚C (3rd Month)	25±2˚C (6th month)
EE %	92.38±8.95	95.73±3.79	85.11±2.46	96.41±3.28	97.94±0.72	84.68±24.28	78.72±4.97
DL %	12.84±1.24	12.49±0.70	11.83±0.34	12.81±0.61	12.77±1.16	11.77±3.37	10.27±0.53
S,S isomer %	57.10±0.23	54.30±0.18	55.02±0.79	52.02±0.25	52.10±0.58	51.41±2.31	47.98±0.25
R,S isomer %	42.90±0.23	45.70±0.18	51.41±2.31	49.58±0.28	47.90±0.58	48.59±2.31	50.42±0.28
Particle Size (nm) (n=6)	301.0±16.27	301.5±22.72	331.20±2.97	306.8±13.03	298.5±7.94	326.40±11.61	480.00 ±16.89
PDI	0.441±0.013	0.458±0.012	0.392±0.02	0.541±0.02	0.476±0.021	0.455±0.04	0.431±0.014
Zeta Potential (mV)(n=3)	-16.70±1.24	-19.10±1.10	-18.10±1.24	-17.40±0.48	-19.70±1.90	-20.60±1.31	-18.40±1.96
DL Changes% (Mean)	100	97.27	92.13	99.77	99.45	91.66	79.98

In case of inulin nanoparticles, the particle size, zeta potential and SAMe concentration were found stable during the 6 month at 5°C, but drug amount was decreased at 25±2˚C by the end of 6th month. This very profound stability results were attributed to the hydrophobic ion pairing with SLS. It is considered that ion pairing stabilized SAMe at molecular level.

According to results, drug content was highly stabilized via inulin nanoparticles compared to pectin nanoparticles. On the other hand, temperature was found to be very effective on the stability of SAMe.

Conclusions:

Among the prepared formulations. inulin nanoparticles were found to be the ideal formulation to maintain the stability of SAMe. Under these circumstances, the temperature of 5±3˚C is suggested as an appropriate storage condition for SAMe loaded inulin nanoparticles.

Acknowledgements

This study is supported by the Turkish Scientific and Technological Research Council (TÜBİTAK Grant number 115S339).

References:

1. Desiderio C., Cavallaro RA, De Rossi A. D'Anselmi F. Fuso A. Scarpa S (2005). *38:*449-456.
2. Jahanban-Esfahlan, A., Dastmalchi S., Davaran S. (2016). International Journal of Biological Macromolecules, 91:703-709.

OP004: DEVELOPMENT AND IN VIVO EVALUATION OF A PULSATILE-RELEASE CAFFEINE FORMULATION

[1,2]Arslan, A., [1,3]Yerlikaya, F.

[1] Elixir İlaç Araştırma ve Geliştirme AŞ, Ankara, Turkey

[2] Hacettepe University, Department of Pharmaceutical Technology, Ankara, Turkey

[3] Lokman Hekim University, Department of Pharmaceutical Technology, Ankara, Turkey, aslihan.arslan@elixirlabs.com.tr; firat.yerlikaya@elixirlabs.com.tr

Introduction:

Sleep inertia is a disabling state of reduced physical and mental drive following awakening (1), which typically lasts for less than 30 minutes but symptoms may persist for several hours in susceptible individuals (2-4). A large portion of healthy adolescents report persistent difficulties to rise in the morning (5) and many shift and on-call night workers exhibit impaired performance and grogginess after waking, which raises important safety concerns in operational settings (6, 7). Furthermore, impaired post-awakening vigilance and mood is highly prevalent in a broad range of neurological and psychiatric conditions (7-10). An adenosine receptor antagonist, caffeine, is widely used to reduce sleep inertia symptoms, yet the initial, most severe impairments are hardly alleviated by post-awakening caffeine intake. Upon awakening, most people take a vitalizing substance immediately afterwards, usually in the form of coffee, which contains the stimulating substance caffeine as its main active ingredient. However, caffeine plasma concentration reaches to its maximum level after two hours it is consumed. This delay time affects the first hours of work schedule or lifestyle. Consequently, traditional strategies such as caffeinated products to counter wake-up difficulties cannot target the initial wake-up phase leaving people without energy in the initial phase after waking-up. To ameliorate this disabling state more potently, we aimed to develop a pulsatile-release caffeine formulation, which is administered before the sleep, releases only insignificant amounts of caffeine during sleep and provides adequate caffeine blood plasma levels before the planned awakening time. Multi-Unit Pellet System Formulations (MUPS) offer several advantages over traditional systems, including predictable *in vivo* release, reduced dose dumping, minimized fluctuations in plasma concentration of drug and flexibility of design of *in vitro* drug release. It provides opportunities to develop a reliable formulation than a single unit formulation and minimize of alteration in drug release profile and formulation behaviour due to unit-to-unit variation, change in gastrointestinal pH and enzyme compositions (11). It was aimed that once orally administered, the formulation does not significantly release caffeine in the initial parts of the gastrointestinal tract while passing through it and being exposed to different pH values varying from strongly acidic in the stomach to slightly basic in the colon. It was further aimed that once the formulation passes to the further parts of the gastrointestinal tract (neutral-to-basic) the release-controlling polymeric system immediately dissolves to provide a rapid release of the caffeine. A rapid release of caffeine is targeted within the first 5-10 hours after the administration. To achieve this target release profile, a polymeric system containing a combination of pH-independent and pH-dependent release modifying agents was preferred.

Materials and Methods:

The pulsatile-release caffeine formulation was manufactured using a fluid bed coater with a Wurster tube (Figure 1) using a bottom-spray approach. The formulation was developed using an inert microcrystalline cellulose core, a drug layer comprising caffeine and a release-controlling layer comprising a polymeric system that is based on methacrylic acid copolymers, which controls the release of caffeine both pH-dependently and pH-independently (Figure 1). In the first layer of the formulation, a suspension containing caffeine as the active ingredient, hypromellose as the binder and purified water as the solvent were used. In the second layer of the formulation, which is the release-controlling layer, a suspension containing methacrylic acid - methyl methacrylate copolymer (1:2) and methacrylic acid - methyl methacrylate copolymer (1:1) as a the pH-dependent release modifying agent, ammonio methacrylate copolymer (Type B) as a the pH-independent release modifying agent, triethyl citrate as the plasticizer, talc as the anti-tacking agent, the mixture of isopropyl alcohol and purified water as the solvent are used. The third layer of the formulation provides red colour of micro pellets and contains a ready-to-use film-coating system and purified water.

Figure 1. A representative illustration of the fluid bed coater with a Wurster tube (left), and the layers of the pulsatile-release caffeine formulation (right).

To evaluate the formulations *in vitro* release studies were conducted. For simulating gastrointestinal tract conditions, the *in vitro* release studies were carried out in the media with a pH transition from 1.2 to 7.2 in a 10-hour period. The details of test conditions were given in Table 1.

Table 1. *In vitro* release test conditions

Media	pH 1.2 (2 h) - pH 6.5 (1 h) - pH 6.8 (2 h) - pH 7.2 (5 h)
Surfactant	None
Stirring Speed	100 rpm
Apparatus	USP Apparatus I
Media Volume	900 ± 1 mL
Temperature	37 ± 0.5 °C

After evaluation *in vitro* release results, the optimum formulation which had the best *in vitro* release profile as a promising pulsatile-release formulation was choosed and it was used in

vivo studies. The *in vivo* caffeine release profile was determined in 10 male individuals. After oral intake at 22:30, the study participants were allowed to sleep from 23:00 - 07:00, while their blood samples were continuously collected from the left antecubital vein at baseline (22:00), and 1.5, 2.5, 3.5, 4.5, 5.5, 6.5, 7.5, 8.5, 9.5, 10.5, 13.5 and 17.5 hours after the administration of the study formulation. The blood samples were analysed using a validated LC-MS/MS method after a suitable sample preparation procedure.

Results:

The pulsatile-release caffeine formulation exhibited an *in vitro* release profile, where not more than 10% of caffeine is released during the first 5 hours and not less than 90% of caffeine is released until the 9th hour (Figure 2). The blood plasma concentration of caffeine reached 5 µM after 4 hours following the administration and the C_{max} was observed at about 10.5 hours following the administration of the developed pulsatile-release caffeine formulation to the human subjects (Figure 2).

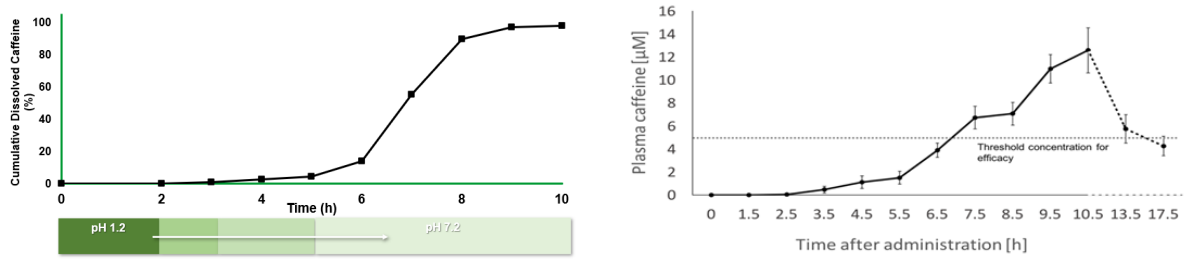

Figure 2. The *in vitro* release profile of the pulsatile-release caffeine formulation (left), and the *in vivo* pharmacokinetic profile of the pulsatile-release caffeine formulation (right).

Conclusions:

The study results showed that the developed formulation exhibited an appropriate pulsatile-release profile, where the *in vivo* caffeine release during sleep was below the clinically significant threshold, which is followed by the rapid release of caffeine with a lag time around eight hours after the administration of the study formulation. It was observed that the *in vivo* release of caffeine was well correlated with the *in vitro* release results of the developed formulation. Based on the *in vitro* and *in vivo* results, it was concluded that a pulsatile-release caffeine formulation was successfully developed. Further clinical efficacy and safety studies are planned to understand the relation of the pharmacokinetics and pharmacodynamics of the developed formulation for the facilitation of the sleep-to-wake transition in sleep-restricted healthy adults.

Acknowledgements

We thank Dr. Dario Dornbierer from the Institute of Pharmacology and Toxicology, University of Zurich, Zurich, Switzerland for his contributions in conducting the *in vivo* experiments of this study.

References:

1. Hilditch CJ, McHill AW (2019). Nature and Science of Sleep, 11:155-65.

2. Hofer-Tinguely et al., (2005). Cognitive Brain Research, 22:323-31.
3. Jewett ME et al., (1999). Journal of Sleep Research, 8:1-8.
4. Tassi P, Muzet A (2000). Sleep Medicine Reviews, 4:341-53.
5. Amaral O et al., (2014). Atención Primaria, 5:191- 4.
6. Hilditch et al., (2016). Industrial Health, 54:528-41.
7. Ohayon et al., (2000). The Journal of Nervous and Mental Disease, 188:340-8.
8. Borisenkov et al., (2015). The Journal of Sleep Research, 24:288-95.
9. Trenkwalder et al., (2011). Movement Disorders Journal, 26:90-9.
10. Trotti LM, Bliwise DL (2014). Neurotherapeutics, 11:68-77.
11. NS Dey et al., (2008). Tropical Journal of Pharmaceutical Research, 7(3): 1067-1075.

OP005: CELLULAR UPTAKE OF POLYMERIC TUBULAR NANOCARRIERS

[1]**Algan, A.H.**, [1]Karataş, A., [2]Besikci, A.,

[1] Ankara University, Department of Pharmaceutical Technology, Ankara, Turkey, kurtoglu@pharmacy.ankara.edu.tr

[2] Ankara University, Department of Pharmacology, Ankara, Turkey, abesikci@ankara.edu.tr

Introduction:

Nanocarriers play a major role for the effective cellular delivery of drugs, due to their small size which facilitates them to extend drug half-life in blood circulation (1). Recent studies demonstrate that, the shape of nanocarrier is a critical parameter affecting circulation time and tumor accumulation and also cylindrical nanocarriers circulate longer giving them more time to reach target tissue (2). Template-assisted synthesis is one of the most promising ways of fabrication polymer tubular nanostructures. Anodized aluminum oxide (AAO) membrane is one of the most popular templates for nanorod/nanotube fabrication by template wetting method (3). Due to effective chemotherapy depends on prolonged exposure of cancer cells to cytotoxic agents, the cellular uptake of drug loaded nanocarriers is an important parameter (4). The aim of this study is to fabricate fluorescent Coumarin-6 (C6) loaded PLGA tubular nanocarriers and evaluate them for cellular uptake into A549 and MCF7cells.

Materials and Methods:

AAO membrane (Anodisc 47, Whatman™) with pore diameter of 200 nm was used for template wetting synthesis. For the optimized formulation poly (d,l lactic-co-glycolic acid) (PLGA) was selected because of its biodegradability and high drug loading capacity. As fluorescent agent lipophilic Coumarin-6 (C6) was selected because of its biocompatibility and stability.

Preparation of tubular nanocarriers

Firstly, C6 dye containing polymer solutions were prepared. Than the templates were immersed into this solution, in tightly closed containers. After loading process polymer embedded membranes were dried at room temperature to remove organic solvent. Etching of the template was performed using aqueous phosphoric acid to dissolve the membrane selectively. Than liberated free nanostructures were collected by vacuum filtration, washed with pure water, and they were freeze dried.

Morphological characterization of nanocarriers

The shape and morphology of nanostructures were observed using Scanning Electron Microscopy (SEM) and Transmission Electron Microscopy (TEM).

Cellular Uptake Studies

Two different cancer cell lines, Human Non-Small Cell Lung Cancer Cells (A549) and Human Breast Cancer Cells (MCF-7), were selected because an anticancer drug was intended to be loaded in nanostructures. Both A549 an MCF7 cells were seeded on Millicell® EZ Slides in DMEM containing high concentration glucose, 2 mM L-glutamine, 1% penicillin/streptomycin

and 10% fetal bovine serum. Cells were incubated for 24 h in a 5% CO_2 incubator (37°C). On the second day after seeding, the growth medium was replaced with fluorescent C6 dye loaded nanocarrier suspension, incubated for 2 hours and 4 hours at 37°C, and the cell monolayers were fixed with 4% paraformaldehyde. The uptake of nanostructures into cancer cells was visualized using a confocal laser scanning microscope (Zeiss LSM 510).

Results:

Morphological characterization of nanocarriers

SEM and TEM images showed that PLGA nanocarriers were obtained successfully in nano dimensions and with smooth surfaced tubular forms. As seen on the SEM image at Fig.1A the diameters of the nanostructures were between 140-160 nm range. And the TEM image at Fig.1B more clearly shows that the length of the nanostructures were between 2-3 µm range.

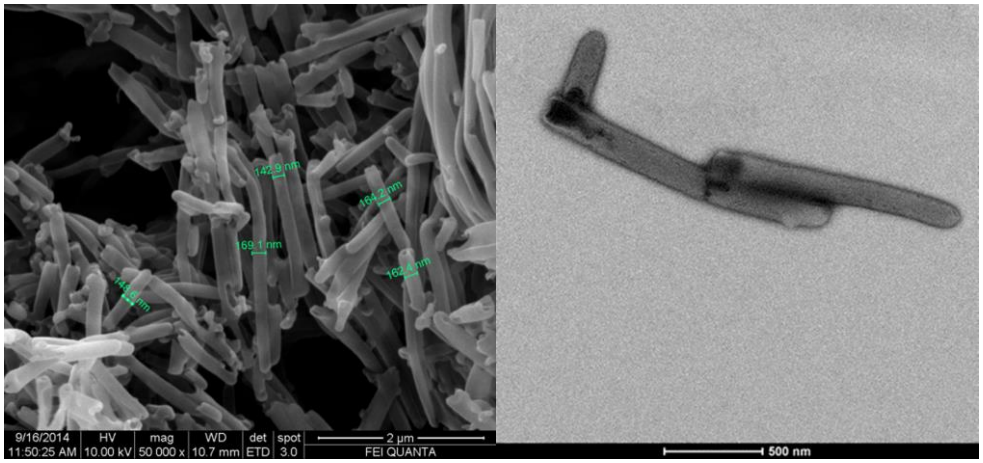

Figure 1. (A) SEM image of PLGA nanaocarriers (left), (B) TEM image of PLGA nanaocarriers (right)

Cellular Uptake Studies

As the result of cellular uptake studies, PLGA tubular nanocarriers were found to be internalized into both A549 and MCF7 cells.

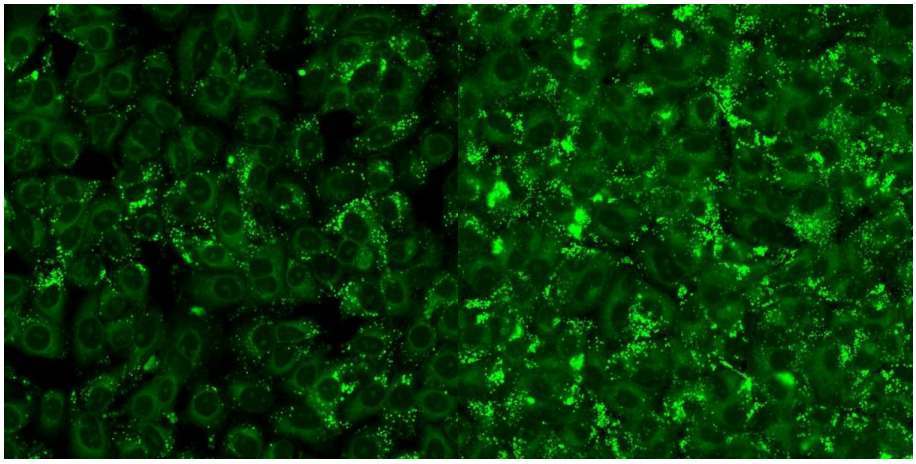

Figure 2. Uptake into A549 cells (A) 2 hours incubation (left), (B) 4 hours incubation (right)

For both cell types it was clearly seen that the green fluorescence intensity increased with the increase of incubation time (Fig.2 and Fig.3). Results suggested that the rate of intracellular accumulation of tubular nanostructures was increased by a time dependent manner.

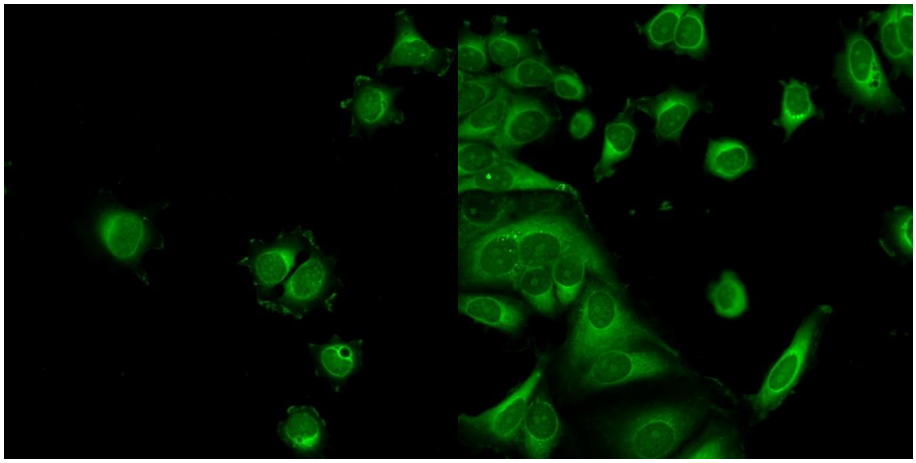

Figure 3. Uptake into MCF7 cells. (A) 2 hours incubation (left), (B) 4 hours incubation (right)

Conclusions:

C6 dye loaded PLGA tubular nanocarriers were successfully fabricated and evaluated for cellular uptake into A549 and MCF7 cells. Tubular nanocarriers were found promising for the delivery of antineoplastic agents.

Acknowledgements

This study was supported by a grant of TUBITAK (SBAG-113S201).

References:

1. Maeda H, Wu J, Sawa T, Matsumura Y, Hori K (2000). J. Control. Release, 65 (1-2): 271-284.
2. Champion JA, Katare YK, Mitragotri S (2007). J. Control. Release, 121 (1–2): 3-9.
3. Son SJ, Bai X, Nan A, Ghandehari H, Lee, SB (2006). J. Control. Release, 114: 143-152.
4. Najar IA, Johri RK. (2014). J. Biosci, 39 (1):139-144.

OP012: FORMULATION AND CHARACTERIZATION OF RESVERATROL LOADED SELF-MICROEMULSIFYING DRUG DELIVERY SYSTEMS (SMEDDS) FOR TOPICAL DRUG DELIVERY

[1]Samancı, B., [1]Yener, F.G., [2]Değim, İ.T.

[1] İstanbul University, Department of Pharmaceutical Technology, İstanbul, Turkey, bulent.samanci@hotmail.com, gulgenyener@yahoo.com

[2] Biruni University, Department of Pharmaceutical Technology, Istanbul, Turkey, tdegim@biruni.edu.tr

Introduction:

Resveratrol (RES) is a natural polyphenolic, which has high antioxidant activity and can reduce skin aging (1). In addition, resveratrol has some improving effects on the skin such as anti-aging, anti-inflammatory, strengthening of skin's natural antioxidant, photo-protective effects, prevention of oxidative stress-induced collagen damage, and protection from UV that induce skin cancer, and sunburn (1,4,5). For polyphenolic compounds such as resveratrol, penetration of the skin is limited due to the low solubility (2). Microemulsions (MEs) are considered suitable drug delivery systems since their easy formulation, thermodynamically stable properties, and facilitating the delivery of both lipophilic and hydrophilic active ingredients (2,3). To overcome the drawback of stability problems and skin bioavailability of resveratrol, it was thought that self micro-emulsifying drug delivery systems (SMEDDs) would be a suitable delivery system. The objective of this investigation was to prepare optimal formulations of MEs and evaluate them according to characterization tests.

Materials and Methods:

Oil-in-water MEs were prepared using Tween 80, olive oil, and distilled water as a surfactant, oily phase, and aqueous phase, respectively. A triangle phase diagram was drawn to determine the amounts of ME components. Points studies were used to determine the ME region on the triangle phase diagram. Some component rates were selected from the ME region to evaluate their stability and other characteristics. Chosen formulations were exposed to stability stress tests such as centrifuge and thermal tests. Characterization studies such as droplet size, size distribution, zeta potential, viscosity, pH measurement were performed on remained intact formulations after stability tests.

Results:

A narrow area on the triangle-phase diagrams came out where oil-in-water microemulsion formed. Transparent systems that were considered as microemulsions were formed in the area In areas where oil and aqua concentrations were low and surfactant concentration was high. It has seemed that while o/w emulsion occurred at the middle up and left area those were riched with water of the diagram, w/o emulsion occurred at the right of the triangle phase diagram where riched by oil phase. Additionally, It was observed that the mixtures with 20-60% water content had gel structures. The water content of systems was above 60% impaired the gel form and resulted in dispersing of the swelled gel. Formulations that have water content above %75 demonstrated better flow properties. However, It was observed that transparent MEs systems formed while the rate of Tween 80 to olive oil was higher than 12:1. It was

observed that olive oil content above %2 revealed dispersion systems that were not quite transparent, as a result of experiments. Since a high concentration of surfactant increase skin irritation, transparent formulations that have a low concentration surfactant were chosen for characterization tests. The droplet size of MEs was measured 24 hours after formulation. Two-peak distribution droplet size was found out in some formulations and they were eliminated. Two formulations were used to incorporate resveratrol and exposed next characterization tests. To detect the effects of incorporating resveratrol into MEs dispersed phase, physical characterization studies were performed. Such as phase separation, cracking, and creaming instability problems were not observed after incorporate resveratrol in ME formulations. Mean droplet size values decreased with the incorporation of resveratrol in both formulations. In terms of the characterization test results, there wasn't a significant difference observed between ME8 and ME9 coded formulations that contained surfactant, oily phase, and aqueous phase at rates 20.4: 1.6: 77.9 and 20.8: 1.6: 77.6, respectively. Characterization test results were as shown in Table 1. In addition, droplet size distributions of ME8 and ME9 coded formulations are shown as in Figure 1 and Figure 2, respectively.

Table 1. Characterization test results of formulations

	ME8	ME8-RES	ME9	ME9-RES
Droplet size (nm)	19.22 ± 0.07	12.34 ± 0.18	12.42 ± 0.16	12.27 ± 0.07
PDI	0.200 ± 0.01	0.103 ± 0.004	0.146 ± 0.001	0.046 ± 0.003
Zeta potential (mv)	-12.2	-1.31	-10.6	-2.13
Zeta deviation (mV)	6.08	71.3	7.45	3.76
pH	6.36 ± 0.03	6.30 ±0.17	6.28 ± 0.01	6.22 ± 0.007
Conductivity (μS/cm)	127.7 ± 0.1	123.4 ± 0.05	124.3 ± 0.08	122. 8 ± 0.06
Viscosity (cP)	11.77 ± 0.15	15.11 ± 1.23	12.07 ± 0.26	16.40 ± 0.48

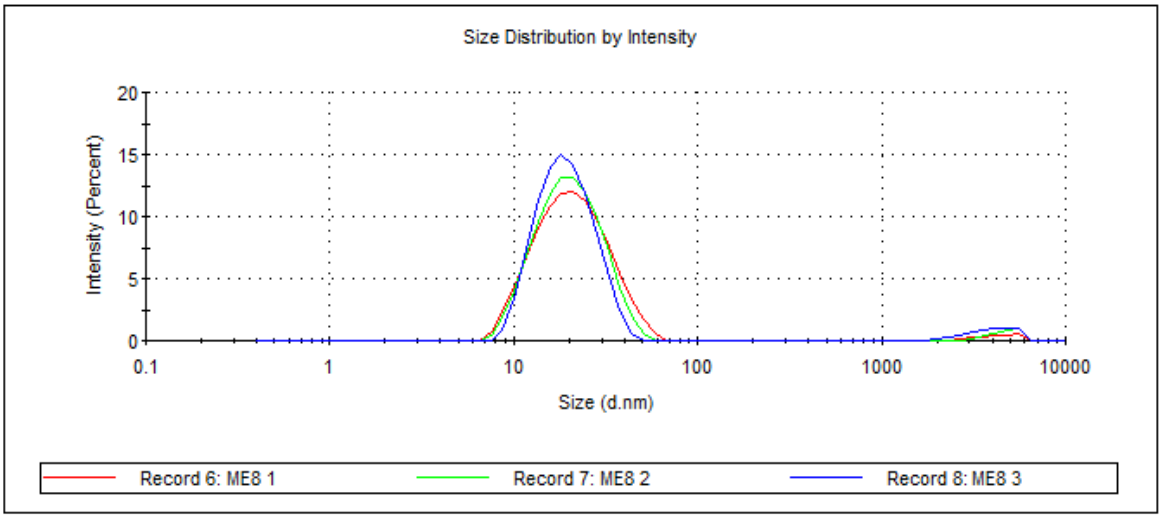

Figure 1. Droplet size distribution of ME8

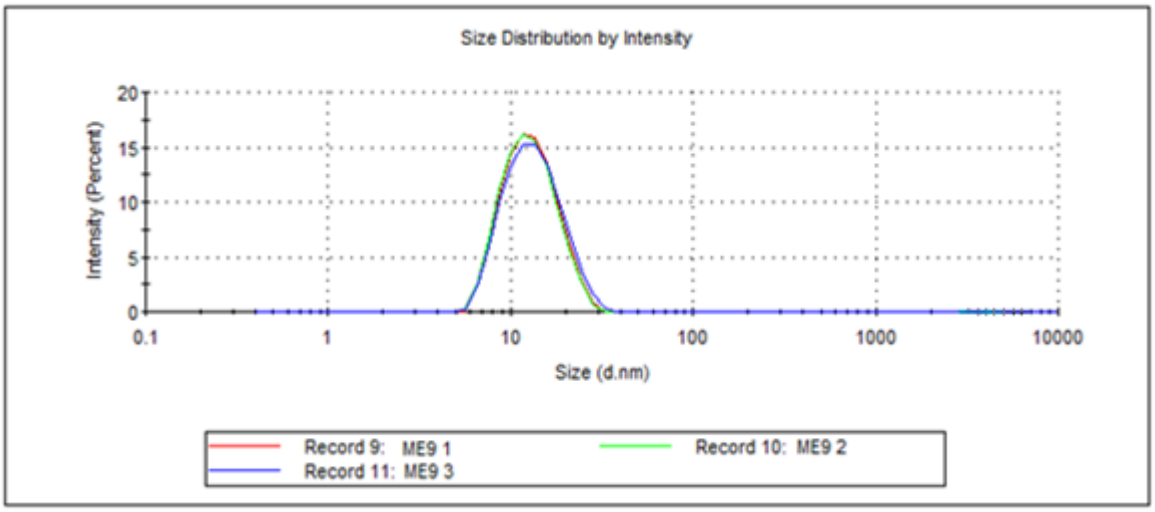

Figure 2. Droplet size distribution of ME9

Conclusions:

Phase diagrams of the components with different ratios have been successfully prepared to determine the ME regions. The optimal amounts of the components were determined to form the most stable ME formulation. The type of and quantities of surfactant, oily phase, and the aqueous phase directly impact the appearance, droplet size, droplet size distribution, type of formulations. ME containing resveratrol was developed, optimized, and characterized for application through the skin. ME prepared by using olive oil, Tween 80, and distilled water in the ratio 1.6: 20.8: 77.6 (in g) was considered as an optimized formulation (ME9) in terms of reducing problems associated with stability. According to both formulations' results, ME9 coded microemulsion formulation was considered the most suitable formulation in terms of droplet size (12,27 ± 0,07) and PDI values (0,046 ± 0,003). In addition, the zeta potential of the ME9 (-2.13 mV) coded formulation is more suitable compared to ME8 (-1.31 mV) in terms of stability.

This study will be very useful and promising to formulate transdermal/topical resveratrol MEs delivery systems both in the pharmaceutical and cosmetics industries. In the future, it is planned to develop ME formulations containing other beneficial active substances for skin care and also the combination of multiple active substances.

Acknowledgements

This study was supported by Scientific Research Projects Unit of Istanbul University (Project code: TDK-2020-35272).

References:

1. Baxter, R, (2008). "Anti-aging properties of resveratrol: review and report of a potent new antioxidant skin care formulation", Journal of Cosmetic Dermatology, 7, 2- 7
2. Juškaité V, Ramanauskiené K, Briedis V, (2015). "Design and Formulation of Optimized Microemulsions for Dermal Delivery of Resveratrol", Evidence-Based Complementary and Alternative Medicine.
3. Lawrence M.J, Rees G.D, (2012). "Microemulsion-based media as novel drug delivery systems", Advanced Drug Delivery Systems Reviews, pp 175-193.

4. Ndiaye, M., Philippe, C., Mukhtar, H., & Ahmad, N. (2011). The grape antioxidant resveratrol for skin disorders: promise, prospects, and challenges. Arch Biochem Biophys, 508(2), 164-170.
5. Zillich, O. V., Schweiggert-Weisz, U., Eisner, P., & Kerscher, M. (2015). Polyphenols as active ingredients for cosmetic products. *International Journal of Cosmetic Science, 37*(5), 455-464.

OP013: DEVELOPMENT OF A PRINTABLE COATING FILAMENT FOR 3D COLON TARGETING TABLETS

[1]Duran, C., [1]Sarısaltık-Yaşın, D., [2]Takka, S.

[1] Dicle University, Faculty of Pharmacy, Department of Pharmaceutical Technology, Diyarbakır, Turkey, diren.sarisaltik@dicle.edu.tr

[2] Gazi University, Faculty of Pharmacy, Department of Pharmaceutical Technology, Ankara, Turkey, takka@gazi.edu.tr

Introduction:

Three-dimensional printing (3DP) technology is the manufacturing process of 3D products by layer to layer from digital designs using a 3D printer. While it has already been widely used in many industries, the 3DP technology is still very new in the pharmaceutical industry (1). The use of 3DP technologies in the pharmaceutical field is promising in the treatment of diseases where the dose varies from person to person or according to the severity of the disease. In colon-specific diseases such as colon cancer or Crohn's disease, in whose treatment antineoplastic agents and corticosteroids are generally used, individual dosing is required to increase the efficiency of the treatment (2). Personalized treatment in oral solid dosage forms produced by conventional methods is generally achieved by using a large number of low-dose drugs or by dividing higher-dose drugs. However, splitting of the tablets may lead to variations in the dose taken. Especially in modified-release tablets such as delayed-release, extended-release, and targeted-release, the division of the tablets may affect the release kinetics of the drugs or lead to burst release as disrupting the integrity of the coating. Thus, dose customization in these tablets is only possible by 3DP methods enabling flexible-dose manufacturing techniques (3). Fused deposition modeling (FDM) is recently the most researched 3DP method for pharmaceutical applications due to lower cost, ease of use and portability, and a wide range of applications.

Eudragit S100 is the most commonly used pH-dependent coating polymer for colon targeting tablets (4). However, it is difficult to produce a formulation including Eudragit S100 by FDM-3DP due to its degradation at the glass transition temperature (5). There is no study in the literature in which Eudragit S100 is printed below its degradation temperature.

This study aims to develop an Eudragit S100 coating filament that can be printed below its degradation temperature by FDM-3DP to be a model for colon-specific tablets.

Materials and Methods:

Citric acid monohydrate, magnesium stearate were donated by Drogsan Pharmaceuticals. Eudragit S100 and triacetin were gifted from Evonik Industries and BASF, respectively.

Preparation of Filaments with Hot Melt Extrusion:

Eudragit S100 was transferred to a mortar and, the required amount of triacetin was dispersed through a pestle. The powder plasticized with triacetin was passed through a 1.50 mm mesh sieve. Other excipients were also sieved onto the plasticized polymer. The powder mixture was then placed in a glass flask and mixed for 15 minutes. Homogeneously mixed powders (30 g)

were extruded at a temperature of 110˚C using a single-screw hot melt extruder with a 1.75 mm-diameter nozzle (Noztec Pro HME, UK).

Diameter, Mechanical and Morphological Properties of the Filaments:

The diameter of the filament was randomly measured from six points by a digital caliper (Dasqua,150mm). Mechanical properties such as the brittleness and flexibility of the filament were manually evaluated by twisting the filament in a spiral and, applying a certain tensile force. Moreover, morphological characteristics such as color, surface roughness, and stickiness of the filament were determined visually. In addition, the structural integrity of the filaments was examined by scanning electron microscopy (SEM, FEI Quanta 250 FEG).

The 3D Printing Process of the Filaments:

The printability of filaments was tested by printing round-shaped tablets (8.99 mm, 8.99mm, 3.68 mm) by an FDM 3D Printer with a 0.4 mm-diameter nozzle (Craftbot 3, Hungary). Tinkercad® (Autodesk, Inc., USA) was used as the computer-aided design (CAD) program to design round-shaped tablets exported as stereolithography (.stl) file into the 3D printer Craftware® software (Craftbot, Hungary). The setting parameters in Craftware® software for tablets were given in Table 1. STL file was converted into ".gcode" format in the software and then the generated G code is transferred to the printer via an external memory disk.

Table 1. The setting parameters of the tablet

The printing temperature	165 ˚C
Platform temperature	50˚C
Layer height	0.2 mm
Extrusion speed	20 mm/s
Traveling speed	120 mm/s
The number of shells	4
The shell thickness	0.8 mm
Infill density	% 50
Infill pattern	Parallel Line

Results:

The filament was extruded at 110˚C. FDM printers generally require a diameter of 1.75 mm, but they can tolerate a 0.05 mm deviation. Thicker filaments cause an interruption in the printing process, while thinner filaments cause air bubble formation in the printed parts. The diameter of the extruded filament was within the suitable limits of 1.74±0.03 mm. Moreover, it is so difficult to work with flexible or brittle filaments in the FDM process. The mechanical properties were considered to be suitable because the filament was resistant to stretching and bending (Figure. 1c,1d). Filaments were white, the surface was smooth and non-sticky (Figure 1a,1b). Besides, the structural integrity and homogeneity of the filaments were demonstrated by SEM analysis (Figure 1e).

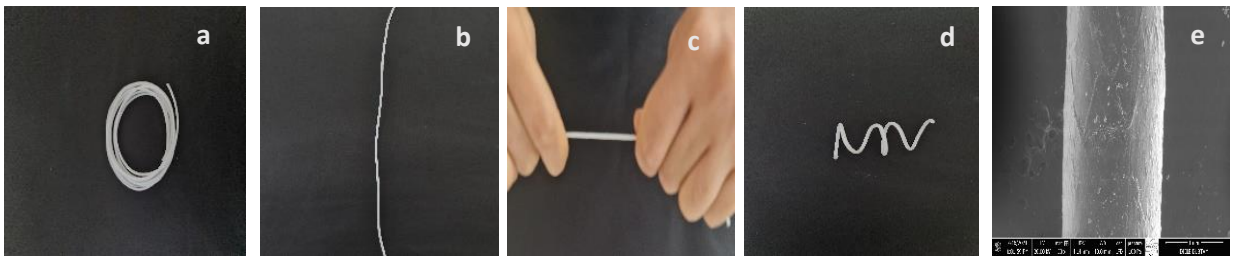

Figure 1. a) the whole filament b) a part of the filament c) The stretching of the filament d) the spiraling of the filament e) SEM image of the filament

The filaments were successfully printed as round-shaped tablets at 165 ºC which was lower than the degradation temperature (173ºC) of the polymer (5) (Figure 2).

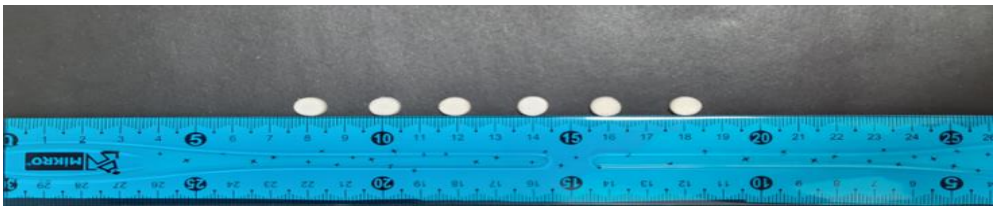

Figure 2. 3D printing of the model tablets

Conclusions:

In this study, Eudragit S100 was printed below its degradation temperature for the first time. This printable filament formulation can be used as a coating layer for a wide range of 3D colon-targeted drugs. The filament formulation developed in this study can be combined with core filaments containing various active ingredients to produce the coated tablets in future studies. The manufacturing of coated tablets by using FDM 3DP can enable personalized treatment without disrupting the integrity of the coating.

Acknowledgments

This study was supported by a grant of TUBITAK (SBAG-219S197)

References:

1. Norman et al., (2017). Advanced drug delivery reviews, 108, 39–50.
2. Charbe, et al., (2017). International Journal of Pharmaceutical Investigation, 7, 47-59.
3. Alhnan et al., (2016). Pharmaceutical research, 33(8), 1817–32.
4. Bruce et al., (2005). European Journal of Pharmaceutics and Biopharmaceutics, 59, 85-97.
5. Gioumouxouzis et al., (2018). AAPS PharmSciTech, 19, 3362–337.

OP014: NICLOSAMIDE LOADED NIOSOME FOR TOPICAL APPLICATIONS: DEVELOPMENT AND IN VITRO CHARACTERIZATION

[1]Yetgin, C., [2]Citlak, H., [1,3]Coban, O.

[1] Karadeniz Technical University, Department of Pharmaceutical Technology, Trabzon, Turkey, cerenyetgin@ktu.edu.tr

[2] Karadeniz Technical University, Faculty of Pharmacy, Trabzon, Turkey, havvagul.citlak@gmail.com

[3] Karadeniz Technical University, Drug and Pharmaceutical Technology Application and Research Center, Trabzon, Turkey, ozlemcoban@ktu.edu.tr

Introduction:

Atopic dermatitis (AD) is a chronic inflammatory skin disease (1). Chronic eczematous dermatitis results in pruritic erythematous, dry, lichenified skin with scaling and excoriations. For AD, current treatment approaches are phototherapy, topical therapy, and systemic therapy. Corticosteroids are generally used for topical treatment. In our study, we chose niclosamide (NIC) for the treatment of atopic dermatitis. NIC was discovered in the late 1950s and is currently used as an antihelmintic drug. In 2018, phase II trials of NIC for the treatment of impetigo and AD were completed (2), thus its future development is focused on atopic dermatitis. Niosomes are vesicular drug delivery systems containing nonionic surfactant in their bilayer structure. They are commonly used topically. Since niosomes have a flexible structure, increase skin penetration of drugs (3, 4). The objective of the investigation was to design a vesicular formulation of NIC, evaluate its ability to topical permeability and improve the therapeutic efficacy of the drug.

Materials and Methods:

Materials: NIC was provided as a gift from Bayer, Turkey. Span 80 was purchased from Doğa Scientific Raw Materials, Turkey, whereas Tween 80 was bought from Fisher Scientific, USA. Sodium chloride (99.5%) and potassium dihydrogen phosphate (99.5%) were supplied from Isolab Laboratories, Germany, while sodium hydrogen phosphate was purchased from Merck Millipore, USA. Cholesterol, sodium hydroxide (≥98%) and dialysis membrane (12000 Da MWCO) were obtained from Sigma-Aldrich, USA. Distilled water used was obtained from a Millipore Milli-Q ultrapure water system in the laboratory.

***Preparation of Niosomes*:** Niosomes containing NIC was prepared by the ethanol injection method (4). We used different ratios of cholesterol (Chol), NIC and surfactant (surf) in the formulations (Table 1). NIC, surfactant and cholesterol in different ratios were dissolved in ethanol. The resulting solution was slowly injected using syringe into distilled water under a magnetic stirrer at 500 or 1000 rpm and at 60°C. Stirring was continued for a further 1 h after injection under same conditions to form niosomes as result of the evaporation of the solvent.

Table 1. Ratios of cholesterol, niclosamide and surfactant in the formulations

Formulation	Chol:surf:NIC (mg)	Surfactant	Charge inducer (mg)	Stirring rate (rpm)
S1	15: 15: 10	Span 80	-	500
S2	15: 15: 5	Span 80	-	500
S3	15: 15: 5	Span 80	1	500
S4	15: 15: 10	Span 80	-	1000
S5	15: 15: 5	Span 80	-	1000
S6	15: 15: 5	Span 80	1	1000
T1	16.2: 55: 5	Tween 80	1	500
T2	16.2: 55: 5	Tween 80	-	500
S7	15: 15: 1	Span 80	-	1000
S7-empty	15: 15	Span 80	-	1000
S8	15: 15: 1	Span 80	1	1000
S8-empty	15: 15	Span 80	1	1000

Chol: cholesterol, **surf:** surfactant, **NIC:** niclosamide

***Entrapment Effiency*:** To determine entrapment efficiency (EE), the unentrapped drug was separated from drug-loaded niosomes by ultra-centrifugation at 15 000 rpm using a cooling centrifuge at 4°C for 1 h. The absorbance of the NIC in the supernatant was measured using a UV-Vis spectrophotometer (Thermo Scientific Multiskan Go, USA) at 291 nm. The amount of entrapped drug was obtained by substracting amount of un-entrapped drug from the total drug incorporated. The entrapment efficiency (EE %) was calculated according to the following equation:

$$EE(\%) = \frac{amount\ of\ entrapped\ niclosamide}{total\ amount\ of\ niclosamide} x100$$

***Particle Size, Zeta Potential, Polydispersity Index of Niosomes*:** The particle size (PS), zeta potential (ZP) and polydispersity index (PdI) of the niosomes were investigated utilizing the Malvern Zetasizer Nano-ZS. After centrifugation, 1 mL of distilled water was added to the precipitate to obtained niosome suspension. 120 µL of this suspension was put into a cuvette and 880 µL of distilled water was added on. All measurements were performed in triplicates at room temperature.

***In Vitro Release*:** In vitro release of NIC from niosomes was conducted by dialysis bag method (5). Dialysis membran were soaked before use in distilled water at room temperature for 24 h. In this study, 20 mL of PBS (pH 7.4) containing 2% Tween 80® was used as a media for enhancing NIC solubility and release study was performed on a magnetic stirrer at 200 rpm and 32°C (figure 1). 2 mL samples were withdrawn from the release media at 15-30-60-90-120-240 min, and an equal volume of fresh release medium was added. The samples were analyzed at 291 nm spectrophotometrically to determine the concentration of NIC.

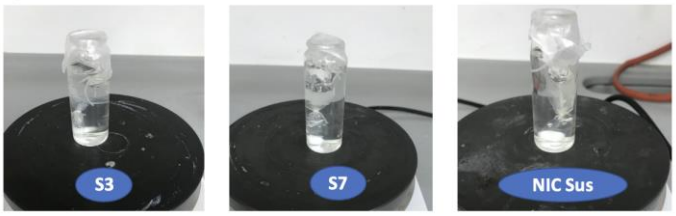

Figure 1. In vitro release studies of S3, S7 formulations and NIC suspension

Results:

Characterization Studies: Ten formulations were prepared to examine the stirring rate, chol:surf:NIC ratio, charge inducer and nonionic surfactant type effect on the characterization of formulations. Tween 80 and Span 80 were used as nonionic surfactants and cetylpyridinium chloride was used as a charge inducer. Low PS and PdI, and highest ZP value were obtained with S3 formulation, whereas lowest PS and PdI were obtained with S7 formulation (table 2). Better results were obtained with formulations containing Span 80. As the HLB value of surfactants increases, the amount of cholesterol required increases. Therefore, niosomes prepared with Tween 80 were thought to have larger PS. In addition, it was observed that cetylpyridinium increased the ZP and all formulations showed high encapsulation efficiency between 94.425% and 99.969%, regardless of parameters. Finally, formulations containing NIC have a lower pH except S8.

Table 2. The particle size, polydispersity index, zeta potansiel, encapsulation efficiency and pH value of formulations.

Formulation	PS (nm)	PdI	ZP (mV)	EE (%)	pH
S1	692.733±421.381	0.567±0.308	-0.283±0.071	99.666	5.43
S2	254.4±11.401	0.297±0.048	-0.856±0.852	97.786	5.44
S3	445.033±6.189	0.643±0.104	-21.833±0.125	99.895	5.78
S4	1266.233±379.554	0.947±0.067	-0.615±0.077	99.772	6.03
S5	416.667±141.132	0.438±0.064	-0.595±0.319	99.413	6.16
S6	845.067±184.532	0.785±0.162	-0.466±0.511	99.969	6.85
T1	3119±1777.875	1±0	0.115±0.36	96.283	5.82
T2	2665±636.784	1±0	-0.242±0.292	94.741	5.63
S7	186.067±1.855	0.156±0.015	0.003±0.885	94.425	6.1
S7-empty	239.233±1.791	0.252±0.03	-0.167±0.365	-	6.22
S8	459.367±9.154	0.381±0.018	-0.403±0.266	99.287	6.67
S8-empty	334.567±1.066	0.271±0.012	-21.3±0.49	-	5.56

PS: particle size, **PdI:** polydispersity index, **ZP:** zeta potential, **EE:** encapsulation efficiency

***In Vitro Release*:** It was observed that NIC suspension released approximately 60% of the drug, while vesicle formulations S3 and S7 showed 40% and 65% drug release respectively within 4 h (figure 2). In this study, since NIC is in suspended form and has low solubility in aqueous media (6), both niosomes were expected to achieve higher release rates. However, 2% Tween 80 used in the release medium may have increased the permeability of the dialysis membrane (7) and therefore caused a decrease in the difference in release rate between the suspension and niosomes. To better observe this difference, the amount of surfactant in the release medium can be reduced or a completely surfactant-free medium can be used.

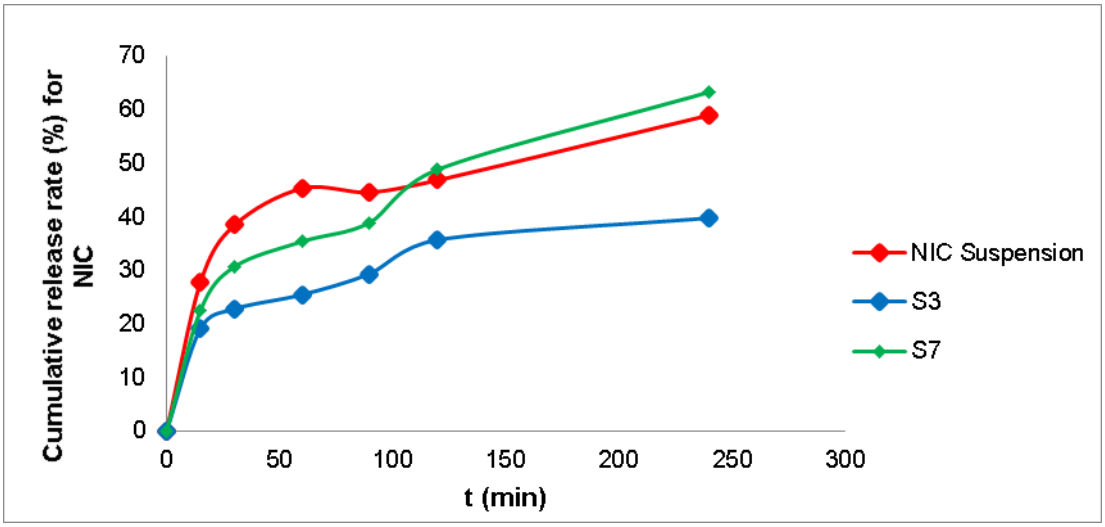

Figure 2. In vitro release profiles of S3, S7 formulations and NIC suspension

Conclusions:

Better results were obtained from niosomes prepared with Span 80 compared to Tween 80. However, no linear relationship was observed between mixing speed and results. The pH values of all formulations are suitable for topical use. When all studies were evaluated, it was observed that the best results were obtained with S7. For topical administration, the resulting formulation can be loaded into the hydrogel and thus the release time of the drug can be extended.

Acknowledgements

This research did not receive any specific grant from funding agencies in the public, commercial, or not-for-profit sectors.

References:

1. Matias CSS (2020). Antibiotic drug development, Technical University of Denmark. (Ph.D. thesis)
2. Butler MS, Paterson DL (2020). Antibiotics in the clinical pipeline in October 2019. J Antibiot., 73:329-364.
3. Bendas ER, Abdullah H, El-Komy MH, Kassem MA (2013). Hydroxychloroquine niosomes: a new trend in topical management of oral lichen planus. Int J Pharm., 458(2):287-95.
4. Kakkar S, Kaur IP (2013). A novel nanovesicular carrier system to deliver drug topically. Pharmaceutical Development and Technology, 18(3):673-685.
5. Aggarwal D, Kaur IP (2005). Improved pharmacodynamics of timolol maleate from a mucoadhesive niosomal ophthalmic drug delivery system. Int J Pharm., 290(1-2):155-9.
6. Yang W, Villiers MM (2005). Effect of 4-sulphonato-calix[n]arenes and cyclodextrins on the solubilization of niclosamide, a poorly water soluble anthelmintic, The AAPS Journal, 7:241-248.
7. Manna S, Wu Y, Wang Y, Koo B, Chen L, Petrechenko P, Dong Y, Choi S, Kozak D, Oktem B, Xu X, Zheng J (2019). Probing the mechanism of bupivacaine drug release from multivesicular liposomes. Journal of Controlled Release, 294:270-287.

OP016: HOW USEFUL ARE MICROSCOPIC TECHNIQUES TO PREDICT DRUGRELEASE PROFILE FROM THE LIPID MICROPARTICLES?

[1]Wolska, E., [1]Sznitowska, M.

[1] Medical University of Gdansk, Department of Pharmaceutical Technology, Gdansk, Poland, eliza.wolska@gumed.edu.pl

Introduction:

Solid lipid microparticles (SLM) as biocompatible and multi-compartment carrier of drug substances are considered as a dosage form for administration by various routes including, for example, oral, topical and parenteral, both in the form of an aqueous dispersion and fine powder. The main advantage of SLM is the relatively simple technology and ability to provide sustained release and action of the active substance. Only effective and permanent incorporation of the drug substance into the lipid matrix of the particles provides the SLM carrier with the aforementioned properties. At the same time, it is a main problem, even in the case of highly lipid soluble substances (1). The aim of the conducted research was to indicate the most advantageous microscopic techniques for the assessment of SLM structure with the potential to detect changes occurring during the release study.

Materials and Methods:

SLM were prepared with two various lipids (Compritol or stearic acid) and two model drug substances: cyclosporine and indomethacin. Tested formulations were obtained both in the form of liquid dispersion (produced by the hot emulsification method) and fine powder (obtained in the process of spray drying (2)).

Physicochemical characterization of the SLM formulations, before and after spray drying, was performed by optical microscopy, scanning electron microscopy (SEM), Raman spectroscopy and atomic force microscopy (AFM) (2). The release of model drug substances (cyclosporine, indomethacin) from SLM was investigated in the membrane-free system.

Results:

The imaging of lipospheres and visualization of structural details were made by various techniques. Optical microscopy was considered the basic tool, useful at every stageof the research as quick and simple technique, that allows both liquid dispersions (Fig. 1A) and solid powders (Fig. 1B) to be observed directly. The main observed properties were the particle size of lipid microspheres which determines the release rate and the shape of the lipospheres influencing the stability of the system. When the drug substance incorporation in the preparation step was incomplete, API particles were clearly visible in the microscopic image, similar as recrystallized drug substance in aqueous phase during storage in unstable systems.

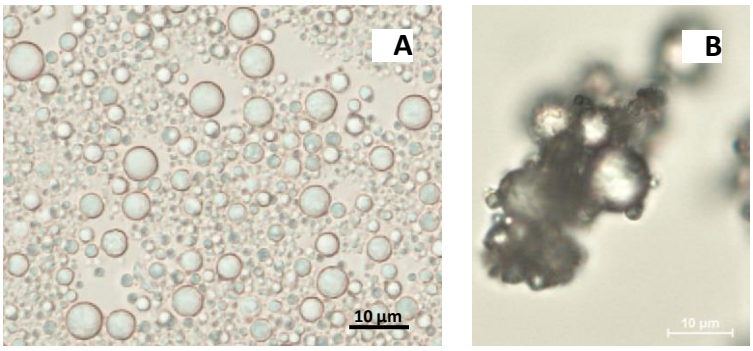

Figure 1. Optical microscopic picture of SLM formulations: (A) solid lipid microparticles dispersion and (B) SLM dry powder

SEM as a high-resolution technique allowed for an in-depth analysis not only of the shape of the obtained microspheres, but above all of their surface structure (Fig. 2A). Despite the high resolution of the obtained images, apart from structural differences, it was difficult to clearly visualize the differences in the surface of placebo lipospheres and those with the drug substance located on the particles surface. In the next stage the SLM surface and the active substance located on it were visualized using the Raman spectroscopy technique. Although model APIs were identified on the SLM surface (Fig. 2B), lipids and other excipients were the dominant components in the maps, mainly due to the low concentration of active substances and their spectral properties. Meanwhile, the AFM microscope was used to compare the viscoelastic properties of placebo and drug loaded SLM surface by measuring the adhesion of the probe tip to the tested surface, which allowed to show characteristic differences (2). Since the fraction of the drug substance responsible for the initiating dose in the release study is located on the surface of the lipid particles, microscopic techniques allowed to observe the differences in the tested formulations and their correlation with the results of the release studies.

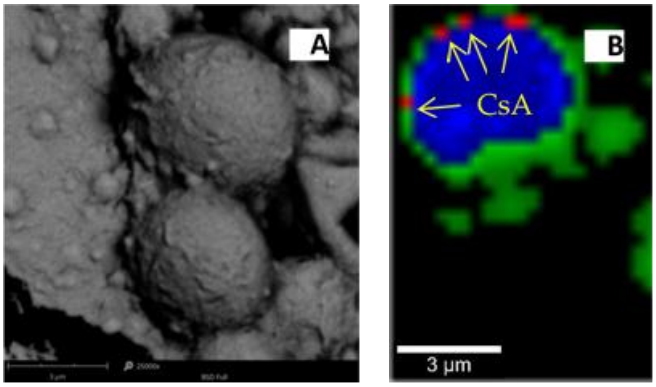

Figure 2. Scanning electron micrographs (A) of SLM powder with cyclosporine and Raman map (B) of SLM with cyclosporine after spray drying (2).

The main factor determining the rate of release of the drug substance from SLM was the lipid forming the matrix of the microspheres. The changes in the release profile observed after spray-drying of aqueous dispersion were also found to be dependent on the lipid of the lipospheres. And finally the so-called "burst effect", which was related to the location of a significant fraction of API on the microparticles surface, was also observed in the obtained release profiles.

Conclusions:

All of the used microscopical methods could be considered complementary and providing valuable information, however SEM and AFM techniques were recognized as the most valuable. In routine inspection, classical optical microscopy can successfully replace the more difficult and time-consuming SEM method. SLM research using Raman spectroscopy will be continued in order to confirm or exclude their suitability for the intended purpose. Regardless of microscopic methods and other instrumental techniques, the resultsof the dissolution studies provide irreplaceable knowledge about the properties of the dosage form and allow the detection of even subtle changes in the distribution and behavior of the drug substance.

Acknowledgements

This study was supported by a grant of the National Science Centre, Poland, 2017/01/X/NZ7/01717.

References:

1. Wolska, E., Sznitowska, M., Chorążewicz, J., Szerkus, O., Radwańska, A., Markuszewski, M. J., ... & Raczyńska, K. (2018). Ocular irritation and cyclosporine A distribution in the eye tissues after administration of Solid Lipid Microparticles in the rabbit model. *European Journal of Pharmaceutical Sciences*, *121*, 95-105.
2. Wolska, E., Sznitowska, M., Krzemińska, K., & Ferreira Monteiro, M. (2020). Analytical techniques for the assessment of drug-lipid interactions and the active substance distribution in liquid dispersions of solid lipid microparticles (SLM) produced de novo and reconstituted from spray-dried powders. Pharmaceutics, 12(7), 664.

OP017: PICKERING EMULSIONS STABILIZED BY CYCLODEXTRIN DERIVATIVES FOR TREATMENT OF ATOPIC DERMATITIS: OPTIMIZATION AND *IN VITRO* CHARACTERIZATION

Aydilek, N., **Kahraman, E.**, Güngör, S.

Istanbul University, Faculty of Pharmacy, Department of Pharmaceutical Technology, Istanbul, emine.kahraman@istanbul.edu.tr

Introduction:

The emulsions have widely used in pharmaceutical applications for many years. The use of stabilizers is required for formulation and providing long-term stability of the emulsions, because they are thermodynamically unstable systems. The synthetic surfactants have mostly been used as stabilizers in the emulsion formulations. However, these surfactants may cause irritation and/or allergic responses in the skin. In order to overcome these problems, Pickering emulsions have emerged for drug delivery in the recent years because of stabilized by adsorption of biopolymers such as chitosan, starch, zein, cyclodextrins or solid particles including hydroxyapatite, colloidal silica, clay, that have emulsifier and non-irritant features (1). Atopic dermatitis is a chronic inflammatory disease characterized by itching, erythema, and eczematous lacerations. The dry skin, irritants, allergies, infection, and so on trigger atopic dermatitis (2). Hence, we aimed to develop surfactant-free formulations exhibiting no irritation/allergic responses in the treatment of atopic dermatitis.

Materials and Methods:

The cyclodextrins (α-CD, β-CD, γ-CD) were obtained as gift samples from Wacker Chemie (Germany). Tacrolimus monohydrate was kindly donated by Bilim Pharmaceuticals (Turkey). The rotor-stator homogenization method was used to prepare Pickering emulsions. Olive oil and a cyclodextrin derivative (in ratios of 1:7, 1:3, 1:1, 3:1 and 7:1, w/w) were weighed, and stirred before adding ultrapure water. Emulsification was conducted using Ultraturrax (IKA, T25 Digital, Germany) at 11000 rpm for 5 min. Tacrolimus monohydrate (0.03%, w/w) was added concurrently with cyclodextrin derivative. After emulsification, phase diagrams of oil/CD/water systems were constructed by observing the presence of phase separation to determine concentration ranges of components for stable Pickering emulsions. Then, the emulsions were characterized in terms of pH, electrical conductivity, homogeneity and rheological behaviours at ambient temperature.

Results:

The concentration ranges of components for stable Pickering emulsions were determined by phase diagrams of oil/CD/water systems. These studies revealed that the emulsions stabilized by γ-CD (28.79-66.67%) contained of much more olive oil for same cyclodextrin derivative ratio than that of the emulsions (17.63-53.75% for the emulsions stabilized by α-CD and 29.74-60.92% for β-CD) (Figure 1), as a result cavity diameter and volume of the cyclodextrins (3). Additionally, α-CD, β-CD and γ-CD cyclodextrin ratios required to form stable emulsions were 7.67-22.19%, 6.87-36.15% and 7.11-34.60%, respectively. Hence, it was decided to utilize the formulations consisting of 8% or 12% of cyclodextrin and 50% of olive oil in order to compare cyclodextrin derivatives and their concentrations in the future studies.

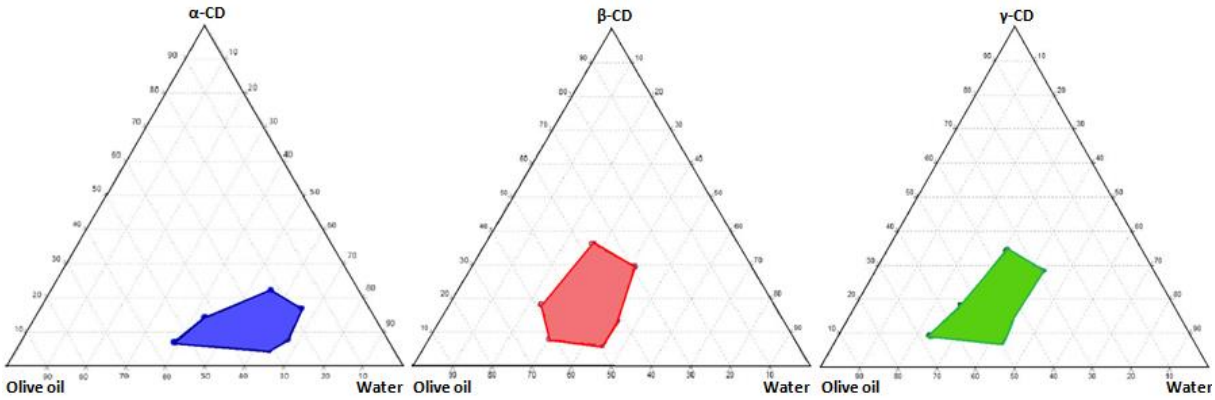

Figure 1. The phase diagrams of oil/CD/water systems

pH values of optimized Pickering emulsions loaded tacrolimus were about 4.5 and 5.5, indicating their feasibility for skin delivery. The electrical conductivity values (in range of 323.3±3.2 and 514.8±5.6 µS/cm) revealed that type of the emulsions was oil in water (O/W) (Table 1).

Table 1. The characterisation of optimized Pickering emulsions (n=3)

Formulation*	pH±SD	Conductivity±SD (µS/cm)	G_I±SD (Pa)	G_{II}±SD (Pa)
8% of α-CD (A8)	4.65±0.04	446.36±5.18	105.914±23.618	18.529±2.987
12% of α-CD (A12)	4.49±0.03	323.33±6.94	-	-
8 % of β-CD (B8)	4.66±0.05	498.43±12.01	17.855±12.426	6.709±4.459
12 % of β-CD (B12)	4.64±0.02	463.96±5.97	178.533±269.464	32.852±40.147
8 % of γ-CD (G8)	4.58±0.01	514.8±17.13	10.765±4987	5.545±2.560
12 % of γ-CD (G12)	4.71±0.05	509.16±6.18	41.039±11837	21.398±6.416

** All of formulations contain 50% of olive oil*

The bright-field microscopy images depicted that the emulsions composed of spherical droplets with high homogeneity, especially ones stabilized by γ-CD (Figure 2). The emulsions stabilized by α-CD exhibited the highest viscosity values, whereas ones stabilized by γ-CD showed the lowest viscosity values (Figure 3). Moreover, the elasticity of the emulsions was found greater than viscous modulus for all of optimized formulations (Table 1).

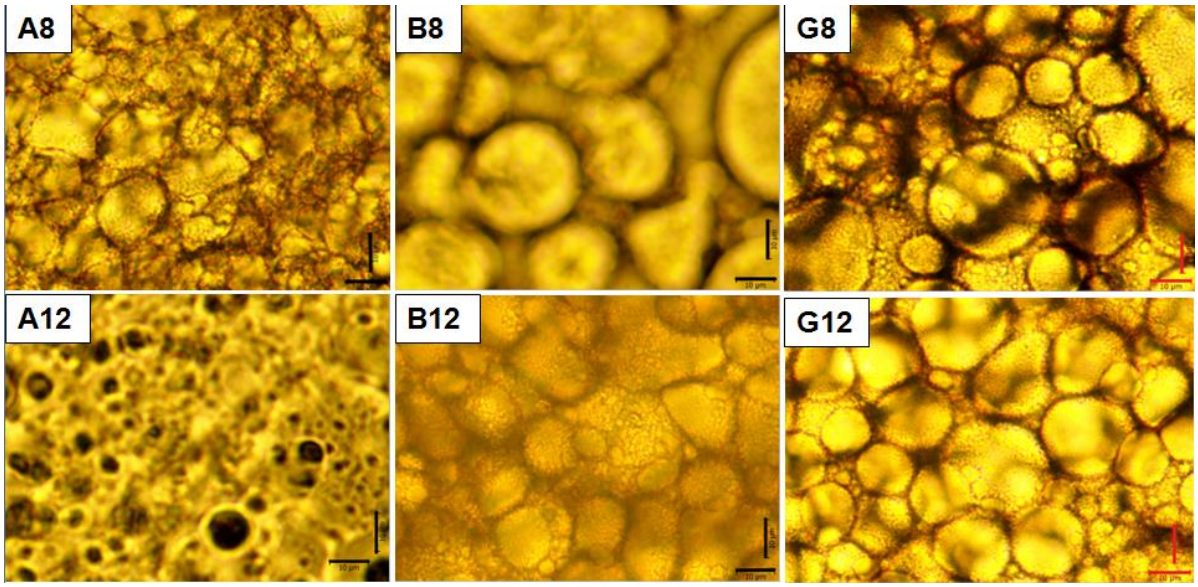

Figure 2. The bright-field microscopy images of optimized Pickering emulsions

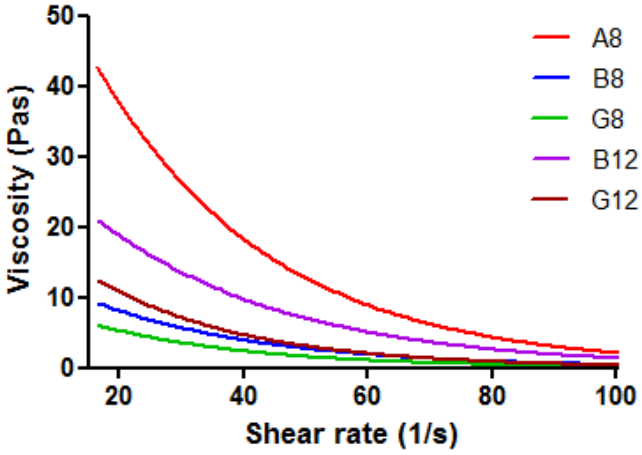

Figure 3. The graph viscosity-shear rate of optimized Pickering emulsions

Conclusions:

The optimization studies and *in vitro* characterization data indicate that Pickering emulsions containing of γ-CD could be promising alternative dosage forms for dermal delivering of tacrolimus in the treatment of atopic dermatitis. However, *in vitro* drug release and permeation studies as well as *in vivo* studies including irritation tests should be performed to support these results and to show efficacy and safety of tacrolimus loaded Pickering emulsions.

References:

1. Albert C, Beladjine M, Tsapis N, Fattal E, Agnely F, Huang NJ (2019). Journal of Controlled Release, 309:302-332.
2. Kahraman E, Aydilek N, Güngör S (2020). Recent Patents on Drug Delivery & Formulation, 14(3):191-200.
3. Ho TM, Howes T, Bhandari BR (2014). Powder Technology, 259: 87–108.

OP019: PREPARATION AND CHARACTERIZATION OF BIGEL SYSTEMS CONTAINING CICLOPIROX AND UREA

[1]Kodan, E., [1]Tirnaksiz, F.

[1] Gazi University, Department of Pharmaceutical Technology, Ankara, Turkey.
esrakodan11@gmail.com, figentirnaksiz@gmail.com

Introduction:

Onychomycosis is a fungal infection of the nail bed and nail plate caused by dermatophytes, non-dermatophyte molds and yeasts (1). It affects approximately 20% of individuals worldwide and accounts for approximately 50% of all nail infections (2). The treatment is performed by using oral and topical antifungal agents alone or in combination. The aim of study is to investigate efficacy of bijels as carriers for dermal delivery of ciclopirox, a broad spectrum antifungal drug. The urea contained in hydrogel, which is outer phase, will increase effectiveness of ciclopirox by contributing to expansion of pores in nail and skin. Bigels are prepared by mixing organogel (oleogel) and hydrogel at certain temperature and ratio at high speed (Figure 1). They are semi-solid systems in which inner phase is dispersed as droplets in outer phase. Bijels are considered that increase penetration of lipophilic active substances in the inner phase by expanding pores in skin and nails when applied topically, since outer phase is water.

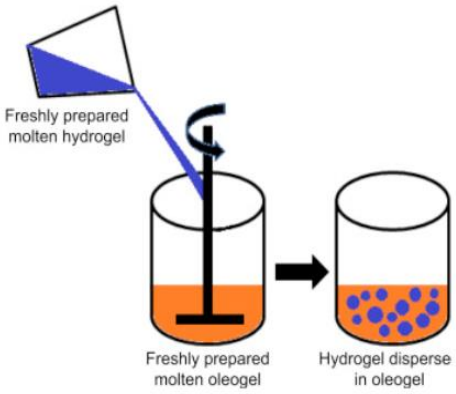

Figure 1. Systematic diagram representing the bigel formulation.

Materials and Methods:

Organogel consists of MCT-oil glyceryl monostearate (GMS), span 80 and ciclopirox, while hydrogel consists of distilled water, urea, Carbopol 974P, tween 80, propylene glycol (PG). After organogel and hydrogel are heated to 70˚C, they are mixed at 6000 rpm. Bigel systems were prepared with 2^3 full factorial designs using different ratios of Carbopol 974P, GMS and MCT-oil (Tablo 1). Optimum formulations were selected according to viscosity, size of oil droplets in

internal phase and centrifuge results of formulations prepared. Oil droplets in outer phase were observed using fluorescent microscope.

Table 1. Composition of hydrogel and organojel formulations.

Ingredients (%)	Hydrogel	Organogel
Carbopol 974P	0,05-0,2	-
Propylene glycol	5-10	-
Urea	20-40	-
Tween 80	q.s	-
D. water	q.s	-
Glyceryl monostearate	-	2-10
Span 80	-	q.s
MCT- oil	-	q.s

Results: Independent variable and response data of 8 formulations prepared according to the Design of Expert-12 are shown in Table 1. As internal phase ratio increased, viscosity increased. As oil droplets in outer phase grew, phase separation was observed in centrifuge performed as an accelerated endurance study. In addition, increase percentage of GMS in organogel increased durability of system. As viscosity increases, structure of bigel changes from shear thinning to shear thickening (Figure 1). The droplet size of bigels varied between 413.6-2287.0 nm (Figure 2).

Table 2. Experimental design and responses for bigel formulations.

Rx	Independent variable 1- Carbopol 974 - %	Independent variable 2- GMS - %	Independent variable 3- MCT-oil - %	Response 1- K (Pa s^n)	Response 2- PB (nm)
D1	0,15	6	34	7.386	599,7
D2	0,05	6	34	2.413	1298,6
D3	0,15	2	34	11.857	1283,0
D4	0,15	2	54	21.100	863,5
D5	0,15	6	54	384.807	413,6
D6	0,05	2	54	11.484	1211,0
D7	0,05	2	34	249	2287,0
D8	0,05	6	54	117.880	476,3

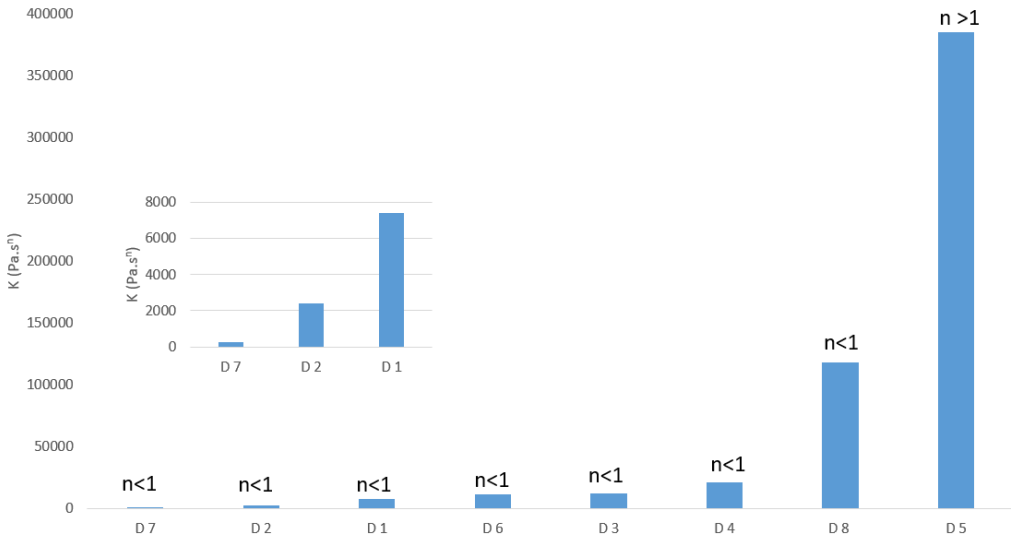

Figure 2. K values of prepared bigel formulations using Design of Expert 12.

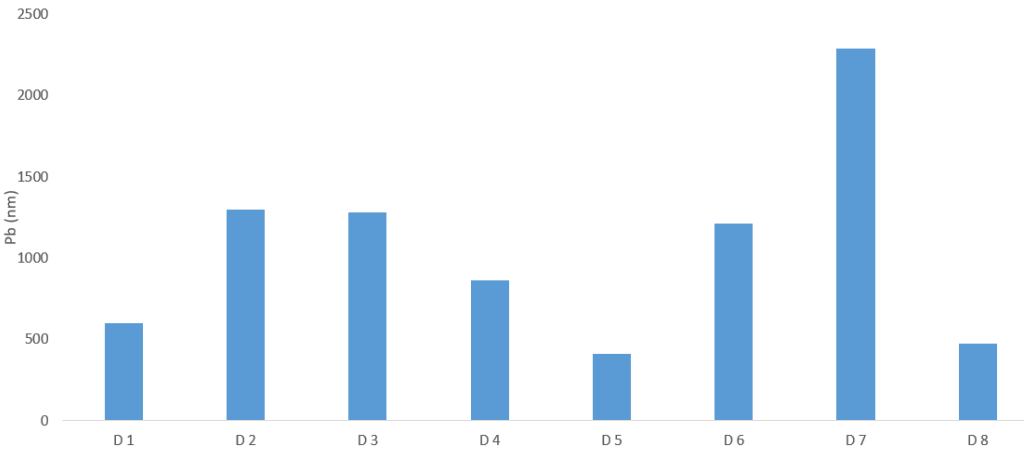

Figure 2. Droplet size of prepared bigel formulations using Design of Expert 12.

Conclusions:

In vitro results have shown that the bigel system is a suitable delivery system for ciclopirox and urea. The viscosity and texture analysis properties have been found suitable for topical application. Three formulations with no phase separation, small droplet size and higher viscosity were selected as optimum. After this, in-vitro release study and ex-vivo permeation study of ciclopirox and urea will be performed.

Acknowledgements

This study was supported by a grant of GAZİ-BAP (02/2020-22)

References:

1. Vlahovic T (2016). Clin Podiatr Med Surg., 33, 305–318.
2. Gupta AK (2018). Expert Review of Anti-infective Therapy, 16:12, 929-938

OP020: STABILITY STUDIES ON MEDICAL DEVICE PREPARED BY VANCOMYCIN-LOADED BONE CEMENT

[1] Zanbak Çotaoğlu, EM., [1]Köse Özkan, C., [1]Eşim O., [2]Kıymacı, M.E., [2] Ünal, N., [1]Savaşer, A., [1]Özkan, Y.

[1] University of Health Sciences, Gülhane Faculty of Pharmacy, Department of Pharmaceutical Technology, Etlik, Ankara, Turkey

[2] University of Health Sciences, Gülhane Faculty of Pharmacy Department of Pharmaceutical Microbiology, Etlik, Ankara, Turkey

Introduction:

'Medical device' means any instrument, apparatus, appliance, software, implant, reagent, material, or other article intended by the manufacturer to be used, alone or in combination, for human beings for one or more of the following specific medical purposes:

- Diagnosis, prevention, monitoring, prediction, prognosis, treatment, or alleviation of disease,
- Diagnosis, monitoring, treatment, alleviation of, or compensation for, an injury or disability,
- Investigation, replacement or modification of the anatomy or of a physiological or pathological process or state,
- Providing information by means of in vitro examination of specimens derived from the human body, including organ, blood and tissue donations,

and which does not achieve its principal intended action by pharmacological, immunological or metabolic means, in or on the human body, but which may be assisted in its function by such means (1, 2).

Bone cement functions as an injection agent to immobilize the prosthesis in joint replacement surgery. The main function of bone cement is to transfer stress from the implant to the bone and increase the load bearing capacity of the system (3, 4).

It can be seen as a complication following joint replacement surgery, and the use of antibiotic-loaded bone cements is potentially used as a clinical practice, helping to reduce the incidence of deep infections.

Vancomycin is a glycopeptide antibiotic used in the treatment of serious gram-positive bacterial infections. Molecular weight 1449 and easily soluble in water (>100mg/mL). The degradation product of CDP-1 has two forms, CDP-1-M (major) and CDP-1-m (minor), possibly conformational isomers formed by hydrolytic ammonia loss. CDP is structurally similar to vancomycin with two carboxyl groups but is biologically inactive (5).

In this study, it is aimed to conduct stability studies by simulating the antibiotic loaded bone cements used in local treatment, the preparation stages of the loaded antibiotics and the in vivo environments that the bone cement will encounter when placed into the body after hardening in order to reduce the incidence of infection. The test methods and results to be

determined in the stability studies will be beneficial in re-evaluating, updating and expanding the existing guidelines.

Materials and Methods:

Within the scope of the stability studies, first, temperature monitoring was carried out during the preparation phase. Release studies of bone cement have been carried out and release amounts / profile and release rates have been determined.

In addition, the structural changes of the prepared bone cement were examined, mechanical strength was also detected. The analysis of the mechanical properties was made based on the test methods in the ISO 5883 standard (6). Antibacterial efficacy testing was performed by Kirby Bauer disk diffusion method in accordance with the European Committee for Antimicrobial Susceptibility Tests (EUCAST) standard (7).

Results:

Most of the cumulative vancomycin release took place over the first week. Detectable, but much lower, levels of vancomycin continued to release for at least four weeks. However, it is not very clear how much vancomycin is released by the formulations and how much remains unreleased in the bone cement 'mix', as the remaining vancomycin in the formulations and the released vancomycin are converted into degradation products.

The mechanical properties of the formulations were tested with the compressive strength and bending strength test methods in ISO 5833. For the bending strength test given in ISO 5883, the average results should be equal to or greater than 50 MPa. The values of all prepared formulations are in accordance with ISO 5883. One-way ANOVA test was applied, and formulations were compared with each other. It was observed that bending strength value decreased as the amount of vancomycin in the formulations increased. The differences between the formulations were not statistically significant.

Comparison of the compression strength of the formulations tested at twenty-four hours with that of the formulations tested after 1 month of elution demonstrated a significant decrease in strength ($p < 0.001$).

As a result of the antibacterial activity studies, it is shown that the increase in the efficiency with the increase of the antibiotic dose. The formulations were store in 37 ℃ SBF for 1 month, samples were taken from here at certain times and its antibacterial activity was checked. Since vancomycin release decreased, the zone diameters also decreased over time.

Conclusions:

Stability evaluations of medical device bone cements loaded with antibiotics will guide future studies with our study. It will also be able to contribute to the work to be done to develop standards such as the relevant ISO.

Acknowledgements

This study was supported by a grant of University of Health Sciences of Turkey- BAP 2021/097

References:

1. The European Parliament And The Council. Regülation On Medical Devices. (Eu) 2017/745 2021.
2. T. C. Sağlık Bakanlığı Türkiye İlaç Ve Tıbbi Cihaz Kurumu. Tıbbi Cihaz Yönetmeliği. Vol. 31499. 2021.
3. Vázquez Lasa B (2008). Poly (Methylmethacrylate) Bone Cement: Chemical Composition And Chemistry. Orthop Bone Cem, 183–205.
4. Vaishya R, Chauhan M, Vaish A. Bone Cement (2013). J Clin Orthop Trauma, (2013). 4(4):157–63.
5. Suchý T, Šupová M, Klapková E, Horný L, Rýglová Š, Žaloudková M, et al. (2016). The Sustainable Release Of Vancomycin And Its Degradation Products From Nanostructured Collagen/Hydroxyapatite Composite Layers. J Pharm Sci, 105(3):1288–94.
6. TS ISO 5833/D1 (2020) Implants for surgery — Acrylic resin cements
7. European Committee on Antimicrobial Susceptibility Testing, Antimicrobial susceptibili ty testing EUCAST disk difussion method, Version 8.0, January 2020.

OP021: PREPARATION AND IN VITRO EVALUATION OF APO-E MODIFIED SOLID LIPID NANOPARTICLES FOR DELIVERY OF HUMANIN PEPTIDE

[1]Topal, GR., [2]Mészáros, M., [2]Porkoláb, G., [2]Szecskó, A., [3]Küçüktürkmen, B., [3]Öz, UC., [2]Deli, MA., [2]Veszelka, S., [3]Bozkır, A.

[1] University of Health Sciences, Gulhane Faculty of Pharmacy, Ankara, Turkey, gizemruya.topal@sbu.edu.tr

[2] Institute of Biophysics, Biological Research Centre, Szeged, Hungary, meszaros.maria@brc.hu, porkolab.gergo@brc.hu, szecskoaniko@gmail.com, deli.maria@brc.hu, veszelka.szilvia@brc.hu

[3] Ankara University, Faculty of Pharmacy, Ankara, Turkey, bozkir@pharmacy.ankara.edu.tr, bbasaran@pharmacy.ankara.edu.tr, umutcanoz@ankara.edu.tr

Introduction:

Alzheimer's disease is the most common type of dementia which ultimately leads to cognitive decline, memory impairment, aphasia and behavioural issues. Current treatments are all symptomatic, so new cures are needed to prevent disease before symptoms occur (1). Due to this reason, many new approaches have been investigated recently. Humanin which is a peptide formed by 24 aminoacids plays a critical role in various biological processes including apoptosis, cell survival, lipid flux, and inflammation. protects the cells and mant studies showed that it is effective on cytotoxicity due to Aβ42 (2). One of the most important problems regarding the treatment of Humanin is the presence of the blood brain barrier, a highly selective diffusion barrier that protects the brain from toxins and other compounds from blood. Solid lipid nanoparticles (SLNs) which is very similar to lipophilic BBB are an alternative carrier system to emulsions, liposomes and polymeric nanoparticles; so we planned to prepare Humanin-loaded SLNs to across the blood-brain-barrier (BBB) easily and the bonding of Apo-E to the SLNs was aimed for targetting. In this study Humanin loaded solid lipid nanoparticles were prepared and evaluated in vitro, subsequently cyctotoxicity and cell uptake of SLNs were determined on SH-SY5Y cells.

Materials and Methods:

Humanin was obtained from Proteogenix and Apo-E from Peprotech. Tripalmitin was a kindly gift from IOI Oleochemical, Germany. Tween 80 was purchased from Sigma, Germany.

Preparation of Solid Lipid Nanoparticles:

SLNs were prepared by homogenization/ultrasonication method that we used our previous study (3). Briefly, %1 (w/v) lipid was melted and surfactant (%1,5 w/v) added to lipid phase and this mixture was heated to 70°C. Afterwards, aqueous phase was also heated to 70°C then these two phase mixed by using homogenisator (Ultraturrax T-25) and sonicated later on. Finally it let to cool down at room temperature. Preparation method can be seen from Figure-1. When Humanin-loaded SLNs were prepared, Humanin was added to lipid phase (%0,01 w/v) and dispersed then preparation procedure was carried on exactly same as explained before.

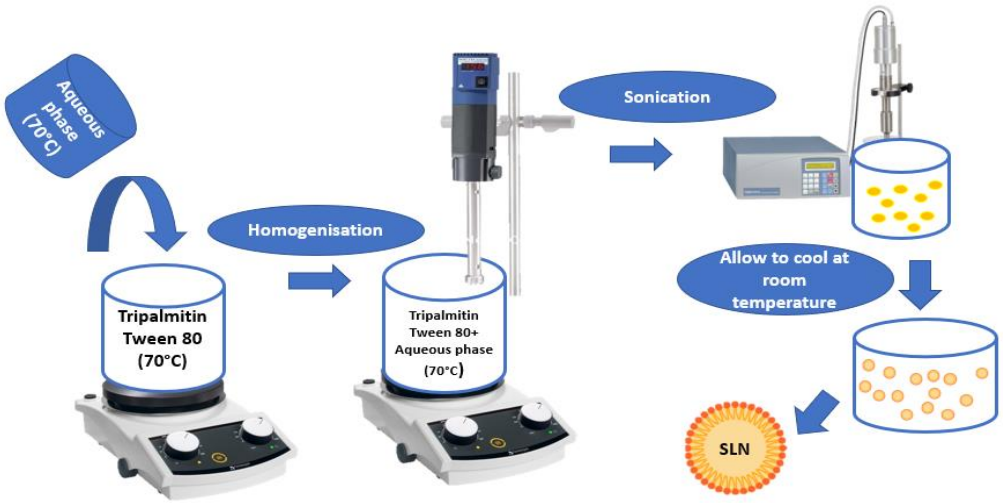

Figure 1. Preparation of SLNs

For brain targeting, SLNs were modified with Apo-E. The functionalization of nanoparticles with Apo-E was carried out as described our previous study (3). SLNs also labelled with Rhodamine B dye for cell culture studies.

Physicochemical Characterization of SLNs:

After preparation of SLNs, particle size, polydispersity index, zeta potential and encapsulation efficiency of SLNs were determined. The particle size and polydispersity index (PDI) of the SLNs were investigated by dynamic light scattering (DLS). For encapsulation efficiency, suspended nanoparticles were centrifuged at 4000 g, 20 min by Amicon Ultra-4 tubes and the amount of encapsulated Humanin was determined by spectrofluorometer at 480 nm excitation and 520 nm emission wavelengths. The results were shown in Table-1.

Table 1. Results for Humanin loaded SLNs

Parameter	Results for Humanin loaded SLNs	Results for Apo-E modified Humanin loaded SLNs
Particle size (nm±SD)	128,1 ± 1,48	167,5 ± 0,8
Polydispersity index (±SD)	0,28 ± 0,04	0,28 ± 0,02
Zeta potential (mV±SD)	-37,7 ± 1,07	-20,3 ± 0,64
Encapsulation efficiency (%±SD)	92,49 ± 0,01	99,99 ± 0,01

Cyctotoxicicity study was performed on SH-SY5Y cells with the modified SLNs by Apo-E for targetting. The effect of SLNs on the viability of SH-SY5Y human neuronal cells tested for 2 hours by MTT viability test. Afterwards, uptake studies also were investigated by modified and non-modified SLNs.

Results:

Humanin SLNs showed the particle sizes around 128 nm. Encapsulation efficiency for optimum formulation 92,49% and Apo-E modified SLNs showed 167,5 nm particle size. After 2 hour incubation Apo-E SLNs didn't show toxic effect on SH-SY5Y cells, all tested concentrations

were safe for neurons after 2 hours of incubation. Apo-E SLNs didn't show any toxic effect on SH-SY5Y cells (Figure-2). The uptake of Apo-E targeted Humanin SLNs was more than 2 times higher in comparison with non-modified SLNs after 2 hours of incubation. The functionalization of the SLNs resulted a significantly better uptake (Figure-3).

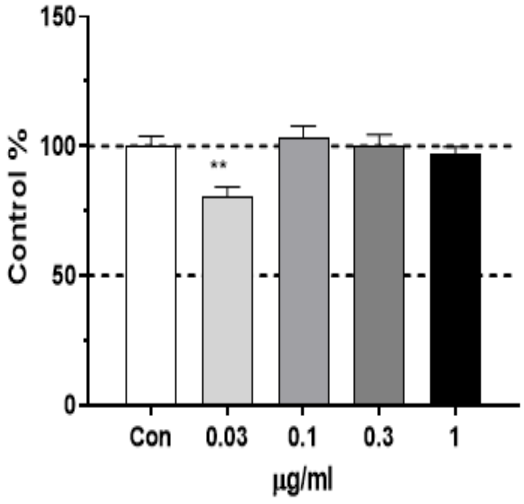

Figure 2. Toxicity of Apo-E Humanin SLNs labelled with Rhodamine B on SH-SY5Y neuroblastoma cells

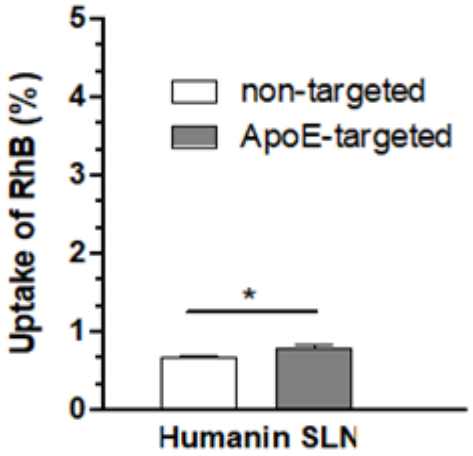

Figure 3. Uptake of SLNs in SH-SY5Y cells

Conclusions:

We achieved to obtain SLNs with a particle size of less than 200 nm which can cross BBB easier and high encapsulation efficiency. SLNs modified with Apo-E successfully and Apo-E SLNs increased the uptake in neurons according to non-modified SLNs. These results may contribute to develop more efficient drug delivery systems for the nervous system.

Acknowledgements

This study was supported by TUBITAK (SBAG-119S124; BİDEB-2214/2211 Scholarship Programs).

References:

1. Ahmed Nel M. et al., (2016). Stem Cells Int, 2016: 8102478.
2. Hashımoto Y. et al., (2001). Biochem Biophys Res Commun, 283(2): 460-468.
3. Topal G.R. et al., (2021). Pharmaceutics, 13(1):38.

OP023: CHEMOSENSITIVE EVALUATION OF METHOTREXATE LOADED NIOSOMES ON BURKITT LYMPHOMA CELLS

[1]Demirbolat, GM., [2]Ergul, M.

[1] Biruni University, Department of Pharmaceutical Technology, Istanbul, Turkey, gulenmelikedemir@gmail.com

[2] Sivas Cumhuriyet University, Department of Pharmacology, Sivas, Turkey, mergulmerve@gmail.com

Introduction:

Methotrexate (MTX), a folate antimetabolite, is one of the widely used therapeutic agents in high doses to treat many solid tumors including Burkitt lymphoma. However, higher doses of MTX lead to decreased bioavailability. It also has low water solubility, low permeability, and poor stability to pH changes (the suitable pH range: 6.5–8.2) (1,2).

Burkitt lymphoma (BL) is an extremely aggressive B-cell Non-Hodgkin's Lymphomas that occurs in adults and children (3). The treatment of BL characterized with rapid cellular growth and division covers intensive combined chemotherapy in order to prevent poor survival. Recently, treatment approaches aiming at decreasing toxicity while retaining efficacy have become prominent (4). In this study, we aimed to investigate *in vitro* anticancer activities of methotrexate loaded niosomes to make remarkable progress in the therapeutic scenario with the help of nanotechnology, which provides higher efficacy with lower doses of drugs.

Materials and Methods:

Methotrexate (MTX), Tween 80, Span 80, cholesterol, chloroform, cellulose acetate membrane, and phosphate buffer saline (PBS) tablets were purchased from Sigma-Aldrich (USA). Raji cell lines human was supplied from American Type Culture Collection (ATCC; USA). XTT (2,3-bis- (2-methoxy-4-nitro-5-sulfophenyl)-2H-tetrazolium- 5-carboxanilide) assay was obtained from Roche Diagnostic (Germany). All other reagents were of analytical grade.

Preparation of Niosomes

Methotrexate loaded niosomes were produced through the thin film method combined with sonication (5). Briefly, a certain amount (15 mM) of Span 80, Tween 80, and cholesterol in chloroform solution was introduced into a round-bottom flask. The solvent was evaporated at 60℃ with a rotation speed of 50 rpm under vacuum by a rotavapor (Buchi R-100, BUCHI Labortechnik AG, Flawil, Switzerland) for 2 h following overnight vacuum application. MTX (16 mg) dispersed in alkaline solution (A; pH:8), PBS (P; pH:7.4) or urea solution (U; pH 6.5) was added onto the lipid film, and then vortex mixing for 10 min and ultrasonic bath for 30 min were applied. The obtained niosome dispersion was used for further investigation.

Characterization of Niosomes

Niosomes were characterized in terms of particle size and distribution, and zeta potential using dynamic light scattering method (Litesizer 500; Anton Paar, Austria). For entrapment efficacy, 1 mL of the niosomes was put into a cellulose acetate membrane (12 kDa MWCO) and kept into 100 mL of medium for 24 h to separate unentrapped free drug. The concentration of unentrapped MTX was measured by UV spectrophotometer (UV-Pharmaspec6100, MAPADA

Instruments) at 304 nm. The amount of entrapped drug was obtained by subtracting amount of unentrapped drug from the total drug (6).

Chemosensitive evaluation

Raji cells (ATCC number CCL-86; Burkitt's Lymphoma) were seeded at a density of 10,000 cells/well in a 96-well culture plate. Cells were treated with a set of MTX samples (pure MTX solution and MTX loaded niosomes in a concentration range of 125 nM to 3.9 nM (dilution factor:2)) for 24 hours. After the incubation time, the medium was removed and wells were washed twice with 200 µL of PBS. For determination of living cells, 100 µL of Dulbecco's modified Eagle medium (DMEM) without phenol red and 50 µL XXT labeling mixture were added to each well and they were incubated for 4 h. The absorbance of XTT-formazan was measured using a microplate reader (Epoch, USA) at 450 nm. All experiments were triplicated. The percentage of cell viability was evaluated by comparison with control group (100% viability).

Results:

The particle size, polydispersity index, zeta potential and entrapment efficiency of MTX loaded niosomes were shown in Figure 1.

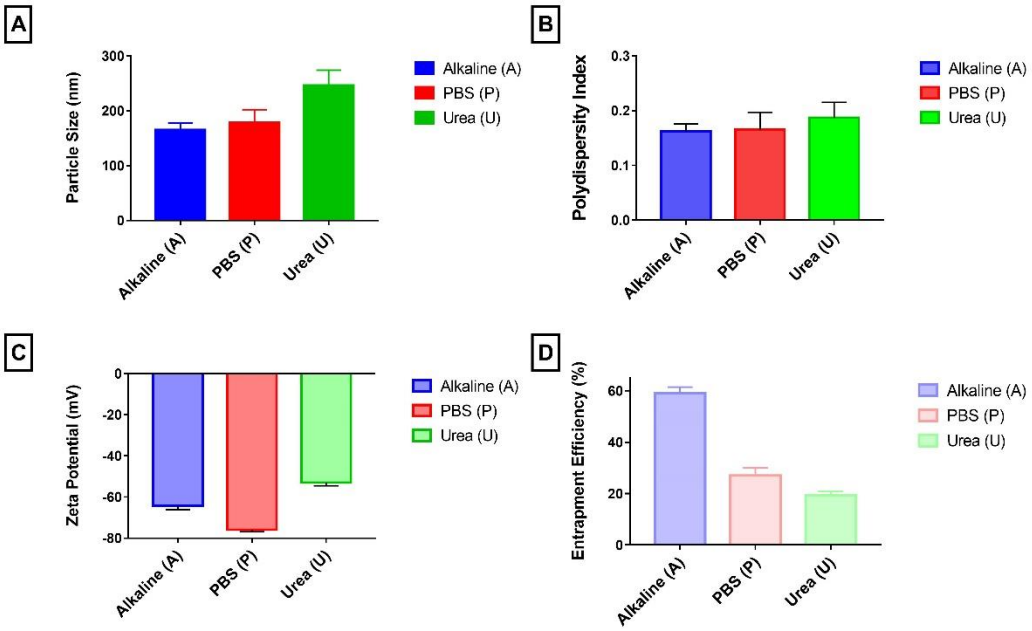

Figure 1. Physicochemical characterization of MTX loaded niosomes; A: particle size, B: polydispersity index, C: zeta potential, D: entrapment efficiency

Niosome formulations were successfully produced in nano-scale (Figure 1.A). As decreasing pH (from alkaline to urea), particle size increased. Polydispersity index was under 0.2 for all formulation (Figure 1.B). It stated that uniform dispersions were obtained. Dispersions with the zeta potential value of ±30 mV or higher are considered to be stable. To this aspect, all niosome formulations were stable (Figure 1.C). The optimum entrapment efficiency of MTX (58.9±2.5 %) was obtained with alkaline solution (Figure 1.D). When the pH decreased, entrapment efficiency also decreased. The solubilization of MTX might affect entrapment efficiency.

The cell viability values after cells exposure to pure MTX and MTX loaded niosomes were given in Figure 2.

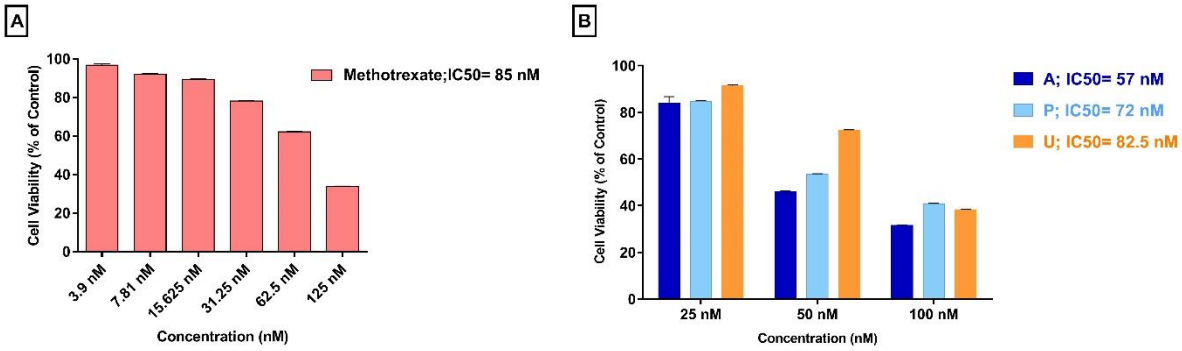

Figure 2. Cell viability and IC_{50} values of; A: pure MTX, B: MTX loaded niosomes

The chemosensitivity of cells to pure MTX was concentration dependent with 85 nM of IC_{50} value (Figure 2.A). The IC_{50} values of niosomes of alkaline solution, phosphate buffer solution, and urea solution were 57 nM, 72 nM, and 82.5 nM, respectively (Figure 2.B). The use of niosomes decreased IC_{50} values of MTX. Niosomes significantly increased the cytotoxic activity of the anticancer agent on the Burkitt Lymphoma cell line. Moreover, alkaline solution boosted their chemosensitivity.

Conclusions:

Developed niosomal formulations were found more effective than pure MTX on cell death in Burkitt lymphoma. In the present study, MTX loaded niosomes using alkaline solution substantially enhanced the chemosensitivity. These promising results might guide to develop an ideal MTX loaded nano-formulation to treat aggressive Burkitt lymphoma.

Acknowledgements

This research did not receive any specific grant from funding agencies.

References:

1. Khan ZA, Tripathi R, Mishra B (2012). Methotrexate: a detailed review on drug delivery and clinical aspects. Expert Opin Drug Deliv, 9(2):151–69.
2. Kapoor K, Nagaıch U (2020). Development And Characterızatıon Of Sustaıned Release Methotrexate Loaded Cubosomes For Topıcal Delıvery In Rheumatoıd Arthrıtıs. Int J Appl Pharm, 33–9.
3. Thomas DA, O'Brien S, Faderl S, Manning Jr JT, Romaguera J, Fayad L, et al. (2011). Burkitt lymphoma and atypical Burkitt or Burkitt-like lymphoma: should these be treated as different diseases? Curr Hematol Malig Rep [Internet], 6(1):58–66. Available from: https://pubmed.ncbi.nlm.nih.gov/21191675
4. Zayac AS, Olszewski AJ (2020). Burkitt lymphoma: bridging the gap between advances in molecular biology and therapy. Leuk Lymphoma [Internet], 61(8):1784–96. Available from: https://doi.org/10.1080/10428194.2020.1747068
5. Bayindir ZS, Yuksel N (2010). Characterization of niosomes prepared with various nonionic surfactants for paclitaxel oral delivery. J Pharm Sci, 99(4):2049–60.
6. Demirbolat GM, Aktas E, Coskun GP, Erdogan O, Cevik O (2021). New Approach to Formulate Methotrexate-Loaded Niosomes: In Vitro Characterization and Cellular Effectiveness. J Pharm Innov [Internet], Available from: https://doi.org/10.1007/s12247-021-09539-4.

OP024: DESIGN AND EVALUATION OF SEMI-SOLID LIPID NANOPARTICLES AS NOVEL NANOCOSMECEUTICALS

Amasya, G.

Ankara University, Faculty of pharmacy, Department of Pharmaceutical Technology, Ankara, Turkey, gamasya@pharmacy.ankara.edu.tr

Introduction:

Nanotechnology is the crucial factor to design and produce next-generation cosmetics. While nanotechnology provides a solution for the active ingredients, it also increases the effectiveness and performance of the product. Nano-cosmeceuticals, which are the hybrid formulations between pharmaceuticals and cosmetics, are produced by transferring nano-drug delivery systems to cosmetics (1). When the cosmetic application of nanomaterials is considered, semi-solid lipid nanoparticles (Semi-solid LNs) are fairly new systems and they exhibit many advantages over other nano-carriers. Semi-solid LNs can be easily produced using only water, physiological lipid and surfactant and they contain a high percentage of solid lipid, unlike SLN&NLC. From the point of the cosmetic industry, the single-step production method of semi-solid LNs allows obtaining low costs products in a short time and the product can be applied directly to the skin without any further process. Because viscoelastic semi-solid structure can be obtained as well as the colloidal size can be protected (2). Conversely, typical SLN&NLC are obtained as an aqueous dispersion due to their production techniques and the second system to carry nanoparticles is necessary both for ease of application and to obtain attractive products for the consumer. On the other hand, semi-solid NLCs contain liquid lipid in their structure and this structural feature of NLC systems can be turned into cosmetic advantages when valuable vegetable oils are used as structural components.

Skin aging is a complex biological process and can be defined as all changes that occur in the normal functions and structure of the skin due to natural or environmental factors. Antioxidants protect the skin by limiting free radical production, which can damage the skin cells. Alpha-lipoic acid (ALA) is one of the strongest and versatile antioxidants and it is an extraordinary radical scavenger. ALA is also recognized to revitalize other antioxidants from their inactive forms. But the major drawback of ALA is that the acid is extremely vulnerable to degradation by the sunlight and is characterized by an unpleasant sulphur smell.

The purpose of this study is to design ALA-loaded novel semi-solid NLC formulations for skin aging and to investigate the contribution of different vegetable oils that can be used as structural units of semi-solid NLCs.

Materials and Methods:

Semi-solid LNs were prepared by the hot homogenization method. Solid lipid - vegetable oil mixture was used to construct the lipid nanoparticles in NLC form and semi-solid structure as well. At first, ALA-loaded main semi-solid SLN formulation was formed using a binary mixture of Precirol® ATO 5 and Stearic acid (Ss-SLN). Then, this initial formulation was modified by adding cosmetically valuable vegetable oils or Myglyol 812® as synthetic liquid lipid to form semi-solid NLC formulations. The composition of semi-solid LNs was given in Table 1. The particle characteristics, including average particle size and size distribution were analyzed by

the technique of Dynamic Light Scattering. The textural properties of semi-solid LNs were investigated by a software-controlled TA.XT Plus Texture Analyzer. *In vitro* and *ex vivo* occlusion tests were carried out to examine the effect of natural vegetable oils on skin hydration. Besides, *ex vivo* skin permeation test was performed to check out the contribution of vegetable oils to dermal uptake of the active molecule. Franz diffusion cells and rat skin sections were used to examine *ex vivo* skin permeation of ALA. All animal experiment was approved by Local Animal Ethics Committee of Ankara University (Approval no: 2019-10-98).

Table 1. Formulation parameters of semi-solid LNs

%	Ss-SLN	Ss-NLC(1)	Ss-NLC(2)	Ss-NLC(3)	Ss-NLC(4)	Ss-NLC(5)
STEARIC ACID	15	7.5	0	0	0	0
PRECIROL® ATO 5	15	7.5	7.5	0	0	0
AVOCADO OIL	0	15	7.5	7.5	0	0
COCONUT OIL	0	0	15	7.5	7.5	0
OLIVE OIL	0	0	0	15	7.5	7.5
ARGAN OIL	0	0	0	0	15	7.5
MYGLYOL812®	0	0	0	0	0	15

Results:

All in vitro characterization results of semi-solid LNs were presented in Table 2. Semi-solid SLN formulation (Ss-SLN) was successfully produced with the average particle size of 265 nm while the PDI value was found smaller than 0.2. Interestingly, when different vegetable oils were added to the formulation, regardless of the lipid type, a decrease in the average particle size was obtained, and an increase was observed in the PDI values. On the other hand, while the zeta potential value of Ss-SLN was measured -23 mV, the addition of liquid lipid resulted in an enhancement in zeta potential. Another important feature of semi-solids is the textural properties for estimating real-life usage and also customers' acceptability. The textural parameters, hardness and cohesiveness of formulations were defined using the force-time graphs obtained by TPA analysis. A lower hardness value is desired in order to remove the semi-solid product from the container and to spread it to the skin surface easily. Cohesiveness gives information about the reconstruction ability and the extent of structural reformation after application of a semi-solid and it has been reported that the semi-solid having a higher cohesiveness value can maintain its physical gel structure for a long time following the application. It can be stated that the presence of liquid lipids contributed positively to textural properties from the point of product performance and consumer compliance. Lipid nanoparticles form an adhesive lipid film layer on the skin surface after application and an increase in occlusive effect is provided by means of the lipid film layer. Thus, the water content of the stratum corneum is increased, TEWL is reduced, and an increase in skin hydration can be achieved. On the other hand, with increased skin hydration, it may be easier for the active molecules to reach the deep skin tissue. Herein, in vitro and ex vivo occlusion tests were performed to investigate the contribution of vegetable oils from different sources to the occlusive effect of semi-solid LNs. According to test results, the occlusion factor of semisolid NLC formulation with avocado and argan oil reached a higher occlusivity after 8h in both in vitro and ex vivo tests and confirming no significant difference with Ss-SLN. Besides, the formulation containing synthetic lipid Myglyol 812® showed the lowest occlusive properties. It can be also claimed that in vitro occlusion test results were correlated with ex vivo results and both methods were capable of simulating skin hydration. Dermal uptake of ALA was measured

by extraction of skin samples with methanol and the amount of ALA penetrated into the skin was measured by HPLC. Ex vivo permeation studies showed that the presence of avocado oil significantly enhanced the accumulation of ALA into the skin. While 93.5 ± 1.3 µg/cm2 of ALA was accumulated into the skin upon 8h with the presence of avocado oil; the percentage of ALA was measured below 60% with formulations containing other vegetable oils and Ss-SLN. The lowest dermal accumulation was obtained in the presence of Myglyol 812®.

Table 2. In vitro characterization results of semisolid lipid nanoparticle formulations

	Particle size (nm)±SD	**PDI±SD**	**Zeta Potential (mV)±SD**	**Hardness (n)±SD**	**Cohesiveness**
Ss-SLN	265.0±1.212	0.189±0.012	-22.7±0.337	1.447±0.07	0.77±0.05
Ss-NLC(1)	229.1±1.250	0.248±0.006	-36.3±0.568	0.320±0.001	0.90±0.02
Ss-NLC(2)	234.6±0.566	0.236±0.009	-36.1±0.794	0.067±0.005	1.03±0.01
Ss-NLC(3)	228.6±2.601	0.279±0.992	-33.1±0.153	0.108±0.005	0.95±0.01
Ss-NLC(4)	245.7±0.757	0.217±0.001	-33.8±0.757	0.169±0.006	0.98±0.02
Ss-NLC(5)	213.6±2.401	0.215±0.08	-32.0±0.568	0.068±0.009	1.04±0.06

Conclusions:

Herein, the advantages of lipid nanoparticles and vegetable oils were successfully combined in the semi-solid LN structure to achieve a synergistic effect on skin hydration and the antiaging effect while the colloidal size and semi-solid consistency were maintained. It can be stated that avocado oil is the most effective vegetable oil to improve skin hydration as well as the skin penetration of active molecules. In conclusion; using vegetable oil to construct semi-solid lipid nanoparticles; is a promising technique for nano-cosmeceuticals due to the ability to target active molecule as well as essential fatty acids into the cells with NLC structure and novel semi-solid lipid nanoparticle formulations were developed as a promising candidate of nano-cosmeceuticals.

References:

1. Kilgman AM. (2005). In: Elsner P, Maibach H, (Eds.) Cosmeceuticals and Active Cosmetics. CRS press Tylor and Francis Group, pp. 1-9.
2. Tarimci N, et al., (2015). A novel approach for topical delivery of SLNs: Semisolid SLNs. Lap Lambert Academic Publishing.

OP025: ROBUST FORMULATION DESIGN USING COMPACTION SIMULATOR AND QBD APPROACH

[1]Özalp, Y., **[1]Khamis, H.**, [1]Jiwa, N., [2]Mesut, B., [3]Aksu, B.

[1] Near East University, Faculty of Pharmacy, Department of Pharmaceutical Technology, Nicosia, KKTC, yildiz.ozalp@neu.edu.tr, hala_khamees@yahoo.com, nailla.jiwa@neu.edu.tr

[2] İstanbul University, Faculty of Pharmacy, Department of Pharmaceutical Technology, Istanbul, Turkey, burcumesut07@windwslive.com

[3] Altinbas University, Faculty of Pharmacy, Department of Pharmaceutical Technology, Istanbul, Turkey, buket.aksu@altinbas.edu.tr

Introduction:

Application of Quality by Design (QbD) approach was used to obtain an optimum formulation and design space. This approach allows formulators to optimize formulations and enhance the product development with built in product quality. The aim was to design optimum compact formulation for Nimesulid using compaction simulator and a QbD approach.

Materials and Methods:

Preformulation studies, solubility study, powder consolidation properties were carried out to charactarize powders used in the formulation. Compressibility parameters were evaluated by compaction simulator Styl'cam 200R (Medelpharm). Binder and disintegrants were selected as key components for poorly soluble Nimesulide. Formulations were produced by direct compression method using 11.28 mm punch. Quality control test results were used as inputs for QbD analysis using MODDE software to obtain a design space.

Results:

Tensile strength values give insight into powder compressiblity which assists in production of a robust formulation. Addition of superdisintegrant (Figure1) affects tensile strength values, hence has limitations during tablet formulation and design.

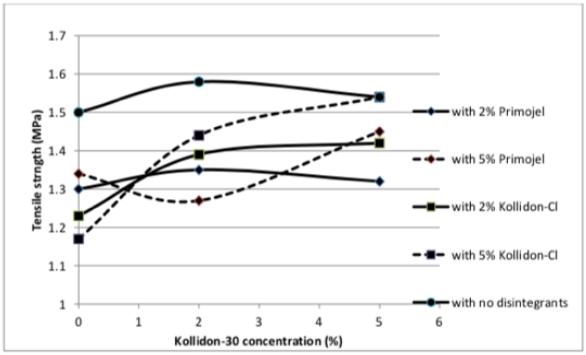

Figure 1. Effect of key excipients on tensile strength at 10kN force

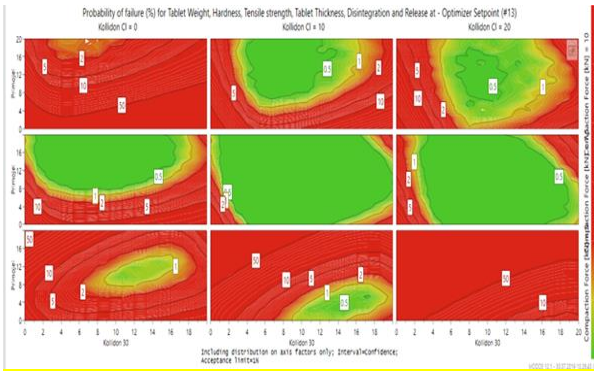

Figure 2. Design space for combination formulations

Figure 2 shows results of QbD analysis, a design space was obtained for all parameters and excipients using QbD analysis. The green zone shows area containing the most robust formulations.

Conclusions:

Compaction simulators are benificial to test the functionality and performance of excipients as well as characterise tabletting properties of powders. They assist in development of robust formulations for industrial production by evaluation of compaction properties. It can be concluded that, characterizing excipients behaviour in the formulation was critical for robust formulation development. Less number of formulation will be use for the quality control tests to optimize the final formulation. QbD can be used to obtain a design space by optimizing excipients and process parameters in order to obtain a robust formulation.

References:

1. Khamis, H. (2019). QbD approach formulation design for poorly soluble drug Nimesulid and evaluations. (Master's Thesis).
2. Aksu, B., & Mesut, B. (2015). Quality by design (QbD) for pharmaceutical area. İstanbul Üniversitesi Eczacılık Fakültesi Dergisi, 45(2), 233-251.
3. Shang, C., Sinka, I. C., Jayaraman, B., & Pan, J. (2013). Break force and tensile strength relationships for curved faced tablets subject to diametrical compression. International journal of pharmaceutics, 442(1-2), 57-64,9.

OP029: PREPARATION OF SILK FIBROIN NANOPARTICLES FROM BOMBYX MORI COCOONS BY DOE APPROACH

Birer, M., Yıldız, A., Acartürk, F.

Gazi University, Department of Pharmaceutical Technology, Ankara, Turkey

Introduction:

Silk fibroin is a natural, protein-based biopolymer produced by silkworm (*Bombyx mori*) and is obtained from silkworm cocoons. It has beneficial features such as biocompatibility, biodegradability, high mechanical resistance, low cost, easy availability, low immunogenicity, and inflammatory response. Silk fibroin nanoparticles attract attention for drug delivery due to their high binding capacity for drugs, controlled drug release properties, and easy preparation. They have also great potential for tissue engineering studies because of their superior mechanical properties and low immunogenicity (1).

Nanoprecipitation refers to a quite simple processing method for the fabrication of polymeric nanoparticles. Generally, the method describes the precipitation of a dissolved material as a nanoscale particle after exposure to a non-solvent that is miscible with the solvent (2).

The aims of the study are performing the silk fibroin extraction and quantification process; preparation of silk fibroin nanoparticles by nanoprecipitation method; investigation of the effects of different stabilizing agents and their concentrations on particle size, and polydispersity index (PDI); optimization of the production method by using a DOE approach.

Materials and Methods:

Silk fibroin was obtained with the Ajisawa method (3) from bombyx mori cocoons, characterized with FT-IR, DSC analyses, and quantified with the Bradford method (4). Kollidon VA64, Poloxamer 188, and Tween 80 were used as stabilizing agents in the nanoprecipitation step at various concentrations. All other reagents and solvents were analytical grade.

Silk fibroin was prepared by the following steps: The beaker containing 1 liter of 0.212 % (w/v) sodium carbonate solution was covered with aluminum foil and left to boil. A part of 2.5 grams of the cocoons was cut into small pieces and added to the boiling solution, after 30 minutes' cocoons were collected and washed with distilled water until sodium carbonate-free cocoons were obtained. Then silk fibers were left to dry at room temperature. Dried silk fibroin was dissolved in $CaCl_2$:ethanol:water at a molar ratio of 1:2:8. The material was dialyzed for 48 hours with the dialysis bag method. After the dialysis step, the silk fibroin solution was filtered with a 0.45 µm membrane filter and then used for the preparation of silk fibroin nanoparticles.

Silk fibroin nanoparticles were obtained by the nanoprecipitation method. Three different stabilizing agents (Tween 80, Kollidon VA64, and Poloxamer 188) at three different concentrations (7.5, 10, 15%) were used for the preparation of nanoparticles. Silk fibroin concentration remained constant at 0.05% and 10 ml of acetone was used as nonsolvent. Acetone stirred at 700 rpm on a magnetic stirrer. An aliquot of 2 ml of silk fibroin solution was added dropwise into the acetone by an automated pump at a 3 ml/h flow rate. After the precipitation of silk fibroin nanoparticles, acetone was removed by rotavapor. Particle diameter and PDI measured by Malvern Zetasizer. Afterward, Tween 80 was chosen as the stabilizing

agent and the process was optimized using a central composite design. For this purpose, two factors (Silk fibroin and Tween 80 concentrations) were used as variables at 3 different concentrations. Concentrations of silk fibroin and Tween 80 were 0.05, 0.1, 0.15, and 7.5, 10, 15 respectively. All other parameters remained constant. Effect of the silk fibroin and Tween 80 concentration on the particle size and PDI was evaluated by experimental design

Results:

Characteristic peaks of silk fibroin were observed in the DSC thermogram at 71 and 296 °C. FT-IR also proved that silk fibroin was purified successfully and all characteristic peaks of silk fibroin were observed in FT-IR spectra as 1620 cm^{-1}-amide I (C=O), 1513 cm^{-1} amide II (N-H), 1230 ve 1444 cm^{-1} amide III (C-N), 694 cm^{-1} amid IV without any impurities.

PDI and particle size results of the nanoparticles are given in Table 1. According to the results Tween 80 was selected as the stabilizing agent and the effect of the SF and Tween 80 concentration on the particle size and polydispersity index (PDI) was evaluated by experimental design. Results of the experimental design are given in Figure 1. According to the experimental design results, it was observed that as the concentration of polymer and stabilizing agent decreased, the PDI and particle size decreased.

Table 1. Effect of stabilizer type and concentration on the particle size and PDI (n=3, mean± standard deviation

Stabilizing agent	Kollidon VA64			Poloxamer 188			Tween 80		
Concentration	**7,5%**	**10%**	**15%**	**7,5%**	**10%**	**15%**	**7,5%**	**10%**	**15%**
Particle size (nm)	1655± 209	434± 42	699± 24	1290± 321	287± 36	1493± 912	966± 121	300± 15	620± 107
PDI	0.730± 0.137	0.328± 0.043	0.217± 0.035	0.602± 0.155	0,321±0. 092	0.525± 0.260	0.841± 0.095	0.152± 0.067	0.344± 0.103

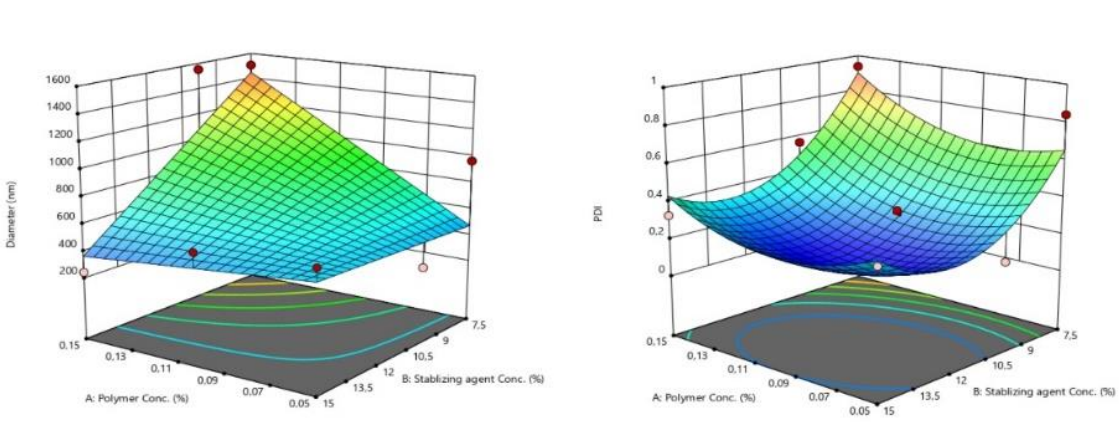

Figure 1. Effect of Tween 80 and SF concentration on the diameter of nanoparticles and PDI

Results showed that the best PDI can be obtained at 0.1% silk fibroin and 12% Tween 80 concentration**.** The smallest particles can be obtained at 0.05% silk fibroin concentration

regardless of Tween 80 concentration. If Tween 80 was used at 15% concentration small particles also can be obtained at 0.1 and 0.15% silk fibroin concentrations.

Conclusions:

Tween 80, Kollidon VA64, and Poloxamer 188 are suitable stabilizing agents for silk fibroin nanoparticle production. Kollidon VA64 was used as a stabilizing agent in the nanoprecipitation method for the first time. Tween 80 was found as the best stabilizing agent among others. The silk fibroin nanoparticle production process can be optimized with the DoE approach.

Acknowledgment

Ayşegül YILDIZ was supported by a scholarship from The Scientific and Technological Research Council of Turkey (TUBITAK) 2211-C National Ph.D. Scholarship Program in the Priority Fields in Science and Technology.

References:

1. Vepari, C., Kaplan, D. L. (2007) Silk as a biomaterial, Progress in Polymer Science (Oxford). 32 991–1007.
2. Schubert, S., Delaney Jr, J. T., & Schubert, U. S. (2011). Nanoprecipitation and nanoformulation of polymers: from history to powerful possibilities beyond poly (lactic acid). Soft Matter, 7(5), 1581-1588.
3. Ajisawa, A. (1997) Dissolution aqueous of silk fibroin with calciumchloride / ethanol solution, The Journal of Sericultural Science of Japan. 67 91–94.
4. Bradford M.M, (1976) A rapid and sensitive method for the quantitation of microgram quantities of protein utilizing the principle of protein-dye binding, Analytical Biochemistry.

OP032: 99mTc-LABELED, COLISTIN ENCAPSULATED, THERANOSTIC LIPOSOMES

[1]Karpuz, M., [2]Ozgenc, E., [2]Atlihan-Gundogdu, E., [3]Senyigit Z.

[1] Izmir Katip Celebi University, Department of Radiopharmacy, Izmir, Turkey

[2] Ege University, Department of Radiopharmacy, Izmir, Turkey

[3] Izmir Katip Celebi University, Department of Pharmaceutical Technology, Izmir, Turkey

Introduction:

Infection represents important burdens for healthy systems all around the world, if not diagnosed in time. The incidence of infection deaths is increasing day by day. The early detection and effective treatment of infection plays an important role to avoid the progression of disease and development of drug resistance (1). Therefore, novel approaches regarding drug delivery systems and conventional antibiotics have been performed to distinguish infection cases from other pathological conditions by more accurate images in diagnosis, decrease the microbial resistance, and increase the uptake of antibiotics in the infected tissue. To that end, in our study, cationic and neutral, colistimethate sodium (CMS) encapsulated, liposomes were prepared, characterized, and radiolabelled with ^{99m}Tc to develop more specific and effective theranostic (therapeutic and diagnostic) agent for infection. Not only the liposome formulations were radiolabelled with Tc^{99m} for SPECT/CT, but also therapy was aimed with CMS encapsulation.

Materials and Methods:

All reagents were of analytical or higher grade and obtained from commercial sources except CMS. Liposomes were prepared by the film-hydration method as given in Figure 1 (2). The lipid phase (40 $mmol.L^{-1}$) of Lipo and Cat-Lipo formulations were prepared by PC:Chol:SA mixtures at molar ratios of 8:2:0 and 7:2:1, respectively. CMS, at a drug-to-lipid mass ratio of 1:8, was added to the PBS (pH 7.4) as the hydration medium in formulations. In characterization studies, the mean particle size, polydispersity index, and zeta potential of liposomes were evaluated with Malvern Zetasizer. After the determination of encapsulation efficiency by electrochemical analysis, the release behaviour of CMS from liposomes was studied by dialysis method. Liposomes were radiolabelled with ^{99m}Tc by tin-reduction method, and the different amounts of $SnCl_2$ were tested to detect the optimum radiolabelling conditions (3). The radiochemical purity of radiolabelled liposome formulations was assessed by thin-layer chromatography at different time intervals for 6 h.

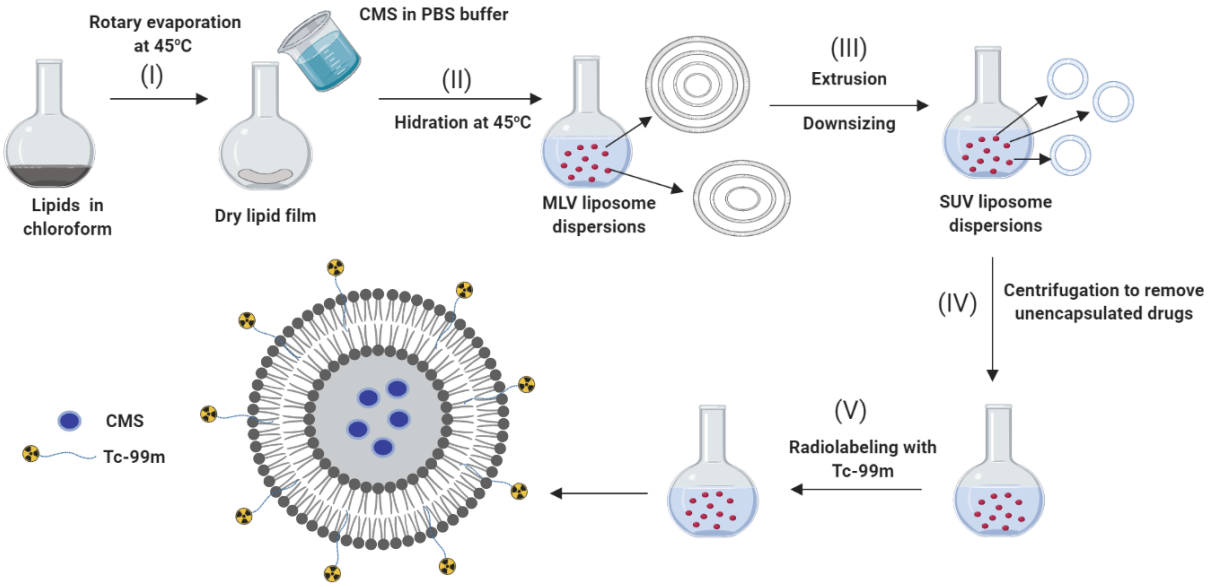

Figure 1. Schematic representation of CMS encapsulated liposomes

Results:

The characterization properties of all liposome formulations are given in Table 1. Particle sizes of all liposome formulations were found between 173 and 217 nm. As expected, the particle sizes of CMS encapsulated formulations were found to be higher than empty liposomes due to their drug content. Thus, the particle sizes of all liposomal formulations were found to be proper to remain longer in blood circulation for targeting infection. The zeta potentials of liposomal formulations were found between −6.5 mV and 2.8 mV. The addition of cationic lipid to lipid content increased the zeta potential. The EE% of CMS in neutral and cationic liposomes were calculated as 70 and 77. CMS was released from cationic and neutral liposomes at the end of 8 and 10 h, respectively. The liposomal formulations were labelled with high efficiency. According to the Figure 2, the radiochemical purity of liposomes was found higher than 90% at different time intervals, and no statistical difference were observed depending on reducing agent amount.

Table 1. Results of characterization studies

Liposome Formulations	Mean Particle Size (nm) ± SD	PDI	Zeta Potential (mV) ± SD	Encapsulation efficiency (%)
Lipo	181 ± 0.9	0.13	-6.5 ± 1.38	-
Lipo/CMS	217 ± 5.0	0.50	-3.3 ± 0.25	70 ± 2.6
Cat-Lipo	173 ± 3.2	0.22	-1.8 ± 0.14	-
Cat-Lipo/CMS	207 ± 5.8	0.47	2.8 ± 0.32	77 ± 2.4

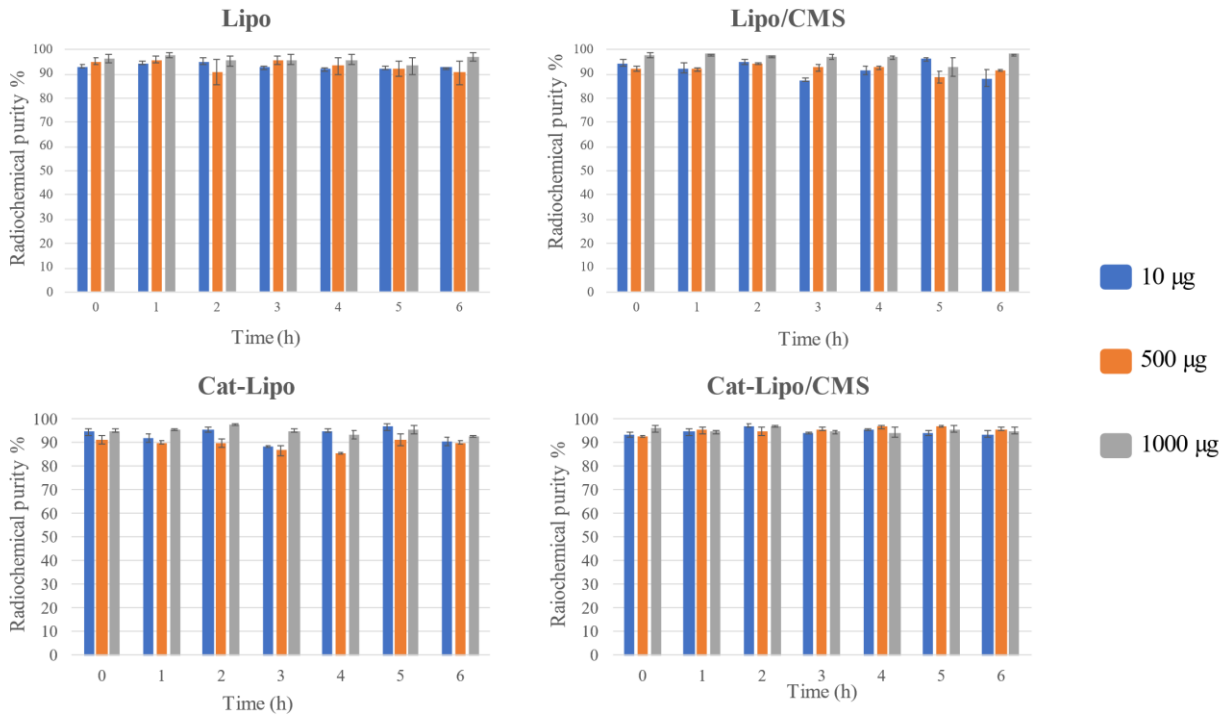

Figure 2. The effect of stannous chloride's amount on the radiolabelling efficiency of liposome formulations *(n=3)*

Conclusions:

By the result of characterization, in vitro drug release, and radiolabelling studies, nanosized, CMS encapsulated liposome formulation was found to be a promising carrier system for the imaging and treatment of infection.

Acknowledgements

The authors would like to thank Polifarma for the generous gift of CMS, and this study was supported by the grant of Izmir Katip Celebi University Scientific Research Projects Coordination Unit, Project No: 2019-GAP-ECZF-0005.

References:

1. Van Giau et al., (2019). Drug Design Development and Therapy, 13:327-343.
2. Bangham et al., (1965). Journal of Molecular Biology, 13:238-252.
3. Saha GB (1979). Fundamentals of Nuclear Pharmacy. Springer, New York, pp 79-94.

OP033: DEVELOPMENT OF PLGA NANOPARTICLES TO PROMOTE ALVEOLAR BONE REGENERATION

[1,2] Ilhan, M., [1]Kilicarslan, M., [3]Alcigir, M.E., [4]Bagis, N., [5]Ekim, O., [6]Orhan, K.

[1] Ankara University, Department of Pharmaceutical Technology, Ankara, Turkey

[2] Izmir Katip Celebi University, Department of Pharmaceutical Technology, Izmir, Turkey

[3] Kirikkale University, Department of Pathology, Kirikkale, Turkey

[4] Ankara University, Department of Periodontology, Ankara, Turkey

[5] Ankara University, Department of Division of Basic Sciences, Ankara, Turkey

[6] Ankara University, Department of Dentomaxillofacial Radiology, Ankara, Turkey

Introduction:

Regenerative treatment usually requires bone grafting. However, grafts are associated with the risk of numerous complications that limit their clinical applications, such as donor site complications, infection, and immune problems (1). For this purpose, it is recommended to modulate the host response with the use of antimicrobials or anti-inflammatories in treatments with regenerative growth factors in dentistry (2,3).

The aim of this study was to prepare and *in vitro* - *in vivo* evaluation of bone morphogenetic protein (BMP) and clindamycin phosphate (CDP) loaded polymeric nanoparticles to accelerate hard tissue regeneration during the dental regenerative process. For this reason, BMP-7, an FDA-approved osteoinductive active pharmaceutical ingredient, was used in the formulations. In addition, disadvantages such as the side effects of BMP at high doses and the difficulty of administration could be eliminated with the poly lactide-co-glycolic acid (PLGA) nanoparticle formulations. Furthermore, a broad-spectrum bacteriostatic CDP used for support the treatment due to its good bone penetration.

Materials and Methods:

BMP-7 was purchased from PeproTech (UK). CDP was a kind gift from Deva (Turkey). PLGA (50:50) (Mw = 24 - 38 kDa), bovine serum albumin (BSA), poly vinyl alcohol (PVA) (Mw = 31 kDa), and enzyme linked immunosorbent assay (ELISA) kit were purchased from Sigma-Aldrich (USA). Bicinchoninic acid protein assay (BCA) kit was purchased from Thermo Fisher Scientific (USA). Dichloromethane was purchased from Lab-Scan (Ireland). Rond burs were purchased from Addent (USA). Decalcification solution (Osteodec), eosin and hematoxylin were purchased from Bio-Optica (Italy).

Preparation of Nanoparticles

PLGA nanoparticles (100 mg) loaded only BMP (4 µg) (F1) or combined with CDP (20 mg) (F2) were prepared by emulsifying and solvent evaporation technique. BSA was used as a model drug for *in vitro* release studies instead of BMP. Briefly, CDP and BMP or BSA was dissolved in 1 mL of distilled water and this solution was used as an internal aqueous phase. The oil phase prepared by dissolving PLGA in 1 mL of dichloromethane. The primary emulsion

was prepared by a probe sonicator (Bandelin, Germany) at 38 % amplitude for 60 s. The primary emulsion was dispersed in 20 mL of 0.3 % PVA solution (external aqueous phase) using a homogenizer at 8500 rpm for 5 min (IKA T25, Germany) to prepare water/oil/water emulsion. Afterwards, the organic solvent was evaporated using magnetic stirrer at 500 rpm at room temperature for 3 h. The suspension was centrifuged at 20000 rpm (Sigma 3-30 KS, Germany) and recovered nanoparticles were lyophilized overnight (Christ Gamma 2-15 LSC, Germany).

Characterization of Nanoparticles

Nanoparticles were characterized by particle size, zeta potential (ZP), encapsulation efficiency (EE) and *in vitro* drug release profiles. Particle size and polydispersity index measured by the dynamic light scattering (Malvern Instruments, UK). EE of clindamycin phosphate, BMP and BSA was determined by high performance liquid chromatography (HPLC), ELISA kit and BCA kit, respectively. Nanoparticles containing 20 ng BSA were dispersed in 1 mL phosphate buffer solution (pH 6.75). After that, the suspension was incubated in a horizontal shaker at 37 °C at 75 rpm. The suspension was centrifuged at 5000 rpm for 15 minutes. The supernatant was collected at predetermined time intervals and the same volume of fresh medium was supplemented. The samples were analyzed by HPLC and BCA kit. All analysis performed in triplicate.

***In vivo* Studies**

Animal experiment protocol was approved by Ankara University Animal Experimentation Ethics Committee (Approval No: 2016-14-146). Regeneration of the bone was evaluated *in vivo* at defected mandibular ramus of Wistar albino rats. Briefly, defect was created in mandible using rond burs. Nanoparticles were implanted into the defect directly. At the proper time intervals (14^{th}, 28^{th} and 42^{nd} days) defected mandibles were analyzed visually and quantitatively by micro-computed tomography (micro-CT). Also, the micro-CT data were compared with histopathological results at mandibular bone tissue.

Results:

The mean particle sizes were between 449.6 ± 19.23 nm (F1-BSA) and 790.9 ± 24.84 nm (F2-BSA). In addition, size distribution was acceptable for all formulations (PDI<0.7). The ZP values were between -18.87 ± 0.87 mV (F1-BSA) and -28.07 ± 0.25 mV (F1). It was observed that the EE (%) values of BMP (F1: 64.15 $\pm$ 5.49 and F2: 68.37 $\pm$ 8.06) and BSA (F1-BSA: 60.17 $\pm$ 11.47 and F2-BSA: 68.23 $\pm$ 13.98) were significantly higher than that of CDP (F2: 42.48 $\pm$ 0.57 and F2-BSA: 44.78 $\pm$ 0.94). Besides, extended release was achieved for up to 3 months in all formulations, and it was observed that CDP was accelerated BSA release (Figure 1.a). As a result of Micro CT quantitative analyses, the least new bone formation and connectivity was observed in the control group at the end of the 2^{nd} week. This showed that bone regeneration started effectively in the treatment groups compared to the control group. In the first two weeks, the highest bone formation was observed with the F2 formulation containing CDP and BMP together (Figure 1.b). Histopathological evaluations were found to be consistent with the results obtained by micro-CT, and it was determined that significant ossification was obtained even after 2 weeks with the F1 and F2 formulations compared to the control group (Figure 1.c).

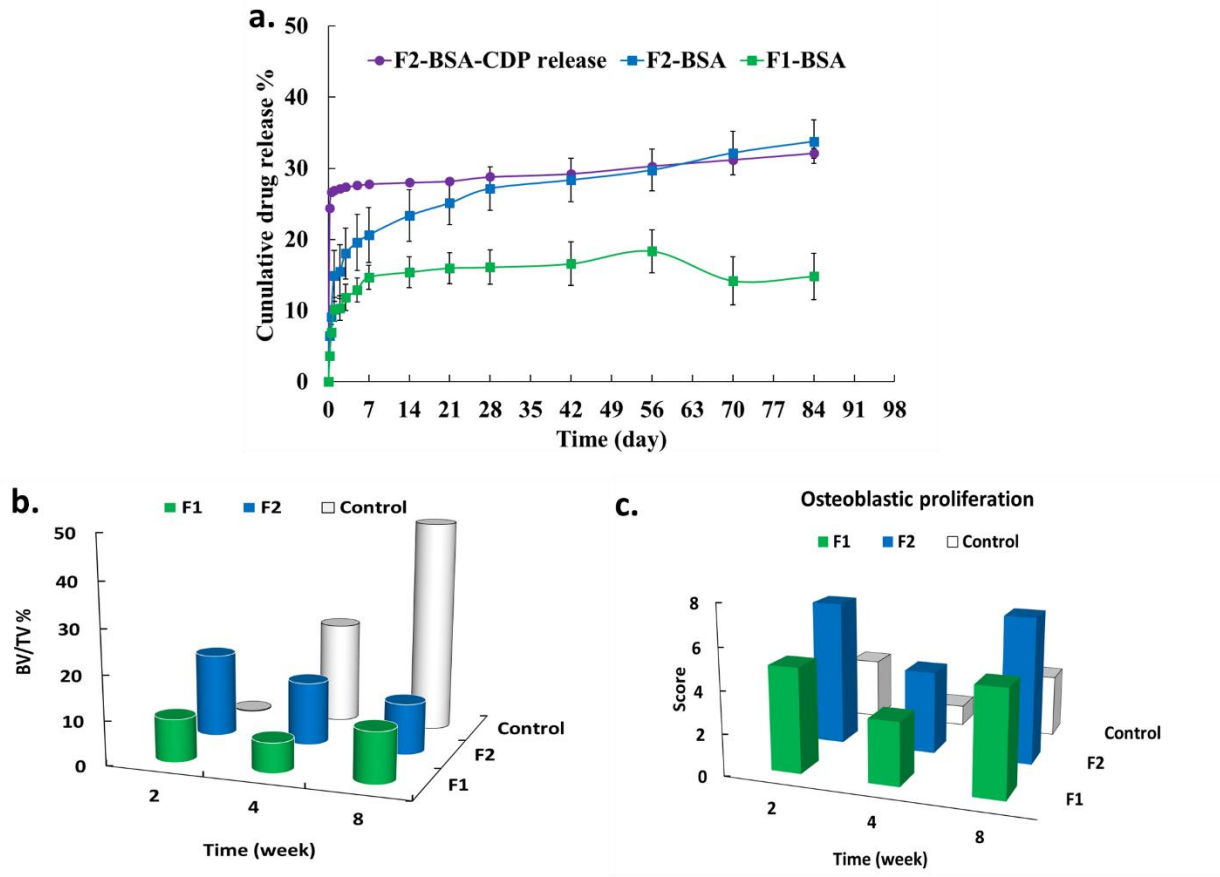

Figure 1. *In vitro* release of BSA and CDP **(a)** and micro-CT **(b)** and histopathological **(c)** evaluations of nanoparticles

Conclusions:

Through *in vitro* assays, sustained release was achieved for more than two months and following *in vivo* experiments, conducted micro-CT and histopathological analysis indicated that the BMP-CDP combination (F2) at a single drug delivery system advanced bone regeneration therapy further than that of only BMP loaded F1 formulation.

Acknowledgements

This study was supported by Ankara University, Coordinator of Scientific Research Projects (Grant number: 17A0234001).

References:

1. Kim JW, et al., (2020). International Journal of Molecular Sciences, 21(14):1-13.
2. Xu X, et al., (2019). Acta Biomaterialia, 86: 235-246.
3. Khajuria, DK, et al., (2018). Arch Oral Biol, 2018. 85: 120-129.

OP038: OPTIMIZATION OF LIDOCAINE BASE NANOSUSPENSIONS WITH EXPERIMENTAL DESIGN

[1,2]Çulcu, Ö., [1]Ilbasmis-Tamer, S., [1]Tirnaksiz, F.

[1] Gazi University, Department of Pharmaceutical Technology, Ankara, Turkey

[2] Agri Ibrahim Cecen University, Department of Pharmaceutical Technology, Agri, Turkey

Introduction:

Lidocaine base (LID) is one of the local anesthetic drugs which is practically insoluble in water so it has low bioavailability (1, 2). Nanosuspensions have a positive effect on the bioavailability of dermally administered drugs by better penetration into the skin (3). The aim of this study was to develop LID nanosuspensions using an experimental design (DoE) approach. Effect of critical formulation attributes (CFAs), critical process parameters (CPPs) and their interactions were determined.

Materials and Methods:

Preparation of Lidocaine Base Nanosuspensions:

LID nanosuspensions were prepared using wet milling method (RETCH® PM100, Germany). LID concentration was kept constant at 2%. Different concentrations (2%, 1%, 0.5% 0.25%, 0.125%, 0.0625%) were tested to determine the optimal concentration for polyvinyl alcohol (PVA) and poloxamer 407(POL). To start to wet milling method, drug and stabilizer solution were stirred with ultraturrax (Heidolph®–Silent Crusher M) at 15.000 rpm-10 min. After the complete wetting of LID particles, wet milling process were applied. The process parameters were selected as 0.5-1mm bead size, 1-2 hour milling time and a milling rate of 200-300 rpm for PVA and 300-400 rpm for POL.

Quality by Design (QbD)

QbD is a systematic approach to product development with predefined goals[4]. DoE approach is used to save time by reducing the number of experiments and to obtain the optimum nanosuspension formulation[5]. In this study, 2^3 factorial design was made using the Design Expert software and the formulation and process parameters were optimized.

Characterization of nanosuspensions:

Particle size measurement of coarse LID powder and post-ultraturrax samples was done with Symphatec HELOS. The particle size (PS), polydispersity index (PDI), zeta potential (ZP) values of nanosuspension were measured using a Malvern Zeta Sizer (Malvern Instruments). Differential Scanning Calorimetry (DSC) was performed with Shimadzu DSC 60 (Shimadzu, Kyoto, Japan) to determine the melting points of the samples and whether there was any interaction between them. Morphologic studies of nanosuspensions were studied with Scanning Electron Microscopy (SEM). In order to determine the short-term stability of the optimum nanosuspensions, stability tests were performed at 25 °C - 4 °C and PS, PDI and ZP values were measured and evaluated at the specified times.

Results:

The Effect of High Speed Mixer on Particle Size

The effects of different mixing rates (10000, 15000 and 20000 rpm) and different mixing times (5, 10, 15 and 20 min) on particle sizes were evaluated in order to determine the most appropriate ultraturrax speed and time. Increasing the mixing speed and time up to a certain value decreased the particle size. At higher speeds and times, the particle size increased again due to friction. It was determined as the optimum ultraturrax for 10 minutes at 15000 rpm.

Determinations of Process Parameters

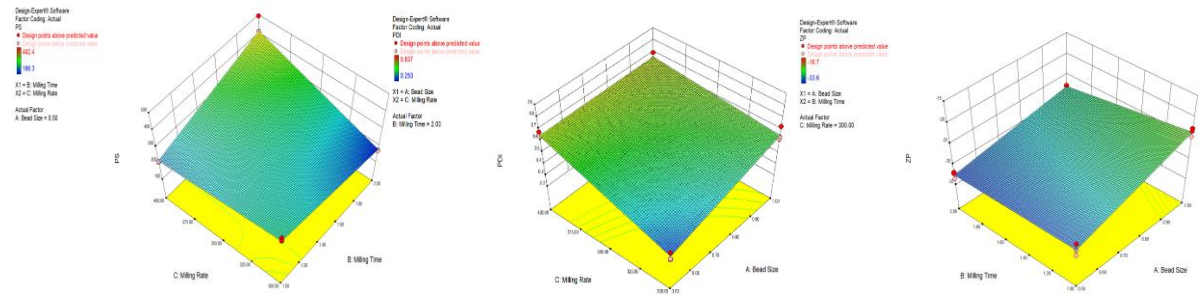

Figure 1. Response surface plot for effect of milling speed, milling time and bead size on POL stabilized nanosuspension

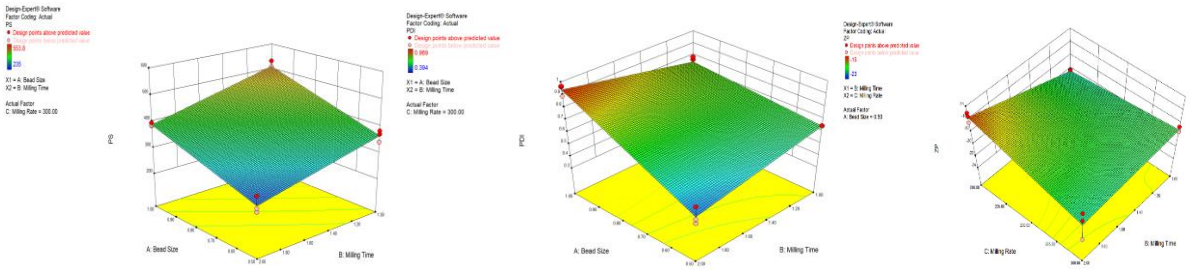

Figure 2. Response surface plot for effect of milling speed, milling time and bead size on PVA stabilized nanosuspension

In order to determine the process parameters, an experimental design was made and graphics were obtained (Figure 1 and Figure 2). According to the graphics, by using smaller bead size and longer mixing time, more suitable PS, PDI and ZP values are obtained. As a result of the experimental design, the most suitable process parameters for both polymers were determined as 0.5mm bead size, 300 rpm and 2 hours.

Differential Scanning Calorimetry (DSC)

DSC studies were performed separately on LID coarse powder, POL, PVA and their physical mixtures. As a result of the study, it was determined that there was no interaction between the drug and excipients.

Short-term Stability Test

Stability studies were carried out to determine the physical stability of POL and PVA nanosuspensions. According to stability studies, POL nanosuspensions were found to be more stable than PVA nanosuspensions. Nanosuspensions prepared using POL are more stable at 25°C, which can be explained by the fact that POL is a thermosensitive polymer.

SEM images of Nanosuspensions

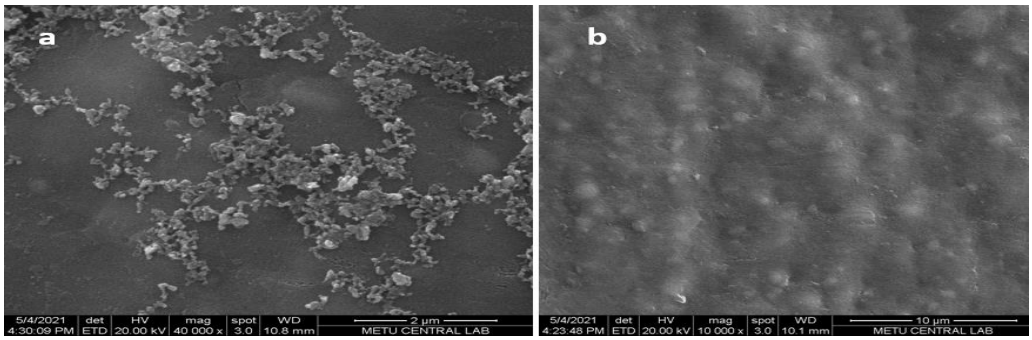

Figure 3. POL stabilized nanosuspension (a) PVA stabilized nanosuspension (b)

SEM studies were carried out with optimum nanosuspension formulations. Approximately, the particle size was found as determined.

Conclusions:

POL and PVA nanosuspensions were produced successfully. POL nanosuspensions were found to be more suitable as they have smaller PS, PDI values. Numerous formulations and process parameters are effective alone or together when preparing nanosuspensions by wet milling method. This study demonstrated the usefulness of QbD approach using DoE to understand the optimum process parameters of LID nanosuspensions.

References:

1. F. A. Maulvi et al., “Lidocaine tripotassium phosphate complex laden microemulsion for prolonged local anaesthesia: In vitro and in vivo studies,” Colloids Surfaces B Biointerfaces, vol. 185, no. August 2019, p. 110632, 2020
2. I. Ullah, M. K. Baloch, and G. F. Durrani, “Solubility of LIDOCAINE in ionic, nonionic and zwitterionic surfactants,” J. Solution Chem., vol. 41, no. 2, pp. 215–222, 2012
3. F. Lai et al., “Nanosuspension improves tretinoin photostability and delivery to the skin,” Int. J. Pharm., vol. 458, no. 1, pp. 104–109, 2013
4. H. B. Grangeia, C. Silva, S. P. Simões, and M. S. Reis, “Quality by design in pharmaceutical manufacturing: A systematic review of current status, challenges and future perspectives,” Eur. J. Pharm. Biopharm., vol. 147, no. September 2019
5. A. N. Oktay, A. Karakucuk, S. Ilbasmis-Tamer, and N. Celebi, “Dermal flurbiprofen nanosuspensions: Optimization with design of experiment approach and in vitro evaluation,” Eur. J. Pharm. Sci., vol. 122, no. July, pp. 254–263, 2018

OP039: DEVELOPMENT AND IN VITRO CHARACTERIZATION OF PREGABALIN LOADED NANOPARTICULAR SYSTEM

[1]Sevinc Ozakar, R., [1]Ozakar, E.

[1]Atatürk University, Faculty of Pharmacy, Department of Pharmaceutical Technology, Erzurum, Turkey, rukiyeso@atauni.edu.tr, emrahozakar@atauni.edu.tr

Introduction:

Nanoparticles are solid, colloidal particles with specific physicochemical properties, ranging in size from 10-1000 nm and made of natural/synthetic polymers or lipids (1, 2). The main target in the design of nanoparticles as drug delivery systems is to control the particle size, surface properties, and the release of active pharmaceutical agents to ensure that the drug acts at the therapeutically optimum dose and speed (3). Pregabalin (PG) resembles gamma-aminobutyric acid (GABA), which is the neurotransmitter of mammals with both structural and pharmacological properties. PG started to be used in the early 1990s. Its primary effect is anticonvulsant, and it is used in epilepsy. However, it also has analgesic, antidiabetic, and anti-inflammatory effects (4, 5). PG has many advantages compared to other antiepileptics as it does not have pharmacokinetic interactions with other drugs or is induced by enzymes (6). Its mechanism of action is still not fully resolved. However, it has been found that it binds to the calcium channel in the central nervous system and reduces calcium flow in the nerve endings. Thus, it is thought to reduce the communication between nerves and be effective in neuropathic pain and epileptic seizures (5, 7). PG is still not registered in any pharmacopeia. PG is recommended in conventional therapy (as capsules) in the treatment of neuropathic pain at the usual dose of 75 mg twice a day or 50 mg three times a day (7). Biodegradable polymers are frequently preferred in biomedical applications because they can be degraded in vivo enzymatically or non-enzymatically and form biocompatible, absorbable or biologically acceptable, non-toxic by-products, and do not require any surgical procedures after drug release after application. These polymers are metabolized and excreted by normal physiological, metabolic pathways (8). Poly lactide-co-glycolide (PLGA) is a polymer approved by the FDA for use in many basic and clinical science studies, disease diagnosis and other applications, and drug delivery on humans (9). The aim of this study is to prepare and characterize PG-loaded PLGA nanoparticles as an alternative to capsules in order to achieve maximum efficiency with low side effects and reduce dosing.

Materials and Methods:

PG was a gift from İlko İlaç (Turkey). PLGA and polyvinyl alcohol (PVA) were purchased from Lactel (USA) and Sigma (Germany), respectively. In the preparation of PG-loaded (10 mg and 12.5 mg) nanoparticles, the nanoprecipitation method was used. PG and PLGA were dissolved in 4 mL of acetone on a stirrer and then this solution was dropped onto the aqueous PVA solution (0.125%, g/mL) with the help of a 26-Gauge injector. After waiting for a while to stir on its own, the evaporator was used at 40 °C to completely remove the organic solvent. Afterward, centrifuged nanoparticles were kept in the freezer during the night and lyophilized for 24 hours (minimum n=3). PG-free nanoparticles were also prepared by the same method. The method was applied exactly without the addition of PG. The morphology, encapsulation efficiency (EE) and loading capacity (LC), yields (Y), particle size, zeta potential, DSC thermograms, FT-IR

spectra of nanoparticles prepared within the scope of characterization studies were examined. The morphology of nanoparticles was evaluated by optical microscope and SEM images. To determine the encapsulation efficiency (EE) and loading capacity (LC), lyophilized PG-loaded nanoparticles (10 mg) were taken into a colored bottle and 10 mL of pH 7.4 phosphate buffer solution was added. The nanoparticles were stirred on a stirrer for 6 hours. It was then filtered to remove polymer residues. A determined amount of ninhydrin solution with DMSO was added to the filtered aqueous solution and kept in an oven at 80 °C for 20 minutes. Ninhydrin has been used as a chromogenic agent. Then, PG amount was determined colorimetrically at room temperature using the previously validated spectrophotometric method. Particle size and zeta potential data were determined using the “Malvern Zetasizer Nano ZSP” (minimum n=3). DSC analyzes, which is frequently used to examine the thermal properties of the formulation components, was performed with “Netzsch STA 409 PC (TG/DSC)”. FT-IR analyzes were performed to examine the interactions of the formulation components with PG them by using the “Bruker VERTEX 70v”.

Results:

The nanoprecipitation method has been successfully applied in the preparation of nanoparticles. Optical microscope and SEM images of PG-free and PG-loaded nanoparticles were given below in Figure 1.

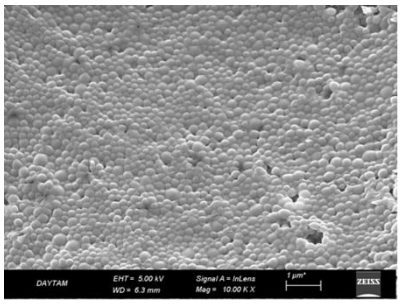

Lyophilized PG-free nanoparticles

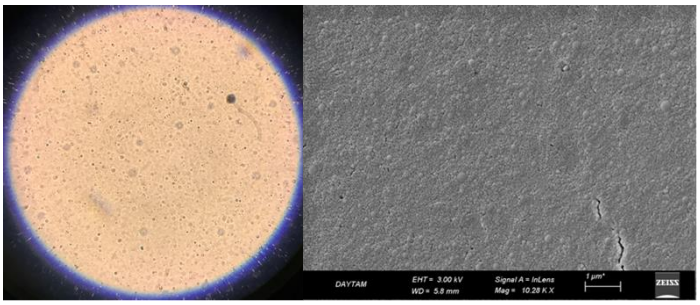

10 mg PG-loaded nanoparticles

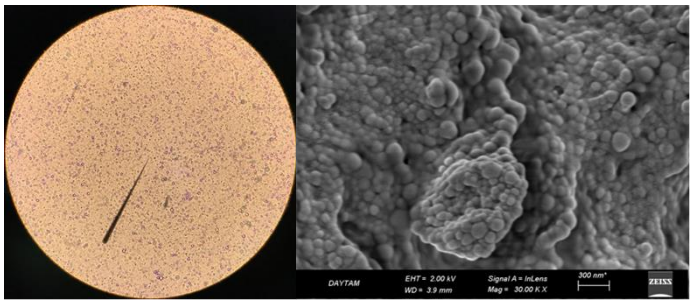

12.5 mg PG-loaded nanoparticles

Figure 1. Optical microscope and SEM images of PG-free and PG-loaded nanoparticles

The EE, LC, Y values are given below in Table 1. When the EE% values were examined, higher EE% values were obtained in nanoparticles containing low-dose PG. As the amount of PG increases, we can say that the hydrophilic structure of PG causes the EE% value to decrease. In the nanoparticle preparation stage, PG diffuses into the aqueous phase during the dropping of the organic phase into the aqueous phase and decreases the EE% value.

Table 1. The EE%, LC%, Y% values of PG-loaded nanoparticles (SD: Standard deviation)

PG Amount in Nanoparticles (mg)	**10**	**12.5**
EE%±SD	17.26±1.47	14.97±2.14
LC%±SD	25.23±1.17	24.11±2.47
Y%±SD	68.41±5.47	69.58±3.45

Particle size and zeta potential values of 10 mg PG-loaded nanoparticles, which have the highest EE% among the prepared nanoparticles, were measured. The particle size and zeta potential values were 135.7±0.48 nm and -22.9±0.8 mV. The zeta potential value is an important particle characteristic as it can influence both particle stability. For physically stable nanoparticles stabilized by electrostatic repulsion only, a minimum zeta potential of ±30 mV is required. However, in the case of both electrostatic and steric stabilization or only steric stabilization, a zeta potential of ±20 mV is sufficient (10). In our formulation, PVA, which provides both electrostatic and steric (electrosteric) stabilization, was used and achieved sufficient stabilization.

The DSC thermogram and FT-IR spectrum of 10 mg PG-loaded nanoparticles were given below in Figure 2. In the DSC thermogram, there was a decrease in the Tg value of PLGA, but no specific PG endothermic Tm peak was observed. In this case, we can say that we have prepared a solid solution; that is, PG is dispersed in the polymeric matrix at the molecular level. In FT-IR spectrum, it can be seen that there was no change in significant peak of PG in nanoparticles, indicating stability of drug in formulation structure.

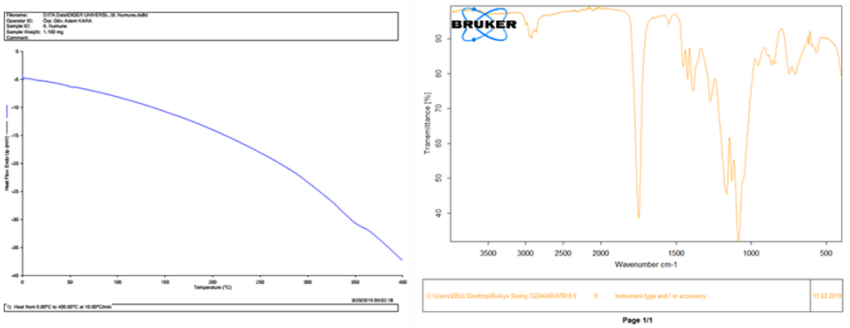

Figure 2. The DSC thermogram and FT-IR spectrum of 10 mg PG-loaded nanoparticles.

Conclusions:

PG-loaded PLGA nanoparticles have been successfully prepared and characterized. However, the amount of PG loaded on the spherical nanoparticles was low due to the hydrophilic nature of PG. Better results can be obtained with additional studies in the future and these nanoparticles can be used as an alternative to conventional treatment.

Acknowledgements

This study was supported by a grant of Atatürk University Scientific Research Projects Coordination Unit (BAP-THD-2018-6547).

References:

1. Neha B, Ganesh B, Preet K (2013). International Journal of Pharmaceutical and Life Sciences, 2(3):107-132.
2. Medina C, Santoz-Martinez MJ, Radomski A, Corrigan OI, Radomski MW (2007). British Journal of Pharmacology, 150(5):552-558.
3. Mirakabad FST, Nejati-Koshki K, Akbarzadeh A, Yamchi MR, Milani M, Zarghami N, Zeighamian V, Rahimzadeh A, Alimohammadi S, Hanifehpour Y, Joo SW (2014). Asian Pacific Journal of Cancer Prevention. 15(2):517-535.
4. Fukasawa H, Muratake H, Nagae M, Sugiyama K, Shudo K (2014). Biological&Pharmaceutical Bulletin, 37(11):1816-1819.
5. Sher N, Fatima N, Perveen S, Siddiqui FA, Sial W (2015). International Journal of Analytical Chemistry, Article ID 241412.
6. Kanwar N, Kumar R, Sarwal A, Sinha VR (2016). Drug Development and Industrial Pharmacy, 42(4):654-660.
7. Jadi RK, Tatikonda A, Reddy PRV, Venisetty RK (2016). International Journal of Pharmaceutical Research and Allied Sciences, 5(3):8-15.
8. Joshi JR, Patel RP (2012). International Journal of Current Pharmaceutical Research, 4(4):74-81.
9. Halder KK, Mandal B, Debnath MC, Bera H, Ghosh LK, Gupta BK (2008). Journal of Drug Targeting, 16(4):311-320.
10. Singare DS, Marella S, Gowthamrajan K, Kulkarni GT, Vooturi R, Rao PS (2010). International Journal of Pharmaceutics, 402(1-2):213-22.

OP041: ACE2 LOADED CATIONIC LIPOSOMES FOR COVID-19 TREATMENT

[1]Arisoy, S., [2]Koçaş, M.,[3]Comoglu, T.

[1] Inonu University, Faculty of Pharmacy, Department of Pharmaceutical Biotechnology, Malatya, Turkey, sema.arisoy@inonu.edu.tr

[2] Selcuk University, Faculty of Pharmacy, Department of Pharmaceutical Technology, Konya, Turkey, meryem.kocas@selcuk.edu.tr

[3] Ankara Univesity, Faculty of Pharmacy, Department of Pharmaceutical Technology, Ankara, Turkey, comoglu@pharmacy.ankara.edu.tr

Introduction:

ACE2 is expressed in the lungs, arteries, heart, kidney, brain and intestines and **it** is an essential component of the renin-angiotensin-aldosterone system. SARS-CoV-2 enters the human body through ACE2 receptors, thus facilitating viral entry into target cells (1). After administration of ACE2 to the lungs, the virus will be able to bind to ACE2 which is given excessively to the body instead of binding to the body's ACE2 receptors (2). Therefore, treatment with a soluble form of ACE2 will be effective with two important parameters. First of all, slow viral entry into the cells and thus reduced viral spread will be provided. And also lungs will be protected from damage caused by blocked function of ACE2 (3). It is reported that the deep canal at the top of ACE2 and the surface of the surrounding ridges are highly negatively charged and the hydrophobic regions are located in these areas (4). For Covid-19 treatment, by using positively charged lipids, ACE2 was planned to adhere to liposomes by electrostatic interaction. In this study, it was aimed to develop decoy liposomes produced with dialkyl cationic lipids such as 1,2-dioleoyl-3-trimethylammonium-propane (DOTAP) and/or 1,2-dioleoyl-sn-glycero-3-phosphoethanolamine (DOPE) and cholesterol for treatment of Covid-19

Materials and Methods:

Materials

Rh ACE2 and cholesterol was purchased from Sigma-Aldrich. DOTAP and DOPE was products of Avanti Lipids.

Methods

Preparation of Liposomes

Cationic liposomes are prepared in DOTAP/DOPE (1:1 molar ratio, S1), DOTAP / DOPE / Chol (cholesterol) (2:1: 1 molar ratio, S2), DOTAP / Chol (1:1 molar ratio, S3) and DOPE / Chol (1:1 molar ratio, S4, liposomes could not be obtained). In order to provide the molar ratio in the formulations, certain volumes of lipid solution were taken and mixed in a 25 mL flask. This solution was dried under pressure in a rotavapor at 80 rpm and 37°C for 15 minutes. Thin lipid film was observed on the inner walls of the flask.

Loading ACE2 into formulations

The thin lipid film was diluted with 1.6 mL of PBS 7.4 to achieve a lipid concentration of 16mmol/L. Formulations were incubated in 2µg/0.8 mL ACE2 PBS 7.4 solution at room temperature for half an hour or 24 hours.

Extrusion of formulations

After the incubation period, formulations were first extruded using 3 µm and then 0.1 µm polycarbonate filters at 50°C for 10 times.

Particle Size and Zeta Potential Measurement

Samples were prepared by taking 50 µL of the products and diluting them with 25 ml of ultrapure water. Particle size(nm), PDI and zeta potential(mV) were measured with Malvern NANOZS (n=3).

Results:

Decoy liposomes carry the binding receptors of viruses in the body and prevent viral infection by allowing viruses to bind to these systems instead of receptors in cells (5).

Table 1. In vitro characteristics of blank liposome formulations

Formulation	Particle Size	PDI	Zeta potential
S1	463,3±9,721	0,511±0,005	45,8±5,43
S2	1077± 0,7	0,574±0,069	54,0±1,40
S3	1254±144,7	0,350±0,267	54,0±4,6

While S1 had only the DOTAP/DOPE combination, cholesterol was added to S2 and S3 formulations by keeping the total lipid concentration constant (Table 1) and particle size was increased.

Table 2. In vitro characteristics of liposome formulations obtained after 24 hours of incubation with ACE2

Formulation	Particle Size	PDI	Zeta potential
S1	326,5±20,96	0,56± 0,425	25,5±5,57
S2	690,3±60,96	0,690±0,125	20,6± 3,28
S3	815,2±12,5	0,796±0,256	29,6±5,62

Table 3. In vitro characteristics of liposome formulations obtained after 1.5 hour of incubation with ACE2

Formulation	Particle Size	PDI	Zeta potential
S1	326,5±20,96	0,56± 0,425	25,5±5,57
S2	690,3±60,96	0,690±0,125	20,6± 3,28
S3	815,2±12,5	0,796±0,256	29,6±5,62

Table 4. In vitro characteristics of ACE2 loaded liposome formulations after filtering through 0.3 µm poly carbonate filter

Formulation	Particle Size	PDI	Zeta potential
S1	369,7±2,845	0,321±0,025	38,5±2,37
S2	577,8±20,18	0,372±0,074	-11,4±1,19
S3	482,5±18,65	0,566±0,140	53,2±3,17

Table 5. In vitro characteristics of ACE2 loaded liposome formulations after filtering through 0.1 µm poly carbonate filter

Formulation	Particle Size	PDI	Zeta potential
S1	269,7±5,254	0,260±0,035	-51,4±1,97
S2	540,1±79,59	0,499±0,123	-43,0±3,69
S3	905,7±129,8	0,571±0,105	-5,14±1,41

Studies have shown that the increasing the incubation time with the protein and liposome formulations increases the loading efficiency. In a study, it was observed that the loading efficiency was increased with the increase of the incubation time up to 1 hour, but the increase in the incubation time after 1 hour did not affect the loading efficiency anymore. In addition, when the incubation temperature was increased from 25°C to 40°C, it was observed that the loading efficiency was decreased. For this purpose, it was concluded that it is more appropriate to compare the loading efficiency of the formulations where the incubation time is half an hour and 24 hours atroom temperature**.** It is thought that when the incubation time of the formulations were increased, the amount of ACE2 which bounds to the surface of liposomes will increase resulting with the increase in particle size. However, after the increased incubation time, a decrease in the size of the particles was observed (Tables 2&3). In addition, in both incubation periods, the zeta potential values of the particles were decreased (Tables 2&3). After extrusion, the zeta potential values of the particles shifted to negative value (Tables 4&5). In literature, it was observed that liposomes containing DOTAP were stable in the pH range of 5-6.7 and the hydrolysis of lipids was accelerated with the increasing pH. The increased rate of hydrolysis for DOTAP-containing liposomes has been attributed to the increased accessibility of the ester linkage between the glycerol backbone and fatty acid tails, thereby promoting hydroxyl catalyzed hydrolysis. In addition, increasing temperature also accelerates hydrolysis (6). Our results accelerated that the liposomes were hydrolyzed.

Conclusions:

The decrease in the zeta potential and particle size in the results show that the structure is distorted. In addition, the formulations were centrifuged at 30.000 rpm for 3 hours and the nanoparticles could not be precipitated. Future studies should be done and discussed for a better design of decoy liposomes loaded with ACE2.

Acknowledgements

This study was supported by TUSEB, Turkish Institutes of Health Presidency (Project No:8783/8974)

References:

1. Lutz, C., et al., (2020). COVID-19 preclinical models: human angiotensin-converting enzyme 2 transgenic mice. Human genomics, 14: 1-11.
2. Kuba, K., et al., (2005). A crucial role of angiotensin converting enzyme 2 (ACE2) in SARS coronavirus–induced lung injury. Nature medicine, 11(8): 875-879.
3. Zhang, H. and Baker, A. (2017). Recombinant human ACE2: acing out angiotensin II in ARDS therapy. Critical Care, 21(1): p. 305.
4. Prabakaran, P., Xiao, X., Dimitrov, D. S. (2004). A model of the ACE2 structure and function as a SARS-CoV receptor. Biochemical and biophysical research communications, 314(1): 235-241.
5. Hendricks, G.L., et al., (2015). Heparin octasaccharide decoy liposomes inhibit replication of multiple viruses. Antiviral Res, 116: 34-44.
6. Vernooij, E., et al., (2002). Chemical hydrolysis of DOTAP and DOPE in a liposomal environment. Journal of controlled release, 79(1-3):299-303.

OP048: ELECTROSPUN NANOFIBERS AS ORAL FAST-DISSOLVING DELIVERY SYSTEM OF RISPERIDONE

Turanlı, Y., Birer, M., Acartürk, F.

Gazi University Faculty of Pharmacy, Department of Pharmaceutical Technology, Ankara, Turkey

Introduction:

Fast-dissolving/disintegrating drug delivery systems (FD-DDSs) address the needs of populations requiring special attention, such as pediatric and geriatric patients. Difficulty in swallowing medicines is often encountered by these patients, leading to non-compliance with medication, which results in ineffective treatment (1). Electrospinning is a straightforward and versatile process by which polymer nanofibers with diameters ranging from a few nanometers to several micrometers can be produced using an electrostatically driven jet of polymer solution or polymer melt. Among all types of DDS, there are some concrete advantages that the electrospun fibers possess for preparing oral FD-DDSs. Fibers have an extraordinary high surface area per unit mass, which facilitates fast release of the active ingredients incorporated in them. Fiber mats have high porosity due to small pore size of the fibers deposited in the fiber membranes (2, 3). Risperidone is a BCS class II compound with low solubility and highly permeability characteristics. It is a medication that works in the brain to treat schizophrenia. Risperidone rebalances dopamine and serotonin to improve thinking, mood, and behavior (4). The objective of the present study is to prepare the orally disintegrating film of risperidone, to provide ease of use and to make sure that schizophrenic patients who want drug rejection take the drug.

Materials and Methods:

Preparation of Electrospinning Solutions

Polyethyleneoxide with three different molecular weights (MW=100000 (WSR N10), 200000 (WSR N80, 600000 (WSR 205)) was used as polymer. Xylitol or Kollidon VA-64 was used as disintegrating agents. A mixture of ethanol, distilled water and acetic acid was used to dissolve the polymer and the risperidone. While preparing the mixtures, the most suitable concentration of polymer to obtain nanofibers was used. In formulations, the disintegrating agent and the polymer was in the same ratio. The drug-polymer ratio is constant for all formulations (Table 1).

Preparation of Nanofibers

For the preparation of nanofibers, the polymer, disintegrating agent, and risperidone were dissolved in solvent mixture and loaded into the syringe. Then the nanofibers were obtained by adjusting the appropriate electrospinning parameters (Table 2). Distance and rotation speed were kept constant in all formulations for nanofiber production.

Characterization of Polymer Mixtures

The properties of polymer solutions are important in the electrospinning process. Therefore, the viscosities, conductivity and surface tension of the polymer solutions were analyzed.

Nanofibers Characterization

DSC and IR analyzes were performed for the characterization of polymers, active substance and formulations Scanning electron microscopy was used for morphological examination of nanofibers. Mechanical characterizations were performed with Texture Analyzer. In addition, disintegration tests and in vitro dissolution tests were performed.

Table 1. The composition of the formulations

Formulations	WSR N10 %	WSR N80 %	WSR 205 %	Xylitol %	Kollidon VA-64 %	Risperidone %	Drug/Total polymer
F1	15	-	-	15	-	3	1/10
F2	-	7.5	-	7.5	-	1.5	1/10
F3	-	-	2.5	2.5	-	0.5	1/10
F4	15	-	-	-	15	3	1/10
F5	-	7.5	-	-	7.5	1.5	1/10
F6	-	-	2.5	-	2.5	0.5	1/10

Table 2. Electrospinning parameters

Formulations	Flow rate (ml/h)	Voltage (kV)	Distance to needle tip to collector (cm)	Rotating speed (rpm)
F1	1.5	20	22	100
F2	1.5	13	22	100
F3	1.5	10	22	100
F4	3.5	14	22	100
F5	2.5	15	22	100
F6	1	7	22	100

Results:

When the DSC thermograms of the formulations were examined, it was determined that the polymer and disintegrating agents kept their characteristic peaks and did not interact with the active substance (Fig. 1a). In the FT-IR analysis, characteristic bands of risperidone, polyethylene oxide, xylitol and Kollidon VA-64 are seen in the formulations (Fig. 1b). There was no significant difference between the surface tensions of the polymer solutions. F1 and F4 formulations prepared with WSR N10 polymer had the highest viscosity value due to the high polymer ratio. The conductivity of the polymer solutions were high accordingly, high voltage had to be applied. In scanning electron microscopy images (Fig. 2), it was observed that nanofibers prepared using Kollidon VA-64 had a smoother surface and larger diameter than that of prepared with Xylitol. While nanofibers prepared with WSR N80+VA-64 had the highest tensile strength, fibers prepared with WSR 205+Xylitol had the highest elongation at break value (Fig. 3). Nanofibers prepared with Kollidon VA-64 disintegrated in a much shorter

time than those prepared with Xylitol (Fig.4). All nanofiber formulations dissolved in neutral medium in a much shorter time than the commercial product. Approximately 75% of F1 and F5 formulations were dissolved within one minute (Fig. 4).

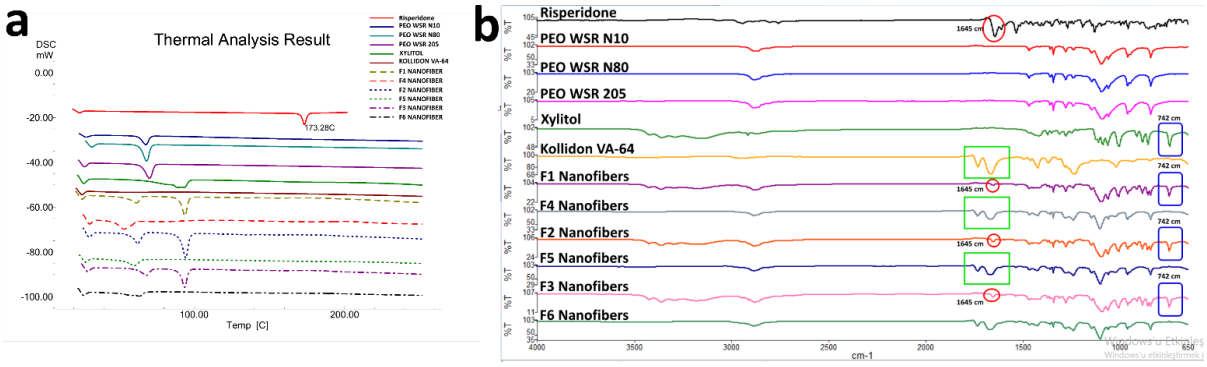

Figure 1. (a) DSC thermogram and (b) FTIR spectra of risperidone, polymers and formulations

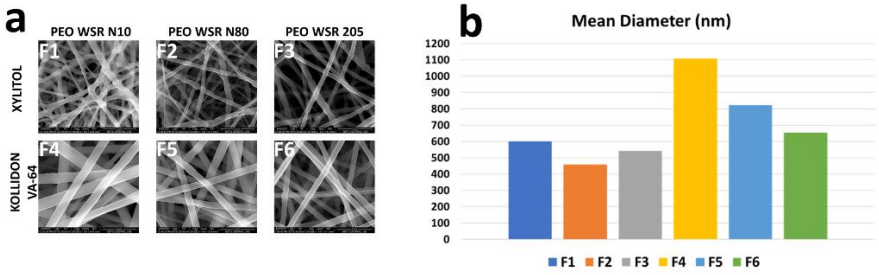

Figure 2. (a) SEM images and (b) mean diameters of nanofibers

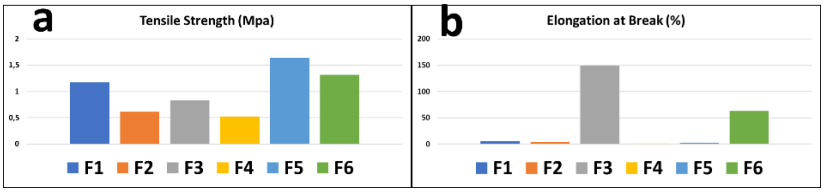

Figure 3. (a) The tensile strenght and (b) elongation at break values of formulations

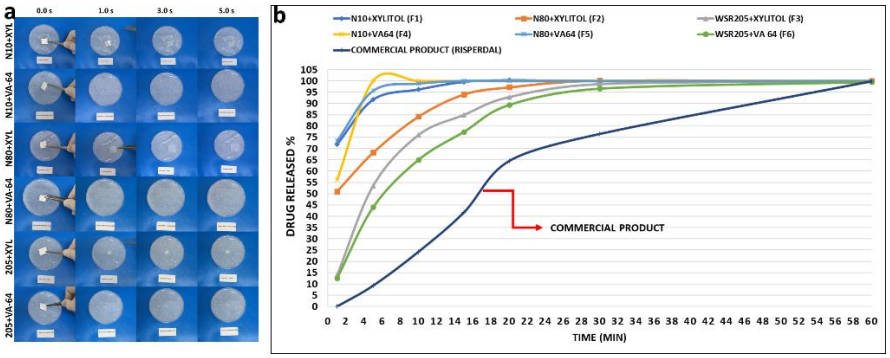

Figure 4. (a) Disintegration tests and (b) in vitro dissolution profiles of formulations

Conclusions:

Electrospun ultrafine fibers have the potential to be used as solid dispersions to improve the dissolution profiles of poorly water-soluble drugs or as oral fast disintegrating drug delivery systems. PEO/XYL or KOLLIDON VA-64 mixture based electrospun nanofiber films could be a suitable alternative to conventional and fast-dissolving/disintegrated tablets available in the market. The beneficial effects of risperidone should be investigated by further cell culture and in vivo studies.

Acknowledgements

Risperidone were generously donated by Deva Pharmaceuticals Istanbul, Turkey.

References:

1. Shukla, D., Chakraborty, S., Singh, S., & Mishra, B. (2009). Chemical and Pharmaceutical Bulletin, 57(4), 337-345.
2. Yu, D. G., Shen, X. X., Branford-White, C., White, K., Zhu, L. M., & Bligh, S. A. (2009). Oral fast-dissolving drug delivery membranes prepared from electrospun polyvinylpyrrolidone ultrafine fibers. Nanotechnology, 20(5), 055104.
3. Birer, M., & Acartürk, F. (2021). Electrospun orally disintegrating film formulation of telmisartan. Pharmaceutical Development and Technology, 26(6), 661-672.
4. Ryan, S., Puzio, H., & Fagan, J. M. (2014). Combating Social Stigma: An Analysis and Overview of Schizophrenics in Society.

OP049: PREPARATION AND CHARACTERIZATION OF TENOFOVIR DISOPROXIL FUMARATE LOADED NANOFIBER FOR VAGINAL DELIVERY

[1]Dik, Z., [2]Saar, S., [2]Tugcu-Demiroz., F.

[1] University of Health Science, Gulhane Faculty of Pharmacy, Department of Pharmaceutical Technology, Ankara, Turkey, zehra.dik@sbu.edu.tr

[2] Gazi University, Faculty of Pharmacy, Department of Pharmacuetical Technology, Ankara, Turkey, fatmanur@gazi.edu.tr

Introduction:

Human immunodeficiency virus (HIV) which causes the acquired immunodeficiency syndrome (AIDS is a virus that can be transmitted in many ways) (1). Approximately around 100 million citizens all over the world are suffering from HIV virus(2).Recently, ARVs have been explored for oral and topical pre-exposure prophylaxis in HIV-negative individuals before exposure to the virus.Topical microbicide products are preferred by people who are at risk of HIV infection, those with long-term toxicity potential due to systemic exposure, or those at risk of periodic HIV exposure(3).Nanofibers are suitable for vaginal drug application with their properties such as high permeability, large surface area, high mucoadhesive strength, reduce toxicity to other organs(4). The basic idea is to protect the vagina from HIV infection by applying nanofiber containing antiretroviral drugs around the time of sexual intercourse. The purpose of this study is to develop mucoadhesive nanofibers preparation by electro-spinning method for vaginal application of Tenofovir Disoproxil Fumarate (TDF). TDF is an FDA and EMA approved antiretroviral drug used to treat HIV(5). As an excipient we used poly vinyl pyrrolidone (PVP) for nanofiber formulations because PVP is a well-known hydrophilic, mucoadhesive, biocompatible polymer(6).

Materials and Methods:

Preparation of Nanofiber Formulation

In the electrospinning process, we prepared polymer blends for our nanofiber formulations using a mechanical stirrer.Blank and TDF-loaded PVP solutions were prepared in different concentrations. For blank formulations PVP dissolved in ethanol at the concentration of 10,12.5, and 15%.

Firstly, 10 mL of the polymer mixture was placed into a plastic syringe injection with a 18-gauge blunt needle and then setup in the electrospinning device and high-voltage electrical potential was applied.

Characterization of Polymer Solutions

To produce electrospun nanofibers, the process parameters were chosen according to our previous study(4).The polymer solutions were characterized in terms of viscosity, conductivity and surface tension. The rheological measurement of the polymer solutions were performed using cone/plate rheometer(Brookfield,DV-III Rheometer).The conductivity measurement of all polymer solutions were carried out using a conductometer (Hanna Instruments, HI 9033, USA).Surface Tension Measurements Of all solutions were carried out using an optical

tensiometer (Attension-Theta Lite, BiolinScientifc, Finland).Surface Tension Values were calculated with Young–Laplace equation using the shape of pendant drops which were formed on the tip of the needle.

Characterization of Nanofiber Formulations

Nanofiber formulations were characterized in terms of contact angle, tensile strength, elongation at break, average fiber diameter, mucoadhesive properties, in vitro diffusion and release kinetics. The morphological properties of all formulations carried out with scanning electron microscopy(Quanta 400 F, FEI Company, USA).Mechanical tests were used to evaluate the mechanical properties. The tensile strength of all nanofiber formulations was calculated using a Texture Analyzer equipped with tensile grip (TA. XTPlus Texture Analyzer, Stable MicroSystems, UK).Tensile strength and elongation at break values of all nanofiber formulations were calculated with stress-strain graphics. The contact angle measurements of the fibers were performed using an optical tensiometer (Attension-Theta Lite, BiolinScientifc, Finland).The ex vivo permeation (through cow tissue) of TDF nanofiber formulations were studied using Franz diffusion cell. All measurements were repeated three times.

Results:

Increase in the polymer concentration from 10% to 15% led to an increase in the viscosity values of all the solutions. An increase in viscosity was observed with TDF loading compared to blank nanofibers. There was no significant difference in surface tension between blank nanofibers. A significant increase in surface tension values of T1, T2 and T3 was observed with the addition of TDF. The decrease in conductivity with the addition of TDF to polymer solutions was not found significant. The viscosity, conductivity and surface tension of the polymer solutions were found suitable to produce nanofibers (Table 1).

Table 1. Different parameters of electrospinning solutions (n=3, mean ± standard deviation)

Formulation Code	Viscosity (cPs)	Surface tension ($mN.m^{-1}$)	Conductivity ($\mu S.cm^{-1}$)
T1	230±4	28,0±0,1	9,4
T2	508±5	27,98±0,06	8,6
T3	683±7	27,6±0,02	7,7
T4	234±4	28,8±0,0	9,1
T5	517±3	28,26±0,07	7,5
T6	827±16	28,15±0,00	7,4

The contact angle of nanofibers was found as 0º. PVP nanofibers havehigh wettability properties due to their hydrophilic nature. An increase of polymer concentration from 10% to 15% caused an increase in tensile strength. The tensile strength and elongation at break were increased with addition of TDF. Morphology and fiber diameter of the electrospun nanofibers were affected significantly from the concentration of PVP. Also The average diameter of nanofibers was increased with loading of TDF for T4 and T5 formulations. Electrospun fibers should have superior mucoadhesive properties to adhere to the vaginal mucosa. In our study, work of mucoadhesion values increased with increasing PVP concentration. Loading of TDF to nanofibers increased the mucoadhesion values. For the T4, T5 and T6 formulations

approximately 80% of the total drug was diffused at the end of 8 hours while 100% diffused at the end of 24 hours. According to the permeability studies, the flux values were found as 115±1 $\mu g.cm^{-2}.h^{-1}$, 130±2 $\mu g.cm^{-2}.h^{-1}$ and 131±2 $\mu g.cm^{-2}.h^{-1}$ and the permeability coefficients were found as 0.05±0.00 $cm.h^{-1}$, 0.0543±0.004 $cm.h^{-1}$ and 0.055±0.001 $cm.h^{-1}$, respectively for T4, T5 and T6. It was seen that mucoadhesive properties, in vitro diffusion, permeation and flux values increased as the concentration of polymers increase.According to the characterization studies, T6 formulation was found most suitable formulation for vaginal use compared to the other formulations (Table 2).

Table 2. Characterization results of nanofiber formulations (n=3, mean ± standard deviation)

Formulation Code	Average fiber diameter (nm)	Tensile strength (MPa)	Elongation at break values (%)	Contact Angle (°)	Work of mucoadhesion ($mJ.cm^{-2}$)
T1	677±131	3.07±0.33	63.87±9.81	0	0,173±0,030
T2	1031±202	3.94±0.73	28.46±7.24	0	0,182±0,021
T3	1564±270	5.87±0.25	15.90±4.93	0	0,212±0,012
T4	877±129	4.04±0.51	64.09±8.85	0	0,234±0,014
T5	1340±210	5.18±0.87	52.89±9.06	0	0,328±0,039
T6	1550±195	6.11±0.11	44.43±5.85	0	0,332±0,012

Conclusions:

Nanofibers are suitable dosage forms for vaginal use. In our study, it was found that the PVP concentration directly affected nanofiber diameter, mechanical, mucoadhesive properties, in vitro diffusion, permeation and flux values of nanofibers. According to permeability results, TDF loaded formulations showed higher permeation and diffusion due to the high porosity of the nanofibers. It was concluded that T6 formulation was found more suitable for vaginal application. TDF loaded nanofibers have potential use for the vaginal drug delivery.

References:

1. Salman, S. M. (2021). Memory and media coverage effect on an HIV/AIDS epidemic model with treatment. Journal of Computational and Applied Mathematics, 385, 113203
2. Shree, B. D. (2021). Application of Topological Indices of Tenofovir Chemical Structures for the Cure of HIV/AIDS Patients. Turkish Journal of Computer and Mathematics Education (TURNCOAT), 12(10), 1693-1706.
3. Young, I., & McDaid, L. (2014). How acceptable are antiretrovirals for the prevention of sexually transmitted HIV?: A review of research on the acceptability of oral pre-exposure prophylaxis and treatment as prevention. AIDS and Behavior, 18(2), 195-216.
4. Tuğcu-Demiröz F. (2020). Electrospun metronidazole-loaded nanofibers for vaginal drug delivery. Drug Development and Industrial Pharmacy, 46, 1015-1025.
5. Gallant, J. E., &Deresinski, S. (2003). Tenofovir disoproxil fumarate. Clinical Infectious Diseases, 37(7), 944-950.
6. Tort, S., Yıldız, A., Tuğcu-Demiröz, F., Akca, G., Kuzukıran, Ö., & Acartürk, F. (2019). Development and characterization of rapid dissolving ornidazole loaded PVP electrospun fibers. Pharmaceutical development and technology, 24(7), 864-873.

OP051: POLYETHYLENEIMINE FUNCTIONALIZED CRYOGEL MEMBRANES AS A CONTROLLED RELEASE SYSTEM

[1]Çetin, K.

[1] Necmettin Erbakan University, Department of Biomedical Engineering, Konya, Turkey

Introduction:

Controlled release systems have some advantages such as utilizing less drug dose, extending the dosing interval, and reducing side effects (1, 2). Because implant systems can deliver high amounts of drugs around the tumor site, the therapeutic effectiveness of chemotherapy may increase while the side effects of the drug decrease (3).

Cryogels, a subclass of hydrogels, are 3D-gel matrices fabricated below freezing temperature of solvents (4). In cryogelation, polymerization takes place as the solvent, usually water, begins to freeze. After the cryogelation is completed, the polymers are thawed at room temperature, allowing the ice to melt and a structure with macropores is formed (5). Contrary to many materials, the use of ice crystals in cryogels instead of toxic pore-forming chemicals such as toluene is one of their biggest advantages. In addition, cryogels do not have a challenging process such as the removal of these toxic porogens after polymerization (6).

Polyethyleneimine (PEI) is a positively charged synthetic polymer with abundant amino groups on its surface (7). PEI is used as an important gene transfection system among all non-viral polymeric carriers due to its high efficiency (8). Due to its amine functional groups, PEI can be utilized to deliver negatively charged drugs such as nucleic acids, peptides, proteins, and so on (9). The objective of the study is to design PEI functionalized cryogel membranes which can be used as a potential delivery system.

Materials and Methods:

The membranes based on 2-hydroxyethyl methacrylate and glycidyl methacrylate, were synthesized via cryopolymerization using ethylene glycol dimethacrylate as a crosslinking agent. After the polymerization step and washing process, PEI was immobilized on the cryogel membranes through the reactive glycidyl groups of the cryogels. Then, Cu(II) ions were chelated on the cryogel membranes through NH_2 groups of PEI. 5-fluorouracil (5-FU) was loaded in the PEI-functionalized cryogel membranes. The percent loading of 5-FU in the PEI-functionalized cryogel membranes is found out using UV/Vis spectrophotometer at 266 nm. *In vitro* release experiments were performed to investigate the effects of pH, and amount of 5-FU on the release rate of 5-FU from modified cryogel membranes in buffer medium.

Results:

Surface area, macroporosity, and the cryogel membranes were found out as 16.2 m^2/g cryogel and 76.7% respectively. Effect of pH on water uptake capacity of the plain and PEI-functionalized cryogel membranes was shown in Figure 1. General surface morphology of the cryogel membranes was investigated using scanning electron microscopy (Figure 2.b). PEI attachment onto cryogel membranes was found to be 77.45 mg/g polymer. The change in the color of the cryogels before and after PEI attachment process was observed by optical images

(Figure 2.a) Release amounts of 5-FU were 78.32 %, 70.61% and 66.48% in 12 h at pH values of 4.0, 6.0 and 7.4, respectively.

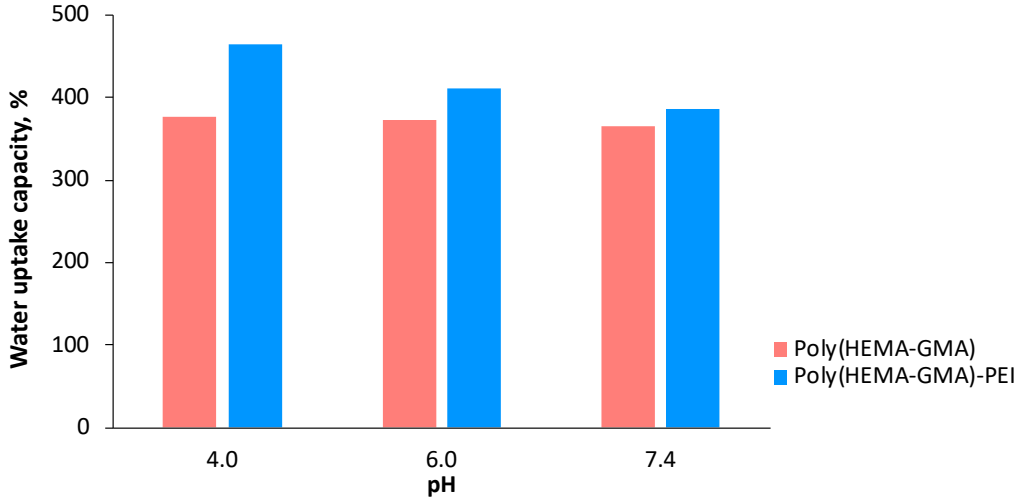

Figure 1. Water uptake capacities of cryogel membranes

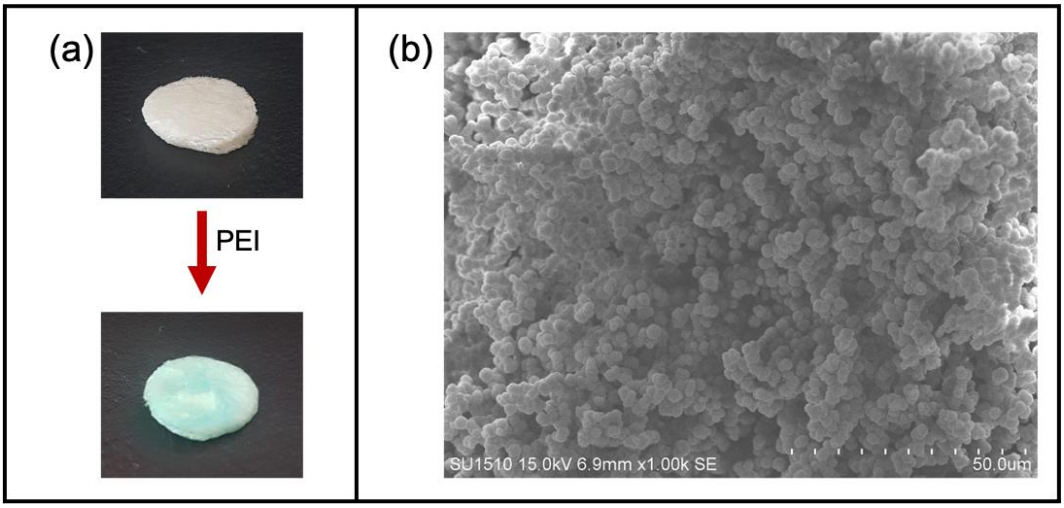

Figure 2. Optical (a) and SEM images (b) of cryogel membranes

Conclusions:

As seen in SEM images, cryogels membranes have a macroporous interconnected flow channels. Unlike plain cryogel membranes, PEI-attached cryogel membranes showed a pH-responsive water uptake capacity. Due to polycationic nature of PEI, swelling degree of the cryogel membranes are increased at acidic environment. According to results of *in vitro* cumulative release studies, cryogel membranes exhibited a burst effect and then slower release rates. Release rates of 5-FU from the PEI-functionalized cryogel membranes were increased by decreasing the medium pH. They showed a pH-responsive behavior as well as higher drug release at lower pH, which also agreed with the swelling ratios as shown in Figure

1. It can be concluded that modified cryogel membranes could be promising candidates for implantable drug delivery systems.

References:

1. Fishbein, I, et al. (2012). In: Siepmann J, et al. (ed). Fundamentals and Applications of Controlled Release Drug Delivery. Springer, New York, United States of America, pp. 445-492.
2. Marudova, M, Yorov, T. (2019). International Journal of Polymeric Materials and Polymeric Biomaterials, 68:99-106.
3. Hanafy, A. F., Yousef, M. I., Mortada, S. A., Molokhia, A. M. (2014). Journal of Taibah University Medical Sciences, 9:14-22.
4. Saylan, Y., Denizli, A. (2019). Gels, 5:20.
5. Çetin, K., Türkmen, D., Qureshi, T., Sağlam, N., Denizli, A. (2016). Hacettepe Journal of Biology and Chemistry, 44:77-86.
6. Arrua, R. D., Causon, T. J., Hilder, E. F. (2012). Analyst, 137:5179-5189.
7. Venkiteswaran, S., Thomas, T., Thomas, T. J. (2016). ChemistrySelect, 1:1144-1150.
8. Yue, Y., Jin, F., Deng, R., Cai, J., Dai, Z., Lin, M. C. M., Kung, H. F., Mattebjerg, M. A., Andresen T. L., Wu, C. (2011). Journal of controlled release, 152:143-151.
9. Feng, M., & Li, P. (2007). Journal of Biomedical Materials Research Part A 80:184-193.

OP058: SYNTHESIS OF NEW PYRAZOLINE DERIVATIVES AND THEIR ANTICANCER ACTIVITIES

[1]Tok, F., [2]Çevik, Ö.

[1] Marmara University, Department of Pharmaceutical Chemistry, Istanbul, Turkey, fatih.tok@marmara.edu.tr

[2] Aydin Adnan Menderes University, Department of Medicinal Biochemistry, Aydın, Turkey, drozgecevik@gmail.com

Introduction:

Cancer is the second leading cause of death worldwide, accounting for nearly 10 million deaths in 2020. Globally one out of six deaths is due to cancer. It was predicted that there were approximately 19.3 million new cancer cases in 2020. This number of cancer cases will reach approximately 30.2 million until 2040 (1, 2). There were many treatment methods such as surgery, radiation, chemotherapy, hormone therapy, immune therapy and targeted therapy. Despite the major advances in the chemotherapeutic management, the use of available chemotherapeutics is often limited mainly due to toxicities, drug interactions and emerging drug resistance (3). Therefore cancer is an important health problem that needs new bioactive molecules for effective treatment methods.

Pyrazolines, an important class of heterocyclic compounds, display numerous biological and pharmaceutical properties such as antimicrobial, analgesic, antioxidant, antidiabetic, anti-inflammatory, anticancer, antidepressant effects (4). These wide range of pharmacological activities of pyrazolines demonstrate the importance of this family of heterocyclic compounds in the area of medicinal chemistry. Different substitutions at N_1, 3rd and 5th position of the pyrazoline ring present a wide variety ofstructural pool for optimization to obtain potent bioactive molecules. Changes in pyrazoline structure offer a high degree of diversity which is useful for the development of new therapeutic agents (5). Furthermore compounds bearing a benzodioxole ring have several biological activities including anticancer, analgesic, antioxidant. The benzodioxol ring is found in many different naturally isolated compounds that have reached the clinic as anticancer agents. For example podophyllotoxin, steganacin, and combretastatin A-2 bearing benzodioxole ring show good anticancer activity (6). From the molecular design point of view, the combination of two pharmacophores into a single molecule represents one of the methods that can be adopted for the synthesis of new anticancer molecules. Therefore, we aimed that a novel series of pyrazoline derivatives bearing benzodioxole ring system were designed and synthesized. The potential anticancer effects of all synthesized compounds were investigated against HeLa, MCF-7 and NIH-3T3 cells by the MTT test.

Materials and Methods:

The new pyrazoline derivatives were synthesized in two steps. Firstly, the Claisen-Schmidt condensation reaction was carried out with a ketone bearing benzodioxole ring and aromatic aldehydes in the absence of ethanolic sodium hydroxide. Then, pyrazoline derivatives from chalcones were obtained with phenylhydrazine hydrochloride or substituted aromatic semicarbazide (Figure 1)(7).

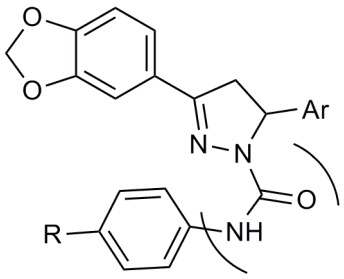

Ar: Substituted aromatic rings
R: H, Cl

Figure 1. The general structure of the synthesized compounds.

The novel pyrazoline derivatives were assayed for their *in vitro* anticancer activity on HeLa, MCF-7 cancer cells and NIH-3T3 normal cells by the MTT test (8).

Results:

All synthesized compounds were confirmed by IR, ^{1}H-NMR and elemental analysis. In the Infrared spectrum, the C=N stretching bands belonging to pyrazolines were observed 1591-1635 cm^{-1}. In the ^{1}H-NMR spectrum, the synthesis of pyrazoline rings was proved by the absence of three doublets of doublet peaks belonging to pyrazoline rings at 2.92–3.28 ppm, 3.70–3.96 ppm and 5.33–5.75 ppm, respectively. The protons belonging to the aromatic ring and the other aliphatic groups were observed with the expected chemical shift and integral values. Also, the elemental analysis of pyrazolines was in agreement with the proposed structures of the compounds. Pyrazolines bearing nitro, bromo and trifluoromethyl substituent on aromatic ring exhibited high cytotoxicity on Hela and MCF-7 cells. Furthermore, their cytotoxicity on NIH-3T3 is quite low. Especially, the compound carrying pyridine ring as an aromatic aldehyde group was found to show high cytotoxicity against HeLa and MCF-7, but lower toxicity to NIH-3T3 normal cells.

Conclusions:

In the present work, new pyrazoline derivatives containing a benzodioxole ring were synthesized and characterized. Their anticancer activities on HeLa, MCF-7 and NIH-3T3 were evaluated by the MTT test. Among these, compound carrying pyridine ring exhibited high cytotoxic effects against both HeLa and MCF-7 with high selectivity index. This molecule can be a lead compound for further anticancer investigations.

References:

1. Ferlay J, Ervik M et al. Global Cancer Observatory: Cancer Today. Lyon: International Agency for Research on Cancer; 2020 (https://gco.iarc.fr/today, accessed February 2021).
2. World Health Organisation,Cancer tomorrow, International Agency for Research on Cancer 2021, (http://gco.iarc.fr/tomorrow).
3. George RF, Fouad et al., (2016). European Journal of Medicinal Chemistry, 112: 48-59.
4. Miguel FB, Dantas et al., (2016). Spectrochimica Acta Part A: Molecular and Biomolecular Spectroscopy, 152: 318–326.

5. Nehra B, Rulhania et al., (2020). European Journal of Medicinal Chemistry, 205:112666.
6. Hawash M, Eid et al., (2020). Heterocyclic Communications, 26: 157–167.
7. Beyhan N, Koçyiğit-Kaymakçıoğlu et al., (2017). Arabian Journal of Chemistry, 10: 2073–2081.
8. Tok F, Abas et al., (2020). Bioorganic Chemistry, 102:104063.

OP059: SYNTHESIS AND STRUCTURE ELUCIDATION OF NEW FENAMATE THIOSEMICARBAZIDE*

[1,2]Coşkun, GP.

[1] Acıbadem Mehmet Ali Aydınlar University, Faculty of Pharmacy, Department of Pharmaceutical Chemistry, İstanbul, Turkey

[2] Sivas Cumhuriyet University, Faculty of Pharmacy, Department of Pharmaceutical Chemistry, Sivas, Turkey , pelin.coskun@acibadem.edu.tr

Introduction:

Thiosemicarbazide compounds have been reported to have diverse biological activities including anticonvulsant, antiviral, anti-inflammatory, antibacterial, antimycobacterial, antifungal, antioxidant and anticancer (1). Therefore, the studies about thiosemicarbazide compounds have recently gained importance and have become important compounds for macromolecules in scientists' new drug development studies in recent years (1, 2, 3). In addition to the wide variety of biological activities of these compounds, they are intermediates in the synthesis of some important heterocyclic compounds. The synthesis of biologicaly active triazoles and thiadiazoles are synthesized via thiosemicarbazide structures. The synthetic procedures of thiosemicarbazides are simple, fast and in good yields. Eventually, they create a wide study of field in medicinal chemistry. In this study, a new and original thiosemicarbazide carrying compound have been synthetized. In the synthetic procedures, microwave irridation was also used. The designed structure is further expected to have COX inhibition activity; especially more selective to COX-2, rather than COX-1.

Materials and Methods:

All chemicals were purchased from Sigma Aldrich and Merck. Melting points were taken on Thermoscientific 9300 apparatus and are uncorrected. Synthesis of the compounds were carried out in the Mikrotest instrument. Merck silica gel 60 F254 plates were used for analytical TLC. The purity of the compounds were controlled on TLC plates precoated with silica gel in a solvent system comprising of petroleum ether:ethyl acetate (50:50, v/v, t: 25°C) mixture as eluent. The spots were located under UV light (254 nm). The microwave synthesis was performed in MARS Cem device. Elemental analyses were performed on CHNS-932 (LECO) instrument. FT-IR spectra were run on Bruker FTIR-Tensor II spectrophotometer. ^{1}H-NMR, ^{13}C-NMR, DEPT and HMBC spectra were obtained on a BRUKER 300 MHz Ultrashield TM instrument (Elemental analysis and ^{1}H-NMR spectrum were performed in İnönü University Scientific and Technological Research Center).

In this study, the ester and the hydrazide derivatives of mefenamic acid are prepared (4). The thiosemicarbazide structure was obtained according to previously reported method (5) (**Figure 1**). Compounds' structure were elucidated by FT-IR and NMR (^{1}H, ^{13}C, DEPT, HMBC) spectroscopic methods and their purity were proven by TLC and elemental analysis.

Results:

The intermediate hydrazide compound was synthesized by a newly developed microwave synthesis method. For thiosemicarbazide structure; C-6; C=S and C=O carbons are not detected in ^{13}C-NMR however, the DEPT and HMBC results proved the formation of thiocarbonile. The correlation between aromatic protons and C-6, C=S and C=O carbons are also determined (**Figure 2; Table 1**).

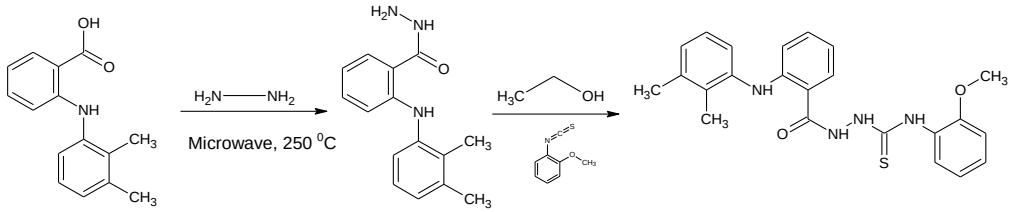

Figure 1. Synthetic route for mefenamic acid thiosemicarbazide with microwave irridation

Thiosemicarbazide compound: White solid. Yield 55%. M.p. 150-152 °C; M.W. 420.52 g/mol; Rf %: 69.23. FT-IR ν max. (cm^{-1}): 3312-3240 (N-H), 2946 (C-H), 1635 (C=O); 1590, 1513, 1491 (Ar-C=C-, C-N and N-H), 1448 (aliphatic C-H), 1350 (C-O), 1259 (C=S), 885-745 (aromatic C-H). ^{1}H-NMR (300 MHz, DMSO-d6/TMS) δ ppm: 2.11 (s, 3H, Ar-CH$_3$), 2.27 (s, 3H, Ar-CH$_3$), 3.74 (s, 3H, O-CH$_3$), 6.75-7.93 (m, 11H, Ar-H), 9.27 (s, 1H, -NH), 9.37 (bs, 1H, -CONHNHCSNH), 9.76 (bs, 1H, -CONHNHCSNH), 10.62 (bs, 1H, -CONHNHCSNH). ^{13}C-NMR (75 MHz, DMSO-d6/TMS) δ ppm: 13.52 (C-13), 20.23 (C-14), 55.66 (C-21), 111.38 (C-17), 117.73 (C-4), 116.64 (C-1), 116.64 (C-5), 119.80 (C-2), 120.30 (C-19), 125.52 (C-11), 125.90 (C-3), 128.00 (C-18), 128.00 (C-20), 129.29 (C-12), 129.82 (C-8), 133.93 (C-10), 137.78 (C-9), 139.78 (C-7), 148.00 (*C-6), 146.00 (*C=S), 153.00 (*C=O) ^{13}C-NMR DEPT (75 MHz, DMSO-d6/TMS) δ ppm: 13.52 (C-13), 20.23 (C-14), 55.66 (C-21), 111.38 (C-17), 117.73 (C-4), 116.64 (C-5), 116.64 (C-1), 119.80 (C-2), 120.30 (C-19), 125.52 (C-11), 125.90 (C-3), 128.00 (C-18), 128.00 (C-20), 129.29 (C-12), 133.93 (C-10), 137.78 (C-9), 138.78 (C-7), 140.00 (C-6), 146 (*C=S), 153 (*C=O). **These carbons are observed in HMBC spectrum.*

HMBC results for thiosemicarbazide compound

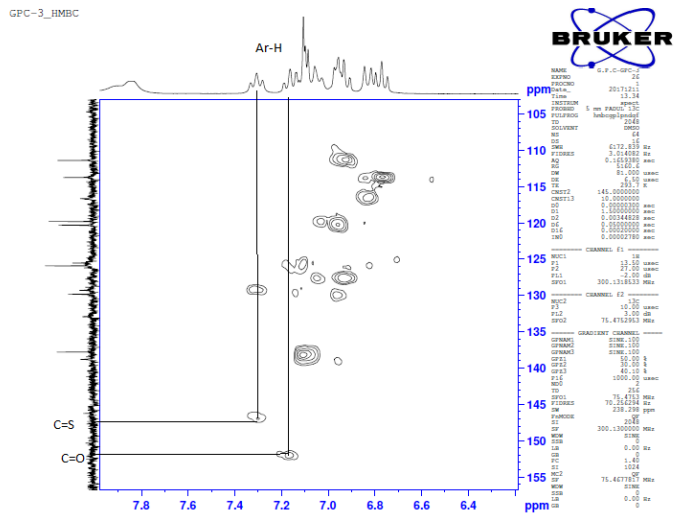

Figure 2. C=O and C=S interactions for thiosemicarbazide compound

The certain contours and the interactions of the atoms are shown in **Table 1**

Table 1. The ^{1}H-^{13}C interactions of thiosemiczarbazide compound

^{1}H	^{13}C
H-13	C-10, C-9, C-13
H-14	C-11, C-10, C-9, C-14
Ar-H	C=S
Ar-H	C=O

Conclusions:

The diverse biological activities of thiosemicarbazide compounds is a key point in designing and developing new drug canditate molecules carrying thiosemicarbazide functionality. Here in this study, the formation of thiosemicarbazide function starting from a non-steroidal anti-inflammatory drug is shown. Following the synthesis of other derivatives, the further biological activity studies will be performed for the novel drug candidate compounds.

Acknowledgement

* This study was supported by a grant of CUBAP (Cumhuriyet University Scientific Research Unit) (ECZ039)

References:

1. Küçükgüzel ŞG, Coşkun GP. (2016). Macromolecular Drug Targets in Cancer Treatment and Thiosemicarbazides as Anticancer Agents. Anticancer Agents Med Chem, 16(10):1288-300.
2. Çıkla P, Arora P, Basu A, Talele TT, Kaushik-Basu N, Küçükgüzel ŞG. (2013). Etodolac Thiosemicarbazides: a novel class of hepatitis C virus NS5B polymerase inhibitors. Marmara Pharm J, 17: 138-146.
3. Dadaş Y, Coşkun GP, Bingöl-Özakpınar Ö, Özsavcı D, Küçükgüzel ŞG. (2015). Synthesis and Anticancer Activity of Some Novel Tolmetin Thiosemicarbazides. Marmara Pharm J,19: 259-267.
4. Reddy LV, Suman A, Beevi SS, Mangamoori LN, Mukkanti K, Pal S. (2010). Design and Synthesis of 1-Aroyl-2-ylidene Hydrazines under Conventional and Microwave Irradiation Conditions and their Cytotoxic Activities. J Braz Chem Soc, 21(1):98-104.
5. Coşkun GP, Djikic T, Hayal TB, Türkel N, Yelekçi K, Şahin F, Ş. Güniz Küçükgüzel ŞG. (2018). Synthesis, Molecular Docking and Anticancer Activity of Diflunisal Derivatives as Cyclooxygenase Enzyme Inhibitors. Molecules, 23(8), 1969.

OP061: SYNTHESIS OF NOVEL HYDRAZONE DERIVATIVES AND EVALUATION OF THEIR INHIBITORY ACTIVITIES AGAINST MONOAMINE OXIDASES AND β-SECRETASE

Sellitepe, H.E., Aksel, A.B.

Karadeniz Technical University, Faculty of Pharmacy, Department of Pharmaceutical Chemistry, Trabzon, Turkey

Introduction:

Dementia is a serious disease that predominantly affects aging patients, especially the elderly population. Alzheimer's disease (AD) is one of the most common causes of dementia and is related to the loss of cognitive functions. Although the mechanism of AD pathogenesis is not fully understood, AD is principally caused by low acetylcholine (ACh) levels, oxidative stress, and β-amyloid plaque deposits (1). AD is associated with decreases in neurotransmitters, particularly ACh, and significant increases in acetylcholinesterase (AChE) and butyrylcholinesterase (BChE) levels (2). In addition, monoamine oxidase (MAO) is responsible for the oxidative deamination of endogenous amines such as serotonin, epinephrine, and other neurotransmitters (3). The amount of MAO increases with aging and neuronal damage, suggesting that MAO inhibition could be effective in treating AD. Importantly, oxidative stress, associated with free radicals and tissue damage, creates an obstacle in the repair of cognitive functions (4). On the other hand, β-secretase (β-site amyloid precursor protein cleaving enzyme 1, BACE-1) is a protease that catalyzes the production and deposition of amyloid-β peptide, and it has been considered a promising target for the treatment of AD (5).

In this study, hydrazide derivatives of ethyl paraben were synthesized in reactions with various benzaldehydes, resulting in 19 tosylated acyl hydrazide derivatives (**3a**–**t**), and their potential biological activities were evaluated by analyzing their inhibitory activities against MAOs, AChE, BChE, and BACE-1 enzymes, as well as their antioxidant activities.

Materials and Methods:

Compounds were synthesized starting from ethyl paraben hydrazide. Then, by the reaction of this compound with various benzaldehydes, hydrazide hydrazone derivatives were obtained. By the reaction of these compounds with tosyl chloride, new tosylated acyl hydrazide derivatives were obtained from **3a** to **3t** (Figure). Structures of the compounds were confirmed via spectroscopic methods.

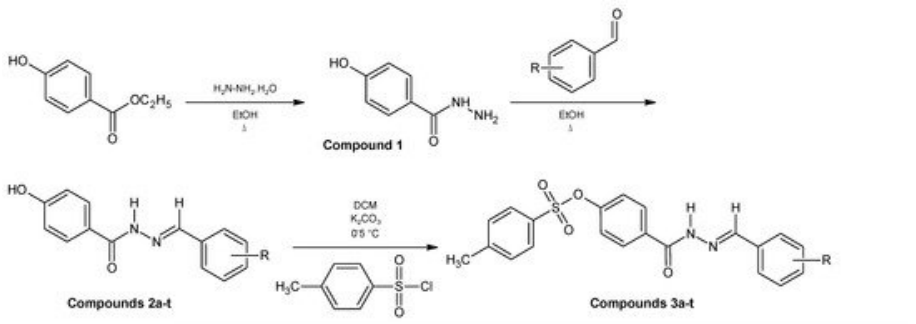

	R		R		R		R
3a	-H	**3f**	3-OCH_3	**3k**	2-Cl	**3p**	4-F
3b	2-CH_3	**3g**	4-OCH_3	**3l**	3-Cl	**3r**	2-NO_2
3c	3-CH_3	**3h**	2-Br	**3m**	4-Cl	**3s**	3-NO_2
3d	4-CH_3	**3i**	3-Br	**3n**	2-F	**3t**	4-NO_2
3e	2-OCH_3	**3j**	4-Br	**3o**	3-F		

Figure. Synthesis of compounds **3a**–**t**.

MAO (6) and BACE-1 (7) activities were evaluated according to the literature. Reversibility and kinetic studies were performed on the most potent inhibitors, i.e., **3o** for MAO-A and **3s** for MAO-B, as previously described (8).

Results:

Among the 19 derivatives, four and three compounds showed effective inhibitory activities against MAO-A and MAO-B, respectively, with residual activities of <50% at 10 μM. Compound **3o** was the most potent inhibitor of MAO-A, with an IC_{50} value of 1.54 μM, followed by **3a** and **3p** (IC_{50} = 3.35 and 4.77 μM, respectively). Compound **3s** was the most potent inhibitor of MAO-B, with an IC_{50} value of 3.64 μM, followed by **3t** and **3a** (IC_{50} = 5.69 and 7.69 μM, respectively). The selectivity index (SI) values of **3s** and **3a** for MAO-B over MAO-A were 4.31 and 0.44, respectively, indicating that **3s** and **3a** are moderately selective for MAO-B and MAO-A, respectively.

In kinetic studies of MAO-A inhibition by **3o**, Lineweaver–Burk plots and secondary plots showed that **3o** competitively inhibited MAO-A with a K_i value of 0.35 ± 0.074 μM. In kinetic studies of MAO-B inhibition by **3s**, Lineweaver–Burk plots and secondary plots showed that **3s** competitively inhibited MAO-B, with a K_i value of 1.97 ± 0.65 μM). These results suggest that **3o** and **3s** are competitive inhibitors for MAO-A and MAO-B, respectively, and compete with the substrate for the active site.

Interestingly, **3e**, **3f**, and **3n** inhibited BACE-1 with IC_{50} values of 8.63, 9.92, and 8.47 μM, respectively, which were lower than the IC_{50} of the quercetin reference. BACE-1 inhibitors have been studied as pharmaceuticals, and some of them have been submitted to phase I–III clinical trials (9).

Conclusions:

It is concluded that **3o** and **3s** are effective MAO-A and MAO-B inhibitors, respectively, and **3e**, **3f**, and **3n** are effective BACE-1 inhibitors. These results suggest that these compounds can be considered potential agents for the treatment of AD.

Acknowledgments

This study was supported by the National Research Foundation of Korea (NRF) grant funded by the Korean government (NRF-2019R1A2C1088967), Republic of Korea, Taif University Researchers Supporting Project (No. TURSP-2020/68 to A. Khames), Saudi Arabia and Scientific Research Projects Coordination Unit of Karadeniz Technical University (Project Number: FLO-2019-7883), Turkey.

References:

1. Cao Z, Song Q, Yu G, Liu Z, Cong S, Tan Z, Deng Y (2021). Bioorganic & Medicinal Chemistry, 35:116074.
2. Lane RM, Potkin SG, Enz A (2006). International Journal of Neuropsychopharmac, 9:101–124.
3. Ege T. Şelimen H (2021). JOTCSA, 8:239–248.
4. Sadaoui N, Bec N, Barragan-Montero V, Kadri N, Cuisinier F, Larroque C, Arab K, Khettal B (2018). Fitoterapia, 130:1–5.
5. Ghosh AK. Osswald HL (2014). Chemical Society Reviews, 43:6765–6813.
6. Oh JM, Jang HJ, Kim WJ, Kang MG, Baek SC, Lee JP, Park D, Oh SR, Kim H (2020). International Journal of Biological Macromolecules, 151:441–448.
7. Jeong GS, Kang MG, Han SA, Noh JI, Park JE, Nam SJ, Park D, Yee ST, Kim H (2021). Journal of Fungi, 7:84.
8. Oh JM, Kang MG, Hong A, Park JE, Kim SH, Lee JP, Baek SC, Park D, Nam SJ, Cho ML, et al. (2019). International Journal of Biological Macromolecules, 137:426–432.
9. Mirand, A, Montiel E, Ulrich H, Paz, C (2021). Journal of Alzheimer's Disease, 81(1): 1-17.

OP062: LIPASE INHIBITOR ACTIVITY AND MOLECULAR MODELLING STUDIES OF NEW PYRIDAZINONE DERIVATIVES

[1]Alagöz, M.A., **[2]Doğan, İ.S.**, [3] Şener, S.Ö., [1]Özdemir, Z.

[1] Inonu University, Department of, Malatya, Turkey, mehmet.alago@inonu Pharmaceutical Chemistry.edu.tr

[2] Karadeniz Technical University, Department of Pharmaceutical Chemistry, Trabzon, Turkey, selinci@gmail.com

[3] Karadeniz Technical University, Department of Pharmacognosy, Trabzon, Turkey, silashener@ktu.edu.tr

Introduction:

Lipids play diverse and important biological roles. Altering the levels of specific lipid species through activating or inactivating their biosynthetic or degradative pathways has been shown to provide either therapeutic benefit or cause disease. Lipases play critical roles in human health and disease (1). The conserved biochemistry across this enzyme class, coupled with certain chemical scaffolds that target serine hydrolases, has enabled the development of inhibitors against many lipases.

Pyridazinone derivatives have been claimed to possess such interesting bioactivity (2). In this context, five pyridazinone derivative compounds **1-5** were synthesized (Scheme 1) and their lipase inhibitory effects were determined. Binding modes of the synthesized compounds to lipase enzyme as well as the key interactions in their active sites were determined via molecular docking simulations. Structure-activity relationships were established upon comparison of the results from the in vitro enzyme inhibition and molecular docking studies.

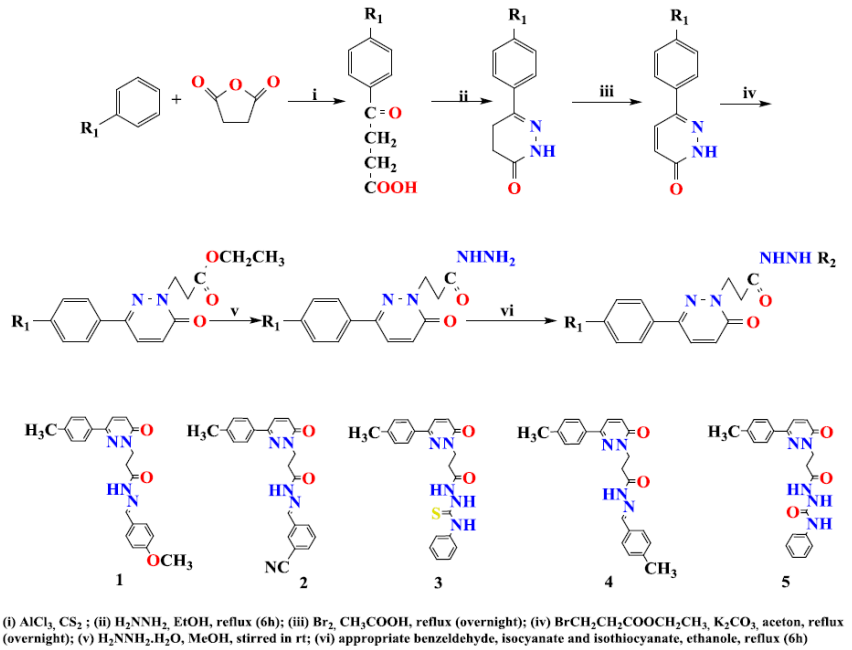

(i) $AlCl_3$, CS_2 ; (ii) H_2NNH_2, EtOH, reflux (6h); (iii) Br_2, CH_3COOH, reflux (overnight); (iv) $BrCH_2CH_2COOCH_2CH_3$, K_2CO_3, aceton, reflux (overnight); (v) $H_2NNH_2.H_2O$, MeOH, stirred in rt; (vi) appropriate benzeldehyde, isocyanate and isothiocyanate, ethanole, reflux (6h)

Scheme 1. Synthesis of compounds **1-5**

Materials and Methods:

Chemistry

All the chemicals used in this study were purchased from Aldrich, Fluka AG and E. Merck. 4-oxo-4-phenylbutanoic acid, 6-substitutedphenyl-4,5-dihydropyridazin-3(2*H*)-one, 6-(4-substitutedphenyl)pyridazin-3(2*H*)-one, ethyl 6-(4-substitutedphenyl)pyridazin-3(2*H*)-one-2-yl propionate and 6-(4-substitutedphenyl)pyridazin-3(2*H*)-one-2-yl propiohydrazide were synthesized according to literature methods.

All title compounds were synthesized in this study as in literature methods according to the as shown in Scheme 1 (3). The progress of reaction was monitored by TLC with Merck Kieselgel F254 plates. Melting points were determined on Electrothermal 9200 melting points apparatus and the values were given uncorrected. The structures of these pyridazinone derivatives were confirmed by their 1H-NMR, 13C-NMR, mass and elemental analysis spectra.

(*E*)-*N*'-(4-methoxybenzylidene)-3-(6-oxo-3-(p-tolyl)pyridazin-1(6*H*)-yl)propanehydrazide (Compound 1)

White crystals; yield: 70 %; mp: 278-80°C; ^{1}H-NMR (DMSO-d_6, 300 MHz): δ (ppm) 2.32 (3H; s; -CH_3), 2.77 (2H; t; -N-CH_2-CH_2-C=O), 3.18 (2H; t; -N-CH_2-CH_2-C=O), 3.83 (3H; s; -OCH_3) 6.97 (1H; d; pyridazinone H^5), 7.0 (1H; d; pyridazinone H^4), 7.05-8.02 (8H; m; phenyl protons), 9.98 (1H; s; -N=CH-) and 11.42, 11.56 (1H; s; -NH-N). ^{13}C-NMR (DMSO-d_6, 300 MHz), δ 20.76 (1C; -CH_3), 30.65 (1C; -N-$CH_2$$CH_2$-C=O), 47.01 (1C; -N-$CH_2$$CH_2$-C=O), 55.07 (1C; -$OCH_3$), 111.07 (1C; 4-methoxyphenyl C^2), 112.89 (1C; 4-methoxyphenyl C^3), 120.94 (1C; 4-methoxyphenyl C^6), 122.44 (1C; 3-methoxyphenyl C^5), 125.62 (1C; =CH), 129.36-130.45 (4C; 4-methylphenyl $C^{2,3,5,6}$), 135.55 (1C; 4-methylphenyl C^1), 138.84 (1C; 4-methoxyphenyl C^1), 142.71 (1C; 4-methylphenyl C^1), 143.22 (1C; pyridazinone C^5), 146.02 (1C; pyridazinone C^6), 158.79 (1C; pyridazinone C^4), 159.45 (1C; 4-methoxyphenyl C^4), 166.39 (1C; CH_2-N-C=O), 172.15 (1C; pyridazinone C^3). $C_{22}H_{22}N_4O_3MS$ (ESI+) calculated: 391.1770, Found: *m/e* 392.2 (M+H; % 100.0).

Biological Activity (Lipase Inhibitory Effect Assay)

Synthesized compounds were evaluated for porcine pancreatic lipase type II (PLL) (EC 3.1.1.3) inhibitory assay by the modified medhod used p-nitrophenyl butyrate (CAS: 2635-84-9) as substrate (4). Compounds and orlistat used as positive control was preapared the range of 6.25, 12.5, 25, 50 and 100 µg/mL concentrations. The percentage of PLL inhibitory effect was calculated using the following equation:

$$\text{PLL Inhibition (\%)} = [[(A-B)-(C-D)]/(A-B)]*100$$

where A is the absorbance in the presence of substrate (control), B is the absorbance without the substrate and compound (blank), C is the absorbance in the presence of substrate and compound (experimental group), and D is the absorbance in the presence of compound (blank of C). Afterwards, the half maximal inhibitory concentration (IC50) values of pridazinone derivatives for PLL were calculated graphically (Figure 1).

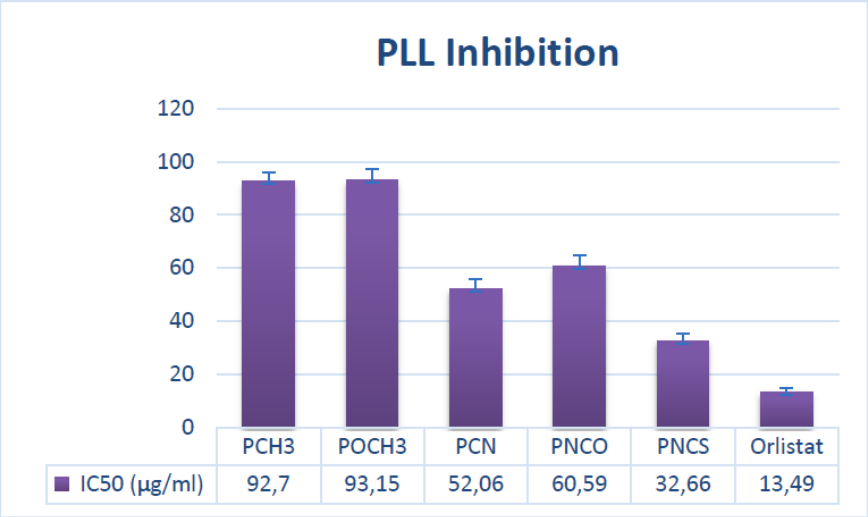

Figure 1. PLL inhibition graphics of synthesized compounds **1-5**.

Molecular Modelling Studies

Molecular docking studies were performed by using Maestro 11.8 (Schrödinger, LLC, NY) molecular modeling software. Three-dimensional structures of compounds were constituted with Maestro11.8 software with the aid of MacroModel software and the OPLS_2005 force field parameters, and were optimized by conjugated gradient method (5). The structure of lipase complex obtained from sus scrofa (PDB ID: 1ETH) retrieved from RCSB (www.rcsb. Org).

Results:

PLL inhibition of synthesized compounds was evaluated against orlistat, is an inhibitor of pancreatic and other lipases. As a result of molecular modeling studies, the docking scores of orlistat and synthesized compounds were calculated and their interactions with the residues in the enzyme active region were examined.

Three of compounds **3**,**4** and **5** show inhibitor activity. Compound **1** and compound **2** did not show inhibitor activity (Figure 2 and Table 1).

Figure 2. Structure of synthesized compounds

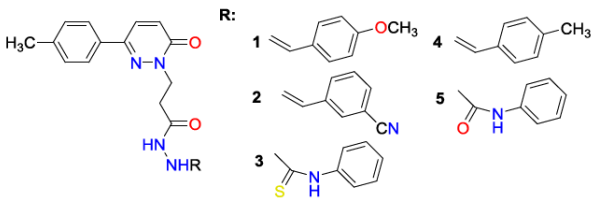

Table 1. PLL inhibition of synthesized compounds **1-5**

Compounds	PLL Inhibition* (IC_{50} (µg/ml) ± SD**)
1	92,70±3,2231
2	93,15±4,2592
3	52,06±3,7526
4	60,59±4,3285
5	32,66±2,8265
Orlistat	13,49±1,2262

*Porcrine pancreatic lipase **Standard deviation

Conclusions:

Compound **3** (**1-(3-(6-oxo-3-*p*-tolylpyridazin-1(6*H*)-yl)propanoyl)-4-phenylthiosemicarbazide)** was found as most active compound by inhibiting at 32.66±2.8265 µg/ml dose. While semicarbazite (compound **5**) coming after thiosemicarbazite (compound **3**) in the activity ranking shows the importance of sulfur in activity; the nitrile, methyl and methoxy sequences (compounds **2,4,1**) of the substituents in *N*-benzilidenhydrazide derivatives show that electron withdrawing groups are important for activity.

Docking scores and activity results are in harmony. Orlistat has been shown to have similar interactions with the most active compound **5**.

References:

1. Tang QJ, Zhang L, Zheng J, Song J, Chen X, Cao W, Xue C, He X, Ma M, Zhao Y. (2021). Food & Functions, DOI:10.1039/D0FO03366A.
2. Dubey S, Bhosle PA. (2015). Medicinal Chemistry Research, 24:3579-3598.
3. Bozbey İ, Özdemir Z, Uslu H, Özçelik AB, Şenol FS, Erdoğan Orhan İ, Uysal M. (2020). Mini Reviews in Medicinal Chemistry, 20:1042.
4. Sridhar SNC, Bhurta D, Kantiwal D, George G, Monga V, Paul AT. (2017). Bioorganic Medicinal Chemistry Letters 27:3749-3754.
5. Doğan, I.S., Saraç, S., Sari, S., Kart, D., Gökhan, Ş., Vural, I., Dalkara, S., 2017. New azole derivatives showing antimicrobial effects and their mechanism of antifungal activity by molecular modeling studiesEur. Med. Chem. 130: 124-138.

OP063: SYNTHESIS AND HUMAN CARBONIC ANHYDRASE INHIBITION STUDIES OF SOME 1,3,4-THIADIAZOLES

[1]Demir-Yazıcı, K., [1]Güzel-Akdemir, Ö.

[1] Istanbul University, Department of Pharmaceutical Chemistry, Istanbul, Turkey

kubra.demir@istanbul.edu.tr, oguzel@istanbul.edu.tr

Introduction:

Human carbonic anhydrases (hCAs) belong to carbonic anhydrases (CAs; EC 4.2.1.1), a ubiquitous family of zinc-included metalloenzyme which catalyzes the reversible conversion of carbon dioxide (CO_2) to bicarbonate (HCO^-) and a proton (H^+).

$$CO_2 + H_2O \longrightarrow HCO^- + H^+$$

hCAs are members of the α-subfamily of CAs and divided into 15 different isoforms (hCA I-XV). Cytosolic isoforms hCA I and II are widespread in the human body while transmembrane isoforms hCA IX and XII are located especially in hypoxic tumour cells, hence also called tumour-related hCA isoforms. Studies for discovering of hCA XI/XII targeted and hCA I/II off-targeted new molecules as a selective carbonic anhydrase inhibitors (CAIs) presents a new approach for anticancer chemotherapy (1-2). To this aim, thirteen new sulfonamido-indole linked 1,3,4-thiadiazole derivatives were prepared (**1**-**12**) and tested with enzyme inhibition assays for their inhibitory activity against four hCA isoforms (hCA I/II and hCA IX/XII).

Materials and Methods:

After the synthesis of the thiosemicarbazide derivatives of 3-phenyl-5-sulfonamido-1*H*-indole-2-carbohydrazide, lead compound (3), with suitable isothiocyanates, new 1,3,4-thiadiazoles (**1**-**12**, Figure 1) were obtained by cyclization in an acidic medium. Crude products were purified with crystallization with ethanol and characterized with spectral and analytical methods (IR, ^{1}H-NMR, ^{13}C-NMR, and elemental analyses). For enzyme inhibition studies a stopped-flow CO_2 hydrase assay was used (4).

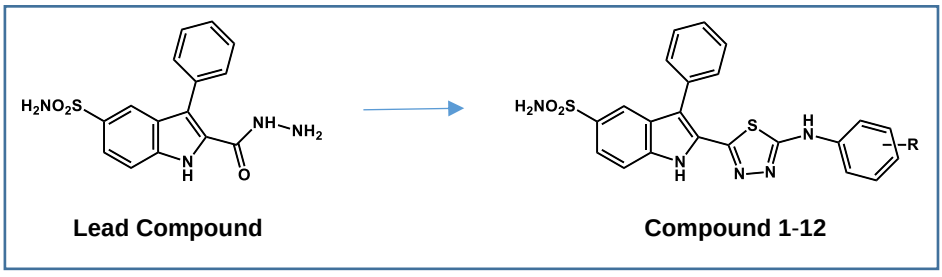

Figure 1. General formula of "**Lead Compound**" and new compounds "**1**-**12**"

Results:

Cyclization of thiosemicarbazide derivatives was proven by spectral and analytical analyses. Enzyme inhibition assays revealed that all new compounds showed selectivity against off-targeted isoforms hCA I/II and very good inhibitory activity against tumour-releated hCA IX/XII at nanomolar level.

Among the newly synthesized 1,3,4-thiadiazole derivatives, four of them have the inhibition value lower than 100 nM (nanomol) against tumour-releated isoforms hCA IX, and all of twelve molecules have the similar feature for hCA XII. One of the molecules were detected as the best inhibitor against hCA IX with the inhibition value lower than 30 nm. Besides, four derivatives showed also very potent inhibitory activity against hCA XII, another tumour-associated isoform with the inhibition value lower than or equal to 30 nm.

Enzyme inhibition studies revealed that the new compounds showed higher selectivity against hCA XII compared to hCA IX. In addition, synthesized 1,3,4-thiadiazole derivatives showed excellent selectivity against targeted tumour releated isoforms hCA XI /XII up to ~ 300 fold over the most abundant isoforms CA I and CAII.

Conclusions:

Three of twelve successfully synthesized and characterized compounds showed K_i values lower than 30 nM against hCA IX or XII with high selectivity ratios over hCA I and II. This study may lead to further development of new thiadiazole derivatives as potent CAIs, as a new anticancer candidates.

Acknowledgements

This study was supported by IU Scientific Research Projects Department (TDK-2018-32263).

References:

1. Supuran, CT (2008). Nature Reviews Drug Discovery, 7:168-181.
2. Demir-Yazıcı et al., (2019). International Journal of Molecular Science, 20:2354.
3. Ergenç et al., (1990)., Die Pharmazie, 45:346-347.
4. Khalifah, RG (1971). Journal of Biological Chemistry, 246:2561-2573.

OP068: MANDELIC ACID-BASED NOVEL SPIROTHIAZOLIDINONES: SYNTHESIS, ANTIMYCOBACTERIAL ACTIVITY AND MOLECULAR MODELLING STUDIES

[1]Trawally, M., [1]Demir-Yazıcı, K., [2,3]Dingiş-Birgül, S.I., [2]Akdemir, A., [1]Güzel-Akdemir, Ö.

[1] Istanbul University, Department of Pharmaceutical Chemistry, Istanbul, Turkey

[2] Bezmialem Vakif University, Department of Pharmacology, Computer-Aided Drug Discovery Laboratory, Istanbul, Turkey

[3] Marmara University, Department of Pharmaceutical Chemistry, Istanbul, Turkey

Introduction:

Tuberculosis (TB), an airborne infectious disease caused by *Mycobacterium Tuberculosis*, is one of the leading death-causing diseases. Experts have declared TB as a global emergency threat and the dire need to combat it. According to the WHO, more than 10 million people were diagnosed with TB and 1.2 million died of it (1). Together with the rapid development of resistance in *M. Tuberculosis*, the long duration of the antitubercular regimen has born the necessity to develop new drugs with a shorter duration of therapy to effectively treat tuberculosis and counteract resistance(2).

Enoyl-[acyl-carrier-protein]-reductase (*Mt*InhA), a target of activated isoniazid, is an NADPH-dependent enzyme lacking in humans and catalyzes the essential step of fatty acid elongation in the biosynthesis of mycolic acid responsible for the virulence of *M. Tuberculosis.* Therefore, targeting *Mt*InhA is one of the most applied methods in the development of antitubercular agents(3).

1,3-thiazolidin-4-one is an intriguing heterocyclic scaffold that affords a wide range of biological activities including antimycobacterial activity(4). Some spirothiazolidinone compounds previously synthesized by Güzel-Akdemir and co-workers inhibited *M. tuberculosis* at low micromolar concentrations (5).

This study is focused on the synthesis and biological assessment of novel mandelic acid-based spirothiazolidinone derivates (figure 1) against *M. tuberculosis,* and the docking studies followed by 50 ns molecular dynamic simulations of the most potent compound to determine whether it exerts its antimycobacterial activity by inhibiting the *Mt*InhA enzyme.

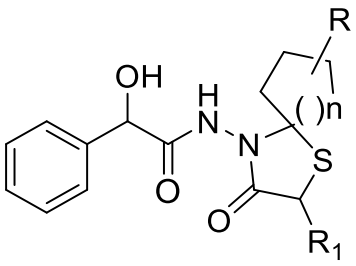

2,3

2a) R= H, R_1=H, n=1
2b) R= 8-CH_3, R_1=H, n=2
2c) R=C_6H_5 , R_1=H, n=2
3a) R= H, R_1=CH_3, n=1
3b) R= 8-CH_3, R_1=CH_3, n=2
3c) R= 8-C_6H_5, R_1=CH_3, n=2

Figure 3

Materials and Methods:

The compounds were prepared from a one-pot sequential reaction of mandelhydrazide, a cyclic ketone and thioglycolic acid/thiolactic acid (Scheme 1). The reaction was heated under reflux with the help of a Dean-Stark trap for 6 hours. Pure compounds obtained were characterized by spectral analyses. The antimycobacterial activity was conducted using MABA and BACTEC 460 radiometric systems. Molecular modeling studies which include docking and molecular dynamic simulations were carried out with MOE, LeadIT, and Schrödinger software packages. Three crystal structures of *Mt*InhA were obtained from the protein data bank (PDB: 4bqp, 4tzk and 4bge), prepared using the 3D protonation module in MOE and eventually energy-minimized with the force field AMBER14:EHT. Flexx docking tool was used to perform the docking calculation. Docked poses were analyzed and subjected to further energy minimization and rescoring with GBVI/WSA force field. To test the stability of the selected poses, a 50 ns molecular dynamics simulation was performed using the Desmond tool of the Schrödinger software package.

Results:

Compound 3c showed growth inhibition of 98% at 6.25 µg/mL and molecular modeling studies of this compound suggested that it may bind to the apo form of *Mt*InhA enzyme (Figure 2).

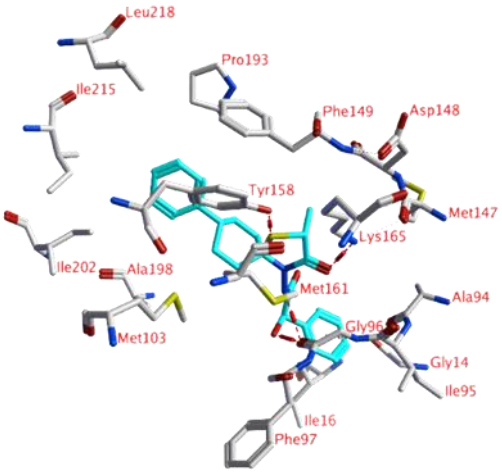

Figure 4. The docked pose of compound 3c in the active site of the apo form 4BGE

Conclusions:

The desired compounds were successfully prepared using a one-pot reaction. The modeling results indicate that the active compounds may bind to the apo form of *Mt*InhA which is a validated target for antimycobacterial drugs.

References:

1. World Health Organization (2020). Available from: http://apps.who.int/bookorders.
2. Tiberi S, Muñoz-Torrico M (2018). Pulmonology, 24:86–98.
3. Martinelli LKB, Rotta M, et al., (2017) Scientific Reports, 7:46696.
4. Nirwan S, Chahal V, et al., (2019). Journal of Heterocyclic Chemistry, 56:1239–53.
5. Güzel-Akdemir Ö, Trawally M, et al (2020), Monatshefte für Chemie ,151:1443-1452.

OP070: DESIGN SYNTHESIS AND IN VITRO BIOLOGICAL ACTIVITIES OF NEW 6,8,9-TRISUBSTITUTED PURINE DERIVATIVES AS PROMISING HSPs INHIBITORS

[1]Kul, P., [1]Tuncbilek, M., [2]Ergul, M., [3]Yenilmez Tunoglu, EN., [4]Tutar, Y.

[1] Ankara University, Department of Pharmaceutical Chemistry, Ankara, Turkey, pkul@ankara.edu.tr, tuncbile@pharmacy.ankara.edu.tr

[2] Sivas Cumhuriyet University, Department of Biochemistry, Erzurum, Turkey mergul@cumhuriyet.edu.tr

[3] University of Health Sciences, Department of Biochemistry, Istanbul, Turkey, nurdanyenilmez@gmail.com

[4] University of Health Sciences, Division on Molecular Oncology, Istanbul, Turkey, yusuf.tutar@sbu.edu.tr

Introduction:

The purine ring forms the basic structure of vital importance biological compounds such as nucleic acids. The use of purine derivatives, precursors of nucleic acids, as antimetabolite chemotherapeutic agents in cancer treatment begins with the idea that nucleic acids have significant roles of cellular proliferation. Instead of treatment with non-selective compounds that show cytotoxic activity by inhibiting the growth of healthy cells as well as cancer cells, treatment with specific inhibition of the targeted molecules known to be associated with cancer disease is preferred (1). Targeting Hsps is an exciting mechanism due to their overexpression in cancer cells and their part on carcinogenesis through proliferation, differentiation, migration and metastasis (2-3). Heat shock proteins (HSPs) are a large family of highly conserved molecular chaperone that are synthesized by cell in response to various stress conditions, especially heat. HSPs protect cells against stress and cell damage by protecting client proteins from degradation, hypoxia, oxidative and thermal stress. HSPs are classified according to their molecular weight. Particularly Hsp70 and Hsp90 subfamilies are observed in cancer cells with highly abnormal amounts (4-5). The overexpression of Hsp70 has been noticed especially in breast, prostate, lung, ovarian, oral, colorectal, hepatocellular carcinoma cells and melanoma. These proteins have anti-apoptotic features explained by more than one mechanism such as; regulating apoptosis by inhibiting stress-induced signals, by preventing mitochondrial membrane permeabilization, and by suppressing caspase activation and DNA fragmentation. Hsp70 also plays role in senescence through effects on the p53-p21 pathway. There is currently no FDA-approved effective drug targeting Hsp70. VER-155008 (Fig. 1) is a purine structure Hsp70 inhibitor that induces apoptosis in BT474 human breast cell line and also induces the Hsp90 substrate protein degradation in HCT116 and BT474 cell lines. The adenosine part of the compound interacts to Hsp70/Bag-1 ATPase domain. (6-7). There are several purine Hsp90 inhibitors such as PU3, PU24FCl, BIIB021 and PU-H71 (Fig. 1). PU3 prevents the cell proliferation in G1 phase in breast cancer cells. PU24FCl is more effective than PU3 but the bioavailability of this compound is also low. BIIB021 induces apoptosis on several tumor cell lines and has good bioavailability. It demonstrates good cytotoxic activity in ESCC cells by regulating the increased apoptotic cells. PU-H71 is another Hsp90 inhibitors which evaluated by Phase I clinical trials in solid tumors and lymphoma (8).

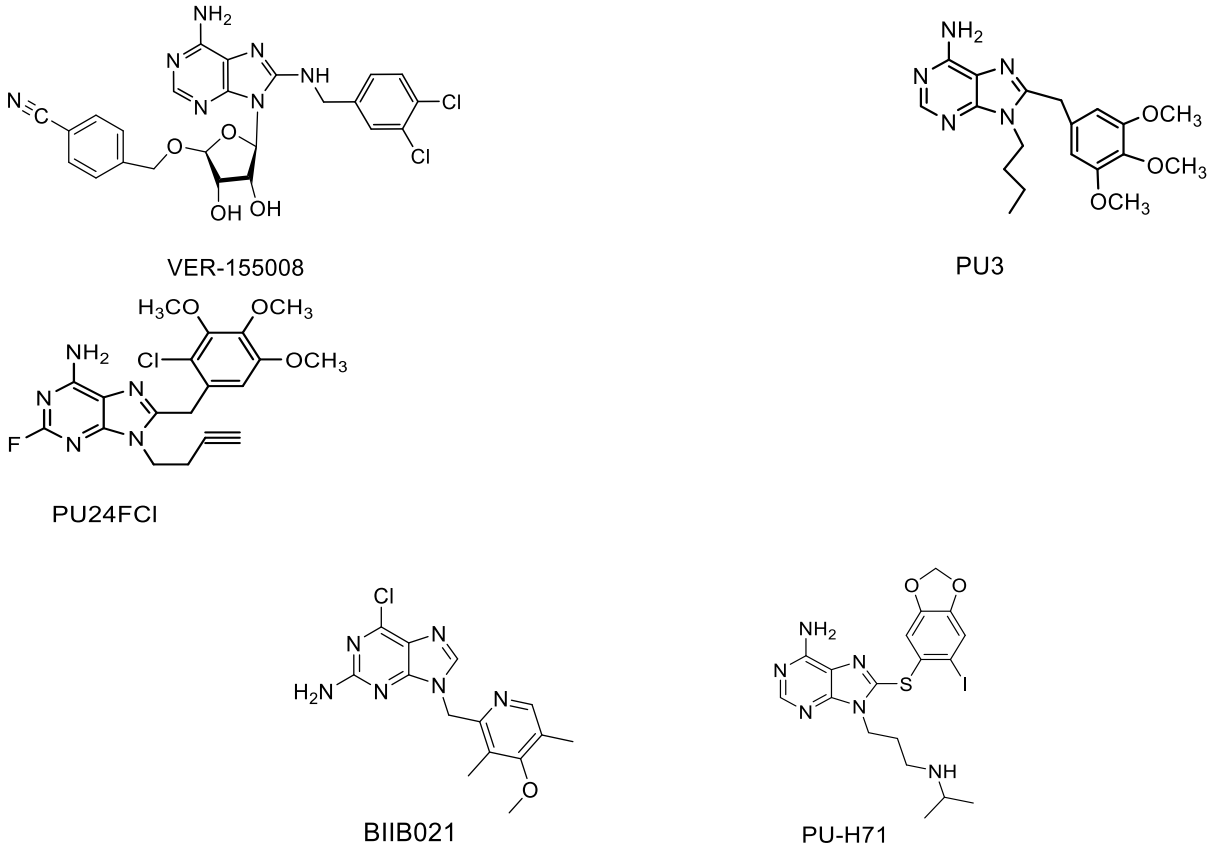

Figure 1. The structures of several Hsp70 and Hsp90 inhibitors

As we mentioned above, many HSPs inhibitors are synthesized and some of them are evaluated for clinical trials, yet there is no FDA approved drug. Considering the synthesized inhibitors; we design, synthesize new 6,8,9-trisubstituted purine analogues and elucidate their biological activities on selected cancer cell lines and perform molecular docking studies on Hsp70 and Hsp90 to find out predicted binding conformation.

Materials and Methods:

The 6,8,9-trisubstituted purine derivatives were readily obtained from commercially available 4,6-dichloro-5-nitro pyrimidine in four steps. The cytotoxicity of this newly synthesized compounds were screened by the XTT cell viability test on breast (MCF7), liver (HepG2), prostate (PC3) and leukemia (K562) cell lines in comparision with the nucleoside analogue Fludarabine *in vitro*. To predict the linkage of the synthesized compounds to the ATPase and SBD domains of HSPs, molecular docking studies were performed using PyRx.

Results:

Among the synthesized 6,8,9-trisubstituted purine compounds, **12** and **15** showed 89% cell viability on MCF7 cell line. Molecular docking results showed that all compounds bind to Hsp70 ATP binding pocket between -8.5 and -10.8 kcal/mol; Hsp70 substrate binding site between -6.5 and -7.6 kcal/mol; Hsp90α between -7.6 and -8.7 kcal/mol; Hsp90β between -8.6 and -9.8 kcal/mol binding energies. Particularly, compound **14** binds to Hsp70 ATP binding site and compound **15** binds to Hsp90 α and 90β with high affinity and good binding energies (Fig. 2)

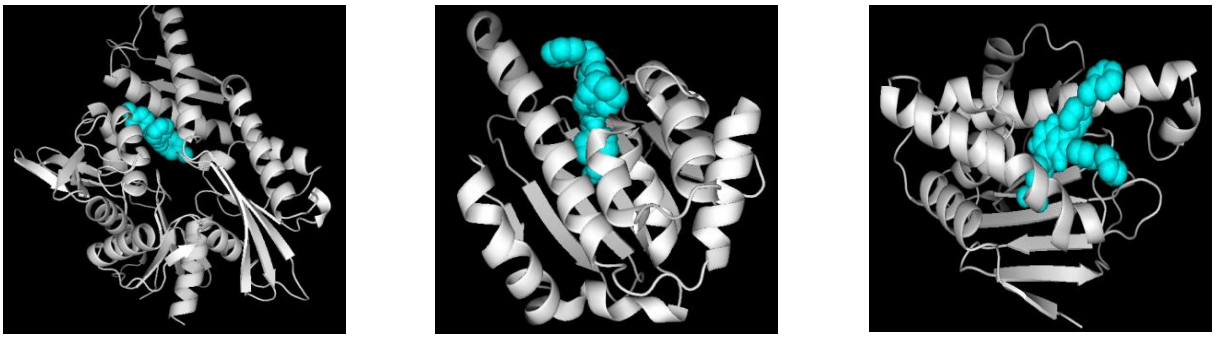

(a) (b) (c)

Figure 2. (a) Interaction between **14** and Hsp70 ATP binding pocket (b) Interaction between **15** and Hsp90α (c) Interaction between **15** and Hsp90β

Conclusions:

Novel purines were prepared and their cytotoxic activities identified. Considering the binding attitudes of the synthesized derivatives in the selected proteins and their binding energies, it is thought that the common skeleton of the compounds can be determined and potential main structure for anticancer drugs in our further studies.

Acknowledgements

Central Laboratory of Pharmacy, Faculty of Ankara University provided support for acquisition of the NMR and mass spectrometer used in this work.

References:

1. Lind MJ., (2020). Medicine. 48(2):90-96.
2. Lianos GD., Alexiou GA., et al. (2015). Cancer Letters, 360(2):114-118.
3. Yun CW., Kim HJ. et al. (2019). Cells, 9(1):60.
4. Chatterjee, S. & Burns, TF. (2017). International Journal of Molecular Sciences, 18(9):1978.
5. Wu, J., Liu, T., et al. (2017). Trends in Pharmacological Sciences, 38(3), 226–256.
6. Elmallah, M. I. Y., Cordonnier, M., et al. (2020). Cancer Letters, 469, 134–141.
7. Massey, A. J., Williamson, D. S., et. al.(2010). Cancer Chemotherapy and Pharmacology, 66(3), 535–545.
8. Taldone, T., & Chiosis, G. (2009). Current Topics in Medicinal Chemistry, 9(15), 1436–1446.

OP071: IDENTIFICATION OF A POTENT INDOLE N-OXIDE DERIVATIVE HIF PHD2 INHIBITOR THROUGH HYBRID VIRTUAL SCREENING.

[1]Sari, S., [2] Tumber A.

[1] Hacettepe University, Department of Pharmaceutical Chemistry, Ankara, Turkey

[2] University of Oxford, Department of Chemistry, Oxford, United Kingdom

Introduction:

Hypoxia-inducible factors (HIFs) are transcription factors that respond to hypoxia by upregulation of a set of genes to enlist survival pathways. Under normoxic conditions HIF is hydroxylated by HIF prolyl hydroxylase (HIF PHD) enzymes, which leads to rapid degradation of HIF. Inhibition of HIF PHD, which naturally occurs in hypoxia, leads to cytoplasmic accumulation of HIF, which then migrates to the nucleus and activates the genes related to a number of cellular responses against hypoxia, e.g., increased erythropoiesis and angiogenesis. Thus, HIF PHD inhibition has been tested as a strategy for the treatment of related conditions such as chronic anemia and impaired wound healing (1). Three isoforms of HIF PHD have been identified so far and type 2 (HIF PHD2) contributes the most to the processes defined above. A number of HIF PHD inhibitors have been clinically approved or tested against anemia in chronic kidney disease (CKD) for hypoxia-related diseases such as anemia (Figure 1). However, current HIF PHD inhibitors are associated with serious side effects like fatal liver necrosis undermining their safety for chronic use (2). In this study we aimed to discover new HIF PHD inhibitors through hybrid ligand- and structure-based virtual screening of commercial compound libraries and validate these hits by *in vitro* testing.

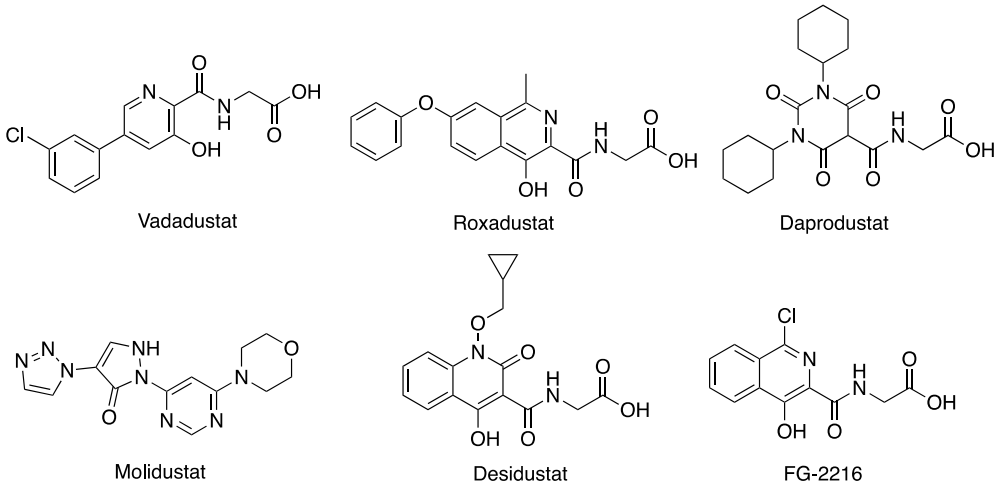

Figure 1. Clinically approved/tested HIF PHD inhibitors for the treatment of anemia in CKD

Materials and Methods:

InterBioScreen (IBS) library was prepared using LigPrep and MacroModel (2020-4, Schrödinger LLC, New York, NY) according to the OPLS3e forcefield parameters (3). Molecular descriptors were calculated using QikProp (2020-4, Schrödinger LLC, New York, NY). Shape similarity screening was performed by Maestro (2020-4, Schrödinger LLC, New York, NY) and molecular docking by Glide (2020-4, Schrödinger LLC, New York, NY) at

standard and extra precision modes (SP and XP) (4). Selected compounds were tested for HIF PHD2 inhibition using solid phase extraction-mass spectroscopy using FG4592 as positive control (5).

Results:

The virtual screening pipeline is outlined in Figure 2. 68,373 compounds from the IBS library were filtered using a set of molecular descriptors related to druglikeness, i.e., molecular weight, number of rotatable bonds, hydrogen bond acceptor and door counts, LogP, and polar surface area. Remaining 63,829 compounds were screened for 3D similarity regarding 16 known HIF PHD2 inhibitors and those with similarity score higher than 0.8 were selected for docking. 4286 compounds were docked to human HIF-PHD2 structure first at SP and then at XP mode. Those with docking score lower than -7.0 kcal/mol were visually evaluated regarding ligand-receptor interactions, leaving 11 candidate compounds for *in vitro* tests (Table 1).

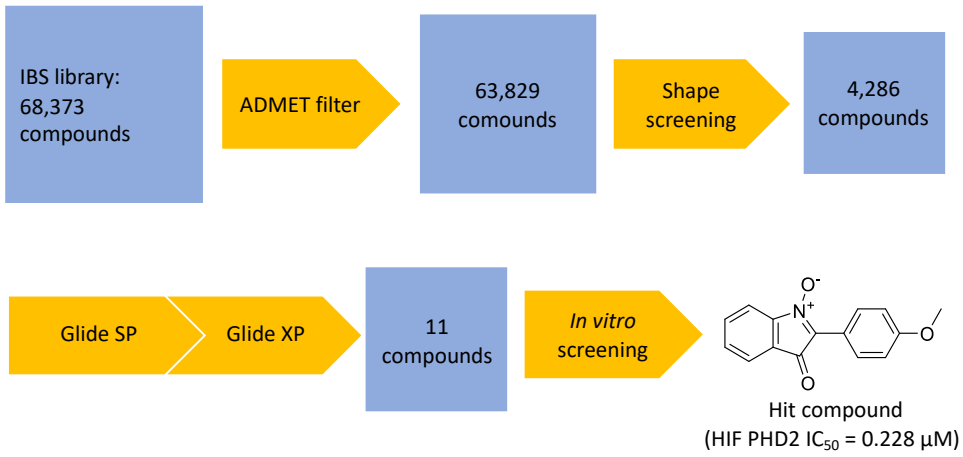

Figure 2. The virtual screening pipeline

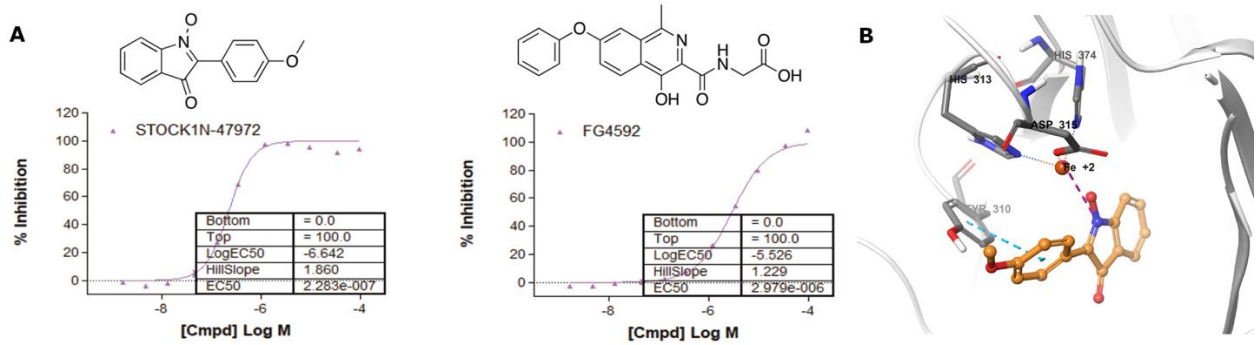

Figure 3. (**A**) Dose-response curves of the hit and the positive control. (**B**) Binding interactions of the hit with the HIF PHD2 active site residues.

Table 1. Selected compounds for the *in vitro* tests and their docking results

Title	Docking score (kcal/mol)	Interactions
STOCK1N-95706	-10.3	Tyr310 (π-π), Asp315 (salt bridge), Arg383 (H bond, π-cation), Trp389 (π-π)
STOCK1N-96247	-10.1	Arg252 (H bond), Tyr303 (H bond), Asp315 (salt bridge)
STOCK1N-47972	-9.4	Tyr310 (π-π), Asp315 (salt bridge)
STOCK1N-07021	-8.2	Asp315 (salt bridge), Arg383 (H bond)
STOCK1N-99176	-7.8	Asp315 (H bond), Tyr329 (H bond), Arg383 (H bond)
STOCK1N-39562	-7.5	Tyr310 (H bond), Tyr329 (H bond), His374 (π-π), Arg383 (H bond), Trp389 (π-π)
STOCK1N-38657	-7.3	Tyr310 (H bond), Tyr329 (H bond), His374 (π-π), Arg383 (H bond), Trp389 (π-π)
STOCK1N-99445	-7.2	Asp254 (H bond), Tyr310 (H bond), Tyr329 (H bond), Arg383 (H bond)
STOCK1N-40546	-7.2	Tyr310 (H bond), Tyr329 (H bond), His374 (π-π), Arg383 (H bond), Trp389 (π-π)
STOCK1N-37117	-7.0	Tyr310 (H bond), Tyr329 (H bond), His374 (π-π), Arg383 (H bond), Trp389 (π-π)
STOCK1N-37206	-7.0	Tyr310 (H bond), Tyr329 (H bond), His374 (π-π), Arg383 (H bond)

Selected compounds were tested against HIF PHD2, their dose-response curves were plotted and EC_{50} values were determined. Among the tested compounds, STOCK1N-47972 (2-(4-methoxyphenyl)-3-oxo-3*H*-indole 1-oxide) was identified as the hit with ca. 13 times lower EC_{50} than FG4592, a clinically tested inhibitor (Figure 3A). The hit compound is an indole *N*-oxide derivative and strongly interacts with the co-factor (Fe^{2+}) and the nearby residues, e.g., Tyr310, and Asp315 (Figure 3B).

Conclusions:

A virtual screening campaign combining the benefits of ligand- and structure-based methods has yielded a highly potent HIF PHD2 inhibitor. The hit compound features indole *N*-oxide scaffold, which has not been reported for such an effect before. Thus, our study opens new venues in terms of future hit-to-lead design of HIF PHD inhibitors through modifications of the identified scaffold.

References:

1. Singh A, Wilson JW, Schofield CJ, Chen R (2020). Scientific Reports, 10(1):1597.
2. Haase VH (2017). Hemodialysis International, 21:S110-S124.
3. Harder E, et al. (2016). Journal of Chemical Theory and Computation, 12(1):281-96.
4. Friesner RA, et al. (2006). Journal of Medicinal Chemistry, 49(21):6177-96.
5. Richardson NL, et al. (2021). Bioorganic & Medicinal Chemistry, 38:116115.

OP074: DEVELOPMENT OF NON-STEROIDAL AMINOTHIAZOLE ANALOGS ACTIVE ON MCF7 CELL LINE AND AROMATASE ENZYME

Sahin, Z.

Istanbul Medipol University, Department of Pharmaceutical Chemistry, Istanbul, Turkey, zsahin@medipol.edu.tr

Introduction:

Breast cancer is one of the most common cancer types. Majority of breast cancers are ER+, thus suppressing estrogen biosynthesis is an important approach for drug design. Aromatase plays a key role in estrogen biosynthesis, its steroidal and non-steroidal inhibitors have their own binding mode. Non-steroidal inhibitors usually contain an azole ring, which is important to coordinate with the active site Fe^{+2}. Based on published works of our group, in this study, we synthesized a series of 9 pyridyl-aminothiazole derivatives for follow-up (Figure 1). Compounds were tested on MCF7 cell line for cytotoxic activities. Induced-fit docking studies were performed on human placental aromatase cytochrome P450 in complex with androstenedione (3EQM) crystal structure for evaluating the binding modes of the most active compound (1). Furthermore, most active compound also evaluated for its intrinsic activity on CYP2C9, 2D6, 3A4 enzymes compared to anastrozole by using induced-fit docking and in silico techniques.

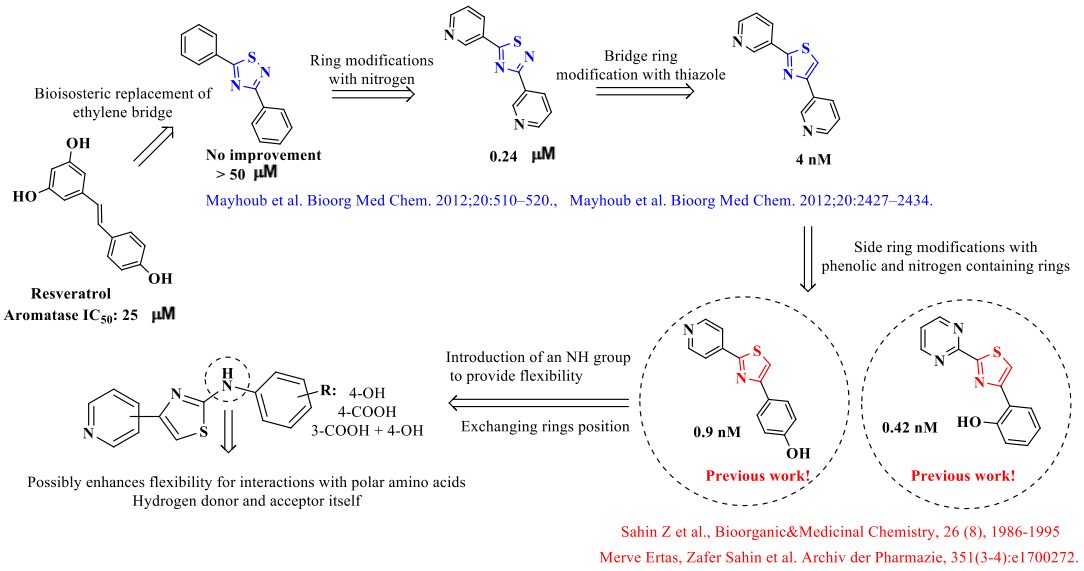

Figure 1. Design and development of the synthesized compounds

Materials and Methods:

Final compounds were synthesized by usual Hantzsch thiazole synthesis (Figure 1). Structure elucidation were successfully realized by IR, NMR and Mass spectrometry. MTT test was applied for antitumor activity. In silico binding and intrinsic activity studies were visualized and processed with Schrödinger Maestro software.

Results:

Compounds were successfully synthesized (Figure 2) and yields were between 60%-80%. IR, NMR and MS results were consistent.

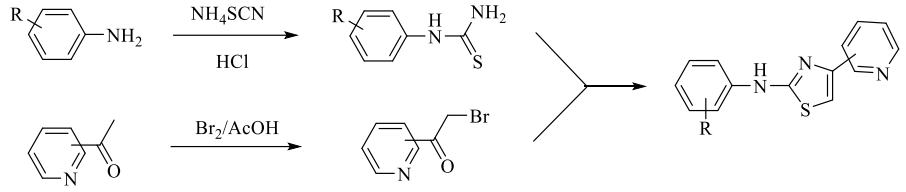

Figure 2. General synthetic method for compound 1-9

Compound 7 (2-hydroxy-5-((4-(pyridin-2-yl)thiazol-2-yl)amino)benzoic acid

Yield: 76%, ^{1}H-NMR (300 MHz, DMSO-d_6, ppm) δ: 6.67 (1H, d, J: 8.67 Hz, Ar), 7.26-7.32 (1H, m, Ar), 7.40 (1H, s, Ar), 7.57 (1H, dd, J: 8.79, 2.75 Hz, Ar), 7.86 (1H, td, J: 7.71, 1.71 Hz, Ar), 7.93-7.98 (2H, m, Ar), 8.54-8.58 (1H, m, Ar), 9.96 (1H, s, NH), 15.55 (1H, s, COOH), ^{13}C-NMR (75 MHz, DMSO-d_6, ppm): 105.81, 105.86, 116.27, 120.77, 122.93, 123.18, 131.35, 137.61, 149.79, 150.72, 152.79, 158.38 (thiazole C_2), 165.61 (Ph-OH), 172.19 (COOH). MS (M+H): 314.

Compound 7, as a novel compound, showed the highest inhibitory activity against MCF-7 cell line. All the compounds showed an activity between 21-55 μM antitumor activity. These results direct the study to measure enzymatic activity on aromatase.

Table 1. Structures and antiproliferative activity of compounds 1-9 on MCF-7 cell line

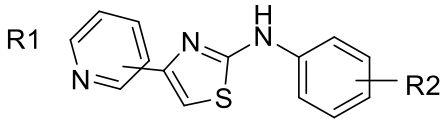

C.no	R1	R2	IC_{50} (MCF7) (μM)
1	2-pyridyle	4-OH	55.17 ± 0.87
2	3-pyridyle	4-OH	53.08 ± 1.02
3	4-pyridyle	4-OH	48.15 ± 2.98
4	2-pyridyle	4-COOH	41.55 ± 1.02
5	3-pyridyle	4-COOH	39.19 ± 0.92
6	4-pyridyle	4-COOH	32.02 ± 1.19
7	2-pyridyle	3-COOH, 4-OH	**21.13 ± 1.15**
8	3-pyridyle	3-COOH, 4-OH	35.20 ± 1.18
9	4-pyridyle	3-COOH, 4-OH	40.09 ± 0.09

Docking results were consistent with Caporuscio et al. lead study (2). Antitumor activity was found 21 μM for compound 7 (2-hydroxy-5-((4-(pyridin-2-yl)thiazol-2-yl)amino)benzoic acid). Other compounds also showed activity between 32-55 μM (IC_{50}) on MCF7 cell line.

Aromatase enzyme structure complexed with androstanedione is reported in prominent publications in this area. According to that docking results, androstanedione 3-oxo group interacts with Asp309 in active site 17-oxo group interacts with Met374. Methyl group at 19th position in a contact with haem group. In this active site, Thr310 is coordinated with heme group but not in interaction with androstandione. In these studies, even if they do not interact with androstanedione, Leu477, Ser478 and Arg115 were represented as key aminoacids in active site (2-4). As shown in Figure 3, pyridine ring of 7 is in interaction with haem group. NH group provided a hydrogen bond with Leu477. Salicylic acid group make a good polar interaction with key amino acids Arg115 and Met374.

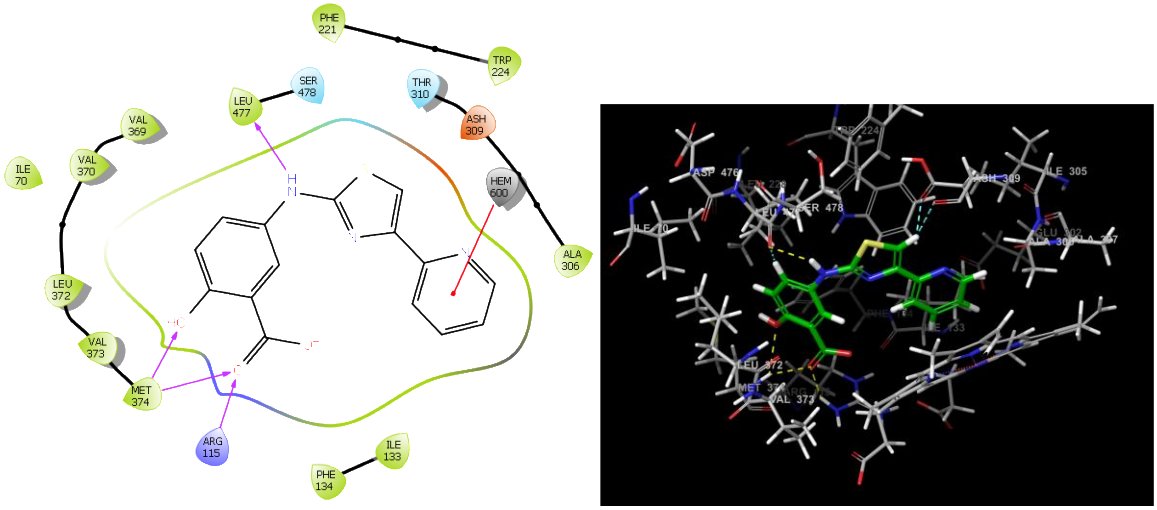

Figure 3. 2D and 3D poses of compound 7 on aromatase (3EQM) active site

Conclusions:

Compounds binding pose gave a functional hydrogen bond donor site following previous studies. Ongoing work will be done to evaluate enzyme binding and developing novel compounds.

References:

1. Sahin Z, Ertas M, Biltekin et al., (2018). Bioorganic & Medicinal Chemistry, 26:1986-1995.
2. Caporuscio F, Rastelli G, Imbriano C, Del Rio A (2011). Journal of Medicinal Chemistry, 54(12): 4006-4017.
3. Ertas M, Sahin Z. et al., Archiv der Pharmazie, 351(3-4):e1700272.
4. Mayhoub et al. (2012). Bioorg Med Chem, 20:510–520.

OP075: THE EFFECT OF SACUBITRIL/VALSARTAN ON PROTEIN EXPRESSION OF DIASTOLIC COMPONENTS IN HFD/STZ INDUCED DIABETIC RAT HEART

[1,3]**Erdogan, B.R.**, [2,3]Yesilyurt Z.E., [3]Karaomerlioglu I.,[3]Muderrisoglu A.E., [3]Arioglu Inan, E.

[1] Izmir Katip Celebi University, Department of Pharmacology, Izmir, Turkey, betulrabia.erdogan@ikc.edu.tr

[2] Gazi University, Department of Pharmacology, Ankara, Turkey, zeynepelifyesilyurt@gazi.edu.tr

[3] Ankara University, Department of Pharmacology, Ankara, Turkey,

remkar22@gmail.com, muderrisoglu@ankara.edu.tr, arioglu@ankara.edu.tr

Introduction:

Diabetes is a chronic, endocrine disease which effects millions of people worldwide. Cardiovascular complications are the major cause of diabetes-related morbidity and mortality (1). People with diabetes have 2-3 times higher risk to develop cardiovascular diseases compared to the individuals without diabetes (2) and more than 32 percent of diabetic patients have concomitant cardiovascular diseases (3). Sacubitril/valsartan is the first compound of ARB/Neprilysin inhibitor (ARNi) combination strategy (4). This compound has been approved in the treatment of heart failure with reduced ejection fraction. Sacubitril/valsartan combination was shown to have beneficial effects on the diabetic heart, however underlying mechanisms remain unclear. We aimed to evaluate possible effect of sacubitril/valsartan on the diabetic heart in terms of expression of SERCA2a (is an indicator of cardiac diastolic function) and phospholamban (PLN) (has an inhibitory effect on SERCA2a function) protein levels compared to valsartan alone.

Materials and Methods:

Western Blot experiment was performed as previously described with minor changes (5). Frozen left ventricle tissues were powdered in liquid nitrogen and homogenized in RIPA buffer, which contains sodium ortovanadate and protease inhibitor coctail. After sonication, samples were agitated at +4°C for 2-hour and centrifuged at 12000 rpm at +4°C and supernatant fraction were obtained for protein level analysis. Samples which contains equal amount of protein (10 or 45 or 100 µg) were loaded onto 4 % acrylamide SDS-PAGE stacking gel and were seperated by 10 % acrylamide SDS-PAGE seperation gel. The proteins were transferred to either polyvinylidene difluoride or nitrocellulose membran at 100 V for 2-hour (10 µg) or 3-hour (45 µg) or 4-hour (100 µg). Membranes were blocked with tris-buffered saline (TBS) containing 5% bovine serum albumine for 1-hour at room temperature to prevent non-specific protein binding. Then membranes were incubated with primary antibodies (SERCA2a, PLN, p-PLN ($PLN^{ser16/thr17}$), GAPDH) at +4°C for overnight. Afterwards, membrane were washed with tris-buffered saline containing 1% Tween20 (TBST) then were incubated with horse radish peroxidase (HRP) conjugated antirabbit secondary antibodies +4°C for 1.5-hour. Membranes were washed with TBST and were incubated with enhanced chemiluminescence (ECL) mix for 1-min, then blots were exposed to film. Films were scanned and protein bands were analyzed by using Image J. Data are expressed as mean ± SD. One-way ANOVA, followed by post-hoc

Bonferroni test was used for multiple comparisons. p-values < 0.05 was considered as statistically significant. All results on the expression level were expressed as % relative intensity.

Results:

The expression of SERCA2a was significantly decreased in diabetic and sacubitril/valsartan treated diabetic group. Although there was a decrease in valsartan treated diabetic group compared to control, it was not found statistically significant (C: 100.00 ± 15.38; D: 73.38 ± 10.05; SV: 73.24 ± 10.44; V: 82.75 ± 18.49) (Fig. A). The expression of PLN was found comparable amoung the groups (C: 100.00 ± 13.08; D: 73.68 ± 5.23; SV: 72.96 ± 10.74; V: 79.56 ± 25.52) (Fig. B). On the other hand, the p-PLN/PLN ratio was significantly decreased in diabetic animals and did not reach to control level with both treatment approaches (C: 100.00 ± 19.33; D: 64.28 ± 13.40; SV: 82.02 ± 16.83; V: 68.59 ± 8.84) (Fig. D). SERCA2a/PLN ratio was not found different among the groups (C: 100.00 ± 22.51; D: 98.21 ± 12.94; SV: 99.62 ± 14.31; V: 106.94 ± 23.26) (Fig. C).

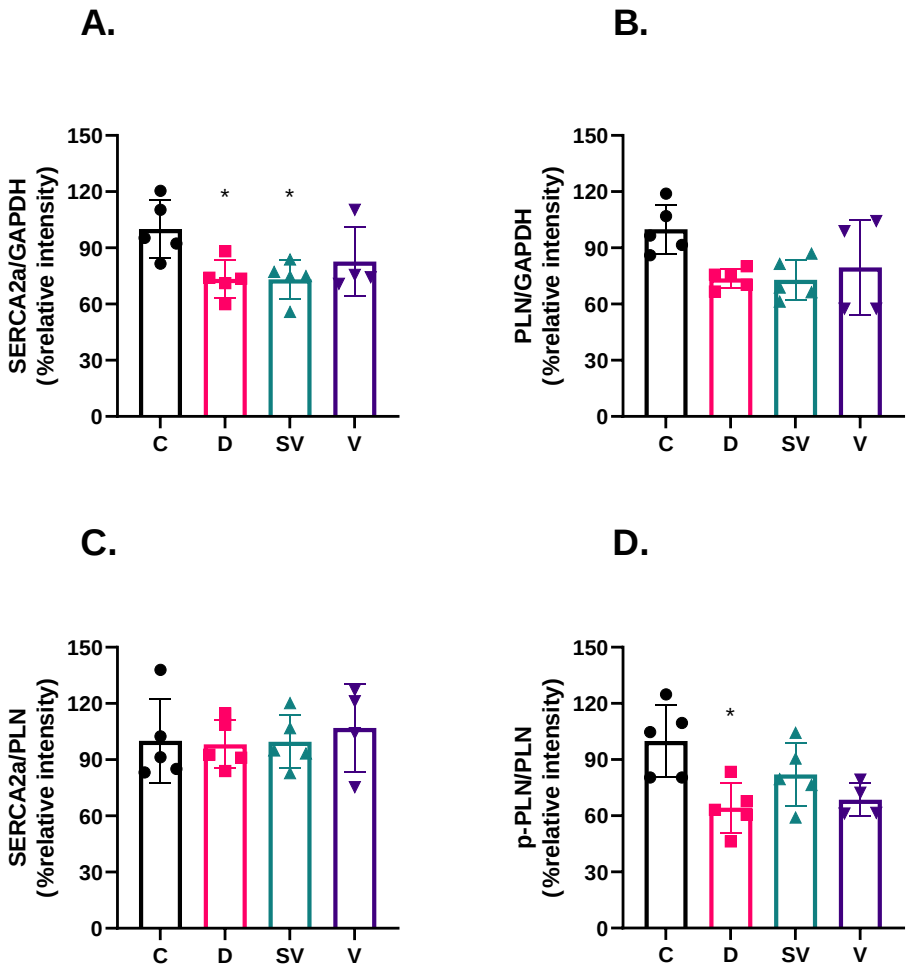

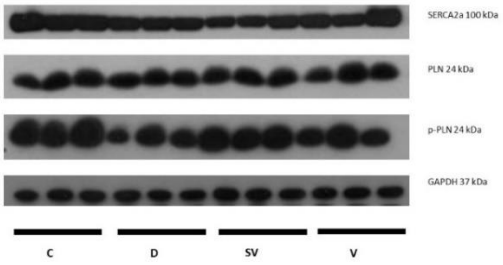

Figure. Protein expression levels **A.** SERCA2a protein expression level normalized to GAPDH. **B.** Phospholamban protein expression level normalized to GAPDH. **C.** The ratio of SERCA2a to phospholamban. **D.** The ratio of phosphorylated phospholamban to phospholamban. C, Control (n=5); D, Diabetic (n=5); SV, Sacubitril/valsartan treated diabetic (n=5); V; Valsartan treated diabetic (n=4). *, p<0,05 compared to control.

Conclusions:

Decreased expression of SERCA2a and reduced p-PLN/PLN ratio in the diabetic group, which are indicators of impaired diastolic function in diabetes, were not improved after the treatment approches. We conclude that sacubitril/valsartan combination may exert its beneficial effect on the diabetic heart through other mechanisms rather than the improvement of diastolic function components.

Acknowledgements

This study was supported by a grant of TUBITAK (SBAG-117S936) and Ankara University Scientific Research Projects Coordination Unit (19H0237004)

References:

1. Gregg et al., (2014). New England Journal of Medicine, 370:1514-1523.
2. DF 2017. IDF Diabetes Atlas 8th Edition. In: International_Diabetes_Federation (ed.) 8th ed.
3. Einarson et al., (2018). Value Health, 21: 881-890.
4. Food And Drug Administration (2015). Center for drug evaluation and research. [https://www.accessdata.fda.gov/drugsatfda_docs/nda/2015/207620Orig1s000OtherR.pdf]
5. Arioglu-Inan et al., (2013). European journal of pharmacology, 718(1-3): 533-543.

OP080: A DROSOPHILA APPROACH TO STUDY THE EFFECTS OF ATYPICAL ANTIPSYCHOTIC DRUGS

[1]Milani, D., [1]Forgiarini, A., [2]Gumeni, S.,[1]Comai, S., [1]Guarato, G., **[1]Orso, G.**

[1] Padova University, Department of Pharmaceutical and Pharmacological Sciences, Padova, Italy,

[2] Department of Biology, School of Science, National and Kapodistrian University of Athens, Greece

Introduction:

Genetic variations in the *DTNBP* gene encoding dysbindin-1 can alter D2 receptor availability and are associated with cognitive response to antipsychotic drug treatment (1). The mechanisms underlying the efficacy and adverse effects induced by these drugs are, to date, not sufficiently explained (2). In *Drosophila*, dysbindin (Dysb) regulates glutamatergic and dopaminergic transmission at neuronal and glial levels, respectively (3). To investigate the role od Dysb in the mechanism of action ofatypical antipsychotic drugs (AAPs), we used *Drosophila* loss of function models of *dysb* to analyse the effects of olanzepine, risperidone and ziprasidone at molecular, cellular and behavioral levels.

Materials and Methods:

Drosophila RNAi and mutant strains (Dysb[1]) of *dysb* were used for loss of function studies; ubiquitous, astrocyte, neuron and glia driver lines were employed to selectively reduce dysb in *Drosophila*. Confocal microscopy was used to identify endo-lysosomal defects in neuronal and glial cells; qRT-PCR to measure the relative expression changes of the receptor transcripts (D1,D2, 5-HT(2A), β1, β2 and β3) and glia transcription factors; climbing and activity tests to investigate behavioral differences. Ziprasidone, risperidone and olanzepine were chronically administrated at 30 um in the food.

Results:

Dysb[1] flies showed increased locomotor activity (as reported previously), increased expression of D2 receptors (up to 10-fold) (Figure 1 and 2), 5-HT(2A) (1.8-fold) and β3 (1.5-fold), a partial loss of glia cells with a concomitant reduction of astrocyte-specific transcription factors expression. A selective downregulation of dysb in astrocytes lead to a defective endolysosomal pathway and the increased of D2 expression (6 fold) . Of note, climbing activity of Dysb1 was increased, whereas the astrocytes selective reduction of dysb caused a decrease in locomotor activity that was associated to a striking hyperexcitability behavior in adult flies. All the tested AAPs drugs restored receptor expressions in a dose dependend manner (Figure 2). However, while risperidone and ziprasidone ameliorated cellular astrocytic defects, olanzepine had the greatest effects at behavioral level (Figure 3).

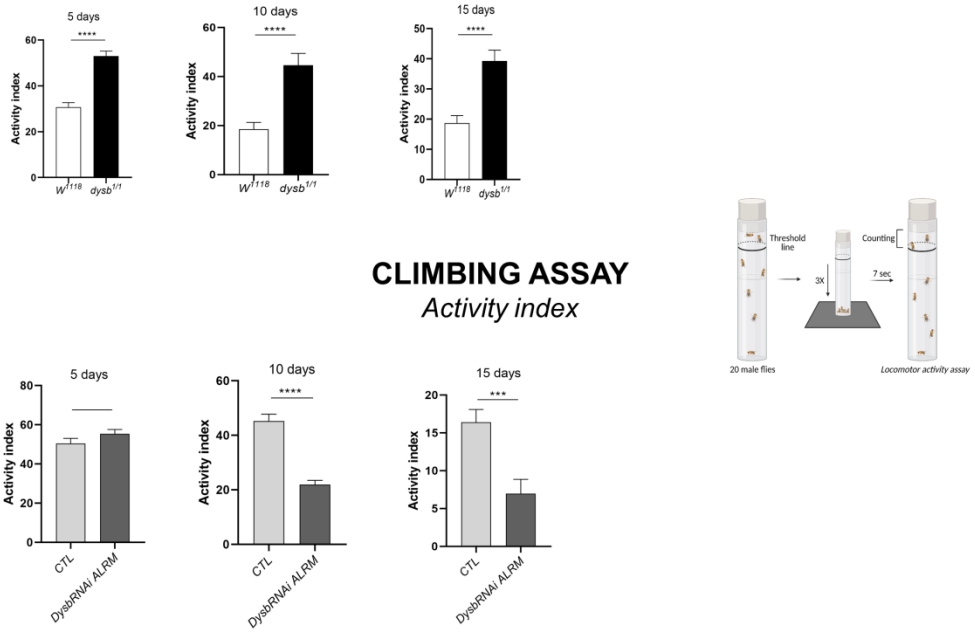

Figure 1. Climbing test on Dys[1] flies (upper gaphs) and after the astrocyte specific dowunregulation of dysb (lower graphs)

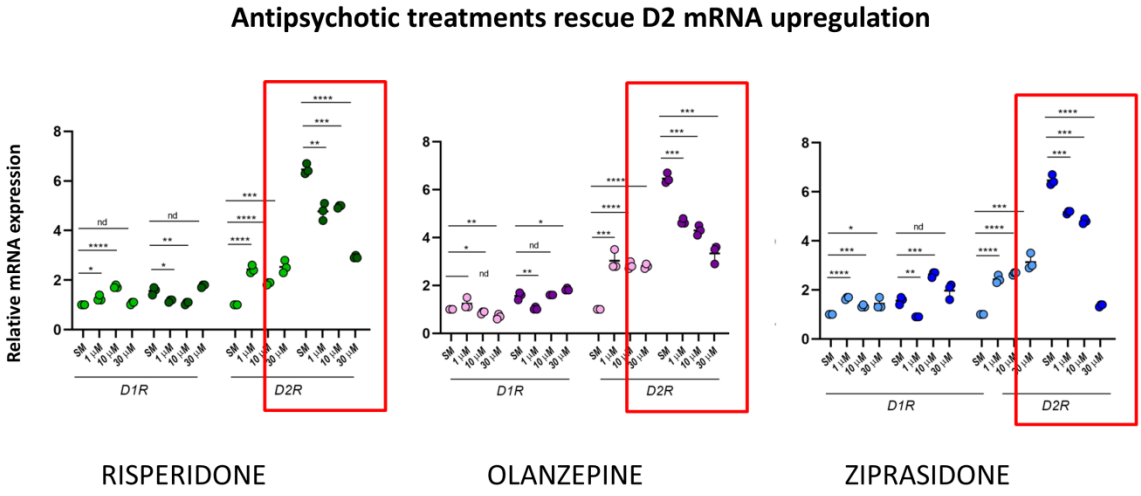

Figure 2. Antipsychotic effects on D2 receptor transciptional levels in control and dysb[1] flies.

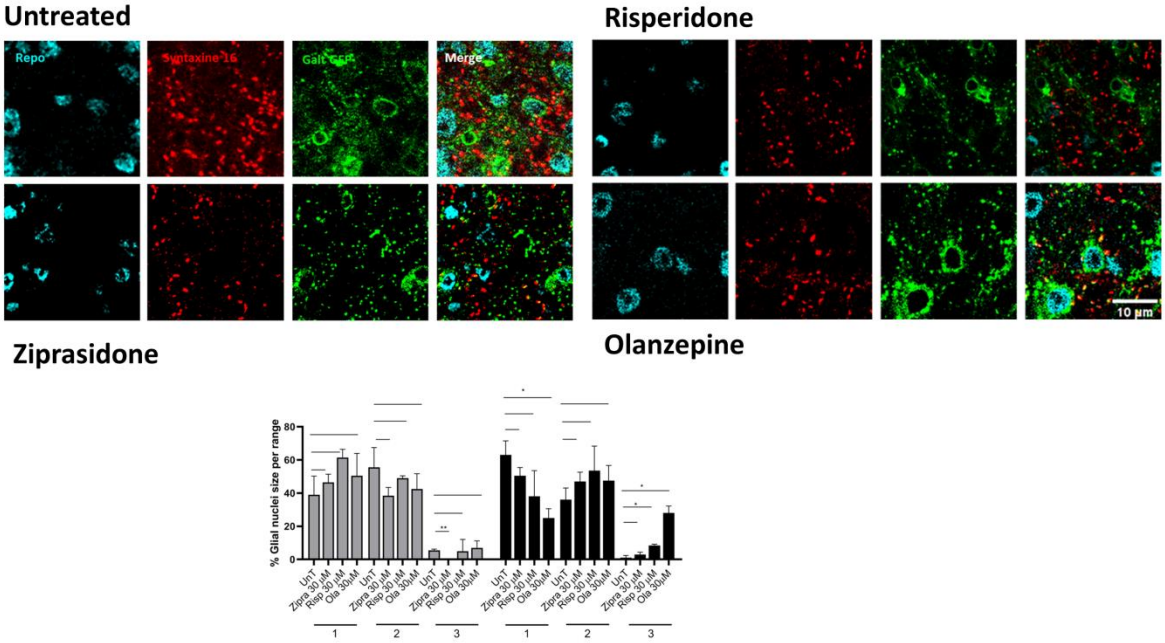

Figure 3. Antipsychotic effects on astrocytes recycling marker Galt-GFP. Glia nuclei are in blu (anti α-Repo) and anti α-syntaxin16 in red (upper panel). On the bottom the quantification of glia nuclei size per range.

Conclusions:

Our data demonstrate that dysb regulates astrocytes specific intracellular recycling, with a consequent modulation of dopaminergic function and thus of the dopamine-related behavioral phenotypes. Importantly, these dysb-dependent mechanisms are differently affected by the AAPs including olanzepine, risperidone and ziprasidone.

Acknowledgements

This study was supported by the Young Investigator grant Ministery of Italian Health.

References:

1. Scheggia,D., Mastrogiacomo,R., Mereu,M., Sannino,S., Straub,R.E., Armando,M., Managò,F., Guadagna,S., Piras,F., Zhang,F., et al. (2018) Variations in Dysbindin-1 are associated with cognitive response to antipsychotic drug treatment. Nat. Commun., 9.
2. Vantaggiato,C., Panzeri,E., Citterio,A., Orso,G. and Pozzi,M. (2019) Antipsychotics Promote Metabolic Disorders Disrupting Cellular Lipid Metabolism and Trafficking. Trends Endocrinol. Metab., 30, 189–210.
3. Shao,L., Shuai,Y., Wang,J., Feng,S., Lu,B., Li,Z., Zhao,Y., Wang,L. and Zhong,Y. (2011) Schizophrenia susceptibility gene dysbindin regulates glutamatergic and dopaminergic functions via distinctive mechanisms in Drosophila. Proc. Natl. Acad. Sci. U. S. A., 108, 18831–6.

OP081: A DROSOPHILA BASED APPROACH TO DEVELOP SPECIES-SELECTIVE VERTEBRATE DRUGS

[1]Guarato, G., [1]Forgiarini, A., [1]Orso, G.

[1] Padova University, Department of Pharmaceutical and Pharmacological Sciences, Padova, Italy, giulia.guarato@studenti.unipd.it, alessia.forgiarini@unipd.it, genny.orso@unipd.it

Introduction:

Here we propose an alternative approach to replace vertebrate models in preclinical research. We are developing fruit-fly models to test Norbormide (NRB) target and its species selective toxicity. NRB is a Rattus-specific toxicant relatively harmless to other species. NRB's lethal effect is due to its vasoactive properties. In rat peripheral arteries NRB causes vasoconstriction, while in rat aorta and arteries of other species tested it induces relaxation (Figure 1) (1).

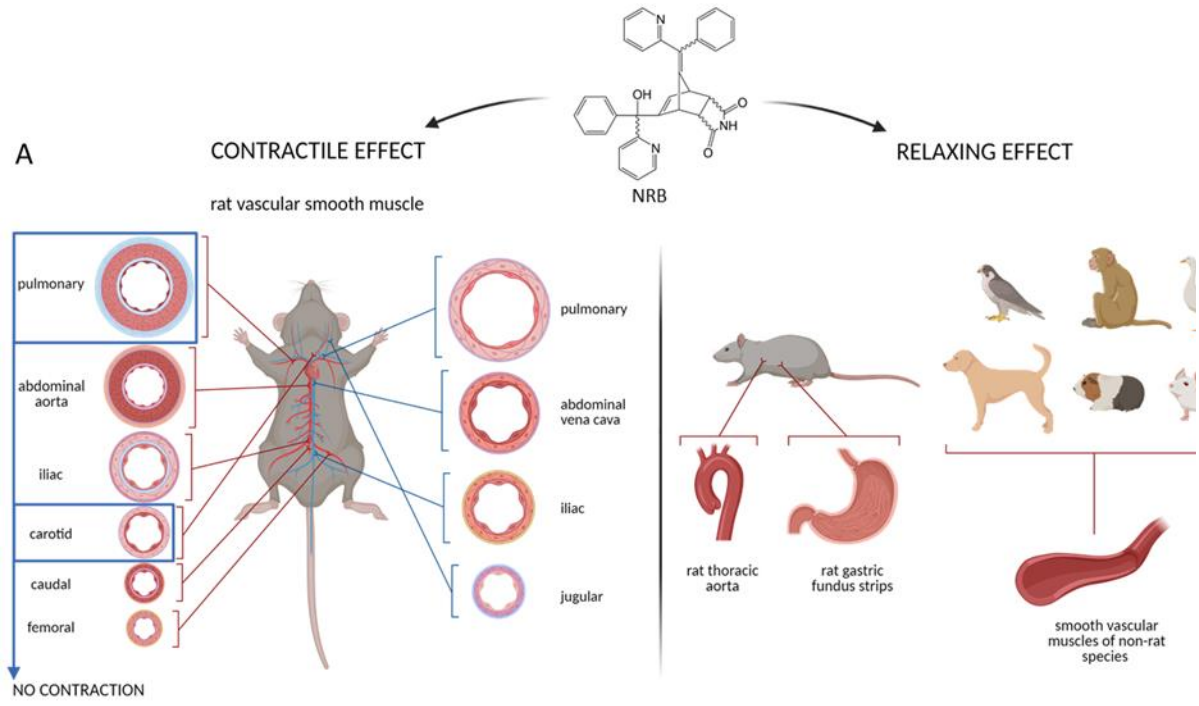

Figure 1. Species- and tissue-selective effects of NRB. (A) NRB exerts its contractile effect in both rat peripheral arteries and veins, with a force of action inversely proportional to the vessel diameter. The carotid and pulmonary artery are an exception and are not contracted by NRB, even if their caliber is smaller than other vessels affected by the drug. (B) In rat thoracic aorta, rat-non vascular muscle and in blood vessels of non-rat species, like birds and other mammalian species (including human), NRB induced relaxation of the musculature

Since its development in the 1960s the mechanism of NRB remains unknown, nevertheless some hypotheses have been postulated. Based on previous data a possible target was proposed to be the KATP channel composed by the SUR2B/Kir6.1 subunits (Figure 2) (2,3). New NRB derivatives were synthetized and tested for vasoconstriction properties and localization in *ex vivo* and *in vitro* tests. We thought to develop *Drosophila* transgenic animals expressing the rat and mouse KATP channels and to characterize NRB derivatives properties.

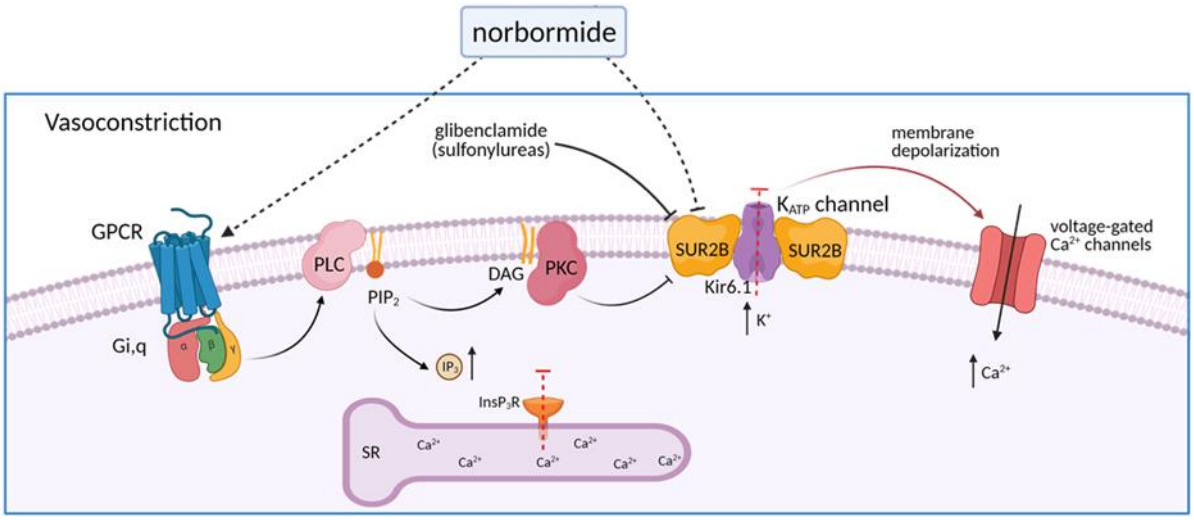

Figure 2. Proposed mechanism underlining NRB vasoconstriction effect in rat vascular smooth muscle cells. The NRB-induced contraction is provoked by the entry of Ca2+ from the extracellular environment. It is proposed that the NRB-induced contraction is mediated by the influx of Ca2+ via activated calcium channels, after the activation of the phospholipase C/protein kinase C (PLC/PKC) pathway.

Materials and Methods:

Rat and mouse cDNAs, with epitope tags, of the subunits of Kir6.1 and SUR2B were cloned in PUAST-ATTB vector for transgenesis in *Drosophila.* Ubiquitous driver lines were used to express the subunits, separately. Immunohistochemistry was used to visualize subunits expression in *Drosophila* tissues. Fluorescent derivatives of NRB were used in live imaging experiments to visualize the subcellular localization in control, downregulated *Drosophila* homologues of SUR2B and Kir6.1 and KATP expressing animals. Toxicity tests were done to evaluate the effects of NRB derivatives on *Drosophila* wild type and KATP models.

Results:

Here we present preliminary data on rat KATP channel expression in *Drosophila*. Our data shows that the inividual expression of KATP channel subunits colocalize with endoplasmic reticulum membrane, as previuolsy shown *in vitro* for these subunits. NRB derivative with NBD or BODIPY groups showed the same localization observed in rat cell lines, with a ER localization for compounds of group 1 of and plasma membrane for group 2. NRB derivatives (with and without fluorophores) were atoxic when administrated to wild type *Drosophilae*. The ubiquitous coexpression of the two subunits (to reconstitute the channel) resulted in a lethal phenotype at embrionic stage. Thus, we coexpressed the channel in selected tissues, for example in the eye (Figure 3).

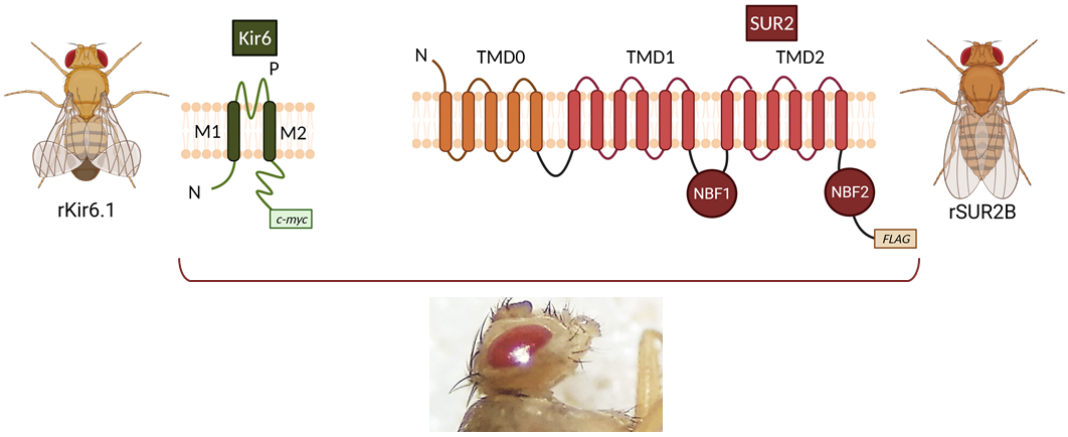

Figure 3. Co-expression of the Kir6.1 and SUR2B subunits in eye tissue. The expression of the two rat subunits in the *Drosophila* eye causes a damage to the tissue.

Conclusions:

Drosophila models expressing species-selctive receptors can be used to replace vertebrate models during preliminary preclinical experimentations allowing the selection of the most promising compounds for future studies.

Acknowledgements

This project was supported by the New Zealand MBIE Endeavor Fund C09X1710 (BH, SB, and) and by the University of Padua, project no. 148125/14 (GO,SB).

References:

1. Cavalli M, Omiciuolo L, Cargnelli G, Cima L, Hopkins B, Bova S (2004) Distribution of the vasoconstrictor and vasorelaxant effects of norbormide along the vascular tree of the rat. Life Sci 75:2157–2165.
2. D'Amore C, Orso G, Forgiarini A, Ceolotto G, Rennison D, Ribaudo G, Jay-Smith M, Hopkins B, Brimble MA, Bova S (2018) Synthesis and Biological Characterization of a New Norbormide Derived Bodipy FL-Conjugated Fluorescent Probe for Cell Imaging. Front Pharmacol 9:1055 Available at: https://www.frontiersin.org/article/10.3389/fphar.2018.01055/full [Accessed May 5, 2021].
3. Saponara S, Fusi F, Spiga O, Trezza A, Hopkins B, Brimble MA, Rennison D, Bova S (2019) The Selective Rat Toxicant Norbormide Blocks KATP Channels in Smooth Muscle Cells But Not in Insulin-Secreting Cells. Front Pharmacol 10:598 Available at: http://www.ncbi.nlm.nih.gov/pubmed/31191321 [Accessed March 6, 2020].

OP087: CONTRIBUTION OF CANNABINOID SYSTEM TO THE ANTIHYPERALGESIC EFFECTS OF ANTIEPILEPTIC DRUGS

[1]Bektas Turkmen, N., [1]Alyu, F., **[2]Okcay, Y.**, [1]Arslan, R.

[1] Anadolu University, Faculty of Pharmacy, Department of Pharmacology, Eskisehir, Turkey, nurcanbektas@anadolu.edu.tr

[2] University of Health Sciences, Gulhane Faculty of Pharmacy, Department of Pharmacology, Ankara, Turkey, yagmur.okcay@sbu.edu.tr

Introduction:

Transient Receptor Potential (TRP) channels are a superfamily of ion channels that are permeable to several cations. Vanilloid receptor subtype-1 (TRPV1) which is a subtype of TRP channels, is the most well-characterized and extensively studied mammalian TRP channel. It is expressed in sensory neurons and is activated by capsaicin, protons, toxins and temperature in the noxious range, making it physiologically important for thermal and chemical nociception. When activated by ligand-binding, TRPV1 allows cation influx, resulting in membrane depolarization, which relays pain information to the brain and a burning and painful sensation. Alterations in TRP channel activity results in mechanical and thermal hypersensitivity and they are possible targets of cannabinoid system mediated analgesia, especially in inflammatory conditions (1,2). Cannabinoids are known to produce analgesia through their CB1 and CB2 receptors. It also has been shown that TRPV1 channels mediate the antihyperalgesic effects of cannabinoids and that TRPV1 channels may present a molecular target for cannabinoids. On the other hand, antiepileptic drugs are shown to exert antihyperalgesic activity in inflammatory pain models and TRPV1 channels are shown to be involved in the antihyperalgesic action of cannabinoids (3,4). Considering this mutual component of analgesic mechanisms, it is aimed to investigate the relationship between these systems and the involvement of cannabinoid system to antihyperalgesic action mechanism of some antiepileptic drugs. In this study it was aimed to investigate the involvement of cannabinoid system to antihyperalgesic action mechanism of antiepileptic drugs in a rat model of TRPV1 agonist capsaicin-induced mechanical hyperalgesia.

Materials and Methods:

80 adult male Sprague-Dawley rats weighing 250-300 g were used. All animals were housed in a well-ventilated room with 12h light/dark cycle at 24 ± 1 °C and allowed free access to food and water *ad libitum.* Pre-treatment with AM251, CB1 receptor antagonist, was followed by pregabalin (50 mg/kg, *i.pl*.), gabapentin (600 µg/paw *i.pl*.), oxcarbazepine (500 µg/paw *i.pl*.), carbamazepine (140 µg/paw *i.pl*.) administrations. Electronic von-Frey apparatus was used to evaluate mechanical hyperalgesia and pain thresholds were recorded at 15, 30, 60, 90, 120, 150 and 180 minutes following the drug injections. Average of three measurements were calculated for each animal. All procedures were performed strictly in accordance with the ethical principles of Helsinki Declaration and was approved by the Local Ethics Committee of Anadolu University, Eskisehir, Turkey (No: 2017-11).

Results:

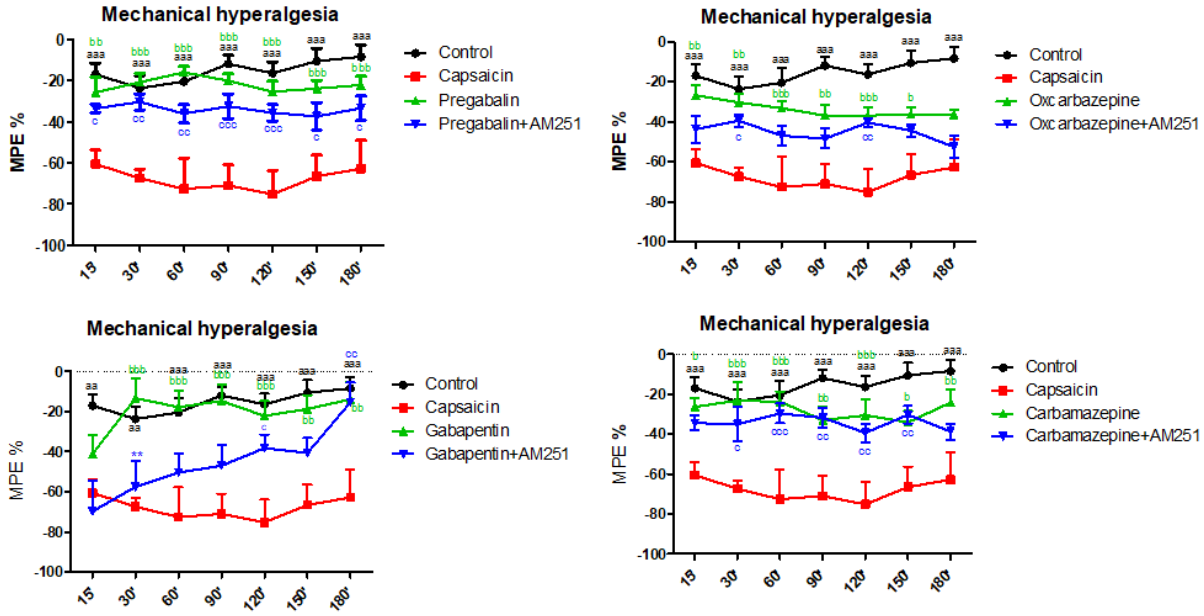

As shown in the figure, in all of the groups, capsaicin reduced the withdrawal responses to mechanical stimuli compared with the control groups. Gabapentin, pregabalin, carbamazepine and oxcarbazepine time-dependently reversed the development of mechanical hyperalgesia. AM251 antagonized the antihyperalgesic effects of antiepileptics in all of the groups in a varying rate.

Conclusions:

The results of this study demonstrate that the mechanisms of action of gabapentin, pregabalin, carbamazepine and oxcarbazepine are associated with TRPV1-cannabinoid pathway. TRPV1 channels are considered to be ionotropic cannabinoid receptors and may be modulated by endocannabinoids. Therefore, these drugs may contribute to the desensitization of TRPV1 channels by altering the endocannabinoid levels.

Acknowledgements

This study was supported by a grant of Anadolu University (BAP – 1905S073).

References:

1. Sisignano et al., (2014). TRP-channels as key integrators of lipid pathways in nociceptive neurons. Progress in lipid research, 53, 93-107.
2. Storozhuk, M.V., & Zholos, A.V. (2018). TRP channels as novel targets for endogenous ligands: focus on endocannabinoids and nociceptive signalling. Current neuropharmacology, 16(2), 137-150.
3. Tomić et al., (2018). Antiepileptic drugs as analgesics/adjuvants in inflammatory pain: current preclinical evidence. *Pharmacology & therapeutics*, *192*, 42-64.
4. Bektaş Türkmen et al., (2018). TRPV-1 channels contributes to antihyperalgesic effects of carbamazepine and oxcarbazepine. Klinik Psikofarmakoloji Bulteni, 28, 75-76.

OP092: EVALUATION OF THE PSYCHOLOGICAL BURDEN OF COVID-19 PANDEMIC ON YOUNG ADULT POPULATION

[1]Aksoy, N., [2]Ongun, E.

[1] Altınbaş University, Department of Clinical Pharmacy, Istanbul, Turkey, nilay.aksoy@altinbas.edu.tr

[2] Altınbaş University, Pharmacy Faculty, Istanbul, Turkey, elif.ongun@ogr.altinbas.edu.tr

Introduction:

Coronavirus Disease is an ongoing global pandemic which has affected the world since December 2019, caused by SARS-CoV-2 (1). In Turkey, the first COVID-19 case was seen in March 2020. Pandemics have serious effects on people's economic, emotional, social, and physical well-being. Lack of social life, time spent following COVID-19 news and being anxious about the future are inevitable reasons for the psychological changes (2,3). Depression, anxiety disorders, insomnia, stress, nervousness, mood instability, and even the most serious effect which is suicidal behavior started to increase during the pandemic. The aim of this study is to determine the psychological effect of the pandemic on the young adult Turkish population.

Materials and Methods:

A survey was performed using Google Forms and included validated questionnaires such as the Patient Health Questionnaire (PHQ-9) for depression, Generalized Anxiety Disorder (GAD-7) for anxiety, and the Insomnia Severity Index (ISI) for sleeping issues. Age, gender, current or previous diagnosis, and drug use were all inquired. The survey was shared on social media and has a 5-day completion deadline. The Altınbaş University Clinical Research Ethic Committee gave their approval to perform this study. Before answering the questions, all participants signed an online informed consent form. The statistical analyses for the PHQ-9, GAD-7, and ISI were performed using SPSS 26 (Statistical Package for the Social Sciences), Gender and age disparities in questionnaire responses were investigated using the Mann-Whitney U-test.

Results:

A total of 177 students took part in the survey and provided responses to the questioners. The vast majority of participants are female 73.5%. The majority of those who responded to the survey were under the age of thirty. Our survey's average age is 24.7±8.3. Only 12 of the 170 students polled were over 35 years old, with 158 being between the ages of 18 and 35. According to responses to the Patient Health Questionnaire (PHQ-9) for depression, the Generalized Anxiety Disorder (GAD-7) for anxiety, and the Insomnia Severity Index (ISI) for sleep issues, severe depression, anxiety, and insomnia were detected in 25.3 %, 25.3%, and 4.1%, respectively. Table 1 describes the severity of these psychological disorders among the student population.

When the study's findings are examined by gender, severe depression (27,2%, 20% in female and male respectively) and anxiety (28% female, 17,7% male) are more common in women, whereas severe insomnia is more common in men (1,6 female,11,1 male), $p<0,05$. When age groups are compared, it is shown that the youthful population <30 years old has the highest

rates of depression, anxiety, and insomnia, p<0,005. Table 2 describes the study's findings examined by gender and age.

Table 1. The severity of the psychological disorders among the student population

Depression			Anxiety			Insomnia		
	n	%		n	%		n	%
Minimal	9/170	5.3	**Minimal**	24/170	14.1	**Minimal**	62/170	36.4
Mild	30/170	17.6	**Mild**	63/170	37	**Subthreshold Insomnia**	66/170	38.8
Moderate	57/170	33.5	**Moderate**	40/170	23.5	**Moderate**	35/170	20.6
Moderately Severe	31/170	18.2	**Severe**	43/170	25.3	**Severe**	7/170	4.1
Severe	43/170	25.3						

Table 2. Psychological disorders in different age and gender groups

Variable	**Gender**		***p* value**
	Male	**Female**	
Severe Depression	20%	27,2%	<0,05
Severe Anxiety	17,7%	28%	<0,05
Severe Insomnia	11,1%	1,6%	<0,05
	Age		***p* value**
	18-35	**>35**	
Severe Depression	27,2%	0	<0,05
Severe Anxiety	26,5%	8,3%	<0,05
Severe Insomnia	4,4%	0	<0,05

Fluoxetine, a Selective Serotonin Reuptake Inhibitor, is the most often prescribed medicine for the treatment of depression, according to research. The second and third most popular alternatives are sertraline and medazepam. Another finding of the study is that Alprazolam, a benzodiazepine medicine, is the most regularly recommended prescription for anxiety problems, whereas herbal remedies like Passiflora Syrup and Melissa Tea were preferred by the majority of the study population to treat insomnia.

Depression, anxiety and insomnia are prevalent psychiatric disorders that affect both men and women at any age. In our study, when a comparison is made between genders, even though major depression and anxiety are more common in women, the incidence of severe insomnia for male (11.4%) is approximately 7 times more than females. This result conflicts with other research that indicates females are more prone to sleep disorders during the quarantine period compared to men (4). Considering the results of the survey, it was determined that there is a significant correlation between the ages of 18-35 and higher rates of psychological disorders. By implementing the quarantine process, the life of the young population has completely changed. Lack of sociality, unemployment and the stress about the future are the major determinant factors to have psychological disorder. Considering these factors, it can be interpreted that the result is predictable for high incidence of 18-35 ages.

A previous study done in the Swedish population concluded that the prevalence of psychological disorders was as follows (moderate 8.1%, severe depression 6.2%; moderate 13.6 %, severe anxiety 10.6%) (5). Although one more study found a similar result in the Bangladesh population with a survey done using the DASS-21, our research's findings percentages are quite higher since a 25.3% of the study population were suffering from severe depression and 18.2% from a moderate one while 25.3% of them were suffering from severe anxiety. When we compare our findings to a study conducted in a similar population prior to the pandemic, we may conclude that the COVID-19 pandemic has resulted in a five-fold rise in the rate of severe depression. May be deduced that the epidemic has had a significant impact on the young people, particularly in terms of disrupting their social lives and increasing future fear (6). Additionally, the most prescribed drug for depressed populations in our research findings was fluoxetine, which is preferred as a first line treatment due to its tolerability in the young population, efficacy and general safety in overdose. Moreover, the most preferred drug for patients suffering from anxiety in our study was alprazolam which is one of the benzodiazepine derivatives and it's generally preferred as a first line treatment due to its broad range of onset, efficacy and varied duration of action.

According to one study done in China in March 2020, the coronavirus epidemic was still in its infancy throughout the rest of the world, despite the fact that it was at a critical level in China at the time. The percentage of people who suffer from moderate insomnia is 6.8%, whereas the percentage of people who suffer from severe insomnia is 1% (7). Another study carried out in Bangladesh later on showed that the level of moderate-severe insomnia has climbed 2-3 times since March 2020 (moderate insomnia is 14.7% and severe insomnia is 3.1%) (8). In our research, it can be concluded that the coronavirus has been at higher levels (moderate insomnia level is 20.6% and severe insomnia level is 4.1%) compared to both studies, although it was done in 2021 after one year of the pandemic. When studies published on different periods are compared, it can be deduced that the prevalence of insomnia rises over time.

Conclusions:

The young population, especially students, are suffering from a variety of psychological disorders that may have been triggered or exacerbated by the COVID 19 pandemic, necessitating the creation of online support programs to help reduce anxiety and treating depression symptoms. Clinical pharmacists should take their role to monitor the side effects of the medications, help prevent withdrawal complications, and ensure continuity of the treatment.

References:

1. Pappa et al., (2020). Prevalence of depression, anxiety, and insomnia among healthcare workers during the COVID-19 pandemic: A systematic review and meta-analysis. Brain, behavior, and immunity, 88, 901–907.
2. de Figueiredo et al., (2021). COVID-19 pandemic impact on children and adolescents' mental health: Biological, environmental, and social factors. Progress in neuro-psychopharmacology & biological psychiatry, 106, 110171.
3. Son et al., (2020). Effects of COVID-19 on College Students' Mental Health in the United States: Interview Survey Study. Journal of medical Internet research, 22(9), e21279.

4. Altena et al., (2020). Dealing with sleep problems during home confinement due to the COVID-19 outbreak: Practical recommendations from a task force of the European CBT-I Academy. Journal of sleep research, 29(4), e13052.
5. McCracken et al., (2020). Psychological impact of COVID-19 in the Swedish population: Depression, anxiety, and insomnia and their associations to risk and vulnerability factors. European psychiatr: the journal of the Association of European Psychiatrists, 63(1), e81.
6. YILDIZ, E.(2021). Evaluation of antidepressant medication use and determination of risk factors for depression among university students in Istanbul. Aurum Journal of Health Sciences, 3(1), 3-18.
7. Lai et al., (2020). Factors Associated With Mental Health Outcomes Among Health Care Workers Exposed to Coronavirus Disease 2019. JAMA network open, 3(3), e203976.
8. Islam et al., (2020). Psychological responses during the COVID-19 outbreak among university students in Bangladesh. PloS one, 15(12), e0245083.

OP097: SMOKING BEHAVIORS IN COVID 19: AN ONLINE SURVEY AMONG 749 UNIVERSITY STUDENTS

Çelik, FG., **Demirel, G.**

[1] Cukurova University, Faculty of Pharmacy, Department of Pharmaceutical Toxicology, Adana, Turkey, gdemirel@cu.edu.tr

Introduction:

The global Covid-19 pandemic started in the first quarter of 2020 and caused many people to die due to lung problems. As a result of such drastic outcomes, addiction levels are expected to change because it is typical to observe changes in smoking addiction levels (as well as other types of addiction) as well during times when societal behaviors change (1).

Due to the Covid 19 pandemic, an unexpected and majör change has appeared in the lifestyles of the population, with an extreme decline of any form of socialization (2). Especially young university students were going through an overwhelming process, as they had to continue their life in isolation. Social distancing and self-isolation strongly impacted university students' lives, affecting in particular lifestyle and smoking behaviors.

Materials and Methods:

A web-based, cross-sectional study was conducted using a survey instrument to obtain responses from university students in Turkey. Approval for the study was obtained from the Republic of Turkey Ministry of Health- Scientific Research Platform (form number 2020-11-01T15_03_42) and Cukurova University Non-interventional Clinical Studies Ethics Committee (project number GO-105 dated 22.11.2020 and decision number 55).

A 30-item survey instrument was developed using the Fagstörm Nicotine dependence test and demographic data including COVID-19. The survey was administered to university students and demographic data, nicotine dependences, and knowledge and perceptions related to COVID-19 were obtained. In this survey, both pre and during Covid-19 dependency level was questioned.

Results:

A total of 749 respondents have been included in the study, aged between 19 and 30 years (54,8% females). Of 749 participants, a total of 571 health science students (medicine, pharmacy dentist, etc) completed the survey. The pre-pandemic and Covid-19 pandemic mean nicotine dependence scores were 3,03 and 2,97, respectively. A difference was seen pre-pandemic ($p = 0.002$) and during pandemic ($p = 0.005$) for those studying in health departments and other departments. Students who have middle socio-economical status had significantly higher nicotine dependence scores pre-covid-19, compared to during the pandemic. ($p=0.027$). Compared to pre and during the pandemic, the mean score of dependence was significantly lower in students whose parents were non-smokers during the pandemic. ($p=0.017$). For students who had to be in quarantine due to their relatives or family members, their dependency level was significantly higher compared to pre-pandemic. ($p=0.011$).

Conclusions:

Stress related to the COVID-19 pandemic appears to affect smokers in different ways, some smokers increase their smoking while others decrease it. While boredom and restrictions in movement might have stimulated smoking, the threat of contracting COVID-19 and becoming severely ill might have motivated others to improve their health by quitting smoking. (3)

From the beginning of the COVID-19 pandemic, supreme evidence has shown that smoking tobacco was a risk factor for pandemic (4). Recent studies demonstrated that smoking is linked to an increased risk of COVID-19 infection (5) and cigarette smokers are at a higher risk of having adverse effects after being contaminated (6). However, the psychosocial effect of the pandemic with related anxiety and stress raised by limitation and fear of illness could lead smokers to increase tobacco use.

As a result of this study, it was observed that their smoking behavior during covid was increased the pre and during pandemic. Consequently, an increase or decrease in addiction levels can be seen because of withdrawal from social life and anxiety caused by a pandemic. During the Covid 19 pandemic, addictions like smoking need exhaustive management, especially among vulnerable young populations such as quarantined people and individuals who are at higher risk for smoking and other addictive behaviors. Thus, necessary planning should be made by relevant health institutions to end smoking addiction and other substance abuse habits by taking advantage of the pandemic periods.

References:

1. Fidanci İ, Aksoy H, Yengil Taci D, Ayhan Başer D, Cankurtaran M (2021). Evaluation of the effect of the Covid-19 pandemic on smoking addiction levels. Int J Clin Pract. https://doi.org/10.1111/ijcp.14012.
2. Wang C, Pan R, Wan X, Tan Y, Xu L, Ho CS, et al (2020). Immediate psychological responses and associated factors during the initial stage of the 2019 coronavirus disease (COVID-19) epidemic among the general population in China. Int J Environ Res Public Health, 17:1729.
3. Bommelé J, Hopman P, Hipple Walters B, Geboers C, Croes E, Fong T, Willemsen M (2020). The double-edged relationship between COVID-19 stress and smoking: Implications for smoking cessation. Tobacco Induced Diseases. https://doi.org/10.18332/tid/125580.
4. World Health Organization. (2020). Smoking and COVID-19: Scientific brief. https://www.who.int/publicatio. [accessed 2020 June 30].
5. Russo P, Bonassi S, Giacconi R, et al. (2020). COVID-19 and smoking: is nicotine the hidden link?. Eur Respir J, 55(6):2001116. doi:10.1183/13993003.01116-2020.
6. Vardavas CI, Nikitara K. (2020). COVID-19 and smoking: A systematic review of the evidence. Tob Induc Dis, 18: 1-4. doi:10.18332/tid/119324.

OP100: EVALUATION OF THE IN-VITRO CYTOTOXIC ACTIVITY OF SUNSET YELLOW IN ACUTE AND CHRONIC DOSING SCENARIOS

[1]Sönmez, K., [1]Dural, E., [2]Süzen, HS.

[1] Sivas Cumhuriyet University, Department of Pharmaceutical Toxicology, Sivas, Turkey, kifayetsonmez@icloud.com, emrahdural@cumhuriyet.edu.tr

[2] Ankara University, Department of Pharmaceutical Toxicology, Ankara, Turkey, sinansuzen@ankara.edu.tr

Introduction:

A synthetic anionic azo dye, sunset yellow (SY) is widely used as colorant and food additives worldwide since its ability to give different shades of orange (1). Sunset yellow is intolerant to salicylates in humans. There are conflicting reports in the literature that its widespread use causes some adverse effects on the health of exposed individuals and, more broadly, on public health. It releases histamine and intensifies asthma symptoms. Long-term and excessive use of sunset yellow causes hives, rhinitis, nasal congestion, allergies, hyperactivity, kidney tumors, asthma, abdominal pain, nausea and vomiting, indigestion and loss of appetite (2). However, genotoxicity and teratogenic activities of SY, as well as developmental toxic activities and potentials of causing oxidative damage are frequently reported (3). Studies carried out and new data obtained highlight the toxicological importance and risk potential of SY exposure (4). In this study, it was aimed to conduct an in vitro-based study to determine the change in cytotoxic activity of SY depending on 1-day acute and 5-day chronic dosing, in order to better represent real human exposures and to make a more accurate risk assessment. In order to determine the effects of the main structure and its metabolite on the cytotoxicity of Sunset yellow, two separate lymphoblastoid cell lines, AHH1 cell, which has CYP450 metabolism activity, and TK6, which do not have this activity, were used.

Material and Methods:

In this study, the human TK6 and AHH1 lymphoblastoid cell lines were used. TK6 and AHH1 cells were cultured with +37 °C, 100% humidity and 5% CO_2 in RPMI 1640 supplemented with 10% horse serum and 1% L-glutamine. The relative population doubling (RPD%) test was used for the determination of cytotoxic effects of SY in different dose concentrations. The RPD % calculation was carried out according to the OECD-487 guideline (5) that given below:

$$\text{RPD\%} = \frac{Number\ of\ population\ doublings\ in\ treated\ cultures}{Number\ of\ population\ doublings\ in\ control\ cultures} \times 100$$

$$\text{Population doubling} = [\log(\text{Post-treatment cell number} \div \text{Initial cell number})] \div \log 2$$

After the TK6 and AHH1 cell suspensions were grown in T75 flasks, they were seeded in 6-well plates at 1 x 10^5 cells/mL (3 mL). This number was recorded as the first day of the RPD% study. On the second day, each plate was dosed with appropriately diluted SY after they were counted by neaubeaur style hemacytometers with a reversed-phase microscope and incubated 24 hours for acute and 5 x 24 hours for chronic study. Here, in accordance with OECD guidelines, a maximum of 1% of the medium, that is, a maximum of 30 µL volume for 3 mL of medium, is used in dosing. For the 24 hours acute SY treatment, at the end of the dosing

time cells were counted by the same way. On third day out of the 5 days chronic treatment, cells were counted and diluted again as to ensure cell number was 1 x 10^5 cell/mL. The cell volume used at this stage was recorded and used as a dilution factor for calculating RPD%. After preliminary tests were made to determine the optimized dose concentrations of Sunset yellow to be used in the experiment, it was decided to use concentrations of 380 µg/mL, 760 µg/mL, 1140 µg/mL, 1520 µg/mL, 1900 µg/ml in the study. Acute doses of SY administered chronically were divided into 5 equal doses. Acute and chronic dosing applications were carried out in 3 replicate experiments for each dose concentration of SY. During the acute and chronic dosing experiment, the cell counts in the flasks should be kept between 1 x 10^5 and 1 x 10^6 µg/mL concentrations in accordance with the OECD-487 guideline.

Results:

In the acute study, it was clearly observed that the cytotoxic activity of SY was dose-dependent at the applied 5 dose concentrations for both cell lines. The RPD% values observed at the concentrations given above in the acute study were 87.75%, 76.48%, 74.09%, 71%, and 66.06%, respectively in the TK6 cell line. RPD% values of chronic dosing were 97.11%, 86.90%, 87.23%, 92.61% and 92.10%. In the AHH1 cell line, same concentrations' RPD% values were found as 89.12%, 76.42%, 74.04%, 72.97%, 65.66%. RPD% values of chronic dosing were 93.68%, 91.47%, 92.91%, 95.29%, 93.65%. For these concentration RPD% values, it was observed that the acute study caused an increase in cytotoxicity by 1.11, 1.14, 1.18, 1.30, and 1.40 times, respectively, compared to chronic application in TK6. As the same, the comparing of cytotoxicity acute to chronic dosing were observed as 1.00, 1.05, 1.13, 1.31, 1.51 in the AHH1 cell line. The RPD% results obtained from acute and chronic dosing of SY to TK6 and AHH1 cell lines are given in Table 1.

Table 1. Comparison of acute and chronic dosing values of SY in TK6 and AHH1 cell lines

TK6				AHH1					
			Fold Change				Fold Change	Fold Change	
								Acute	Chronic
Conc. (µg/mL)	Acute	Chronic	Act/Chr	Conc. (µg/mL)	Acute	Chronic	Act/Chr	TK6/AHH1	TK6/AHH1
N.Cont.	100.00	100.00	1.00	N.Cont.	100.00	100.00	1.00	1.00	1.00
380	87.75	97.11	1.11	380	94.04	93.68	1.00	1.07	0.96
760	76.48	86.90	1.14	760	87.29	91.47	1.05	1.14	1.05
1140	74.09	87.23	1.18	1140	81.91	92.91	1.13	1.11	1.07
1520	71.00	92.61	1.30	1520	72.87	95.29	1.31	1.03	1.03
1900	66.06	92.10	1.39	1900	61.98	93.65	1.51	0.94	1.02

It has been determined that acute exposure to SY causes cytotoxic effects in both TK6 and AHH1 cell lines in a dose-dependent manner. However, it was observed that the presence of CYP450 activity in cells in acute SY dosing did not have a significant effect on the toxicity of SY, but in chronic dosing, it had a modest effect on reducing toxicity (Table 1, Figure 1).

Conclusions:

There are some in vitro studies on the cytotoxic activity of SY in the literature. For example, Yadav et al. (2013) found that the cytotoxicity of SY is dose-dependent. In this study, the highest non-cytotoxic dose of SY was found to be 250 µg/mL. Here, the cytotoxic activity of

SY was found to increase significantly at higher doses (500 and 1000 µg/mL) (6). Similar results were obtained in our study. Kuş and Eroglu (2015) found that SY concentrations of 30 and 40 mg/mL were cytotoxic (7). These concentration values are approximately 30-40 times higher than the SY concentrations we evaluated in our study. In our study, cytotoxic effect was observed even at acute initial dose in TK6 and AHH1 cell lines. Contrary to these data, Haveric et al. (2018) reported that SY concentrations of 450, 900, 1800 and 3600 µg/mL in in vitro human lymphocyte cultures were neither genotoxic nor cytotoxic (8).

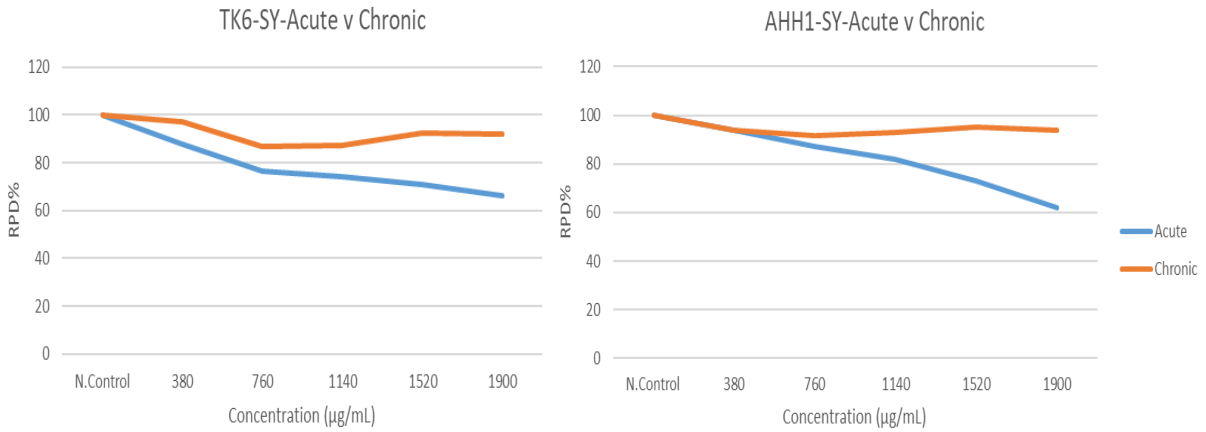

Figure 1. Comparison of acute and chronic dosing treatment values of SY in AHH1 and TK6 cell lines.

In this study, which we performed in cell culture in vitro, SY was dissolved in the highest concentration that can be dissolved in water (and then sterilized with a 0.22 µm injector tip filter) and applied to the cell culture study and caused dose-dependent cytotoxicity in both lymphoblastoid cell lines in acute dosing. In chronic dosing, however, dose-independent cytotoxicity was observed both in TK6 and AHH1 cell lines, although less than in acute dosing. While the presence of bioactivation (CYP450 activity) did not significantly contribute to the cytotoxic effect of SY in acute dosing, it contributed positively in chronic dosing (Figure 1).

As a result of the study, the presence of cytotoxic effect of SY at the relevant concentrations was determined. In order to elucidate the toxic effect mechanism of SY, it is recommended to evaluate the mitochondrial damage activity using the MTT test and to determine the free radical damage-inducing activity using the DCFDA test. In addition, it is recommended to investigate its genotoxic activity using the single cell rational COMET test, and its mutagenic activity using the HPRT test. Our laboratory studies to determine other toxic effects of SY continue.

Acknowledgements

This study was supported by the Scientific and Technological Research Council of Turkey (TÜBİTAK) under the scope of the University Students Research Projects Support Program, known as TÜBİTAK2209A, with the number 1919B012001095 in the 2020/2 term.

References:

1. Wood R et al., (2004). İnternational Journal of Food Science and Tecnology, 1-14.
2. ANON (2002). Ministry of Agriculture and Rural Affairs and Ministry of Health, Turkish Food Codex, Colorants Used in Food.

3. Osman M Y et al., (2002). Br J Biomed Sci., 59: 4, 212-217.
4. European Food Safety Authority, (2011). EFSA Journal, 9: 9, 2349.
5. OECD, Test No. 487 (2010). In Vitro Mammalian Cell Micronucleus Test.
6. Yadav A et al., (2013). Toxicol Lett, 217: 3, 197-204.
7. Kus ve Eroglu (2015). Pak J Pharm Sci., 28: 1, 227-230.
8. Haverić A et al., (2018). Cell Mol Biol, 28: 64, 87-91.

OP106: EVALUATION OF IN VITRO CYTOTOXIC ACTIVITY OF HYDROXYCHLOROQUINE

[1]Önal, Ş., [1]Dural, E., [2]Süzen, H.S.

[1] Sivas Cumhuriyet University, Faculty of Pharmacy, Department of Pharmaceutical Toxicology, Sivas, Turkey

[2] Ankara University, Faculty of Pharmacy, Department of Pharmaceutical Toxicology, Ankara, Turkey

Introduction:

Hydroxychloroquine (HCQ) is an anti-malarial medication that has been utilized as treatment for a variety of autoimmune diseases, such as rheumatoid arthritis, systemic lupus erythematosus, and other inflammatory and dermatologic conditions (1). It is also reported to be used as the treatment agent for the COVID-19 pandemic in many countries (2). However, it has been reported that HCQ has very serious toxic effects, especially on the cardiovascular system. HCQ's side and adverse effects are gastrointestinal effects (vomiting, stomache ache, etc.), skin related effects (skin rash, itching, hair loss), retinopathy, conduction disturbances and cardiomyopathy. HCQ may cause irreversible retinopathy. Retinopathy occurs particularly with high dose and long-term use of HCQ. Cardiac side effects are rarely reported, but in some cases can be severe and irreversible. They comprise conduction disturbances and cardiomyopathy – often with hypertrophy, restrictive physiology and congestive heart failure (3). Although many serious toxic effects have been reported, the number of studies on cytotoxicity is very limited.

In this study, it was aimed to conduct an *in vitro*-based study to determine the change in cytotoxic activity of HCQ depending on 1-day acute and 5-day chronic dosing, in order to better represent real human exposures and to make a more accurate risk assessment. For this purpose, two separate lymphoblastoid cell lines named TK6 and AHH1 were used.

Materials and Methods:

In this study, a human TK6 and AHH1 lymphoblastoid cell lines were employed. The cell lines AHH1 and TK6 (CYP450 activity-competent and-deficient, respectively) were cultured in RPMI 1640 supplemented with 10% horse serum and 1% L-glutamine in an 80 cm^2 flask at 37°C, 5% CO_2 with 100% humidity. The relative population doubling (RPD%) test was used to determine the cytotoxic effects of HCQ at different dose concentrations. In the calculation of RPD%, OECD's guideline numbered 487 was used (4). RPD% calculation formula is given below:

$$\%RPD = \frac{Number\ of\ population\ doublings\ in\ treated\ cultures}{Number\ of\ population\ doublings\ in\ control\ cultures} \times 100$$

Population doubling = [log (Post-treatment cell number ÷ Initial cell number)] ÷ log 2

Initially, cells were seed in the 6-well plate as 1 x 10^5 cell/mL. After 24 hours, they were counted by neubauer style hemacytometers with a reversed-phase microscope and then were dosed with the proper appropriate concentration of chemical agents. For 24 hours after the cells were

treated with HCQ, at end of the dosing time cell were counted by the same way and it was calculated according to the %RPD equation. On third day out of 5 days chronic treatment, cells were counted and diluted again as to ensure cell number was 1 x 10^5 cell/mL.

The cells were maintained at concentrations between 1 x 10^5/ml and 1 x 10^6/ml during to the study. Acute and chronic dosing applications were carried out in 3 replicate experiments for each dose concentration of HCQ. Although the acute dosing study was performed by applying the total dose to the cells in a single time within 24 hours, chronic dosing was performed by applying the same total dose divided into fractions to the cells on 5 days.

Cell suspensions were prepared at 1 x 10^5 cells/mL and treated with serial dilution with one of the chemicals described above for 24 h and 5 days (acute and chronic, respectively). In the 5-day chronic exposure study, when the 3rd dosing day was reached, the cells in the flasks were counted to keep the number of cells within the desired range. Then, the volume was adjusted to keep cells at 1 x 10^5/mL. The cell volume used at this stage was recorded and used as a dilution factor for calculating RPD%. After the preliminary tests were made to determine the optimized dose concentrations of HCQ to be used in the experiment, it was decided to use values of 20, 40, 60, 80 and 100 µM in the study.

Results:

It was clearly observed that the cytotoxic activity of HCQ was dose-dependent at the applied 5 dose concentrations not only in the acute but also the chronic study. In this study performed with TK6 and AHH1 cells, the RPD% results obtained from acute and chronic dosing applications with HCQ chemical are given in Table 1.

Table 1. Comparison of acute and chronic dosing treatment values of HCQ in TK6 and AHH1 cell lines

TK6				AHH1					
			Fold Change				Fold Change	Fold Change	
								Acute	Chronic
Conc. (µM)	Acute	Chronic	Chr/Act	Conc. (µM)	Acute	Chronic	Act/Chr	AHH1/TK6	TK6/AHH1
N.Cont.	100.00	100.00	1.00	N.Cont.	100.00	100.00	1.00	1.00	1,00
20	98.84	100.01	0.99	20	60.50	93.52	1.50	1.63	0.94
40	75.22	89.65	0.84	40	39.75	89.35	2.97	1.89	1.00
60	71.52	77.62	0.92	60	25.95	79.75	4.10	2.75	1.03
80	38.20	28.18	1.36	80	12.26	72.52	41.64	3.11	2.57
100	25.47	-24.39	-1.04	100	-1.66	62.71	-4.17	-5.34	-2.57

It was observed that the cytotoxic effect of HCQ in the AHH1 cell line which has CYP450 activity increased in a dose-dependent manner in acute exposure. Contrary to this result, the chronic cytotoxic effect of HCQ increased dose-dependently in TK6 cells.

Conclusions:

The number of *in vitro* studies on HCQ is so limited in the literature. HCQ cytotoxicity in melanocytes was found to be concentration-dependent by Li et al. (2016). The concentration-dependent cytotoxicity was observed when the concentration of HCQ was >7.4 µM. The

cytotoxic effect was not observed when the concentration of HCQ was <3 µM (5). HCQ dose concentrations observed to be cytotoxic in this study performed with acute dosing were consistent with the dose concentrations found to be cytotoxic in our study.

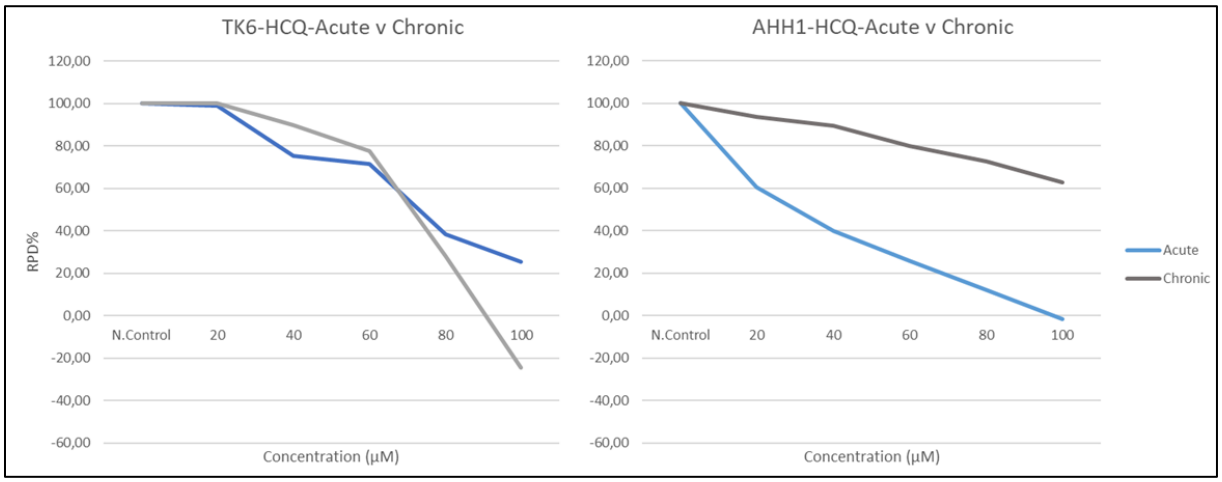

Figure 1. Comparative representation of acute and chronic dosing-induced cytotoxicity values of HCQ in both TK6 and AHH1 cell line

In our study both in acute and chronic study, TK6 and AHH1 cell lines, it was clearly observed that the cytotoxic activity of HCQ was dose-dependent at the applied 20, 40, 60, 80 and 100 µM concentrations (Figure 1). Metabolism activities reduce the cytotoxicity of HCQ. In the absence of CYP450 activity, the cytotoxic effect of HCQ was increased in chronic dosing. The data we have obtained so far indicate that the structure responsible for the cytotoxicity of HCQ is itself (main structure), and the metabolite/s formed as a result of metabolism activities reduce the toxicity of HCQ. This suggests that HCQ-related toxicity reported in the literature is dependent on differences in individual metabolic activities. Therefore, further testing which may include its metabolite is recommended to find out the cause of this cytotoxicity of the substance. For this purpose further tests which are XTT, micronucleus (MN), Comet assay, DCFDA and HPRT were suggested for elucidation of HCQ *in vitro* toxic effect mechanism. Our research group are still working on this chemical for elucidation of its toxic effect mechanism.

Acknowledgements

This study was supported by the Scientific and Technological Research Council of Turkey (TÜBİTAK) under the scope of the University Students Research Projects Support Program, known as TÜBİTAK2209A, with the number 1919B012002217 in the 2020/2 term.

References:

1. Schlesinger PH, Krogstad DJ, Herwald BL (1988). Antimalarial Agents: Mechanisms of Action. Antimicrobial Agents And Chemotherapy, 32(6): 793-798.
2. Yao X, Ye F, Zhang M, Cui C, Huang B, Niu P (2020). In Vitro Antiviral Activity And Projection Of Optimized Dosing Design Of Hydroxychloroquine For The Treatment Of Severe Acute Respiratory Syndrome Coronavirus 2(SARS-CoV-2). Clinical Infectious Diseases, 71: 732-739.
3. Tönnesmann E, Kandolf R, Lewalter T (2013). Chloroquine Cardiomyopathy. Immunopharmacology And Immunotoxicology, 35(3): 434-442.
4. OECD Guidelines (2010). Test No. 487: In Vitro Mammalian Cell Micronucleus Test.

5. Li D, Hu W, Ma H, Liu W, Yang Q, Zhao G (2016). Hydroxychloroquine protects melanocytes from autoantibody-induced injury by reducing the binding of antigen-antibody complexes. Molecular Medicine Reports, 14: 1275-1282.

OP108: POSSIBLE EFFECT OF CHELATION TREATMENT ON METABOLOMIC AND LIPIDOMIC ANALYSIS IN LEAD EXPOSURE

[1]Çetin, T., [2]Samadi, A., [3]Reçber, T., [2]Eser, B., [2]Yalcinkaya, A., [2]Öztaş, Y., [3]Nemutlu, E., Lay, İ., [1]Sabuncuoğlu, S.

[1] Hacettepe University, Faculty of Pharmacy, Department of Pharmaceutical Toxicology, Ankara, Turkey, *tugcecetin06@gmail.com, *suna@hacettepe.edu.tr

[2] Hacettepe University, Faculty of Medicine, Department of Biochemistry, Ankara, Turkey

[3] Hacettepe University, Faculty of Pharmacy, Department of Analytical Chemistry, Ankara, Turkey

Introduction:

Lead (Pb) is a widely preferred heavy metal in the industry due to its useful physicochemical properties. It can get in the human body through food, water, soil and air (1). Because it is not biodegradable and has a slow elimination rate, it tends to accumulate in the body. Pb has important toxic effects in biological systems such as hematopoietic, renal, reproductive, and central nervous systems (2). Chelation agents are used in its treatment and intravenous sodium calcium edta ($CaNa_2EDTA$) is one of the important chelation agents used in the treatment (3). Oxidative stress is considered to be the main mechanism of Pb poisoning. It has a strong electron sharing property that aids in covalent bond formation. Covalent bonds formed between Pb and sulfhydryl groups in antioxidant enzymes ultimately render them ineffective (1, 2). Cholesterol, an important component of the cell membrane in mammalian tissues, is a molecule sensitive to oxidation reactions due to its structure. The main metabolites formed as a result of the oxidation of cholesterol are oxidation products known as oxysterols (4). Studies have shown that oxysterols formed by auto-oxidation in particular play a role in the pathogenesis of diseases such as atherosclerosis, neurological diseases and cancer (4,5). Sphingosine 1-phosphate (S1P) is a signal sphingolipid. They play an important role in a variety of cellular processes that are largely associated with inflammation and apoptosis (6). Metabolites are intermediate products of biochemical reactions and are important chemical molecules that are involved in or arise during the functioning of many different metabolic cascades in the living cell. Metabolomic analysis is the most ideal method for diagnosing disease or investigating the effects of toxic agents on phenotype (7). The present study was designed to investigate the possible influence of chelation treatment on metabolomic and lipidomic profile.

Materials and Methods:

Heparinized blood and urine samples were collected from occupationally Pb exposed workers (age 36±7.6 years, n=42) before and after chelation therapy. Pb workers with chronic illness, chemotherapy/radiotherapy treatment, viral infection and not requiring chelation therapy (with a blood Pb level of 35 µg/dl) were not included in the study. Consent was obtained from 42 individuals diagnosed with Pb poisoning and two different blood samples and urine were collected before and after chelation therapy. Oxysterol derivatives formed by autoxidation 7-ketocholesterol (7-KC), 3β, 5α, 6β trihydroxy cholestane (triol) and S1P levels were analyzed by LC-MS/MS. Metabolomic analyzes were performed with GC-MS/MS.

Results:

7-KC and triol levels before chelation were measured as 37.35 ± 2.53 ng/ml and 41.81 ± 2.54 ng/ml while after chelation they were 22.91 ± 4.49 ng/ml and 17.64 ± 3.42 ng / ml, respectively ($p < 0.001$). S1P levels were measured as 60.76 ± 15.03 ng/ml before chelation and 48.79 ± 10.75 ng/ml for afterwards. In addition, pathway analysis was made using the metabolites determined in the metabolomic studies. The results showed that important pathways such as aspartate, glutamate, homocysteine metabolisms, mitochondrial electron transport chain, as well as sphingolipid metabolism and linolenic and linoleic acid metabolism pathways were affected (Figure 1).

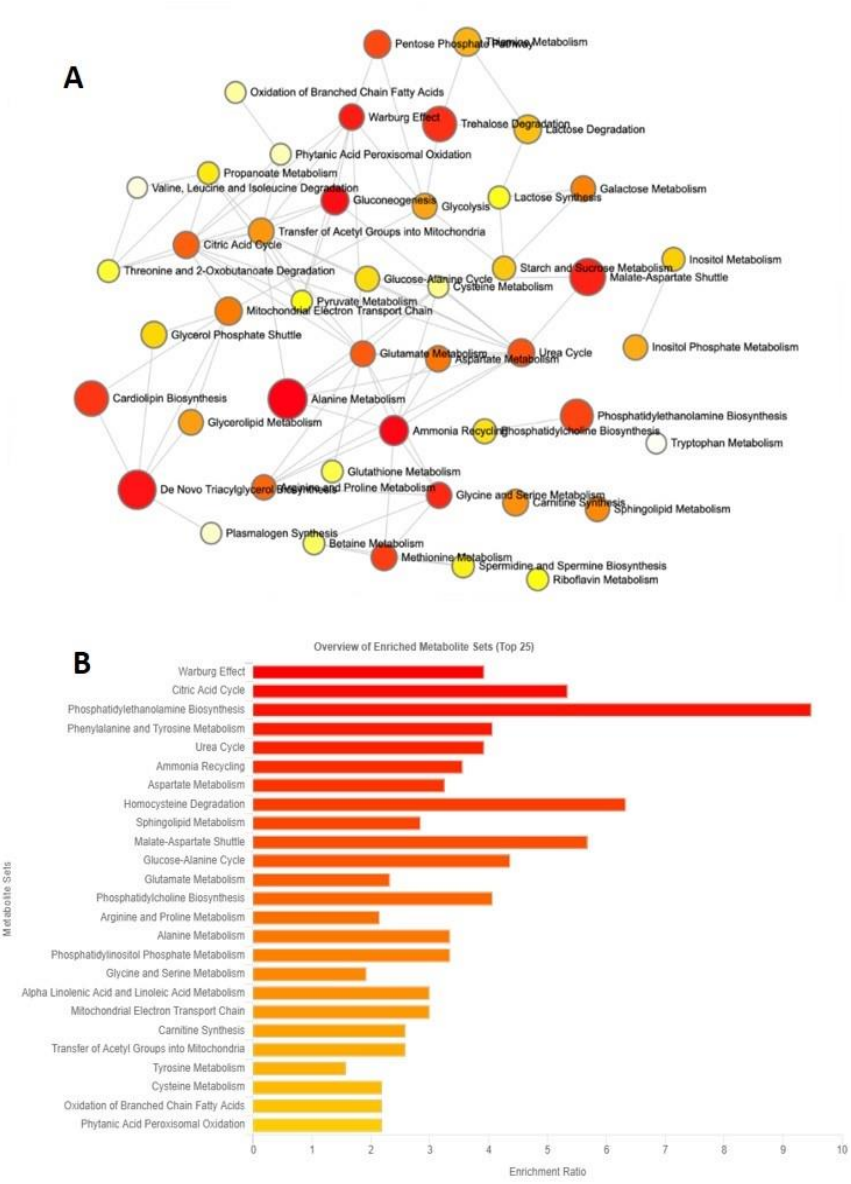

Figure 1. General altered pathways before and after chelation therapy (A) and pathways derived from enriching pathway analyzes of statistically significant altered metabolites (B).

Conclusions:

In a study conducted with workers exposed to Pb, 137 patients were studied and two groups were formed according to the level of Pb exposure. In these groups, cholesterol oxidation was

evaluated by measuring 7-KC levels and oxidative lipid damage was evaluated by measuring malondialdehyde (MDA) levels. As a result of the study, while no significant change was observed in 7-KC levels, it was determined that lipid peroxidation was induced (8).

In a study investigating the plasma metabolomic profile of Pb exposure, analyzes were performed on toenail and blood samples collected from the study group. 858 metabolites were measured in samples collected from a total of 399 individuals, and 154 of them were found to be significantly associated with blood Pb. At the end of the study, it was determined that Pb exposure was effective in metabolites and metabolomic pathways associated with oxidative stress and immune dysfunction (9).

In this experiments, it was determined that the chelation treatment reversed the increased cholesterol auto-oxidation when compared before and after chelation treatment, and S1P levels decreased with chelation treatment. Considering the effect of chelation therapy on the parameters of Pb toxicity, the main mechanism of which is oxidative stress, it can be concluded that antioxidant supplements to be used may help reduce Pb toxicity and prevent oxidative lipid damage caused by the oxidative stress mechanism. The metabolomics data obtained also revealed changes in many metabolite profiles with which lipid pathways (e.g. sphingolipid metabolism) are related, and it was concluded that it is necessary to carry out large-scale lipidomic studies by increasing the number of patients in the future. This is also the first pilot study related to Pb toxicity was evaluated with all its parameters.

References:

1. Klaassen CD, Amdur MO (2013). Casarett and Doull's toxicology: the basic science of poisons. Mc Graw Hill Education, United States of America.
2. Sachdeva C, et al., (2018). Lead: Tiny but Mighty Poison. Indian Journal of Clinical Biochemistry, 33(2):132-46.
3. Čabarkapa A, et al., (2015). $CaNa_2EDTA$ chelation attenuates cell damage in workers exposed to lead-a pilot study. Chemico-biological interactions, 242:171-8.
4. Brown AJ, Jessup W (2009). Oxysterols: sources, cellular storage and metabolism, and new insights into their roles in cholesterol homeostasis. Molecular aspects of medicine, 30(3):111-22.
5. Aksu N, et al., (2020). Evaluation of oxysterol levels of patients with silicosis by LC–MS/MS method. Molecular and cellular biochemistry, 467(1):117-25.
6. Dai L, et al., (2017). Sphingosine kinase 1/sphingosine1-phosphate (S1P)/S1P receptor axis is involved in ovarian cancer angiogenesis. Oncotarget, 8(43):74947.
7. Griffiths W, et al., (2007). Metabolomics and metabolite profiling: past heroes and future developments. European journal of mass spectrometry, 13(1):45-50.
8. Kasperczyk S, et al., (2005). Lipids, lipid peroxidation and 7-ketocholesterol in workers exposed to lead. Human & Experimental Toxicology, 24(6):287-95.
9. Kelly RS, et al., (2020). Metabolomic signatures of lead exposure in the VA Normative Aging Study. Environmental Research, 190:110022

OP118-DESIGN OF A NOVEL NANOSENSOR FOR THE DETERMINATION OF CARDIAC INOTROPE DRUG

[1]Unal, D.N., [1]Selcuk, O., [2]Süslü, İ., [1]Uslu, B.

[1]Ankara University, Faculty of Pharmacy, Department of Analytical Chemistry, Ankara, Turkey, dnunal@ankara.edu.tr, ozgselcuk@ankara.edu.tr, buslu@pharmacy.ankara.edu.tr

[2] Hacettepe University, Faculty of Pharmacy, Department of Analytical Chemistry, Ankara, Turkey, isuslu@hacettepe.edu.tr

Introduction:

Milrinone (MIL) is a selective phosphodiesterase-3 enzyme inhibitor used in the treatment of heart failure. Although amrinone is a bipyridine derivative, MIL is more effective and has fewer side effects than amrinone. MIL has a positive inotropic and vasodilatory effect by inhibiting cAMP degradation (1,2). Several analytical methods, including gas chromatography (3), high-performance liquid chromatography (4,5), and spectroscopic(6) been used to determine MIL in pharmaceutical formulations and biological fluids. To the best of our knowledge, no electrochemical studies have been conducted on the determination of MIL with bare or modified electrodes. Electrochemical sensors have some extraordinary features such as rapid determination, easy preparation, suitability to miniature chip technology, and working electrodes can be modified with various nanomaterials thanks to developing nanotechnologies. The aim of our study is electrochemical detection of milrinone using flower-like zinc oxide (ZnO) modified nanodiamond decorated carbon paste electrode (ZnO/nD@CPE).

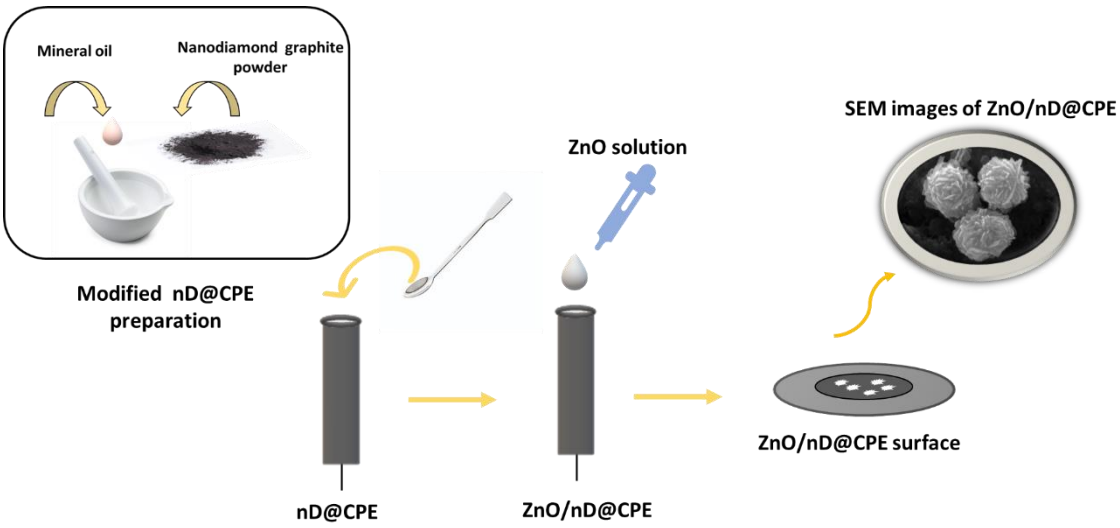

Figure 1. Fabrication of ZnO/nD@CPE for MIL determination

Materials and Methods:

The voltammetric measurements were performed using PalmSens EmStat 4 potentiostat (DropSens, Metrohm, Turkey) with PSTrace 5.8 software. CPE (Ø = 3 mm) as working electrode, platinum wire as an auxiliary electrode, and Ag/AgCl as reference electrode (KCl 3 M, BAS) used for all measurements. In order to modification of CPE, graphite powder and diamond nanoparticles were mixed well to get a uniform mixture. Then, mineral oil was added, and the mixture was mixed with mortar and pestle to get a soft paste. ZnO/nD@CPE was prepared by dropping an optimized amount of ZnO suspension onto the nD@CPE surface and drying. Electrochemical measurements were performed with differential pulse voltammetry (DPV). The general morphologies of the modified electrode surfaces were characterized by SEM and IR spectroscopy. Electrochemical characterization of ZnO/nD@CPE was performed cyclic voltammetry (CV) and electrochemical impedance spectroscopy (EIS) techniques.

Results:

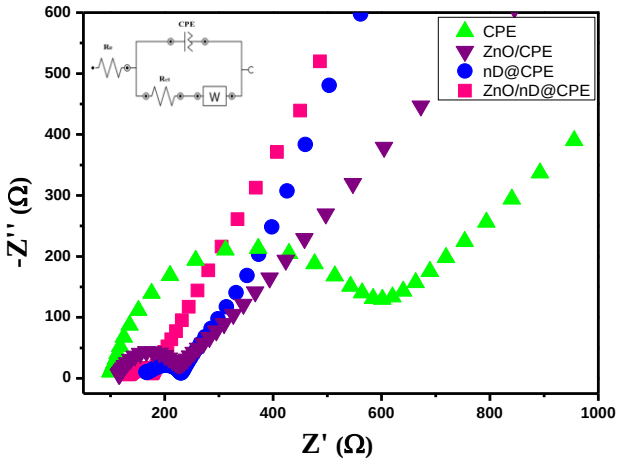

Figure 2. Nyquist plots of electrochemical impedance spectra (Inset: modified Randles equivalent circuit) at; Bare CPE, ZnO/ CPE, nD@CPE, and ZnO/nD@CPE, respectively.

EIS analysis is a important tool for predicting the mechanism of MIL sensor. Fig. 2 illustrates the Nyquist plot for bare CPE, ZnO/CPE, nD@CPE and ZnO/nD@CPE in the presence of 0.1 M KCl with 5 mM $K_3[Fe(CN)_6]/K_4[Fe(CN)_6]$. R_{ct} values for the bare CPE, ZnO/CPE, nD@CPE and ZnO/nD@CPE are found to be 442.5, 95.4, 46.6 and 30.9 Ω, respectively. From the observed R_{ct} value, it is clear among the studied sample ZnO/nD@CPE exhibit the lowest charge transfer resistance suggesting the better electron-transfer mobility at the interface.

The effect of key parameters such as modifying agent amount, dropping volume, pH of buffer solution, and scan rate was studied and optimized to achieve the best response for the electrochemical behavior of the MIL. ZnO/nD@CPE increases MIL electrochemical oxidation signals ~5 fold compared to CPE. Therefore, ZnO/nD@CPE has been chosen as the most suitable surface for MIL detection. In the linear range from $6x10^{-7}$ to $1x10^{-5}$ M, the limit of detection (LOD) was found as $1.42x10^{-7}$ M using ZnO/nD@CPE for determination of MIL.

Conclusions:

In the current study, a new ZnO/Diamond modified CPE was successfully produced and then applied as a new electrochemical sensor to study the electrochemical behavior of the MIL at pH 4.0 BRBS. The current curing performance of the modified electrode was verified from the improved interface and surface area properties obtained from EIS and CV experiments..

In summary, we have developed a novel nanosensor for the determination of MIL. Sensitive detection of the MIL was performed for the first time using an electrochemical method. Electrode conductivity for sensing was substantially changed by modifying ZnO with flower structure to nD@CPE surface. The determination of MIL in bulk, ampoule, human serum, and urine samples was successfully performed by the DPV method. Our developed nanosensor work opens up a novel avenue for electrochemical drug analyses.

Acknowledgements

The authors would like to thank VEM İlaç San. ve Tic. A.Ş, (Istanbul, Turkey) for chemical substances and their pharmaceutical dosage form support.

References:

1. Brocks, D. R., Spencer, T. J. and Shayeganpour, A. (2005). A sensitive and specific high performance liquid chromatographic assay for milrinone in rat and human plasma using a commercially available internal standard and low sample volume. Journal of Pharmacy and Pharmaceutical Sciences, 8(2), 124–131.
2. Edelson, J. et al. (1983). High-performance liquid chromatographic analysis of milrinone in plasma and urine. Intravenous pharmacokinetics in the dog. Journal of Chromatography B: Biomedical Sciences and Applications, 276(C), 456–462. doi: 10.1016/S0378-4347(00)85117-8.
3. Gackowski, M., Koba, M. and Kruszewski, S. (2020). Comparison of UV- and Derivative-Spectrophotometric and HPTLC UVDensitometric Methods for the Determination of Amrinone and Milrinone in Bulk Drugs. Current Pharmaceutical Analysis, 16(3), 246–253. doi: 10.2174/1573412914666180627141659.
4. IKEDA, Y. et al. (1991). Periandradulcins A, B and C: Phosphodiesterase inhibitors from Periandra dulcis Mart. Chemical and Pharmaceutical Bulletin, 39(3), pp. 566–571. doi: 10.1248/cpb.39.566.
5. Magiera, S. et al. (2011). GC-MS method for the simultaneous determination of β-blockers, flavonoids, isoflavones and their metabolites in human urine, Journal of Pharmaceutical and Biomedical Analysis. Elsevier B.V., 56(1) 93–102. doi: 10.1016/j.jpba.2011.04.024.
6. Nadur, N. F. et al. (2021). The long and winding road of designing phosphodiesterase inhibitors for the treatment of heart failure. European Journal of Medicinal Chemistry. Elsevier Masson SAS, 212, 113123. doi: 10.1016/j.ejmech.2020.113123.

OP119: ASSESSMENT OF ANTIOXIDANT AND ANTICANCER ACTIVITIES OF ACHILLEA PHRYGIA EXTRACT LOADED CHITOSAN NANOPARTICLES

[1]Taşkın, D., [2]Doğan, M.

[1] University of Health Sciences Turkey, Department of Analytical Chemistry, İstanbul, Turkey

[2] University of Sivas Cumhuriyet, Department of Pharmaceutical Biotechnology, Sivas, Turkey

Introduction:

The use of plant extracts with antioxidant and anticancer activity has been recommended for the treatment of some diseases (1). Despite superior properties of extracts and essential oils of medicinal plants, they also have undesirable properties such as low pharmacokinetic profile and solubility, lack of active substance targeting, and irregular release profile (2). Thanks to the smart carrier systems containing herbal active substances, the side effects of the plants are reduced, and the plant extracts become more effective (3). Nano-particular systems are widely used due to their controlled release properties, high encapsulation efficiency and ease of application. Therefore, the application of plant extracts with such a delivery system is more appropriate in terms of efficacy and side-effect profile (4). Polymers such as cellulose, chitosan, dextran, polyvinyl alcohol, polyvinyl prolidon are used in the preparation of nanoparticles. In this study, chitosan, a natural polymer with cationic and biocompatible properties, was used. The release profile and encapsulation efficiency of chitosan are very suitable, and the absence of any toxic effects and side effects are the reasons for preference (5). The aim of this research was to prepare a chloroform extract of *Achillea phrygia* and test its antioxidant and cytotoxic properties. Then, on the most effective extracts, nanoparticles (NPs) were synthesized, and the biological activities of the free forms of the extracts were compared to the NPs forms.

Materials and Methods:

Antioxidant, and cytotoxic activities of eight fractions (from A to H) obtained using column chromatography from *A. phrygia* chloroform extract, which was found to have a stronger effect than methanol extract in MCF-7 cell line, were evaluated. Antioxidant capacities of the extracts were found by FRAP, DPPH and CUPRAC methods. The cytotoxic activities of all fractions were evaluated on MCF-7 and HT-29 cell lines using the XTT cell viability assay (6). Then, NPs were prepared with most active fraction by combining with chitosan using the ionic gelation method (7). The particle size and zeta potential of nanoparticles were determined by using a Zetasizer Nano ZS instrument (Malvern Instruments Ltd, UK).

Results:

The results showed that the B fraction exhibited the strongest antioxidant activity with significantly higher ($p<0.05$) DPPH radical scavenging activity (IC_{50} 0.399±0.091 mg/mL), CUPRAC (1.713±0.065 mMTE/mg analyte) and FRAP results (40.984±0.201 mM$FeSO_4$/mg analyte) than the other fractions (Table 1). In cells treated with B extract, the cell viability of HT29 and MCF7 cells were found as 56.338 ± 1.220 and 64.764 ± 1.368, respectively (Figure 1).

Table 1. Antioxidant capacity results of the fractions, references and nanocapsules

Extracts/standarts/NPs of B extract	DPPH (IC_{50}: mg/mL)	FRAP (mM$FeSO_4$/mg analyte)	CUPRAC (mMTE/mg analyte)
A	1.399±0.929	36.307±0.698	0.422±0.008
B	**0.399±0.091**	**40.984±0.201**	**1.713±0.065**
C	0.573±0.094	38.694±1.007	1.681±0.078
D	0.621±0.017	32.501±0.550	**2.149**±0.108
E	0.861±0.123	36.372±0.806	1.609±0.088
F	0.565±0.095	32.050±0.349	1.351±0.065
G	1.189±0.335	29.018±0.403	0.779±0.025
H	0.650±0.123	28.050±0.201	0.682±0.003
B capsule	1.014± 0.078	21.758± 0.197	0.780± 0.030
Ascorbic Acid	0.0028±0.0004		3.213±0.076
BHT		86.004± 8.914	

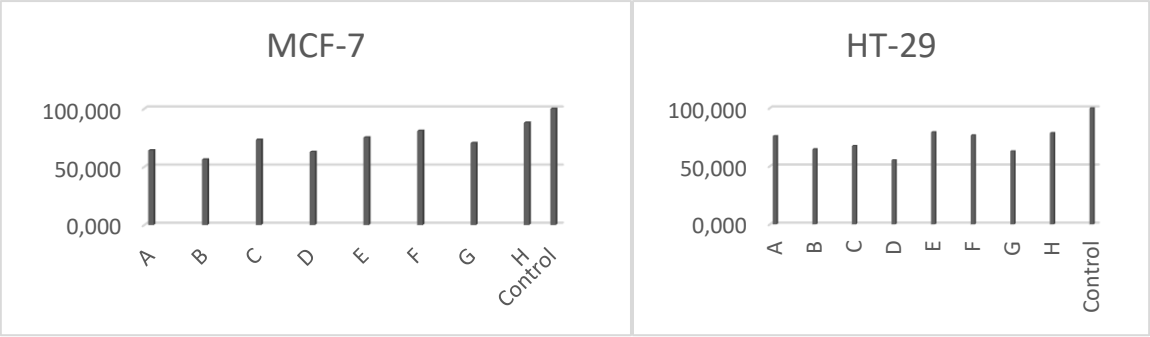

Figure 1. Cell viability results of chloroform extracts of the plant. Cells were treated with samples at a concentration 40 µg/mL. Cell viability of the control group was determined as 100%.

When we evaluated the cytotoxic effects of the extracts on MCF-7 and HT-29 cells, it was observed that B chloroform extract had stronger cytotoxic potential. Based on these results, NPs containing B extracts were prepared, and the extracts and NPs containing the extracts were treated with MCF-7 and HT-29 cells at 40µg/mL (Figure 2). XTT cell viability results explain that NPs containing B chloroform extract of *Achillea phrygia* have desirable high anticancer activity.

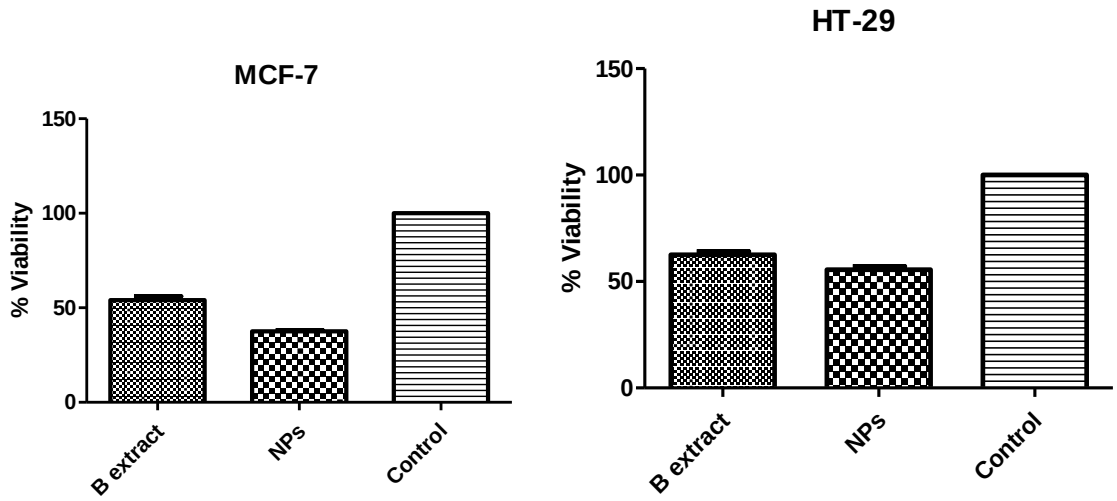

Figure 2. Cell viability results of B chloroform extract and NPs.

Conclusions:

Chitosan NPs containing the most active B extract were prepared. In cell culture studies, the anti-proliferative and anticancer effects of the extract embedded in chitosan, a carrier system, were evaluated. XTT cell viability results explain that NPs containing B chloroform extract of *A. phrygia* have desirable high anticancer activity. While the antioxidant activity of chitosan NPs was close to the unencapsulated extracts, the anticancer activity gave better results. This finding shows that NPs made from chloroform extract may be useful in preclinical and clinical cancer research.

Acknowledgement

This study was supported by a grant of TUBITAK (SBAG-116S509). Our heartfelt thanks to Prof. Dr. Turan Arabacı for collected and identified the plants.

References:

1. DeSantis CE, Lin CC, Mariotto AB, Siegel RL, Stein KD, Kramer JL, et al. (2014). CA: A Cancer Journal for Clinicians 64: 252–271.
2. Silva MM, Calado R, Marto J, Bettencourt A, Almeida AJ, Gonçalves L (2017) Marine Drugs 15: 370.
3. Watkins R, Wu L, Zhang C, Davis RM, Xu B (2015). International Journal of Nanomedicine 10: 6055-6074.
4. Martinho N, Damgé C, Reis CP (2011). Journal of Biomaterials and Nanobiotechnology 2: 510-526.
5. Ghorani-Azam A, Sepahi S, Riahi-Zanjani B, Ghamsari AA, Mohajeri SA, Balali-Mood, MJ (2018). Journal of Research in Medical Sciences, 23:26.
6. Wolf NB, Kuchler S, Radowski MR, Blaschke T, Kramer KD, Weindi G (2009). European Journal of Pharmaceutics and Biopharmaceutics, 73: 34–42.
7. Calvo P, Remunan-Lopez C, Vila-Jato JL, Alonso MJ (1997). Journal of Applied Polymer Science, 63: 125-132.

OP123: ELECTROCHEMICAL DETERMINATION OF ANTINEOPLASTIC DRUG IN HUMAN PLASMA BY MODIFIED GLASSY CARBON ELECTRODE

[1]Mehmandoust, M., [1]Erk, N., **[2]Tiris, G.**

[1] Ankara University, Department of Analytical Chemistry, Ankara, Turkey, Nevin.Erk@pharmacy.ankara.edu.tr, mehamndoust@ankara.edu.tr

[2] Bezmialem Vakif University, Department of Analytical Chemistry, Istanbul, Turkey, gizem.tiris@gmail.com

Introduction:

Topotecan (TPT) is semisynthetic unoriginal of the herb alkaloid camptothecin and is used as an anti-tumor and inhibitor of topoisomerase I. Comptothecin accompanied by its derivatives create a prominent type of anti-tumor drugs. (1-3). An antineoplastic agent used to treat ovarian cancer. The purpose of this work is to complete the straight oxidation of TPT and then to enhance a new electrochemical method for the sensitive and fast detection of TPT. Chemically, TPT (S)-10-[(dimethylamino)methyl]-4-ethyl-4,9-dihydroxy-1H-pyrano(3',4':6,7)-indolizinol (1,2b) quinoline-3,14-(4H,12H)-dione hydrochloride shown in Figure 1.

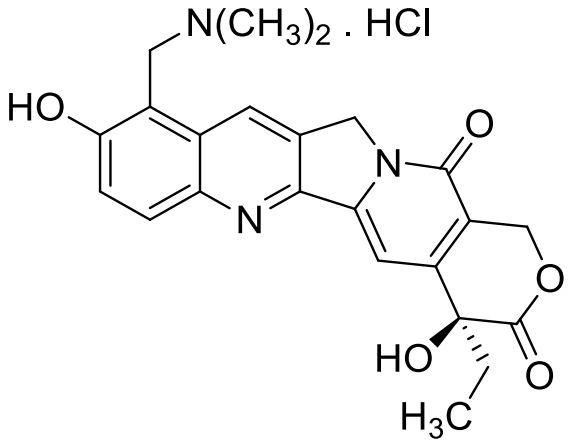

Figure 1. Structure of TPT hydrochloride

Materıals and Methods:

TiO_2 NPs and 2DMoS_2 NFs were ultrasonicated for 20 min in separately 2.0 mL of deionized water to prepare the TiO_2 and 2D-MoS_2 dispersions. Then, 1.0 µL of various concentrations of 2D-MoS_2 was dropped on the GCE and permitted to dry at room temperature then 1.0 µL of diverse concentration of TiO_2 solution was reformed onto GCE and permitted to dry up at room temperature.

Results:

DPV method was used to verify the electroanalytical capacity of 2D-MoS_2/TiO_2 to detect TPT. The anodic signal increased linearly with the rising of TPT concentration in the one ranges of 0.01–18.44µM. The limit of detection (LOD) and limit of quantification (LOQ) values were calculated, respectively. The electrochemical reaction in such an appropriate concentration range was plenty to exhibit the fairly high sensitivity of the sensor to TPT.

The electrochemical response from TPT at bare GCE, TiO_2/GCE, 2D-MoS_2/GCE, and 2D-MoS_2/TiO_2/GCE was investigated by cyclic voltammetry (CV) techniques in BR buffer. Compared to bare GCE, TiO_2/GCE, 2D-MoS_2/GCE, and 2D-MoS_2/TiO_2/GCE, a definite rise in peak current was gained at the 2D-MoS_2/TiO_2/GCE, which illustrate that the presence of 2D-MoS_2 and TiO_2 ameliorate the sensitivity of the sensors for the TPT detection.

The repeatability and reproducibility of 2D-MoS_2/TiO_2/GCE were investigated by analyzing 1.0 µM TPT solution at diverse times in a day (repeatability) and using five independent electrodes of TPT solution (reproducibility), respectively. The respective RSD quantities were obtained to for repeatability and reproducibility, respectively. The consequences demonstrated that 2D-MoS_2/TiO_2/GCE has good repeatability and reproducibility in conjunction with TPT.

The selectivity of 2D-MoS_2/TiO_2/GCE for TPT detection was performed by DPV technique in the existence of diverse interfering substances such as glucose (GL), ascorbic acid(AC), uric acid(UA), 5-fluorouracil(FL), and l-cysteine(CS) under optimal electrochemical situations. The efficiency of selectivity of the 2D-MoS_2/TiO_2/GCE modified electrode as an electrochemical sensor was observed using the DPV method.

The TPT peak currents of the developed electrochemical sensor gave a linear response in the concentration range of 0.01 to 18.44 µM. This sensing platform showed a steady response, appropriate LOD, and great selectivity.

Conclusions:

GCE was modified with 2D-MoS_2/TiO_2 and the electrochemical behavior of TPT was investigated. The results of proposed this voltammetric study shows that the reaction is an irreversible. The proposed 2D-MoS_2/TiO_2/GCE system offers excellent features, including low-cost, simple, rapid, good stability, and sensitivity response to TPT with applicability to real sample analysis.

Acknowledgements

This work was supported by the Scientific Research Projects Commission of Ankara University (Project Number: 19L0237001 and 19L0237004)

References:

1. Garst, J., (2007). Therapeutics and clinical risk management, 3(6):1087.
2. Rajan, R., et al., (2013). Industrial Crops and Products, 43:472-476.
3. Kim, J.H., et al., (1992). International Journal of Radiation Oncology Biology Physics, 22(3):515-518.

OP131: QUANTITATIVE PYRROLIDONYL ARYLAMIDASE ASSAY FOR GROUP A STREPTOCOCCUS PYOGENES DETECTION WITH IMAGE ANALYSIS

[1]Eryilmaz, M., [2]Boyaci, I.H., [1]Tamer, U.

[1] Gazi University, Faculty of Pharmacy, Department of Analytical Chemistry, Ankara, Turkey,

[2] Hacettepe University, Department of Food Engineering, Ankara, Turkey, utamer@gazi.edu.tr

Introduction:

Pharyngitis is inflammation of the pharanx, mainly caused by Group *Streptococcus pyogenes* (GAS) and the diagnosis of GAS performs mainly with rapid antigen tests. These tests are easy to perform however the results must be confirmed with plate counting method, which is a gold standard in this field (1). GAS colonies are formed on blood agar plates after 24-48 hours and definitive identification should be done with biochemical tests, such as pyrrolidonyl arylamidase (PYR) activity test (2). In this work, PYR test was transformed to a quantitative assay instead of defining the colony with aid of magnetic gold nanoparticles (AuNPs). GAS was targeted with the modified nanoparticles and incubated in the broth and red color was evaluated with the image analysis.

Materials and Methods:

Magnetic AuNPs were synthesized and modified with anti-GAS antibody. The capture of GAS with cotton swabs and the related steps are optimized in our previous study (3). After capturing of GAS and washing the unbound magnetic AuNPs, 400 µL of complex was added to 500 µL of PYR-broth and incubated 38°C for 4 hours. Then, 25 µL of DMACA reagent was added and red color formation was the sign of GAS presence as schematized in Figure 1.

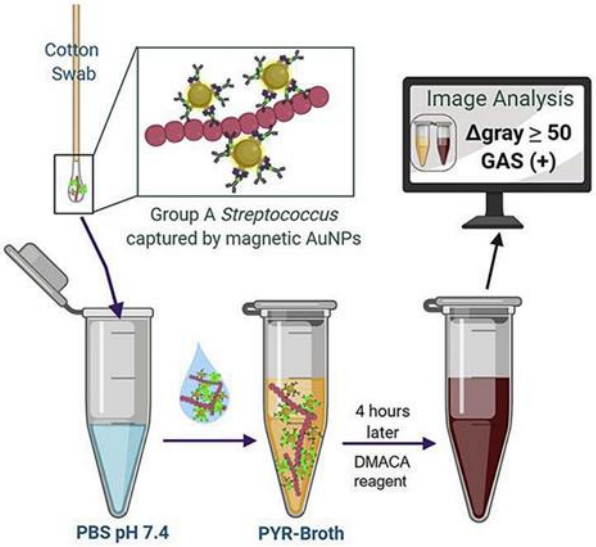

Figure 1. Steps of proposed quantitative PYR assay and red color change as GAS presence in the sample (4).

The color difference between sample and blank was evaluated with image analysis, proposing a formula of (Δgray = gray value of the blank – gray value of sample), since gray value is a brightness calculation with RGB channels of the image. Therefore, bigger values than 50 (Δgray ≥ 50) were selected as the GAS presence in the sample. In addition, PYR amount in broth, incubation time, effect of ambient light was optimized and practical sample was evaluated.

Results:

The linear correlation was found between the log of bacteria count ($1.5 \times 10^4 – 1.5 \times 10^7$ CFU/mL of GAS) and mean gray of RGB with a linear equation of y = 22.839x - 56.845 and a R^2 of 0.9685 between the log of bacteria. (Figure 2). The limit of detection and limit of quantification were calculated as 3.3×10^2 and 4.2×10^2 CFU/mL of GAS, respectively. In addition, the critical point of the study was an interference of *Enterococcus faecalis* and there was not significant effect and proposed assay worked selectively with a practical sample, obtaining Δgray values for GAS bigger than 50.

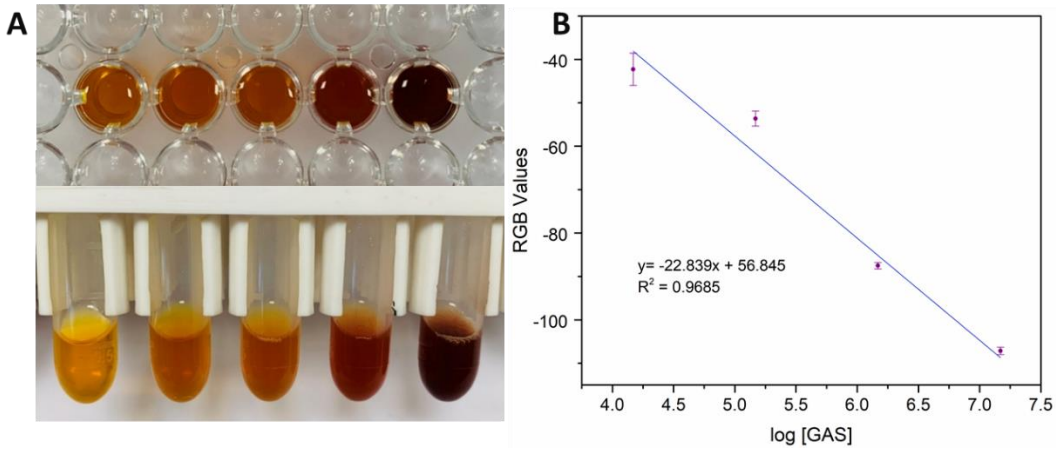

Figure 2. (A) Red color change depending on the increase of bacteria count, **(B)** Linear correlation between bacteria count and RGB values.

It was also critical that a regular ambient light and a white background should be existed for image analysis since there was difference only in dim light as given in Table 1. The measurement of blank was improved accuracy of the assay. Place B enables the brightest values, whereas place F gives the darkest gray values. Δgray values did not show significant differences between the places except the experiment in dim light, place F. In place F, Δgray values are 59.2 ±2.41 and this observation can be expected since the values are dependent on the brightness. Furthermore, 4 hours incubation was efficient enough to obtain β-naphthylamine in the presence of GAS, using PYR as a substrate, and observing the red color change.

Table 1. Effect of ambient light on gray values in the image analysis [4].

	Place	I Blank – Sample		II Blank - Sample		III Blank - Sample		Δgray
A	Laboratory (Holding)	134.3	49.6	133.2	47.7	132.3	47.5	85.0 ± 0.35
B	White box (Holding)	148.9	61.5	157.3	64.4	147.8	61.2	88.9 ± 2.80
C	White box (X-axis)	113.4	40.4	124.4	43.7	141.8	44.3	83.73 ± 10.22
D	White box (Glass tube)	123.1	46.1	137.8	48.1	122.2	46.4	89.4 ± 0.57
E	Laboratory (Glass tube)	140.7	52.3	138.4	53.6	137.9	45.6	88.5 ± 3.06
F	Laboratory, Dim light (Glass tube)	85.3	28.5	89.1	26.6	84.8	26.5	59.2 ± 2.41

Conclusions:

Here, selective and sensitive assay for GAS detection was performed with PYR using image analysis. This was the first study for PYR using as a probe for quantifying GAS without the back-up of the plate counting method. There was not also requirement of antigen extraction as it was in rapid antigen tests and GAS could be detected directly collected with swab. Thus, the proposed work has advantages in terms of test duration and sensitivity, comparing to the gold standard.

References:

1. Bisno, A.L. (2001) N. Engl. J. Med. 344 (3), 205-2011
2. Gieseker, K.E., et al., (2003) Pediatrics, 111 (6) e666-e670.
3. Eryilmaz, M., et al., (2019) Analyst, 144, 3573-3580.
4. Eryilmaz, M. et al., (2020) Talanta, 212, 120781.

OP133: FABRICATION OF 2D-G-C3N4/SDS/GNPS AS AN ELECTROCHEMICAL SENSOR FOR BIOMEDICAL APPLICATION

[1]Mehmandoust, M., [1]Erk, N.

[1] Ankara University, Department of Analytical Chemistry, Ankara, Turkey,
Nevin.Erk@pharmacy.ankara.edu.tr, mehamndoust@ankara.edu.tr

Introductıon:

Doxorubicin (DOX) is a famous anticancer drug with many side effects that make it crucial to determine it in an actual sample (1). Figure 1 exhibits the chemical structure of doxorubicin (IUPAC name: (7S,9S)-7-[(2R,4S,5S,6S)-4-Amino-5-hydroxy-6-methyloxan-2-yl]oxy-6,9,11-trihydroxy-9-(2 hydroxyethyl)-4-methoxy-8,10-dihydro-7H-tetracene-5,12-dione).

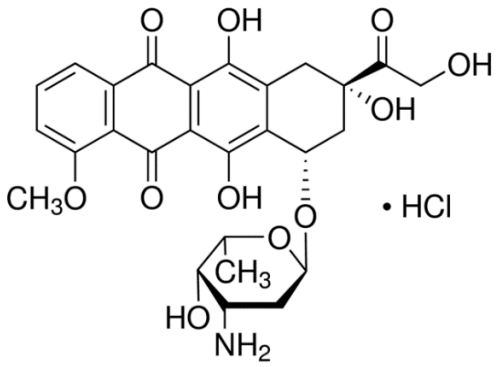

Figure 1. The chemical structure of DOX

In the present study, the electrochemical properties of novel nanocomposite were studied on screen-printed electrode modified with 2D-g-C_3N_4/SDS/GNPs nanocomposite. The novelty of this work is the successful synthesis of 2D-g-C_3N_4/SDS/GNPs nanocomposites and their application sensing toward the electrochemical determination of doxorubicin on a screen printed electrode (SPE) in the real samples. The presence of sodium dodecyl sulfonate (SDS) on the surface of electrode was caused an outstanding stability for developed electrode (2,3).

Materıals and Methods:

Doxorubicin, melamine ($C_3H_6N_6$), graphene nanoplatelets (GNPs), sodium dodecyl sulfate (SDS) were purchased from Sigma Aldrich company, and screen printed electrodes (SPE) were purchased from Metrohm Drop Sens. All of these substances are analytical grade, and water di-ionized were utilized. Britton-Robinson buffer (B-R) was used in all steps. The SPE electrode was modified with a certain concentration of nanocomposite. The electrochemical properties of the developed were observed by several methods such as differential pulse voltammetry (DPV), cyclic voltammetry(CV), and chronoamperometry (CA) under optimal conditions.

Results:

The AdsDPV for the oxidation peak of DOX on the SPE electrode and modified electrodes, applied out in 0.1M Britton–Robinson buffer at pH of 6.0 with 0.1mM DOX. The bare SPE did

not exhibit any peak in the absence of DOX, showing that the faradic reactions on the bare sensor did not occur. A favorable electrochemical response of 2D-g-C_3N_4/SDS/GNPs/SPE, the oxidation of 0.1 mM DOX, explicated a result of the increased sensitivity, electrode surface area, and development of the electrochemical response of the GNPs support with 2D-g-C_3N_4. The results endorsed that the developed sensor (2D-g-C_3N_4/SDS/GNPs/SPE) effectively increases the electro-catalytic ability to oxidize DOX.

The interfering effects were examined in the presence of selected organic and inorganic compounds. No response to up to 200-fold of ascorbic acid, dopamine, glucose, uric acid, l-cysteine, potassium nitrate, sodium sulfate, and potassium chloride was obtained. No remarkable signal change was obtained in the presence of interfering agents. The repeatability of the developed sensor was performed by taking five repetitive measurements of 1.0 µM DOX with a single modified electrode in BRT buffer at pH 6.0. Moreover, the reproducibility between multiple electrodes was conducted by comparing I_{pa} of 1µM DOX. The long-term stability of 2D-g-C_3N_4/SDS/GNPs/SPE was also observed. In the long-term stability experiments, AdsDPV responses of 1.0 µM DOX at 2D-g-C_3N_4/SDS/GNPs/SPE were obtained for five weeks . It showed a appropriate stability for the modified electrode. Finally, the reusability of 2D-g-C_3N_4/SDS/GNPs/SPE was observed. 2D-g-C_3N_4/SDS/GNPs/SPE is not a disposable electrode. It can be used at least 8 times by washing with 0.1 M BR buffer (pH 6.0).

Conclusıons:

Herein, for the first time, we fabricated a novel electrochemical sensing platform based on 2D-g-C_3N_4/SDS/GNPs nanocomposite for the determination of trace level of DOX in real samples. The 2D-g-C_3N_4/SDS/GNPs/SPE were found to be excellent for the determination of DOX. The principal advantages of the 2D-g-C_3N_4/SDS/GNPs/SPE are sensitivity, repeatability, reproducibility, stability, reusability and selectivity in the presence of interfering agents. On the other hand, the applicability of 2D-g-C_3N_4/SDS/GNPs/SPE to the rapid analysis of DOX in the real samples demonstrates the excellent ability for practical application.

Acknowledgements

Ankara University's Scientific Research Projects Commission funded this research. (Project Number: 21B0237005 and 19L0237004). M.O. thanks the Turkish Academy of Sciences (TUBA) for partial support.

References:

1. Minotti, G., Menna, P., Salvatorelli, E., Cairo, G., Gianni, L. (2004). Anthracyclines: Molecular Advances and Pharmacologic Developments in Antitumor Activity and Cardiotoxicity, ASPET.
2. Arulraj, A.D., Vijayan, M., Vasantha, V.S. (2015). Highly selective and sensitive simple sensor based on electrochemically treated nano polypyrrole-sodium dodecyl sulphate film for the detection of para-nitrophenol, Analytica chimica acta, 899: 66-74.
3. Cao, Y., Smith, P., Heeger, A.J. (1993), Counter-ion induced processibility of conducting polyaniline, Synthetic Metals 57(1) 3514-3519.

OP134: QSRR-ANN MODELLING IN β-CD-MODIFIED RP-HPLC

[1]Djajić, N., [1]Krmar, J.,[1]Otašević, B., [1]Malenović, A., [1]Protić, A.

[1] University of Belgrade – Faculty of Pharmacy, Department of Drug Analysis, Belgrade, Serbia, nevena.maljuric@pharmacy.bg.ac.rs, jovanak@pharmacy.bg.ac.rs, biljana.otasevic@pharmacy.bg.ac.rs, andja@pharmacy.bg.ac.rs, anna@pharmacy.bg.ac.rs

Introduction:

Cyclodextrin (CD) is a macrocyclic oligosaccharide composed of several glucose units, bound together in a particular truncated conical-like cylinder, forming an internal lipophilic cavity delimited with hydrophilic outer surface. This structure enables CD to form inclusion complexes with wide variety of organic relatively hydrophobic molecules, which is recognized as the most valuable characteristic of CD, responsible for its widespread usage (1–3). The complexation process is generally governed by the size complementarity between the ligand molecule and CD cavity. Upon complexation physical, chemical and biological properties of complexed molecules are altered resulting in numerous positive effects, such as increased bioavailability, solubility, chemical stability and efficacy of drugs, while side effects are reduces (4). The largest field of practical utilization of CD in pharmaceutical industry is mainly based on the solubilizing capacity. Apart from its usage in pharmaceutical, food or cosmetics industry, CD has an important role as mobile phase additive in reversed-phase high performance liquid chromatography (RP-HPLC) (5, 6). CD added to RP-HPLC mobile phase interacts with investigated compound, solvent components and stationary phase surface. Therefore, the retention is influenced by the distribution of a compound between CD dissolved in the mobile phase, free CD and formed inclusion complex adsorbed onto the stationary phase, and stationary phase itself (1, 2). The complexity of CD-modified RP-HPLC systems arises from the possibility of forming multiple various interactions, while resolution and separation efficiency depend on different experimental conditions, such as type and concentration of applied CD, mobile and stationary phase characteristics, as well as column temperature. Although it is known in which way the compound is distributed among the components of the HPLC system, researchers are still not completely familiar with the influence of molecular structure and experimental parameters on retention in these kinds of systems, and especially with the influence of inclusion complexes structures. Which retention mechanisms would prevail and lead the retention is still a question.

For that reason, the main research goal was to reveal the structural characteristics affecting the inclusion complexation and retention in these kinds of chromatographic systems by means of quantitative structure-retention relationships (QSRRs) built with an aid of artificial neural networks (ANNs). Risperidone, olanzapine and their related compounds are selected as model substances on the basis of diversity in ionization ability and lipophilicity, which enables the coverage of a proper analytically challenging chemical space. Among CDs, β-CD is preferred over others when dealing with pharmaceutical compounds, since it is able to accommodate most heterocyclic and aromatic compounds within its cavity.

Materials and Methods:

HPLC experiments were conducted on Dionex Ultimate 3000 (U)HPLC. Factors influencing the retention behaviour, namely pH of the aqueous phase, the content of acetonitrile in the mobile phase (%, v/v), column temperature (°C) and concentration of employed β-CD in the aqueous phase (mM) in corresponding ranges were varied according to the plan of experiments. Experimental plan was obtained in Design Expert 7.0.0 via central composite design.

Mixed QSRR model included large pool of molecular descriptors, complex association constants and experimental parameters as model inputs towards the retention factors of selected model substances, as outputs. Molecular descriptors were calculated for the geometrically optimized conformations of examined model substances in Dragon 6.0.7 software. Complex association constants, as descriptors describing the formed inclusion complexes were calculated on the basis of inclusion complexes structures proposed in molecular docking study performed in AutoDock v4.2. QSRR-ANN modelling was performed in STATISTICA Neural Networks.

Results:

Nowadays, almost unlimited number of descriptors could be possibly assigned to a certain compound. Therefore none of the molecular characteristics would be neglected. However, model load caused by descriptors carrying the same information could be a problem. For that reason, the adequate selection of descriptors to be included in the model is crucial. Firstly, all mutually correlated descriptors with correlation coefficient higher than 0.9, were excluded. Afterwards, uncorrelated molecular descriptors, complex association constants and experimental parameters were subjected to multiple linear regression analyses to identify those with significant influence on retention of examined model substances, which would be included as ANN inputs. The dataset was composed of 210 cases, divided into three subsets, namely training (147 cases), validation (32 cases) and test set (31 cases). The assignment of cases was performed in a random manner. Constructed ANN was multilayer perceptron with 11-7-1 topology (Figure 1), trained with back propagation algorithm. Learning rate set to 0.1, while momentum was 0.3. The obtained network showed good predictive and descriptive ability reflected through low values of root mean square error (RMSE) together with high coefficient of determination (R2) values (approximately 1). To illustrate, RMSE for training, validation and test set were 0.3884, 0.2666 and 0.3401, respectively, while R2 values for the same subsets were 0.9912, 0.9959 and 0.9953, respectively.

To evaluate the individual influence of each of the descriptors on retention, the difference in the highest and lowest retention factor value across the investigated range of the descriptor's values was calculated. The highest ratios were associated with the following descriptors RDF075m, UE, Mor04v and CATS2D_08_PL, making them the most contributing towards the selected output. RDF075m descriptor shows the three-dimensional mass distribution calculated at a distance of 7.5 Å from the geometrical centre of the molecule and it refers to steric factors at the same distance. Groups approximately 7.5 Å distant from the geometrical centre of risperidone, olanzapine and related compounds in their optimized conformations were determined (Figure 2). These groups were the same ones involved in the complexation process according to previously performed NMR study. Identified groups and their steric factors are the most important for the formation of inclusion complexes, and, in this way, the

value of RDF075m contributes to the retention of the selected compounds. The importance of Mor04v confirms the influence of molecular size and shape in retention in these kinds of chromatographic systems, while CATS2D_08_PL accounts for lipophilicity.

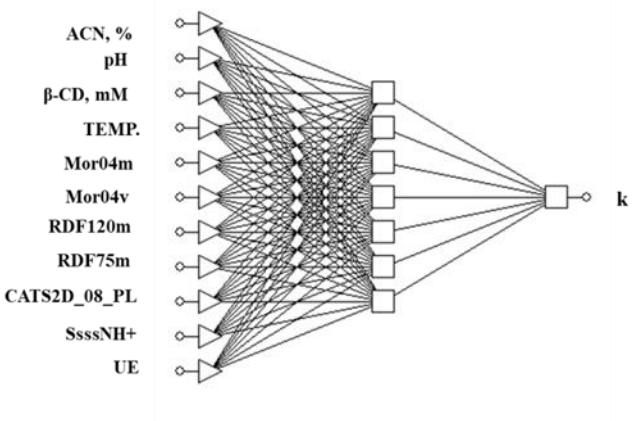

Figure 1. ANN with 11-7-1 topology

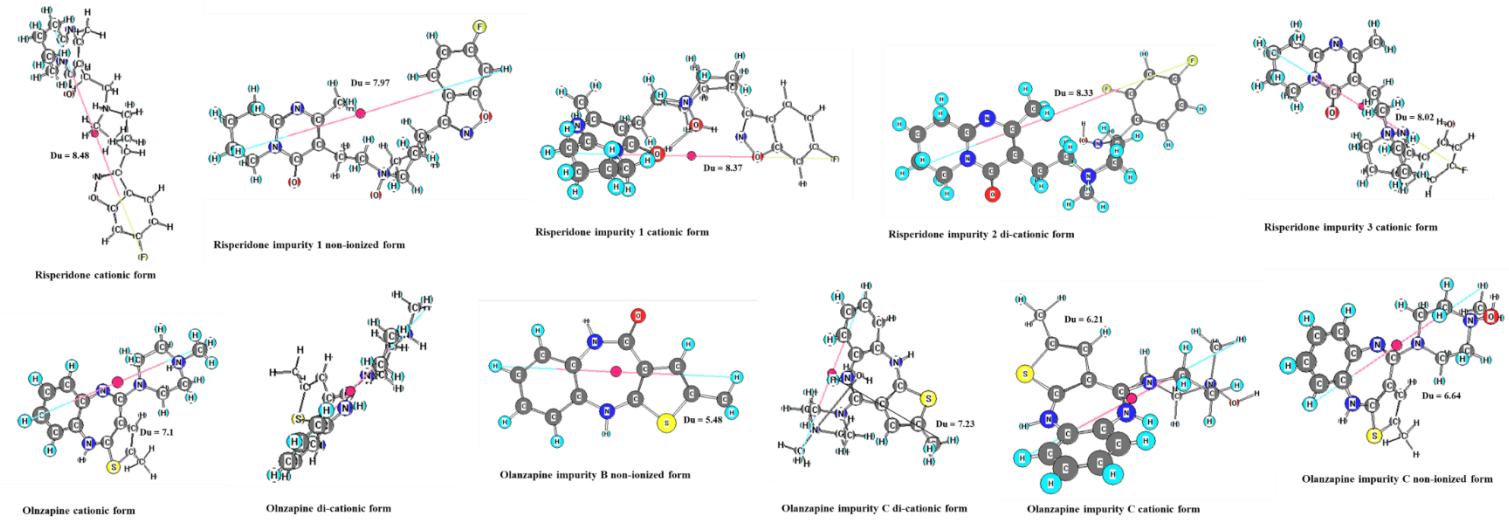

Figure 2. Groups approximately 7.5 Å distant from the geometrical centre of each model substance in its geometrically optimized conformation

Conclusions:

The current study resulted in development of QSRR-ANN with remarkable performances, which enabled the elucidation of the molecular features significantly influencing the retention in β-CD-modified RP-HPLC. The pronounced effect of molecular structure on retention was best described through RDF075m, followed by UE, Mor04v and CATS2D_08_PL. Retention behaviour is also highly affected by molecular size and shape, as well as lipophilicity of the investigated compounds. Moreover, the size and polarity of the chosen CD should not be neglected, due to the consequent structural fit.

Acknowledgements

This study was supported by the Ministry of Education, Science and Technological Development of the Republic of Serbia (Project no. 451-03-9/2021-14/200161).

References:

1. Szejtli J (1998). Introduction and general overview of cyclodextrin chemistry, Chemical Reviews. 98 (5): 1743–1754.
2. Dodziuk H (2006). Cyclodextrins and their complexes: chemistry, analytical methods, applications. John Wiley & Sons.
3. Szente L et al., (2016). Analytical characterization of cyclodextrins: History, official methods and recommended new techniques. Journal of Pharmaceutical and Biomedical Analyses. 130:347-65.
4. Del Valle E.M (2004). Cyclodextrins and their uses: a review, Process Biochemistry. 39 (9):1033–1046.
5. Maljurić N et al., (2018). Quantitative structure–retention relationship modeling of selected antipsychotics and their impurities in green liquid chromatography using cyclodextrin mobile phases, Analytical and Bioanalytical Chemistry. 410(10):2533-50.
6. González-Ruiz V et al., (2011). Eco-friendly liquid chromatographic separations based on the use of cyclodextrins as mobile phase additives, Green Chemistry.13 (1):115–126.

OP135: ELECTROCHEMICAL INVESTIGATION OF SURFACTANT EFFECT ON THE ETODOLAC AND THIOCOLCHICOSIDE SIGNALS

Selcuk, O., Erkmen, C., Bozal-Palabiyik, B., Uslu, B.

Ankara University, Faculty of Pharmacy, Department of Analytical Chemistry, Ankara, Turkey
ozgselcuk@ankara.edu.tr,cmrkmn@gmail.com,
burcinbozal@hotmail.com,buslu@pharmacy.ankara.edu.tr

Introduction:

As a non-steroidal drug having significant analgesic and anti-inflammatory effects etodolac (ETO) and as a semi-synthetic sulphur derivative of colchicoside having similar effects thiocolchicoside (TCC) are combined to establish a quick analgesic effect for the treatment of serious pain emerged at diseases like vertebral colon syndrome, severe trauma, and surgery operations (1,2). The pharmacokinetic properties of both drugs remained same in the combined form, while the analgesic effect of this combination is stronger (3). Because of these characteristics, it is vital to determine the concentration of each drug found in pharmaceutical preparations in order to perform quality control studies. The literature reveals various methods for simultaneous determination of ETO and TCC from different samples including high performance liquid chromatography (HPLC) (4,5), high performance thin-layer chromatography (HPTLC) (6) and spectrophotometric methods (7,8) This study, on the other hand, which utilizes an electrochemical method for the first time for the simultaneous determination of ETO and TCC, aims to present a novel approach based on differential pulse voltammetry (DPV) at glassy carbon electrode (GCE) in the presence of sodium dodecyl sulphate (SDS).

Materials and Methods:

In performing electrochemical measurements, a conventional three-electrode cell based on a working, reference (Ag/AgCl) and auxiliary electrodes (platinum wire) was connected to PalmSens EmStat 3 potentiostat (DropSens, Metrohm,Turkey) with PSTrace 5.5 software. Before each measurement, in order to activate the GCE surface, the electrode was polished with Al_2O_3 (0.05 micron) slurry on a synthetic cloth and then it was rinsed with pure water. For voltammetric studies, 1.0 mM stock solutions of ETO and TCC were prepared separately in methanol and 10 mM stock solution of anionic surfactant SDS was prepared in water; these solutions were kept in refrigerator at dark. Working solutions, in which 20% methanol ratio was kept constant, were prepared anew just before the assay by diluting stock solutions with the selected buffer solution. For quantitative analysis studies, studied substances are taken in appropriate quantities and diluted with pH 6.0 BR buffer including 20% methanol and 70 µM SDS. The applicability of the proposed method is shown by studying at tablet (Etotio® tablets, each containing 400 mg ETO and 8 mg TCC). To study accuracy of the proposed method, recovery studies were performed using the standard addition method.

Results:

This method aimed to achieve simultaneous determination of ETO and TCC sensitively by adding SDS via DPV. Given the 50-fold amount of ETO compared to TCC (400 mg ETO and 8 mg TCC), increasing the oxidation signal of TCC is very significant for simultaneous determination. The DPV results revealed that addition of 70 µM SDS almost doubled the peak current of TCC, it did not have an effect on ETO. SDS addition did not change both peak potentials as well. The reason of increase in TCC signal after addition of SDS can be the electrostatic interaction between negatively charged hydrophilic SDS film and positively charged TCC molecule. In sum, the SDS addition resulted in TCC signal increase, which contributed to more sensitive simultaneous determination.

Validation studies were performed by measuring the linear range, LOD, LOQ, within day and between days precision and accuracy. The linear range obtained by DP voltammograms are found between 1.0 µM and 80 µM for both compounds in pH 6.0 BR buffer solution in the presence of 70 µM SDS at GCE with "r" values of 0.998 and 0.999 for ETO and TCC, respectively. The detection limit values of ETO and TCC were calculated as 0.11 and 0.20 µM, respectively. For precision studies, the relative standard deviation (RSD %) values were calculated for peak currents and potentials of studied compounds and found less than 1% for within day and less than 2% for between days measurements. The tablet analysis results were found consistent with ETO and TCC amounts given in tablet label. For accuracy measurements, recovery studies were made from tablet. % recovery data was found as 99.21% for ETO and 99.29% for TCC from tablet with RSD% value smaller than 1%.

Conclusions:

This study aims to achieve a DPV method in the presence of SDS at GCE and a simple, fast, low-cost and versatile electrochemical method for simultaneous determination of ETO and TCC in tablets was proposed. At optimized conditions, the method showed linear responses for the concentrations of ETO and TCC between 1 µM and 80 µM with detection and quantification limits of 0.11 µM and 0.38 µM for ETO and 0.20 µM and 0.67 µM for TCC, respectively. The contribution of SDS was an increase in the TCC signal; this is significant considering the lesser amount of TCC in the tablet. This study is the first electrochemical study for simultaneous determination of ETO and TCC on GCE in the presence of surfactant and offered an excellent sensitivity.

Acknowledgements

The authors would like to thank Nobel Drug Company (Istanbul, Turkey) for chemical substances.

References:

1. C. de Miranda Silva, A. Rocha, E. Tozatto, L.M. da Silva, E.A. Donadi, V.L. Lanchote (2016). Enantioselective analysis of etodolac in human plasma by LC-MS/MS: Application to clinical pharmacokinetics, J. Pharm. Biomed. Anal. 120 (2016) 120–126. https://doi.org/10.1016/j.jpba.2015.12.009.
2. R.A. Weideman, K.C. Kelly, S. Kazi, A. Cung, K.W. Roberts, H.J. Smith, G.A. Sarosi, B.B. Little, B. Cryer (2004). Risks of clinically significant upper gastrointestinal events with etodolac and naproxen: A historical cohort analysis, Gastroenterology. 127, 1322–1328. https://doi.org/10.1053/j.gastro.2004.08.016.

3. D. Riendeau, M.D. Percival, S. Boyce, C. Brideau, S. Charleson, W. Cromlish, D. Ethier, J. Evans, J.P. Falgueyret, A.W. Ford-Hutchinson, R. Gordon, G. Greig, M. Gresser, J. Guay, S. Kargman, S. Léger, J.A. Mancini, G. O'Neill, M. Ouellet, I.W. Rodger, M. Thérien, Z. Wang, J.K. Webb, E. Wong, L. Xu, R.N. Young, R. Zamboni, P. Prasit, C.C. Chan (1997). Biochemical and pharmacological profile of a tetrasubstituted furanone as a highly selective COX-2 inhibitor, Br. J. Pharmacol. 121(1)105–117. https://doi.org/10.1038/sj.bjp.0701076.
4. M.P. Mascia, E. Bachis, N. Obili, E. Maciocco, G.A. Cocco, G. Pietro Sechi, G. Biggio (2007). Thiocolchicoside inhibits the activity of various subtypes of recombinant GABAA receptors expressed in Xenopus laevis oocytes, Eur. J. Pharmacol. 558 (1-3) 37–42. https://doi.org/10.1016/j.ejphar.2006.11.076.
5. N.A. El-Ragehy, M.M. Ellaithy, M.A. El-Ghobashy (2003). Determination of thiocolchicoside in its binary mixtures (thiocolchicoside-glafenine and thiocolchicoside-floctafenine) by TLC-densitometry, Farmaco. 58 (6) 463–468. https://doi.org/10.1016/S0014-827X(03)00050-8.
6. F.C.W. Sutherland, M.J. Smit, L. Herbst, J. Els, H.K.L. Hundt, K.J. Swart, A.F. Hundt. (2002). Highly specific and sensitive liquid chromatography-tandem mass spectrometry method for the determination of 3-desmethylthiocolchicine in human plasma as analyte for the assessment of bioequivalence after oral administration of thiocolchicoside, J. Chromatogr. A. 949 (1-2) 71–77. https://doi.org/10.1016/S0021-9673(02)00008-0.
7. M. Albayrak, F. Demirkaya-Miloglu, O. Senol, E. Polatdemir (2019), Design, optimization, and validation of chemometrics-assisted spectrophotometric methods for simultaneous determination of etodolac and thiocolchicoside in pharmaceuticals, J. Anal. Sci. Technol. 10 (1)1-8. https://doi.org/10.1186/s40543-019-0176-2.
8. A.D. Dhiware, P.B. Deshpande, S. V. Gandhi, S. Nair, S. Vanjari (2013). A simple and sensitive RP-HPLC method for simultaneous estimation of Atorvastatin Calcium, Ezetimibe and Fenofibrate in combined tablet dosage form, Res. J. Pharm. Technol. 6(10)1085–1088.

OP137: NEW SCHIFF BASE LIGAND-COMPLEXES AS CARBONIC ANHYDRASE AND CHOLINESTERASE ENZYME INHIBITORS: SYNTHESIS, CHARACTERIZATION AND *IN VITRO* / *IN SILICO* EVALUATION

[1]Tuna Yıldırım, S., [2]**Gügercin, R.S.**, [3]Duran H.E., [4]Türkeş, C.

[1] Erzincan Binali Yıldırım University, Faculty of Pharmacy, Department of Analytical Chemistry, Erzincan, Turkey, stuna@erzincan.edu.tr

[2] Erzincan Binali Yıldırım University, Health Sciences Institute, Department of Pharmaceutical Sciences, Erzincan, Turkey, rgugercin@gmail.com

[3]Kafkas University, Faculty of Medicine, Department of Medical Biochemistry, Kars, Turkey, haticeesra4990@gmail.com

[4] Erzincan Binali Yıldırım University, Faculty of Pharmacy, Department of Biochemistry, Erzincan, Turkey, cuneyt.turkes@erzincan.edu.tr

Introduction:

Schiff bases are compounds containing the azomethine group (-HC=N), which was first reported by Hugo Schiff in 1864 and formed as a result of the reaction of a primary amine with an active carbonyl compound, usually carried out by acid-base catalysis or heat. Moreover, they are helpful chelates because of their ease of preparation, structural variety and steric, and electronic control mechanisms. There are also considered "privileged ligands" and are widely used due to their versatile synthesis and good solubility.

In azomethine derivatives, the C=N bond is important for biological activity and the nitrogen atom of azomethine plays a role and interacts in the formation of components in normal cell processes. It is known that heterocyclic structures containing an azole ring system and a phenol derivative have a wide range of biological applications such as antifungal, antibacterial, antimicrobial, antioxidant, anticancer, antitumor, antiulcer, anti-inflammatory and antipyretic applications (1, 2). Thus, these compounds have extensive pharmacological activity. With the use of some metal complexes mainly in cancer treatment, their importance in the medical world is gaining day by day and therefore synthesis for the field of health is increased. Furthermore, it is known that these compounds are used in agriculture, in the production of dyes, in the production of polymers, in the plastics industry, in the electronics industry, in the aircraft industry, in analytical chemistry and various branches such as liquid crystal technology (3).

In the present work, we have conducted an investigation that involved the synthesis, characterization and biological activity of novel metal complexes of 5-fluorosalicylidene-4-chloro-o-aminophenol to discover novel multitarget human carbonic anhydrase (*h*CA) I, II and cholinesterase (AChE and BChE) inhibitors.

Materials and Methods:

In this study, firstly, the ligand of 5-fluorosalicylidene-4-chloro-o-aminophenol was synthesized by the reaction of 5-fluorosalicylaldehyde and 4-chloro-o-aminophenol in the absolute ethanol at 60 ^{o}C by the catalyzed of p-toluenesulfonic acid (4). The dark orange product obtained as a result of the reaction was allowed to stand overnight and then filtered. The product was washed

several times with hot distilled water, ethyl alcohol, and diethyl ether. The resulting product was dried under a vacuum and stored in a desiccator [$C_{13}H_9NO_2FCl$ (W: 265.67 g/mol), yield: 61.00%]. Later, the complexes of this ligand were prepared with Co(II), Ni(II), Cu(II), Zn(II), Cd(II), Mn(II), Pb(II), Hg(II), Fe(II) and UO_2(II) in acetate forms at pure EtOH. The product obtained as a result of the reaction was left to rest overnight and filtered. The obtained product was washed several times using hot distilled water, ethyl alcohol and diethyl ether. The product was dried under vacuum and stored in a desiccator. All compounds were characterized using spectroscopic techniques. Lastly, in vitro inhibitory effects of the new complexes on *h*CAs and AChE were determined using Verporte's and Ellman's methods and the IC_{50} values of all these compounds were calculated (6, 7).

Results:

It is understood that the LH ligand forms products with M^{2+} salts with a metal : ligand ratio of 1:2 from the elemental analysis of the complexes of the LH ligand. In the thermograms of the complexes, there was no mass loss in the range of 25-260 ^oC. This shows that there is no coordination and crystal water in the complexes. In other words, the data obtained from the thermogram supports the results of elemental analysis.

When the IR spectrum of the LH ligand taken in KBr is examined, it is seen that the characteristic IR peaks belong to C=N and O-H stretching vibrations. The spectrum has a sharp peak is observed at 1630 cm^{-1}, which indicates the presence of –CH=N (imine) group in the structure. In addition, the tensile vibration of the O-H group was observed at 3420 cm^{-1}. The disappearance of the peak observed at 1640 cm^{-1} in the IR spectrum of 5-fluorosalicylaldehyde, which is the starting material, belonging to the -C=O stretching vibration and the formation of a peak belonging to the -C=N stretching vibration instead of this peak, supports the completion of the reaction. The IR spectra of the metal (II) complexes of the LH ligand were examined in KBr, a change was observed in the stretching vibrations of the –C=N group and the bending vibrations of the phenolic O-H group. The characteristic C=N stretching vibration observed at 1630 cm^{-1}, indicating the presence of imine in the ligand, shifted to the low frequency region of 1610-1615 cm^{-1}. This observed shift can be explained by the coordination of the nitrogen atom in the azomethine group with the metal during the formation of the complex. In other words, the nitrogen atom has entered into coordination by giving its unshared electrons to the metal ion. In addition, the shift in the O-H peak in the ligand shows that phenolic O-H loses its proton and enters coordination with the metal ion. Besides, it has shifted in complex structures, which is the characteristic band for phenolic C-O stretching vibration observed at 1279 cm^{-1}. This shift supports the coordination of deprotonated phenolic oxygen with metal ions during complex formation. As in the ligand, the O-H stretching vibration in complexes is in the form of a broad peak in the region of 3400-3450 cm^{-1}.

As a result, all of the Schiff base complexes were found to be bidentate ligands involving the imino nitrogen and phenolic oxygen atoms in the complexes. The structures of ligand and complexes were identified using FT-IR, ^{1}H-NMR, ^{13}C-NMR, UV-Vis, XRD, SEM techniques. And then, *in vitro* studies, novel metal complexes of 5-fluorosalicylidene-4-chloro-o-aminophenol were determined to be potent inhibitors of *h*CAs and ChEs.

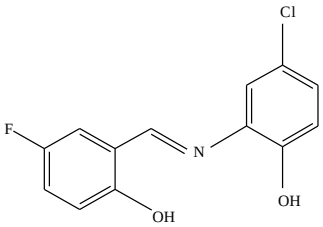

Ligand [LH]

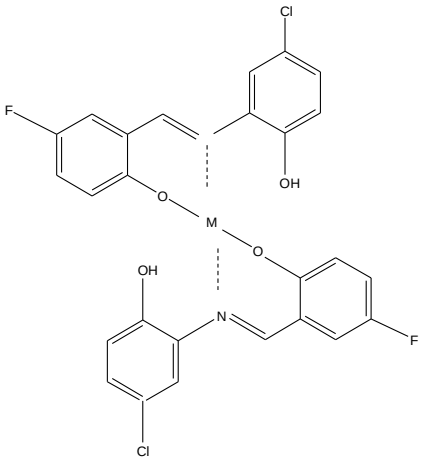

Complex [ML_2]

Analytical and Physical Data of Ligand and Its Complexes of [LH]

Compound	Formula	W (g/mol)	Color	μ eff	Yield (%)	Elemental Analysis, % Calculated (Found)		
						C	H	N
LH	$C_{13}H_9NO_2FCl$	265.67	Dark Orange	-	61.00	58.77 (58.76)	3.41 (3.36)	5.27 (5.19)
[Co(L)$_2$]	$CoC_{26}H_{16}N_2O_4F_2Cl_2$	588.26	Dark Brown	4.09	41.00	53.08 (53.11)	2.74 (2.88)	4.76 (4.69)
[Ni(L)$_2$]	$NiC_{26}H_{16}N_2O_4F_2Cl_2$	588.02	Brown	2.71	46.00	53.11 (53.02)	2.74 (2.63)	4.76 (4.71)
[Cu(L)$_2$]	$CuC_{26}H_{16}N_2O_4F_2Cl_2$	592.87	Dark Green	1.70	44.00	52.67 (52.39)	2.74 (2.81)	4.72 (4.69)
[Zn(L)$_2$]	$ZnC_{26}H_{16}N_2O_4F_2Cl_2$	594.71	Yellow	Dia.	44.00	52.51 (52.39)	2.71 (2.68)	4.71 (4.67)

Conclusions:

Schiff bases have a very broad pharmacological activity, and studies in medicine and pharmacy on these compounds and their metal complexes gain importance day by day. In the current research, a new Schiff base ligand, 5-fluorosalicylidene-4-chloro-*o*-aminophenol (LH) was synthesized from the reaction of 5-fluorosalicylaldehyde, an aromatic aldehyde and 4-chloro-*o*-aminophenol and with these Schiff base ligands Co(II), Ni(II), Cu(II), Zn(II), Cd(II), Mn(II), Pb(II), Fe(II), Hg(II), UO_2(II) complexes were prepared. The structures of the obtained Schiff bases and complexes were elucidated using elemental analysis, IR, ^{1}H-NMR, ^{13}C-NMR, UV-Vis, magnetic susceptibility and thermogravimetric analysis techniques. The results indicated that the complexes displayed the potent inhibition on both *h*CAs and ChEs when compared with acetazolamide and tacrine. According to the findings, the synthesized complexes may represent interesting lead agents and might maintain further structural guidance to explore and design more potent *h*CAs and ChEs inhibitors.

Acknowledgements

This study was supported by the Research Fund of Erzincan Binali Yıldırım University (grant number TSA-2021-756).

References:

1. Ayman A., Abdel Naby M., Aboaly M., (2011). Synthesis, Structural Characterization, Thermal Studies, Catalytic Effeciency and Antimicrobial Activity of Some M(II) Complexes with ONO Tridentate Schiff base N-Salicylidene-o-aminophenol, Journal of Molecular Structure, 22(8).
2. Sharaby, C.M. Amine, M.F. Hamed, A.A. (2017). 'Synthesis, structure characterization and biological activity of selected metal complexes of sulfonamide Schiff base as a primary ligand and some mixed ligand complexes with glycine as a secondary ligand', J. Mol. Struct., 1134, 208-216.
3. Liu, X., Carolina Manzur, C., Novoa, N., Celedón, S., Carrillo, D., Hamon, J. R. (2018). Multidentate Unsymmetrically-Substituted Schiff Bases and Their Metal Complexes: Synthesis, functional materials properties and applications to catalysis, Coordination Chemistry Reviews, 357, 144–172.
4. Tuna, S., (2010). Aromatik Amin İçeren Schiff Bazı Ligandlarının Sentezi, Karakterizasyonu ve Bazı Geçiş Metal Komplekslerinin İncelenmesi, Doktora Tezi, Fen Bilimleri Ens., Elazığ.
5. Uçan, Y. S., (2014). Synthesis, Spectral, Thermal and Magnetic Studies of Cobalt(II), Nickel(II), Copper(II), Zinc(II) and Cadmium(II) Complexes with N_2O_2 Donor Groups, Russian Journal of General Chemistry, 84, 1819-1824.
6. Türkeş, C., Arslan, M., et al., (2019). Synthesis, biological evaluation and in silico studies of novel N-substituted phthalazine sulfonamide compounds as potent carbonic anhydrase and acetylcholinesterase inhibitors. Bioorganic Chemistry, 89, 103004.
7. Durgun, M., Türkeş, C., et al., (2019). Synthesis, characterisation, biological evaluation and in silico studies of sulphonamide Schiff bases. Journal of Enzyme Inhibition and Medicinal Chemistry, 35(1), 950-962.

OP139: LC-MS/MS AND LC-DAD METHODS FOR ROBUST DETERMINATION OF GLYCEROL PHENYLBUTYRATE IN BIOLOGICAL FLUIDS AND HIGH-RESOLUTION MASS SPECTROMETRIC IDENTIFICATION OF FORCED DEGRADATION PRODUCT

[1,2]Özcan, S., [1,2]Can, N.Ö.

[1] Anadolu University, Faculty of Pharmacy, Department of Analytical Chemistry, Eskisehir, Turkey, saniyeozcan@anadolu.edu.tr

[2] Anadolu University, Faculty of Pharmacy, Doping and Narcotic Compounds Analysis Laboratory, Eskisehir, Turkey.

Introduction:

Urea cycle disorders are congenital metabolic errors that result from defects in any of the six enzymes involved in the hepatic removal of ammonia from the bloodstream and its conversion to urea secreted by the kidneys. Such disorders are mainly of two types: deficiencies in specific enzymes required to convert fat or carbohydrate into energy or to break down amino acids or other metabolites. If these compounds are not processed as a result of any deficiency in the pathway, they accumulate and have a toxic effect (1). Ammonia formation is particularly toxic to the central nervous system and some tissues, causing astrocyte swelling and subsequent permanent damage (2). Glycerol phenylbutyrate (GPB) was approved by the FDA in the USA, EU, and Canada in 2013 for the treatment of urea cycle disorders that cannot be managed with protein restriction and/or amino acid supplementation in patients 2 months of age and older. There are limited data on the use of nitrogen conjugation agents in very young patients who may have immature pancreatic exocrine function (3).

When we look at the literature, although it has been 7 years since GPB approval, the data for analysis are extremely limited. Existing studies on the analysis of the active substance are generally in the form of analytical determination as a pillar of the pharmaceutical study. In addition, no study has been done so far about the determination of DAD in the detector by HPLC. In the current study; a novel fully validated liquid chromatography method has been developed for the analysis of GPB in pharmaceutical formulations, human plasma and urine.

Materials and Methods:

Studies were performed using a Nexera XR series liquid chromatograph, which was composed of a DGU-20A3R on-line degasser, 2 × LC-20AD gradient pumps, a SIL-20AC autosampler, a CTO-10ASVP column oven, a FCV20AH6 high-pressure flow line selection valve, and a CBM-20A communications bus module; two different detectors, LCMS-8040 triple quadrupole mass spectrometric detector for mass-based detections and SPD-M20A photodiode array detector for absorbance-based detections (all from Shimadzu, Kyoto, Japan). Also, Shimadzu LC LabSolutions 3.43 SP1 data integration software was used for instrumental control and data processing.

The liquid chromatographic separations were succeeded with using a Supelco Ascentis® Express F_5 reversed-phase column (100 × 4.6 mm, 2.7 µm I.D). The mobile phase was composed with 1 mM ammonium acetat buffer and acetonitrile (25:75, *v/v*, pH=5.3). The flow rate was 0,5 mL/min, injection volume was determined as 1 µL. Compounds were monitored

at 200 nm using PDA detector. In the mass detection, the maximum ionization peak obtained in the positive mode was observed in the Q3 scan, and so the MRM+ mode was selected.

Table 1. MRM conditions of GPB in LC-MS/MS analyses

Compound	Precursor Ion	Product Ion	Q1 Pre Bias (V)	CE(V)	Q3 Pre Bias (V)
GPB	548.35	367.20	-34.0	-19.0	-25.0
		147.05	-20.0	-33.0	-26.0

Results:

The method was fully validated according to ICH Q2 (R1) guideline and also forced degradation studies were carried out comprehensively. The linearity of GPB was carried out in the concentration range. For each concentration, the analysis was done 3 times in replicates. The correlation obtained is quite suitable for the low concentrations studied.

Parameter	LC-DAD	LC-MS/MS
Linearity range	2.8-111.7 (µg/mL)	1.40-55.84 (ng/mL)
Slope (intraday, n=10)	6741.5	3897.9
Intercept (intraday, n=10)	-3310.3	1549.7
Regression coefficient (intraday, n=10)	0.9986	0.9985
Limit of dedection	689 ng/mL	0.105 ng/mL
Limit of quantitation	957 ng/mL	1.149 ng/mL
Retention time (min)	4.95	5.01
Precision for area (n=6)	0.126	0.299
Injection precision for retention time (n=6)	0.051	0.142
USP Tailing (T)	0.951	1.113
Number of theoretical plates (N)	9088	7054

In order to determine the accuracy value of the method, urine and plasma samples were prepared and recovery experiments were performed. Recovery experiments were carried out for three points of the calibration graph as 80%, 100% and 120%. For this, recovery was calculated by adding standard LUMA solution at certain concentrations to the pseudo formulation solution. The data calculated from the recovery experiments are given in the Table 2. RSD and SD were also calculated to show the precision of the results.

The forced degradation solutions was examined and identified using LCMS-IT-TOF. It has unique capabilities allow both quantitative and qualitative determination. We were analyzed same liquid chromatography conditions. GPB has only one degradation product in acid, base and oxidative medium. This degradation product was identified with using high resolution mass spectrum. Based on its ESI-IT-TOF spectrum, it was identified via CID fragmentation with m/z ratio three hundred sixtyseven as a precursor ion product. It is a novel degradation product. New degradation product is revealed by beta elimination reaction. So the molecule is unstable and not resistant to harsh conditions.

Table 2. Recovery experiments for GPB for both detectors

LC-DAD	URINE SAMPLES			Precision	Accuracy	
	Added (µg/mL)	Found (µg/mL)	SD	RSD (%)	Recovery (%)	Error (%)
	44.672	42.335	0.216	0.511	98.69	-1.03
	55.840	53.856	0.399	0.740	96.45	-3.55
	67.008	66.317	0.348	0.525	94.77	-5.23
	PLASMA SAMPLES			Precision	Accuracy	
	Added (µg/mL)	Found (µg/mL)	SD	RSD (%)	Recovery (%)	Error (%)
	44.672	42.114	0.128	0.304	94.27	+1.8
	55.840	53.657	0.162	0.301	96.09	-3.9
	67.008	68.193	0.440	0.644	101.8	-5.73
LC-MS/MS	URINE SAMPLES			Precision	Accuracy	
	Added (ng/mL)	Found (ng/mL)	SD	RSD (%)	Recovery (%)	Error (%)
	22.336	22.335	0.227	1.01	99.99	-0.01
	27.920	28.102	0.022	0.083	100.7	+0.70
	33.504	33.088	0.087	0.262	98.76	-1.24
	PLASMA SAMPLES			Precision	Accuracy	
	Added (ng/mL)	Found (ng/mL)	SD	RSD (%)	Recovery (%)	Error (%)
	22.336	22.359	0.084	0.376	100.1	+0.11
	27.920	27.924	0.145	0.519	100.0	+0.01
	33.504	32.902	0.197	0.598	98.20	-1.80

Conclusions:

To sum up with the analysis of pharmaceutical formulation, human urine and plasma and detection of degradation products was made successfully in HPLC, LC-MS/MS, and LCMSMS-IT-TOF. This newly validated method was transferred to another laboratory with its stationary phase for interlaboratory comparison study in HPLC. In the other HPLC instrument, the validated method was examined and proved method suitability.

Acknowledgements

This study was supported by a grant of Anadolu University Scientific research Projects Commission (Project No: 2005S061).

References:

1. Leonard, J., & Morris, A. (2002). Urea cycle disorders. Paper presented at the Seminars in neonatology.
2. Waisbren, S. E., Cuthbertson, D., Burgard, P., Holbert, A., McCarter, R., Cederbaum, S., & Consortium, U. C. D. (2018). Biochemical markers and neuropsychological functioning in distal urea cycle disorders. Journal of Inherited Metabolic Disease: Official Journal of the Society for the Study of Inborn Errors of Metabolism, 41(4), 657-667.
3. Berry, S. A., Longo, N., Diaz, G. A., McCandless, S. E., Smith, W. E., Harding, C. O., Robinson, B. (2017). Safety and efficacy of glycerol phenylbutyrate for management of urea cycle disorders in patients aged 2 months to 2 years. Molecular genetics and metabolism, 122(3), 46-53.

OP143: INHIBITION OF TYROSINASE BY NON-STEROIDAL ANTI-INFLAMMATORY DRUG: AN ELECTROCHEMICAL APPROACH

Kurbanoglu, S., Erkmen, C., Demir, Y., Uslu, B.

Ankara University, Faculty of Pharmacy, Department of Analytical Chemistry, Ankara, Turkey skurbanoglu@gmail.com, cmrkmn@gmail.com, yelizzdemirr@gmail.com, buslu@pharmacy.ankara.edu.tr

Introduction:

Tyrosinase Tyr (EC 1.14.18.1) was discovered by Schoenbein in 1856 in edible fungi, also knowns as phenol oxidase, catecholase, phenolase, catechol oxidase or polyphenol oxidase. Tyr is one of the enzymes commonly found in nature and it is also multifunctional enzyme containing copper. Tyr causes hyperpigmentation and hypopigmentation in mammals, and it is vital to control enzyme activity with Tyr inhibitors (1). In literature, researchers concluded that non-steroidal anti-inflammatory drugs to possess inhibitory potential against Tyr activity. Furthermore, it is reported that diclofenac also inhibits melanogenesis. Therefore, diclofenac showed inhibition through monophenolase or diphenolase activity of Tyr followed by spectrophotometric method (2). There is no report on the electrochemical investigation of Tyr inhibition by diclofenac. For this purpose, enzyme-based biosensor platforms decorated with different nanomaterials have often been proposed. In this study, a novel amperometric nanobiosensor was constructed from poly(3,4-ethylenedioxythiophene) nanoparticles (PEDOT NPs) decorated graphene quantum dots (GQDs) to investigate the dual determination of catechol (CAT) and anti-inflammatory drug diclofenac.

Materials and Methods:

To prepare nanobiosensor, 2 µL GQDs nanomaterial suspension was dropped onto the working surface of the screen printed electrode (SPE) and allowed to dry at room temperature. 1 µL PEDOT NPs were dropped onto SPE/GQDs surface and allowed to dry at room temperature in the next step. Then, the 5 µL Tyr enzyme was dropped on the surface of SPE/GQDs@PEDOT NPs by crosslinking with 0.25% GA crosslinking agent.
Chronoamperometric (CA) determination of CAT was performed using the optimized SPE/GQDs@PEDOT NPs/Tyr nanobiosensor under stirring conditions within a working potential of −0.2 V at 300 rpm. 1.0 mM of the related substrate was added after achieving a steady-state current. In order to perform inhibition studies of Tyr, a stock solution of diclofenac was prepared in ultra-pure water and diluted with PBS for inhibition time and inhibition concentration studies. Afterward, SPE/GQDs@PEDOT NPs/Tyr nanobiosensor was inserted into the eppendorfs containing diclofenac solutions and allowed diclofenac to inhibit immobilized Tyr. Moreover, for incubation time and concentration studies, developed nanobiosensor was kept at different times in diclofenac solutions containing different amounts of diclofenac. In the final step, CA measurements were carried using inhibited nanobiosensor for catechol. Tyr inhibition was followed by the decrease in CAT response, and relative inhibition of Tyr by diclofenac was calculated.

Results:

Prior to detection and inhibition studies, amounts of GQDs, PEDOT NPs, Tyr, pH, and measuring temperature were optimized. Dual detection and determination of CAT and diclofenac were further investigated using SPE/GQDs@PEDOT NPs/Tyr nanobiosensor. Continuous addition of CAT, with different and increased concentrations under optimized conditions and linear relation was obtained between 0.005 and 11 µM CAT with LOD value as 0.002 µM, and LOQ value as 0.001 µM. In the second step, the developed SPE/GQDs@PEDOT NPs/Tyr nanobiosensor was used to investigate Tyr inhibition by diclofenac through the decrease in CAT response. Inhibition % is calculated as:

$$Inhibition\% \ \frac{I_0 - I_P}{I_0} x100$$

where I_0 current corresponds to the enzyme activity of the nanobiosensor when the inhibitor diclofenac is not present. Lower steady state-currents (I) refer to the CAT response after inhibition with diclofenac. Firstly, the incubation time was optimized since inhibition needs time. For optimizing the incubation time, firstly, the CA response for 10 µM CAT is recorded. The same nanobiosensor is incubated in 5 mM diclofenac for different incubation times (1, 5, 10, 15, 30, and 60 min). The optimum incubation time was found as 15 min with an inhibition % of 51.6 ± 0.86 (Fig. 1A). Fig. 1B shows the change of the inhibition % with diclofenac concentration. In the linear range of 0.5−10 mM diclofenac, the inhibition effect of diclofenac on Tyr was followed. Using this inhibition strategy, the inhibition effect of diclofenac can be observed with the LOD value of 0.2 mM.

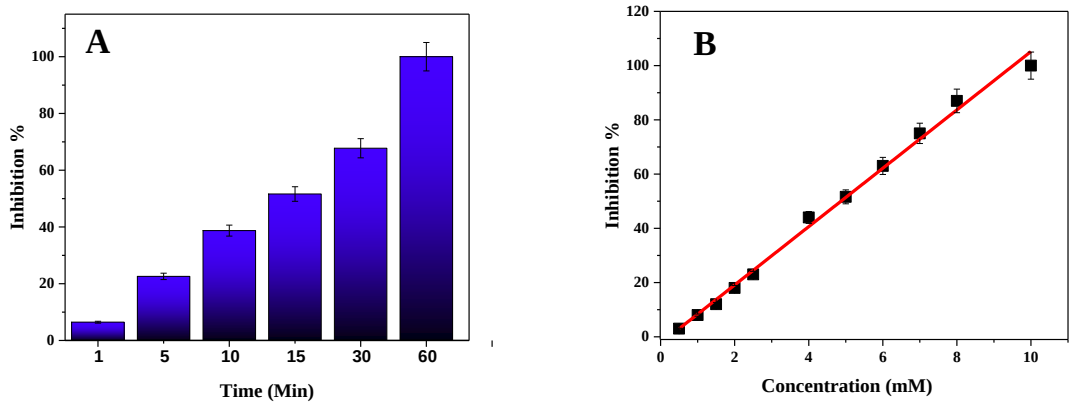

Figure 1. Effect of time on inhibition for diclofenac, B) Concentration *vs.* inhibition% graph for diclofenac.

After optimization of the inhibition conditions, inhibitory strength, which is expressed as the I_{50} value, which is the half-maximal inhibitory concentration where 50 % inhibition is followed at a specific substrate concentration, was calculated. Hence, I_{50} was reported as 4.87 mM diclofenac (3).

Conclusions:

The developed biochemical strategy of this electrochemical nanobiosensor would provide excellent potential for analysis of other substrates of Tyr, immobilization of different enzymes, and inhibition studies for other drugs, pesticides, ions etc. Hence, it is suggested that the designed sensor is a perfect marker to show Tyrosinase inhibition using electrochemical

methods. This way, a diclofenac-based cosmetic cream formulation can be an alternative to the cosmetic market.

Acknowledgements

The authors would like to thank VEM İlaç San. ve Tic. A.Ş, (Istanbul, Turkey) for chemical substances and their pharmaceutical dosage form support.

References:

1. Erkmen C, Kurbanoglu S, Uslu B, (2020). Sensors and Actuators B: Chemical, 316: 128121.
2. Sato, M. Toriyama, (2011). International Journal of Molecular Sciences, 12: 3998–4008.
3. Yung-Chi C, Prusoff, W.H., (1973). Biochemical Pharmacology, 22 3099–3108.

OP150: IN VITRO BIOLOGICAL EFFECTS OF ENDEMIC ANATOLIAN SPOTTED NEWT DERMAL VENOM: A POTENTIAL ACTIVE PHARMACEUTICAL INGREDIENT (API) FOR DRUG DELIVERY SYSTEMS

[1,2]Karış, M., **[3]Çimik, A.**, [4]Gürel-Gürevin, E., [5]Öztürk, A.A., [6]Kıyan, H.T.

[1] Ege University, Faculty of Science, Department of Biology, Zoology Section, Izmir, Turkey

[2] Nevşehir Haci Bektaş Veli University, Acigöl Vocational School of Technical Sciences, Program of Laboratory Technology, Department of Chemistry and Chemical Process Technologies, Nevşehir, Turkey, mertkaris@nevsehir.edu.tr

[3] Anadolu University, Graduate School of Health Sciences, Department of Pharmacognosy, Eskisehir, Turkey, alpercimik@anadolu.edu.tr

[4] Istanbul University, Faculty of Science, Department of Biology, Istanbul, Turkey, egurel@istanbul.edu.tr

[5] Anadolu University, Department of Pharmaceutical Technology, Eskisehir, Turkey, aaozturk@anadolu.edu.tr

[6] Anadolu University, Department of Pharmacognosy, Eskisehir, Turkey, htkiyan@anadolu.edu.tr

Introduction:

Neurergus strauchii strauchii Steindachner, which is a member of the *Salamandrid* genus, has a haemolytic dermal venom (1). Previously, the dermal venom microflora of *Neurergus* sp. has been reported to exhibit antimicrobial activities against pathogene microorganisms (2) The main goal of this study is research on the *in vitro* anti-inflammatory, antioxidant and antimicrobial activities of dermal venom of *Neurergus strauchii*. *In vitro* anti-inflammatory, antioxidant and antibacterial effects of dermal venom of *Neurergus strauchii* were determined by using *in vitro* COX-1 & COX-2, DPPH scavenging assays and agar microdilution method. The total protein amount of the secretion was determined by using BCA Protein Assay Kit.

Materials and Methods:

In vitro anti-inflammatory activity

In vitro cyclooxygenase-1 (COX-1) and cyclooxygenase-2 (COX-2) enzyme inhibitory activities of formulations were evaluated using method described in (3,4) also by using commercial Biovision COX-1 & COX-2 inhibitor (fluorometric) kits. SC560 and Celecoxib were used as COX-1 and COX-2 positive controls respectively.

In vitro antioxidant activity-Free radical scavenging assay (DPPH test)

The scavenging effect of the samples on DPPH free radical was determined using a modified method of Brand-Williams (5). The free radical scavenging activity of the samples was expressed as percentage of inhibition calculated according to Equation:

$$\%Inh: (A_{control} - A_{sample)} / A_{control}) \times 100$$

Where $A_{control}$ is the absorbance of the control (containing all reagents except the test compound),

A_{sample} is the absorbance of the sample with added DPPH. The IC_{50} values were obtained by plotting the DPPH scavenging percentage of each sample against the sample concentration. Data were analyzed using the SigmaPlot software (Version 12.0).

Antimicrobial activity

Microorganisms and culture conditions

Probiotic microorganism strains were obtained from Christian Hansen© culture collection. Routine culture was performed on MRS Agar(Biokar Diagnostics©, Ref: BK089HA) for *Lactobacillus reuterii* DSM 17938 and *Bifidobacterium animalis* ssp. *lactis* B94 microorganisms (6). All agar plates were incubated at 37ºC for 24 -36 h. Several colonies of each microorganism were then suspended in 0.9% NaCl and cell suspensions were adjusted to c.10^8 CFU mL^{-1} and 0.5 Mc Farland turbidity (7).

Agar dilution minimum inhibitor concentration (MIC) method

Bacteria were assessed for susceptibility to the samples using the agar dilution assay, which was performed according to method M7-A7 from the Clinical Laboratory Standarts Institute (CLSI) (8). Chloramphenicol was used as positive control. Stock solution of the samples were prepared in sterile distilled water at 200, 400 and 400 µg/mL, Chloramphenicol was dissolved in 10% (v,v) respectively. Appropriate volumes of the samples stock solutions in sterile distilled water and MRS agar were combined result in final concentrations of 400 µg/mL, 200 µg/mL and 100 µg/mL for active ingredients and 100 µg/mL, 50 µg/mL and 25 µg/mL for the the samples. Inocula were prepared as described earlier, and agar plates were inoculated using a sterile pipet sets that delivered a 50µL inoculum spot, corresponding to c. 10^4 CFU per spot. Plates were incubated for 24 h at 37ºC, and minimum inhibitory concentrations (MICs) were then determined as the lowest concentration inhibiting growth (9).

Results:

The total protein amount of the secretion was found at 1700 µg/mL. IC_{50} results of venom were calculated as 157.9770, 96.84, 11.6873 µg/mL for *in vitro* COX-1 & COX-2, DPPH inhibitons respectively. Antimicrobial activity MIC results of venom were determined as >400µg/mL against both of the microorganisms.

Conclusions:

Venom inhibited all enzyms and DPPH on related concentrations. It is safe on obligatory and facultative anaerobic microorganisms. This result supports the texistence of probiotic dermal venom microflora (2). The results of this study indicated that link between related enzyme activities and probiotic microorganism protective activity. More detailed analysis will be cconducted in the future stages of the study, and different drug delivery systems will be designed and characterized by using the relevant substance as an API.

References:

1. Arikan, H and Cicek, K. (2014). North-Western Journal of Zoology, 10 (1): 190-209.
2. Parto, P. et al., (2014). Asian Herpetological Research, 5(3):204-208.

3. Vgzquez, M.T. et al., (1997). Eur. J. Med. Chem. 32:529-534.
4. Xingxian, Z. et al., (2009). Patent No: CN 101412670.
5. Brand-Williams, W. et al., (1995). WT-Food science and Technology, 28:25-30.
6. Vinderola, C.G. and Reinheimer, J.A. (1999). International Dairy Journal, 9:497-505.
7. Boorn ,K.L. et al., (2010). Journal of applied microbiology, 108:1534-1543.
8. Clinical and Laboratory Standards Institute, Methods for Dilution Antimicrobial Susceptibility Tests for Bacteria That Grow Aerobically; Approved Standard – Seventh Edition. Wayne, PA: CLSI, 2020.
9. Mota, C.R.A. et al., (2009). Revista da Sociedade Brasileira de Medicina Tropical, 42:250-254.

OP152: METABOLOMICS AND ACETYLCHOLINESTERASE INHIBITORY ACTIVITY STUDIES ON DACTYLIS GLOMERATE L. AND HORDEUM MURINUM L.

[1]Gonulalan, E.M., [2]Kahraman, C.

[1] Afyonkarahisar Health Scinces University, Department of Pharmacognosy, Afyonkarahisar, Turkey, murat.gonulalan@afsu.edu.tr

[2] Hacettepe University, Department of Pharmacognosy, Ankara, Turkey, cigdemm@hacettepe.edu.tr

Introduction:

Metabolomics (Phytomics in plants) is defined as a comprehensive quantitative and qualitative analysis of all metabolites present in a particular cell, tissue or organism (1). Alzheimer's disease is an age-related, irreversible, progressive neurodegenerative disease (2). Acetylcholinesterase inhibitory compounds and extracts can be effective on Alzheimer's and are used (3). In this study acetylcholinesterase inhibitory activities and metabolic profiles of *Dactylis glomerata* L. and *Hordeum Murinum* L. (Poaceae) were investigated.

Materials and Methods:

In this study methanolic extracts of aerial parts from *Dactylis glomerata* L. and *Hordeum Murinum* L. were used. For theacetylcholinesterase inhibitory activities, Acetylcholinesterase from *Electrophorus electricus* (Type-VI-S, EC 3.1.1.7), acetylthiocholine iodide (ATCh-I), and 5,5′-dithiobis-(2-nitrobenzoic acid) (DTNB) were purchased from Sigma. The inhibitory activities were determined spectrophotometrically by Ellman's method with slight modifications (4). Phosphate buffer (pH 7.6) and different concentrations of extracts were incubated with enzyme solution for 10 min at 25 °C. Then DTNB (1.25 mM), for the enzymatic reaction, was added and the reaction was initiated by adding ATCh-I (7.5 mM), as a substrate. The change of absorbance at 412 nm was measured kinetically. Galantamine is used as positive control. GC-MS and LC-QTOF-MS is used to determine metabolic profiles. GCMS-QP2010 Ultra instrument is used for GC-MS analysis (Mass range: 50-650 dalton). Fiehn RTL Library is used to identify metabolites. Agilent 6530 instrument is used for LC-QTOF-MS analysis. Molecular formula and structure prediction was performed using RIKEN tandem mass spectral database (ReSpect)that plant specific ms/ms based database.

Results:

1690 primary metabolites by using gas chromatography-mass spectrometry (GC-MS) 296 of them were annotated using retention index libraries. 25635 mass spectral features have been detected by using liquid chromatography quadrupole time of flight mass spectrometry (LC-QTOF-MS) and 305 of them were annotated using retention index libraries.

GC/MS Based Metabolomic Profiling (Major metabolites)

Super Class	Class / Sub Class / Parent	Number of Metabolites
Benzeneoids	Benzene and substituted derivatives	20
	Phenols	8
Lipids and lipid-like molecules	Fatty Acyls	27
	Prenol lipids	8
Organic acids and derivatives	Amino acids, peptides, and analogues	49
	Dicarboxylic acids and derivatives	7
	Hydroxy acids and derivatives	8
	Keto acids and derivatives	6
Organic oxygen compounds	Carbohydrates and carbohydrate conjugates	53
Organoheterocyclic compounds	Azoles, Indoles and derivatives, Pyridines and derivatives, etc..	28
Phenylpropanoids and polyketides	Cinnamic acids and derivatives, Flavonoids, Phenylpropanoic acids, etc..	24

LC-QTOF-MS Based Metabolomic Profiling (Major metabolites)

Metbolite Type	Number of Metabolites
Anthocyanidin-3-O-glycosides	9
Anthocyanidin-5-O-glycosides	5
Flavonoid-3-O-glycosides	12
Flavonoid-7-O-glycosides	14
Flavonols	6
Hydroxybenzoic acid derivatives	4
Hydroxycinnamic acids	4
Methoxyphenols	7
7-hydroxycoumarins	4

Acetylcholinesterase Inhibitory Activities (% Inh.)

Plant Name	100 µg/mL	200 µg/mL
Dactylis glomerata L.	4,18	18,15
Hordeum murinum L.	3,86	13,13

Conclusions:

This study is the part of a project (Totally 152 species and 41 families). Acetylcholinesterase Inhibitory Activity Assay and metabolomics studies applied to 152 different species and compared. According to metabolic profiles of two plants we expected acetylcholinesterase inhibitory activities because of many possible active metabolite that we determined. But, it is a fact that synergy and antagonism play a important role of the whole metabolite instead of single metabolite. That's why there is no significant acetylcholinesterase inhibitory activity. Further studies will be performed for investigate antagonistic interactions.

Acknowledgements

This study was supported by grant from Afyonkarahisar Health Sciences University Scientific Research Projects (Project No: 19.TEMATİK.007)

References:

1. Fiehn, O., Kopka, J., Dörmann, P., Altmann, T., Trethewey, R.N., Willmitzer, L. (2000) Metabolite profil- ing for plant functional genomics. Nature Biotechnology, 18(11):1157-61.
2. Rao, R.V., Descamps, O., John, V., Bredesen, D.E. (2012). Ayurvedic medicinal plants for Alzheimer's disease: a review. Alzheimer's research & therapy, 4(3):1-9.
3. Björkholm, C., Monteggia, L.M. (2016). BDNF-a key transducer of antidepressant effects**,** Neuropharmacology, 102:72-79.
4. Ellman, G.L., Courtney, K.D., Andres, V., Featherstone, R.M. (1961). A new and rapid colorimetric determination of acetylcholinesterase activity. Biochemical Pharmacology, 7 (2), 88-95.

OP153: A COMPARATIVE ANALYSIS ON ANTIOXIDANT PROPERTIES, PHENOLIC COMPOSITION AND HPTLC EXAMINATION OF SIDERITIS SCARDICA SUBSP. SCARDICA INFUSION AND HYDROALCOHOLIC EXTRACT

[1]Bardakcı, H., **[2]Yıldırım, E.B.**, [1]Barak, T.H.

[1] Acıbadem Mehmet Ali Aydınlar University, Faculty of Pharmacy, Department of Pharmacognosy, Istanbul, Turkey,
hilal.bardakci@acibadem.edu.tr, timur.barak@acibadem.edu.tr

[2] Acıbadem Mehmet Ali Aydınlar University, Faculty of Pharmacy, Istanbul, Turkey,
elif.yildirim1@live.acibadem.edu.tr

Introduction:

On account of an imbalance between antioxidative protective systems and the generation of oxidizing substances, including free radicals, the human body is continuously exposed to significant oxidative stress (1). The production of free radicals leads to cell damage and death, speeds up aging, and causes a variety of diseases such as cardiovascular diseases, cancer, Parkinson's disease, and others (1). Antioxidants are thus thought to be useful components for preventing oxidative stress-related illnesses (1). Phenolic compounds, in particular, exhibit substantial antioxidant activity among the many different types of phytochemicals (1). Various phytochemical analyses focused on the occurrence of flavonoids and phenolics, as these chemical substances are partly responsible for pharmacological activity of *Sideritis scardica* (2). In this study, we aimed to comparatively determine the antioxidant potentials of EtOH extract and infusion prepared from the aerial parts of *S. scardica* subsp. *scardica* by using various *in vitro* methods as well as to characterize their phenolic compositions by High Performance Thin Layer Chromatography (HPTLC) technique.

Materials and Methods:

Infusion and 80% ethanolic extracts were prepared from the aerial parts of the *S. scardica* subsp. *scardica*. The extracts were investigated for their antioxidant capacities using DPPH radical scavenging activity method and FRAP, CUPRAC, TOAC assays. Total phenolic, phenolic acid, and flavonoid contents were also assessed spectrophotometrically. Quantification of chlorogenic acid was performed by using HPTLC.

Results:

Total phenolic, flavonoid and phenolic acid contents were measured as 198.60±5.83 mg gallic acid equivalents (GAE)/g, 29.27±1.44 mg quercetin equivalents (QE)/g, 99.27±3.00 mg caffeic acid equivalents (CAE)/g for ethanolic extract, and 209.91±9.34 mg gallic acid equivalents (GAE)/g, 20.66±3.65 mg quercetin equivalents (QE)/g, 227.93±3.82 mg caffeic acid equivalents (CAE)/g for infusion, respectively (Table 1). The IC_{50} values for DPPH radical scavenging activity were measured as 2047.84 µg/ml and 1981.38 µg/ml with comparison of BHT for ethanolic extract and infusion, respectively (Table 2). CUPRAC, FRAP and TOAC antioxidant capacities were determined as 228.15±2.93 mg ascorbic acid equivalents (AAE)/g, 0.97±0.02 Mm $FeSO_4$ equivalents/g, 338.60±5.23 mg ascorbic acid equivalents (AAE)/g for ethanolic extract and 208.53±9.09 mg ascorbic acid equivalents (AAE)/g, 0.95±0,03 Mm

$FeSO_4$ equivalents/g, 323.25±2.76 mg ascorbic acid equivalents (AAE)/g for infusion, respectively (Table 2). Ethanolic extract and infusion of *S. scardica* subsp. *scardica* were found to contain chlorogenic acid as 1.31 and 1.52 w/w%, respectively (Table 3).

Table 1. Results of *in vitro* phenolic profile assays

Assay	Infusion (2%)	EtOH (80%) Extract
Total phenolic content[a]	209.91 ± 9.34	198.60 ± 5.83
Total flavonoid content[b]	20.66 ± 3.65	29.27 ± 1.44
Total phenolic acid content[c]	227.93 ± 3.82	99.27 ± 3.00

a Results were expressed as the mean of triplicates ± standard deviation (S.D.) and as mg gallic acid equivalents (GAE) in 1 g sample.
b Results were expressed as the mean of triplicates ± standard deviation (S.D.) and as mg quercetin equivalents (QE) in 1 g sample.
c Results were expressed as the mean of triplicates ± standard deviation (S.D.) and as mg caffeic acid equivalents (CAE) in 1 g sample.

Table 2. Results of *in vitro* antioxidant assays

Assay	Infusion (2%)	EtOH (80%) Extract
DPPH scavenging activity (IC50)[a]	1981.38 ± 12.38	2047.84 ± 19.72
FRAP[b]	0.95 ± 0.03	0.97 ± 0.02
CUPRAC[c]	208.53 ± 9.10	228.15 ± 2.93
Total antioxidant capacity[c]	323.25 ± 2.76	338.6 ± 5.23

IC_{50} value of the reference compound "BHT" in DPPH scavenging activity is found to be 469.28 ± 2.47 µg/ml
FRAP activity of the reference compound "BHT" is found to be 4.26 mM ± 0.29 $FeSO_4$ eq. in 1 g sample.
a Results were expressed as the mean of triplicates ± standard deviation (S.D.) and DPPH activity was expressed as IC_{50} in µg/ml equivalents.
b Results were expressed as the mean of triplicates ± standard deviation (S.D.) and as mM $FeSO_4$ equivalents in 1 g sample.
c Results were expressed as the mean of triplicates ± standard deviation (S.D.) and as mg ascorbic acid equivalents (AAE) in 1 g sample.

Table 3. Results of HPTLC quantification

Extract	Chlorogenic acid (w/w%)
80% EtOH	1.31
Infusion	1.52

Conclusions:

The antioxidant activities of ethanolic extract and infusion of *S. scardica* subsp. *scardica* were virtually comparable, but the total phenolic acid contents differed significantly. Furthermore, HPTLC analysis showed that chlorogenic acid content is higher in infusion when compared to ethanolic extract. These results support the folkloric use of *S. scardica* subsp. *scardica* as infusion. Moreover, HPTLC analysis was conducted on *S. scardica* subsp. *scardica* extracts, for the first time to our knowledge.

References:

1. Bardakci H, Cevik D, Barak TH, Gozet T, Kan Y, Kirmizibekmez, H. (2020). Biochemical Systematics and Ecology, 92:104120.
2. Todorova M, Trendafilova A. (2014). Journal of Ethnopharmacology, 152:256-265.

OP156: IN THE FIGHT AGAINST BACTERIA: AERIAL PARTS OF PEGANUM HARMALA L.

[1]Guragac Dereli, FT., [2]Onem, E., [3]Ozaydın, AG.

[1] Suleyman Demirel University, Department of Pharmacognosy, Isparta, Turkey, tugcedereli@sdu.edu.tr

[2] Suleyman Demirel University, Department of Pharmaceutical Microbiology, Isparta, Turkey, ebruonem@sdu.edu.tr

[3] Suleyman Demirel University, YETEM-Innovative Technology Application and Research Center, Isparta, Turkey, ayseozaydin@sdu.edu.tr

Introduction:

The increase in the rate of bacterial diseases caused by multi-drug resistant bacterial strains has become a global health problem in recent years. This situation has increased the interest in the research of phytochemicals that are effective in the treatment of bacterial infections caused by resistant microorganisms (1).

Materials and Methods:

This study aimed to evaluate the antibacterial and anti-swarming motility activities of the methanolic extract of aerial parts of *Peganum harmala* L. and determine the chemical characterization of the phytochemical composition of its. Plant material was collected from Kahramankazan, in July 2020. A voucher specimen (AEF 30713) is kept in the herbarium of Ankara University Faculty of Pharmacy. 50 grams of powdered plant material was subjected to solvent extraction using methanol at room temperature for 48 hours. The extract was filtered and the filtrate was evaporated by using a rotary evaporator at 40°C to dryness in vacuo. The microdilution method was used to determine the minimum inhibitory concentrations of the extract against some Gram-positive and Gram-negative bacteria. *Bacillus cereus* ATCC 11778, *Staphylococcus aureus* ATCC 25923, *Methicillin-Resistant Staphylococcus aureus* (MRSA) ATCC 43300, *Escherichia coli* ATCC 25922 and *Pseudomonas aeruginosa* PAO1 strains were used for antibacterial activity test. Sterile 96-well microplates were used for this assay. Bacterial strains were cultured overnight at 37 °C in Muller Hinton Broth. Two-fold serial dilutions were made by adding 100 µl of sample to the wells containing Muller Hinton broth medium. Microplates added with 5 µl of the bacterial suspension were incubated overnight at 37°C. After incubation, the microplates were evaluated. The lowest concentration without bacterial growth was determined as the minimum inhibitory concentration (MIC).

As swarming migrations play an important role in quorum sensing-mediated biofilm formation in uro-pathogens, such as *P. aeruginosa* PAO1, we examined the anti-quorum sensing potential of the plant extract against quorum-sensing dependent swarming motility in this strain. 200 µl of the plant extract was added to the medium containing 8 grams of nutrient broth, 1 gram Bacto-agar and 0.5 %glucose. 5 µl of the overnight culture of supernatant was inoculated into the centre of the medium and incubated at 37 °C for 16-18 hours. At the end of the incubation, the swarming motility was determined by measuring the diameter of the spread from the point of inoculation to the environment. The results were evaluated by comparing with the PAO1 strain, which has a swarming motility characteristic.

Phytochemical analysis of the extract was carried out on a High-Performance Liquid Chromatography (HPLC) system. HPLC conditions are presented in **Table 1.**

Table 1. HPLC analysis conditions

Chromatographic Conditions	Time (min.)	A (%)	B (%)
	0	93	7
Detector: Photo Diode Array Detector (λ max. : 278 nm)	20	72	28
Autosampler: SIL–10AD vp	28	75	25
System controller: SCL-10A vp	35	70	30
Pump: LC-10AD vp	50	70	30
Degasser: DGU-14a	60	67	33
Column heater: CTO-10 A vp	62	58	42
Column: Agilent Eclipse XDB C-18 (250 mm × 4.6 mm), 5 µm	70	50	50
Column temperature: 30 °C	73	30	70
Mobile phases: A: Acetic acid– Water (3:97 V/V), B: Methanol	75	20	80
Flow rate: 0.8 mL / min.	80	0	100
Injection volume: 20 µL	81	93	7

Results:

Results of the microdilution test **(Table 2)** revealed that MIC values of the extract which are effective on different bacteria were in the range of 0.9-1.76-mg/ml.

Table 2. Results of the microdilution test

BACTERIA	***Peganum harmala* L.** MIC (mg/mL)	***Gentamicin*** MIC (mg/mL)
S. aureus ATCC 25923	1,76	0,0125
MRSA ATCC 43300	1,76	0,0125
B. cereus ATCC 11778	0,9	0,0125
E. coli ATCC 25922	1,76	6,25
P. aeruginosa PAO1	1,76	6,25

As shown in **Figure 1&2,** the extract showed observable inhibition against the swarming of PAO1. It was found that the extract inhibited the swarming ability of PA01 by 85 % at a concentration of 58 µg/ml.

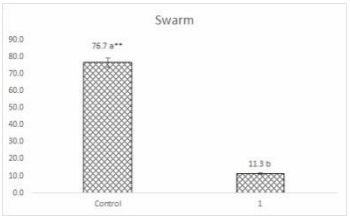

Figure 1. Results of the anti-swarming assay

**Differences between mean values followed by different letters of plant extracts are statistically significant at $p<0.01$.

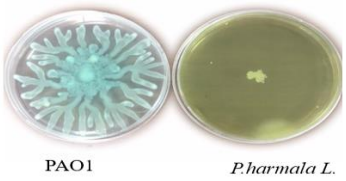

Figure 2. Effect of plant extract on swarming motility *(Scale bar = 30 mm)*

The results obtained from HPLC analysis **(Table 3)** indicated that *p*-hydroxybenzoic acid and chlorogenic acid were the main phytoconstituents. It was also determined that the extract contains flavonoids including hesperidin, quercetin and luteolin and phenolic acids including cinnamic acid, sinapinic acid, ferulic acid, *p*-coumaric acid and vanillin.

Table 3. Results of the HPLC analysis

PHYTOCHEMICALS	CONCENTRATIONS (µg/mL)	RETENTION TIME (min)
p-hydroxybenzoic acid	115,3	14,60
Chlorogenic acid	68,7	16,17
Vanillin	2,3	22,23
p-coumaric acid	4,7	26,06
Ferulic acid	12,0	30,23
Sinapinic acid	25,8	31,90
Hesperidine	0,7	56,14
Cinnamic acid	0,6	69,00
Quercetin	18,3	72,94
Luteolin	18,1	75,40

Conclusions:

Phenolic plant secondary metabolites are among the most investigated naturally occurring phytochemicals due to their health-promoting benefits. These phytocompounds have attracted a scientific interest in terms of their various biological activities, especially their antioxidant properties. Additionally, some studies in recent years have provided evidence of the anti-quorum sensing and anti-biofilm activities of the phenolic phytoconstituents. Especially, flavonoidal compounds have been documented to interfere with the regulation of quorum sensing associated pathways in PAO1 (2).

In conclusion, considering the literature data it is thought that the antibacterial and anti-swarming activities of the methanolic extract prepared from the aerial parts of *P. harmala* may be due to the synergistic effect of phenolic phytochemicals in its content.

References:

1. Lambert RJW, Skandamis PN, Coote P, Nychas GJE (2001). Journal of Applied Microbiology, 91: 453–462.
2. Asfour, H. Z. (2018). Anti-quorum sensing natural compounds. Journal of Microscopy and Ultrastructure, 6(1), 1-10.

OP158: LAMIACEAE MEMBERS USED IN ANATOLIA TRADITIONALLY FOR RESPIRATORY DISEASES FROM THE PERSPECTIVE OF BACTERIAL AND VIRAL INFECTIONS

[1]Zare, G., [1]Diker NY., [1]Tatlı Çankaya, İİ.

[1]Hacettepe University, Faculty of Pharmacy, Department of Pharmaceutical Botany, Sıhhiye, Ankara, Turkey,
golshanzare@gmail.com, yagmurkumser@gmail.com, itatli@hacettepe.edu.tr

Introduction:

Anatolia is the host of most old civilizations besides the rich flora, a wide range of topography and climate. Since ancient time, people use plants and herbal drugs to treat most of the common diseases especially fever, cough, cold, and fatigue and there are so much documented or not documented information related to using the medicinal plants in this area. Respiratory diseases are among the globally most common diseases, in which the majority of the population experiences at least one of them from mild to severe annually. These diseases can be highly contagious and cause the death of more than millions of people every year. These diseases are mainly caused by viruses and bacteria and can vary from mild disorders, such as the common cold, influenza, and pharyngitis to chronic or life-threatening illnesses like asthma, pneumonia, and severe acute respiratory syndromes. These diseases despite their proximity are often avoidable, and most of the time the prevention costs are much less than treatment (1). The ability to control and eliminate diseases cause such as bacteria and viruses besides the improvement of the immune system with beneficial nutrition such as vitamins and antioxidants can be significantly reduced the damage. This study aimed to evaluate the documented Lamiaceae plants from Anatolia used traditionally to treat respiratory diseases from the perspective of bacterial and viral infections.

Materials and Methods:

In this context, we evaluated 187 ethnobotanical researches (between 1991-2020) to prepare the list of the most frequently used Lamiaceae species in Anatolia. Then we studied the books, reviews and scientific studies on biological activities and phytochemical analysis of these taxa too.

Results:

According to our extended research results, Lamiaceae is the most prominent family with 28 genera and 101 citations as traditional therapeutics for the treatment of respiratory diseases such as cough, bronchitis, asthma, colds & flu, shortness of breath (Figure 1). The Lamiaceae family is a diverse plant group with a cosmopolitan distribution. This family is considered an economically and medicinally important group of aromatic plants with rich sources of essential oils. Phytochemical analysis of the Lamiaceae has reported the presence of flavonoids, terpenoids, especially essential oils and fatty acids. Essential oils are known as the origin of the complex secondary metabolites, especially terpenoids and are often associated with broad-spectrum antibacterial properties (2, 3). The antiviral activity is attributable to polyphenols including proanthocyanidins and tannins, phenolic acids, such as rosmarinic acid, the low-molecular glycoside-forming compounds of chlorogenic acid, caffeic acid, their derivatives, as well as some alkaloids (4, 5). Carnosol, caffeic acid, a polysaccharide named

prunellin, and different types of polyphenol salvianolic acids from different genera of Lamiaceae exhibited notable antiviral activities against a large spectrum of enveloped and unenveloped viruses (DNA and RNA) such as HIV, human influenza virus and respiratory syncytial virus (6).

The genera that showed the highest citations frequency were *Thymus* (52 citations), *Mentha* L. (49 citations), *Salvia* L. (40 citations), *Origanum* L. (27 citations), *Sideritis* L. (20 citations), *Teucrium* L. (15 citations), *Thymbra* L. (10 citations), *Rosmarinus* L. (9 citations), *Stachys* L. (9 citations) and *Melissa* L. (7 citations) respectively. These genera are among the most popular folk remedy for the treatment of respiratory diseases (Figure 2).

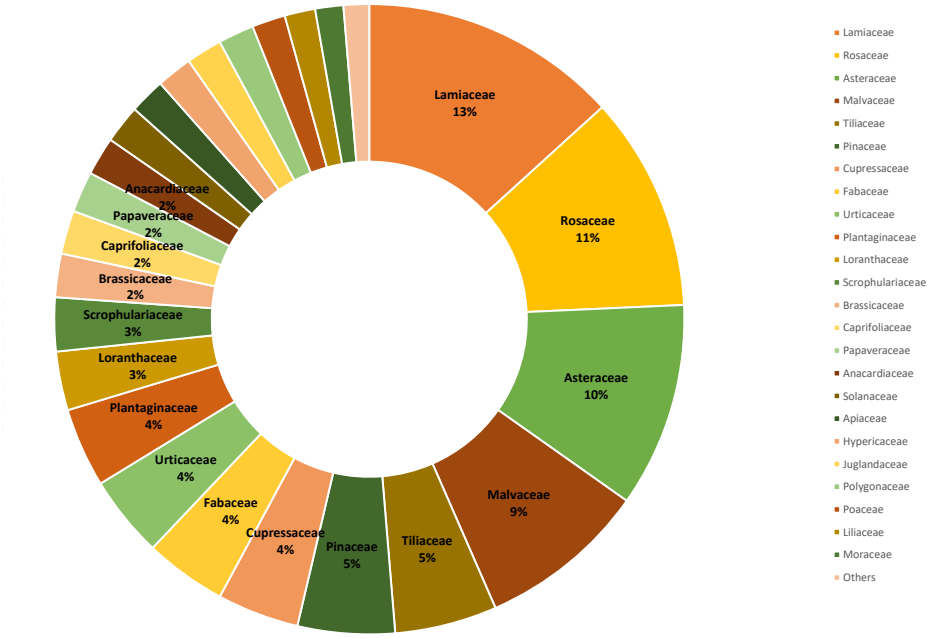

Figure 1. The number of citations per families related to medicinal plants for the treatment of respiratory diseases

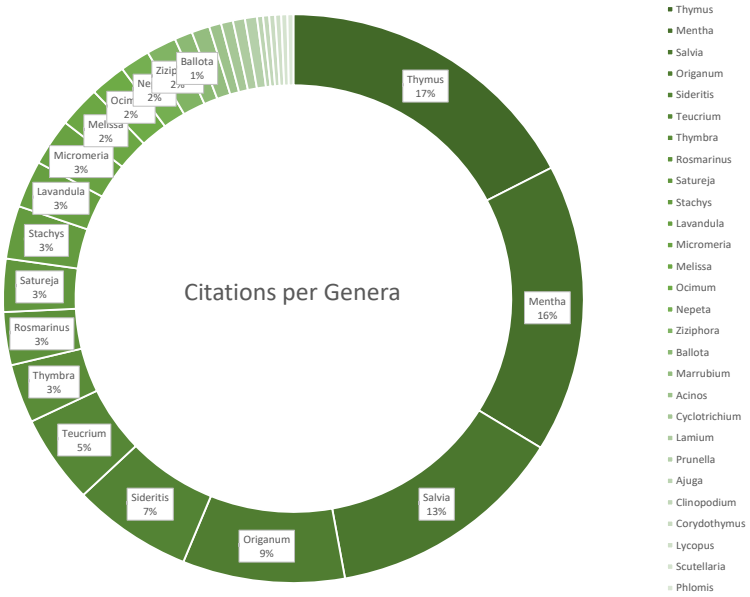

Figure 2. The number of citations per genera belonging to Lamiaceae related to medicinal plants for the treatment of respiratory diseases

Conclusions:

Local people in Anatolia for treatment of cold & flu extensively use a wide spectrum of Lamiaceae family members including *Mentha longifolia*, *Mentha x piperita*, *Origanum vulgare*, *Salvia* sp., *Thymus* sp. and *Sideritis* sp. The presence of a wide range of therapeutic compounds in these medicinal plants has shown beneficial advantages in terms of antioxidant, antibacterial, antiviral, antitussive, antipyretic, and immunomodulatory activities. According to results, some taxa that have a higher potential for the development of new drugs is suggested concern to the common use of taxa by local people in different areas, wide distribution and availability of them.

References:

1. Ferkol T, Schraufnagel D (2014). The global burden of respiratory disease. Annals ATS 11(3), 404-406.
2. Altintas, et al., (2013). Characterization of volatile constituents from *Origanum onites* and their antifungal and antibacterial activity. J. AOAC Int. 96(6), 1200-1208.
3. Assaeed, A., Elshamy, A., El Gendy, A.E.-N., Dar, B., Al-Rowaily, S., Abd-ElGawad, A., 2020. Sesquiterpenes-rich essential oil from above ground parts of *Pulicaria somalensis* exhibited antioxidant activity and allelopathic effect on weeds. Agronomy 10(3), 399.
4. Raja, R.R., (2012). Medicinally potential plants of Labiatae (Lamiaceae) family: an overview. Res. J. Med. Plant 6(3), 203-213. https://doi.org/10.3923/rjmp.2012.203.213
5. Gilling, et al. (2014). Antiviral efficacy and mechanisms of action of oregano essential oil and its primary component carvacrol against murine norovirus. J. Appl. Microbiol. 116(5), 1149-1163.
6. Bekut, et al. (2018). Potential of selected Lamiaceae plants in anti(retro)viral therapy. Pharmacological Research 133, 301-314.

OP161: THE IMPORTANCE OF DROSOPHILA MELANOGASTER AS A MODEL ORGANISM IN PHYTOCHEMICAL ACTIVITY BIOASSAY FOR NEUROLOGICAL DISEASES

[1]Emecen, G.

[1] Hacettepe University, Faculty of Science, Department of Biology, Ankara, Turkey, guzin@hacettepe.edu.tr

Introduction:

Drosophila melanogaster "fruit fly" is one of the most popular, a well understood, high-throughput and cost effective model organism being used more than 110 years to study the different biological aspects related to the development and diseases. The most attractive aspects of this fly include compact genome size and rapid generation time. The *Drosophila* genome has only 4 chromosomes and has been sequenced and detected about 14.000 genes. This number is in comparison to the human genome, which is predicted to have 24.000 genes encoding for proteins. Despite the different sizes of their genomes, it is now known that over 70% of human genes have functional orthologs in *Drosophila*. In particular, axis polarity, metabolic processes, organogenesis and neural development genes are so highly conserved that substitution of fly genes by mammalian genes and vice versa quite often ensures correct functioning. Unlike simpler model organisms, flies exhibit rather complex behaviors that are relevant to mammalian or other higher organism behaviors. These include circadian rhythms, sleep, learning and memory, courtship, feeding. Many of the molecular and genetic components of these behaviors were first elucidated in the fly and then subsequently identified in mammalian systems. The neurotransmitters and molecular mechanisms mediating these behaviors and activities are highly conserved with higher organisms, as well as humans(1). By means of these advantages, pharmacological properties of plants/plant-derived components on behavior can be studied by performing the fly behavior assays, memory and learning studies in the diseased model organism without ethical concerns. Moreover, *Drosophila* has been successfully used for identifying new drug candidates for the neurodegenerative diseases and for evaluating the efficacy and safety of these candidates.These successes in drug development highlight the enormous potential of *Drosophila* as a tool for the neuropharmacological study of medicines candidates (2).

Materials and Methods:

Survivorship assay: In flies feeding with desired plants/components any extension in survival will suggest the life extension associated with phytochemicals.

Behavioral assays:

Behavior is genetic makeup of an organism and is a link between the molecular and physiological prospect of biology and the environmental changes.

- Larval behavioral assays are helpful for early detection of the disease and for the study of the effect of phytochemicals on larval behavior.

- Adult behavior assays of *Drosophila* include courtship, locomotor and phototaxis. These are important identification of neuroprotective potential associated with many plants/compounds.

Courtship (mating) behavior assay is being used to examine flies sexual behavior and neuronal coordination. The cumulative effect of these processes give rise to its motor behaviors and associated with learning and memory of the fly.

Locomotor behavior, such as Alzheimer's (AD), Parkinson's (PD) and Huntington's disease (HD), SMA motor dysfunctions/locomotor impairment is one of the key parameter of the disease progression and it is well studied in the flies.

Phototaxis assay is a visual behavior assay which is controlled by the fly neural system and is associated with learning and memory of the fly. The phototaxis response supplemented with phytochemicals will suggest the neuroprotective potential of these substance

In vivo AChE and BChE enzyme inhibition: In our laboratory, via feeding larval and adult stage in vivo AChE and BChE enzyme inhibition are also studied to determine non-alkaloid effective phytochemicals in Alzheimer's disease (3).

Rpd3 protein and histone acetylation levels in *D. melanogaster* model of SMA:

This study aimed to determine the treatment conditions that can be used in HDAC inhibitor research in the *D. melanogaster* model of SMA (4). With this method we adapted to our laboratory, started to identify phycochemicals with HDAC inhibitory potential.

Results:

We have been investigating the effects of plants/plant-derived components (phytochemicals) on neuromuscular diseases as SMA(spinal muscular atrophy), Alzheimer's and Parkinson's via following assays, in our Hacettepe University, Department of Biology, Functional and Evolutionary Genetics Laboratory.

One of the neuropharmacology studies in our laboratory, it was aimed to determine the appropriate stages that can be used in HDAC inhibitor research in *Drosophila* model with SMA disease. In addition, it is aimed to create a suitable infrastructure for investigating the effects of HDAC inhibitors that have been previously synthesized and will be synthesized hereafter in vivo. These experiments are still ongoing our laboratory in partnership with Hacettepe University Faculty of Medicine - Medical Biology Department.

In another ongoing study, the effect of some phenolic compounds on acetylcholinesterase inhibition is examined with the neuroprotective effect model of *Drosophila melanogaster*.

These responses of flies which applicated phytochemicals of this project *Drosophila* are will reveal the neuroprotective potential of the relevant substance. The *Drosophila* strains developed to study human diseases and are selected from the *Drosophila* Genetic Reference Panel (DGRP), which includes 205 strains with different genetic backgrounds (5). When we take the results into the GWAS analysis, we will reveal other genes that share the same metabolic pathways with the acetylcholinesterase enzyme. Thus, we will have taken the significant step towards revealing known and unknown many genes in Alzheimer's disease. Our results can be considered as important outputs in all aspects, since no such study has yet been conducted with DGRP strains. We are carrying out this study together with Gazi University - Faculty of Pharmacy.

Conclusions:

These studies and our references emphasize the advantage of *D. melanogaster* as a model organism for its use in pharmacological activity studies specifically related to neurological diseases, with our previously reported or ongoing experiments in our laboratory. A growing body of evidence supports the notion that a large part of the pathophysiology of neurodegenerative diseases is well conserved in *Drosophila*. Furthermore, *Drosophila* is a simple in vivo model, which can be used for evaluating the efficacy of a drug at various levels: whether it enters an animal body, targets neurons, or exerts its protective effect in not only cells but also in tissues. Therefore, *Drosophila* has been successfully used for identifying new drug candidates for the neurodegenerative diseases and for evaluating the efficacy and safety of these candidates. These successes in drug development highlight the enormous potential of *Drosophila* as a tool for the pharmacological study of traditional medicines.

References:

1. Nichols C., (2006). Drosophila melanogaster neurobiology, neuropharmacology, and how the fly can inform central nervous system drug discovery, Pharmacology & Therapeutics, 112: 677–700.
2. Lee S.H, Min K.J, (2019). Drosophila melanogaster as a model system in the study of pharmacological interventions in aging, Translational Medicine of Aging 3: 98-103.
3. Erdoğan – Orhan İ, (2020). Bitkisel Kaynaklı Bazı Fenolik Bileşiklerin Anti-Alzheimer, Anti-Melanojenik ve Cilt Yaşlanması Üzerine Etkilerinin In vitro, In vivo ve In Silico Yöntemlerle İncelenmesi, Gazi Üniversitesi BAB Projesi
4. Hazır C, (2021). Sma'lı Drosophıla Melanogaster Modelinde Rpd3 Proteini Ve Histon Asetilasyon Düzeylerinin Araştırılması, Hacettepe Üniversitesi, Tıbbi Biyoloji Programı, Yüksek Lisans Tezi.
5. Mackay T, Richards T.F., et al.,(2012). The Drosophila melanogaster Genetic Reference Panel, Nature, 482, 173-8.

OP162: NEPETA TRANSCAUCASICA GROSSH.: CHEMICAL COMPOSITION AND ALPHA GLUCOSIDASE INHIBITORY ACTIVITY OF ESSENTIAL OIL AND ANATOMICAL PROPERTIES OF DIFFERENT PARTS OF THE PLANT

[1]Yuca, H., [2]Karakaya, S., [3]Yılmaz, B., [1]Guvenalp, Z.

[1] Ataturk University, Faculty of Pharmacy, Department of Pharmacognosy, Erzurum, Turkey, hafize.yuca@atauni.edu.tr, guvenalp@atauni.edu.tr

[2] Ataturk University, Faculty of Pharmacy, Department of Pharmaceutical Botany, Erzurum, Turkey, ecz-songul@hotmail.com

[3] Ataturk University, Faculty of Pharmacy, Department of Analytical Chemistry, Erzurum, Turkey, yilmazb@atauni.edu.tr

Introduction:

Nepeta transcaucasica Grossh. (Lamiaceae), named as 'kaf pisik otu' in Anatolia, belongs to *Nepeta* genus that is represented in Turkey by 33 species and 40 taxa, 19 of them are endemic. In previously studies showed that *N. transcaucasica* has antibacterial and anticandidal activities (1-3). The plant contains flavonoids with aglycons as cirsimaritin, xanthomicrol, salvigenin, gradenin-B, apigenin and genkwanin. Also, it has luteolin and apigenin 7-glucosides and 7-glucuronides, nepetin, hispidulin 7-glucosides and 7-glucuronides (4). Nepeta species can be divided into two groups, as nepetalactone-containing and nepetalactone-less species. In a study, nepetalactone (18.5 %) and 1,8-cineole (14.4 %) were detected as the main compounds of *N. transcaucasica* essential oil while in another study, they were as 4aa,7a,7ab-nepeta-lactone, 4aa,7a,7aa-nepetalactone, caryophyllene oxide, and 1,8-cineole/linalool in Turkey (2, 5). In Lithuania, the main compounds determined as citronellol (17.69 %), aα,7β,7aα-nepetolacton (14.34 %), geranial (9.05 %) and geranyl acetate (8.20 %) in essential oil (6).

Diabetes mellitus (DM) is an endocrine disease characterized by hyperglycemia. Approximately 85–95% of people with DM have type II DM, which is a chronic metabolic disease caused by the inability of the body to secrete sufficient insulin or the development of insulin resistance (7, 8). *α*-Glucosidase and *α*-amylase can hydrolyze carbohydrates; thus, inhibitors of these enzymes are considered useful drug candidates for type II DM therapy (9). Long-term use of synthetic enzyme inhibitors, such as acarbose, may cause various side effects, such as flatulence and abdominal problems (10). Natural *α*-glucosidase inhibitors have thus been presented as a beter alternative to control postprandial hyperglycemia as they exhibit minor or no side effects (11).

The aim of our study is characterizing essential oil obtained from aerial parts of the plant and evaluating for *α*-glucosidase inhibitory activity, as well as making anatomical examination of different parts of the plant.

Materials and Methods:

The aerial parts of *Nepeta transcaucasica* Grossh. (Lamiaceae) were collected in Palandöken, Erzurum City, Turkey on 13th of July 2020. The plant material was authenticated by Songül

KARAKAYA. A voucher specimen was deposited at the Biodiversity Application and Research Center, Ataturk University, Erzurum, Turkey.

The aerial parts were dried in a sun-free environment away from moisture by providing proper air circulation and powdered (100 g). Then, the essential oil obtained by hydrodistillation with Clevenger apparatus.

The GC/MS Analysis was performed by using Agilent 6890N Network GC System with Agilent 5977B Series Mass Selective Detector (MSD).

The *α*-glucosidase enzyme inhibitory effect of essential oil was determined according to method of Bachhawat (12).

Transverse and superficial sections were taken manually from plant parts in 70% alcohol and prepared with Sartur reagent for anatomical examinations by using light microscope (Zeiss 415500-1800-000) and photographed with a digital camera (Zeiss 51425).

Results:

Essential oil yield was 0.4 % (v/w). The major compounds of essential oils were found as *cis*-nepetalactone (92.5 %) and *trans*-nepetalactone (5.5 %). In addition, *β*-copaene (0.6 %), caryophyllene oxide (0.5 %), eucalyptol (cineol, 0.2 %), spathulenol (0.2 %), γ-elemene (0.2 %), *α*-bourbonene (0.2 %), and 3,4-dimethyl-3-cyclohexene-1-carbaldehyde (0.1 %) were the other compounds in the essential oil.

Essential oil exhibited *α*-glucosidase inhibitory activity with an IC_{50} value of 7966.88 µg/mL compared to the positive control, acarbose (IC_{50} = 4199.05 µg/mL).

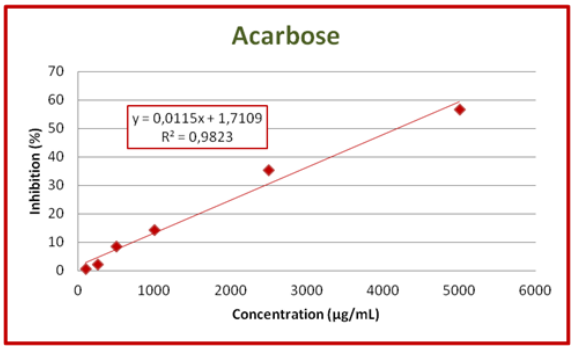

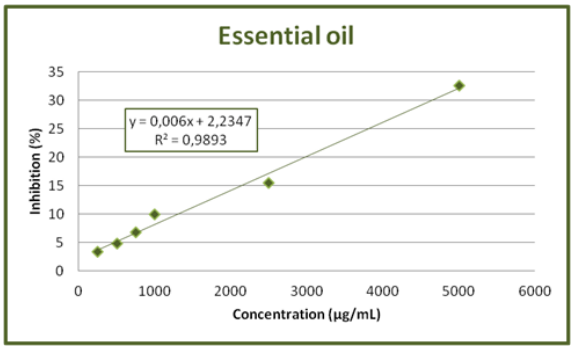

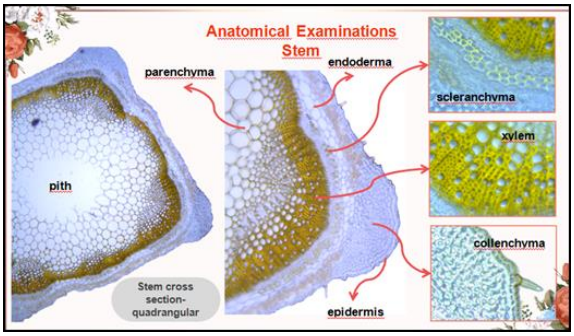

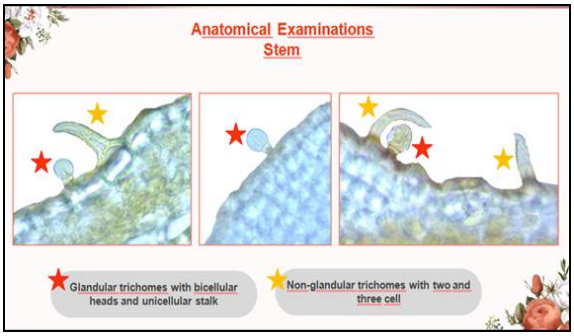

The stem cross section was quadrangular. There were glandular trichomes with bicellular heads and unicellular stalk on stem.

Stomatas were on the upper and lower surface of the leaf. There were glandular trichome with unicellular head, unicellular stalk and Lamiaceae type glandular trichomes on leaf. In addition, Lamiaceae type glandular trichomes were found on petals and sepals.

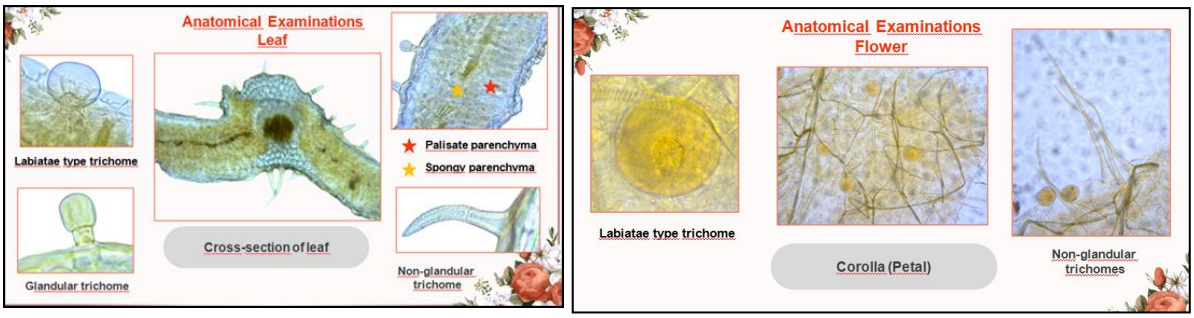

Conclusions:

Nepetalactones were determined as major compounds of essential oil of *Nepeta transcaucasica*. Essential oil was not found as a potent *α*-glucosidase inhibitor. Essential oil was found at different types of glandular trichomes of the plant. These data will contribute to the taxonomic classification of the plant.

References:

1. Güner A, Aslan S, Ekim T, Vural M, Babaç MT (2012). Turkey Plant List (Vascular Plants), Nezahat Gökyiğit Botanical Garden and Flora Research Association, Istanbul.
2. İşcan G, Köse YB, Demirci B, Başer KHC (2011). Chemistry & Biodiversity, 8(11):2144-2148.
3. Öztürk A (2009). Asian Journal of Chemistry, 21(8):6440-6444.
4. Tomas-Barberan FA, Gil MI, Ivancheva S, Tomas-Lorente F (1992). Biochemical Systematics and Ecology, 20(6):589-590.
5. Kilic Ö (2018). Journal of Essential Oil Bearing Plants, 21(6):1706-1711.
6. Baranauskienė R, Bendžiuvienė V, Ragažinskienė O (2019). Food and Chemical Toxicology, 129:269-280.
7. Cowie CC, Eberhardt MS (1996). Diabetes 1996: Vital Statistics, American, Diabetes Association, Virginia.
8. Maritim AC, Sanders RA, Watkins JB (2003). Journal of Biochemical and Molecular Toxicology, 17:24–38.
9. Broadhurst CL, Polansky MM, Anderson RA (2000). Journal of Agricultural and Food Chemistry, 48:849–852.
10. Fred-Jaiyesimi A, Kio A, Richard W (2009). Food Chemistry, 116:285–288.
11. Al-Azzawie HF, Alhamdani MS (2006). Life Sciences, 78:1371–1377.
12. Bachhawat JA, Shihabudeen MS, Thirumurugan K (2011). International Journal of Pharmacy and Pharmaceutical Sciences, 3:267-274.

OP163: IN VIVO ANTI-ANGIOGENIC AND ANTI-INFLAMMATORY POTENTIALS OF R(+) OR S(-) LIMONENE LOADED EUDRAGIT® RS 100 NANOPARTICLES

[1]Kıyan, H.T., [2]Öztürk, A.A.

[1] Anadolu University, Department of Pharmacognosy, Eskisehir, Turkey, htkiyan@anadolu.edu.tr

[2]Anadolu University, Department of Pharmaceutical Technology, Eskisehir, Turkey, aozturk@anadolu.edu.tr

Introduction:

R(+) and S(-) limonene are major compounds of *M. spicata* essential oil have been reported to be used in treatment due to their antimicrobial, anticancer, anti-angiogenic, anti-inflammatory and antioxidant effects and as well as in cosmetics and as sweetener in drinks (1). We aimed to design and characterize R(+) or S(-) limonene loaded nanoparticles (NPs) and investigate their *in vivo* anti-angiogenic and anti-inflammatory potentials.

Materials and Methods:

Preparation of nanoparticles

Eudragit RS 100-based NPs were prepared by following the nanoprecipitation technique with some modifications (2).

The in vivo anti-angiogenic and anti-inflammatory activity

The fertilized hen eggs and chemicals

The fertilized eggs were obtained from Has Tavuk Company (Bursa and Sivrihisar, Turkey). Agarose was purchased from Fluka (Spain) and Sodium dodecyl sulfate (SDS) was purchased from Fluka-Biochemika (Germany). (±)-Thalidomide was purchased from Sigma-Aldrich (Germany).

Preparation of test samples

Eudragit RS 100-based NPs (5 mg/mL), (±)-Thalidomide and SDS (5 mg/mL) for anti-angiogenic and Hydrocortisone (5 mg/mL) for anti-inflammatory activity were dissolved in a 2.5% (w/v) agarose solution. For ease of application pellets of these solutions (10 µL) were prepared and applied dropwise on circular stainless-steel supports of 5 mm diameter and cooled to room temperature for solidification and applied on to the chick chorioallantoic membrane (CAM).

The in vivo chick embryo chorioallantoic membrane (CAM) and Hen's Egg Test on the Chorioallantoic Membrane (HET- CAM) assay

The fertilized hen eggs were previously incubated for 72 h at 36.5°C and a relative humidity of 80%. The eggs were positioned in a horizontal position and rotated several times. Then the eggs were opened on the snub side. Before the opening 10-15 mL of albumin were aspirated from a hole on the pointed side. At two third of the height (from the pointed side) the eggs were

traced with a scalpel and after that the shells were removed with forceps. The cavity was covered with film and the eggs were incubated at 36,5°C at a relative humidity of 80% for further 72 h. If the formed CAM had approximately a diameter of 2 cm one pellet (1 pellet/egg) was placed on it. The eggs were incubated for one further day and then evaluated under the stereomicroscope. For every test compound 10-15 eggs were utilized. All samples were tested in triplicate in different times.

For the evaluation of the anti-angiogenic effect, a semi-quantitative score system was used as shown in Table 1. Scores were calculated using formula (1) for scoring. As controls (±)-Thalidomide and sodium dodecyl sulphate (SDS) at the concentration of 50 µg/pellet were also tested. As blank, CAMs treated with solidified agarose-solution in pellet form (2.5%, w/v) were also included. Each experiment was performed in triplicate (3).

The HET-CAM method was performed as described in the previous work of Öztürk and Kıyan, 2020 (4). Antiinflammatory effects were evaluated by using a scoring system (Table 2) and followed the conversion of the score index in the proportional inhibition of inflammation (Table 3). A characteristic strongly vascularized granuloma which was induced by SDS was observed on the CAM with star-like capillaries surrounding the pellet (Figure 1). If SDS was applied together with the antiinflammatory test compounds, normalization of the membrane irritation is observed (Figure 1).

Table 1. Semi-quantitative score system of anti-angiogenic effect on CAM after treatment

Scale	Anti-angiogenic Effect	Effects observed on CAM after treatment
< 0.5	Inactive	No change (Normal embryo growth).
0.5-0.75	Weak	No capillary free area. Area with reduced density of capillaries around the pellet not larger than its own area.
> 0.75-1	Strong	Small capillary free area or area with significantly reduced density of capillaries. Effects not larger than double the size of the pellet.
> 1	Very strong	Capillary free area around the pellet at least doubles the size of the pellet.

Formula used for scoring:

$$Average\ score = \frac{Number\ of\ eggs\ (score\ 2)\ x\ 2 + number\ of\ eggs\ (score\ 1)\ x\ 1}{Total\ number\ of\ eggs\ (score\ 0,\ 1,\ 2)}$$

Table 2. The Semi-quantative score system of antiinflammatory effect on CAM after treatment

Category	Type	Effects observed on CAM after treatment
1	Irritated	The granuloma is strongly vascularized. A network of capillaries is formed starlike around the granuloma.
2	Weakly irritated	The granuloma is poorly vascularized. A thin network of capillaries is formed starlike around the granuloma.
3	Weakly normalized	The granuloma is somewhat smaller than in category 1 and 2 and only poorly vascularized. The starlike network of vessels is hardly recognizable.
4	Normalized	No granuloma or only a kind of ‘‘scar’’ can be observed (if the granuloma regresses a non-vascularized scar is left). The network of vessels is normal (as the control).

Table 3. The score index in the proportional inhibition of inflammation

İnhibition (%)	Antiinflammatory Effect
≤ 40	No antiinflammatory effect
40-55	Uncertain antiinflammatory effect
55-70	Weak antiinflammatory effect
70-85	Good antiinflammatory effect
> 85	Strong antiinflammatory effect

Statistical analysis

All the statistical analyses were performed by using the Graphpad Prism 6.0 statistical software for Windows. The significance was calculated using one-way analysis of variance (ANOVA). Analysis of variance was used to demonstrate statistical significance between different doses with a Tukey’s multiple comparison post-test. All results were expressed as mean ±SD. Levels of $P<0.05$ were considered statistically significant.

Results:

According to the results, NPs at the concentration of 50 µg/pellet including R(+) limonene and S(-) limonene as 4 µg/pellet showed strong *in vivo* anti-angiogenic potentials with anti-angiogenic scores of 0.93 ± 0.1 and 0.74 ± 0.05 and no membrane irritation and embryotoxicity compared with (±)-Thalidomide (0.8 ± 0.05) (Figure 1).

R(+) and S(-) limonene NPs also exhibited strong *in vivo* anti-inflammatory activities with 75.00 ± 12.50% and 80.00 ± 11.18% inhibition values compared with Hydrocortisone (81.25 ± 8.84%) (Figure 1).

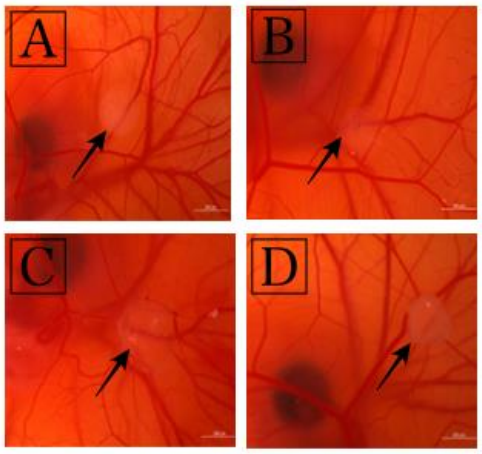

Figure 1. *In vivo* anti-angiogenic and anti-inflammatory effects of R(+) and S(-) limonene NPs. **A:** strong anti-angiogenic effect of R(+) limonene NP, **B:** strong anti-angiogenic effect of S(-) limonene NP, **C**: strong anti-inflammatory effect of R(+) limonene NP, **D:** strong anti-inflammatory effect of S(-) limonene NP.

Conclusions:

Plant derived natural angiogenesis inhibitors including plant extracts, essential oils and their volatile compounds used to treat cancer and inflammatory diseases, are seen promising as good alternatives to synthetic ones due to their low side effect profiles and different mechanisms of effect.

Acknowledgements

This study was financed by Anadolu University Scientific Research Project Foundation (No: 1905S054.).

References:

1. Erasto P and Viljoen AM (2008). Natural Product Communications, 3 (7):1193-1202.
2. Öztürk AA et al. (2020) Drug Development and Indusrial Pharmcy, 46 (4): 682-695
3. Kıyan HT et al. (2014). Pharmaceutical Biology, 52(1):44-50.
4. Öztürk AA and Kıyan HT (2020). Microvascular Research, 128:103961.

OP164: SEARCH OF POTENTIAL MARINE NATURAL PRODUCTS AGAINST COVID-19

[1]Uras, IS., [2,3]Ebada, SS., [4,5]Konuklugil, B.

[1] Agri Ibrahim Cecen University, Department of Pharmacognosy, Agri, Turkey, ibrahimseydauras@hotmail.com
[2] Ain-Shams University, Department of Pharmacognosy, Cairo, Egypt, sherif_elsayed@pharma.asu.edu.eg
[3] Mu'tah University, Department of Pharmaceutical Chemistry, Al-Karak, Jordan, ss_ebada@mutah.edu.jo
[4] Ankara University, Department of Pharmacognosy, Ankara, Turkey, belma.konuklugil@gmail.com
[5] Lokman Hekim University, Department of Pharmacognosy, Ankara, Turkey

Introduction:

The development of vaccines has come to a certain point to end the new coronavirus (SARS-CoV-2) pandemic that has affected humanity for more than a one and a half. Scientists continue to research in order to develop an effective drug against the virus that has killed more than 3 million people (1). The aim of this study is present our findings and bring together the result of other studies on marine secondary metabolites from the studies carried out to end COVID-19 epidemic and to draw attention to the importance of studies on marine natural products for drug research.

Materials and Methods:

The fungus *Aspergillus terreus* was separated from the annelide *Spirorbis* sp., which was collected from Marmara Sea, Istanbul, Turkey in July, 2018. For identification, this fungus was cultured on Sabouraud 4% dextrose agar (SDA, Merck, Germany) at room temperature for a week in an incubator (Nüve, Turkey). The fungus was identified as *Aspergillus terreus* (GenBank accession number MT273950) based on DNA amplification and ITS (internal transcribed spacer) sequencing data analysis, as reported previously in the literature.

The fungal strain was cultivated on a 100 mL solid rice medium prepared by autoclaving (100 g of rice and 100 mL of distilled water containing 3.5% artificial sea salt in a 60-piece 2000 mL Erlenmeyer flask). Fermentation continued for 30 days at room temperature away from light under static conditions. To discontinue the fermentation process, ethyl acetate (EtOAc) (3 x 350 mL) was added to each flask to stop the growth of cells. After adding EtOAc, flasks were shaken for 12 h, then filtered, and EtOAC filtrate was pooled and evaporated under reduced pressure until yielding a solid residue. The crude extract was then partitioned between n-hexane and 90% aqueous MeOH by liquid–liquid fractionation, where both fractions were collected and dried up under vacuum. The aqueous 90% MeOH phase was subjected to vacuum liquid chromatography to yield subfractions.

Docking study was done using the procedure we reported and validated earlier. Tested compounds were downloaded from Pubchem (www.pubchem.ncbi.nlm.nih.gov), accessed on 10 May 2021) or built from the 2D structures. Ligands and proteins were prepared as reported earlier (2). Docking analysis and image preparation were done using PyMol. The proposed binding mode of the isolated compounds with neutrophil elastase (NE) and SARS-CoV-2 main protease (Mpro) was studied using Autodock Vina and a method similar to what we reported

earlier (3). Here, crystal structures of NE (PDB ID:1H1B) and SARS-CoV-2 Mpro (PDB ID: 6LU7) were used. Prepared and co-crystalized ligands were docked in a grid box in the active site (25 x 25 x 25 $Å^3$), centered on cocrystalized ligand) using exhaustiveness of 16. For each ligand, the top nine binding poses were ranked according to their binding affinities and the predicted binding interactions were analyzed. The pose with the best binding affinity and binding mode similar to co-crystalized ligand was reported.

The protective effects of the samples against human coronavirus 229E (HCoV-229) were determined similarly to the described method (4). Huh7 cells (human liver carcinoma cell line) were infected with 9TCID50 (median tissue culture infectious dose) of each coronavirus 229E in the presence or absence of the compounds or vehicle. After incubation at 33^OC for 6 days, the surviving cells were then stained with MTT (3-[4.5-dimethylthiazol-2-yl]-2,5-diphenyl tetrazolium bromide). The percentage of surviving cells was then calculated.

Results:

Thousands of compounds were subjected to preliminary evaluations in studies and hundreds of compounds with drug-like properties were studied. As a result, it has been found that some marine natural products have a potent inhibitory effect by binding to COVID-19 M^{Pro} (Main Protease) (5). In this study four compounds isolated from marine derived *Aspergillus terreus* fungi were assessed for their in silico COVID-19 main protease (Mpro) inhibitory activities. Among the tested compounds only butyrolactone I revealed significant activity that makes butyrolactone I a potential lead entity for developing new remedy to treat and/or control the currently devastating COVID-19 pandemic.

It has also been shown from other studies that sulfated polysaccharides from marine organisms inhibit different stages of the viral infection process within the host cell and Plitidepsin is a peptide found in *Aplidium albicans* tunicate, which is currently used in cancer treatment, has also been found effective against COVID-19 and phase 3 clinical studies have been initiated recently (6).

Conclusions:

Two butenolides, butyrolactons I and III, along with one meroterpenoid, terretonin and a prenylated hydroxybenzaldehyde derivative were isolated from a marine-derived fungus *Aspergillus terreus*. Molecular docking studies exhibited a possible potential role of butyrolactone I for inhibiting SARS-CoV-2 main protease, an essential enzyme for producing the viral functional proteins. These results shed more light on butyrolactone I and other butenolide derivatives as potential candidates for developing lead compounds that may pave the way for producing new pharmaceuticals against SARS-CoV-2 and/or its pathological effects, in particular, ARDS, granting additional time for the immune system to fight for the patient's life. The marine habitats are excellent homes to countless organisms and microorganisms and thousands of bioactive marine natural products have been isolated from these sources until now. The results revealed in the compiled studies show that marine natural products have a very important place in efforts to develop new drugs against the COVID-19 virus. Despite the reported antiviral activity of isolated marine metabolites, structural modifications showed the importance in targeting and efficacy.

Acknowledgements

S.S.E. acknowledges The Scientific and Technological Research Council of Turkey (TÜBITAK) for a financially supported visiting scientist fellowship. Authors declare that there is no conflict of interest in this study.

References:

1. WHO COVID-19 Dashboard. Geneva: World Health Organization, 2020. Available online: https://covid19.who.int/ (last cited: [02.05.2021]).

2. Ebada et al., (2020). In vivo antiulcer activity, phytochemical exploration, and molecular modelling of the polyphenolic-rich fraction of Crepis sancta extract. Inflammopharmacology, 28, 321-331.

3. Ebada et al., (2020). Anti-inflammatory, antiallergic and COVID-19 protease inhibitory activities of phytochemicals from the Jordanian hawksbeard: Identification, structure-activity relationships, molecular modeling and impact on its folk medicinal uses. RSC Adv, 10, 32128-38141.

4. Hsieh et al., (2020). Rosmarinic acid exhibits broad anti-enterovirus A71 activity by inhibiting the interaction between the five-fold axis of capsid VP1 and cognate sulfated receptors, Emerging Microbes & Infections, 9:1, 1194-1205

5. Taglialatela-Scafati O (2021). New Hopes for Drugs against COVID-19 Come from the Sea. Marine Drugs, 19(2), 104-105.

6. Trial to Determine the Efficacy/Safety of Plitidepsin vs Control in Patients With Moderate COVID-19 Infection (Neptuno) Available online: https://clinicaltrials.gov/ct2/show/record/NCT04784559 (last cited: [02.05.2021]).

OP165: THREE NEW ANTIMICROBIAL NATURAL COMPOUNDS FROM *SCORZONERA AUCHERIANA*

[1]Erik, İ, [1]Yayli, N., [2]Coşkunçelebi, K., [3]Karaoğlu, ŞA

[1] Karadeniz Technical University, Department of Pharmacognosy, Trabzon, Turkey, ishakerik@ktu.edu.tr
[2] Karadeniz Technical University, Department of Biology, Trabzon, Turkey, kamil@ktu.edu.tr
[3] Recep Tayyip Erdogan University, Department of Biology, Rize, Turkey, sengul.karaoglu@erdogan.edu.tr

Introduction:

Scorzonera aucheriana (Asteraceae/Compositae), a perennial herb, belongs to the genus *Scorzonera* which consists of over 52 species, and 32 of these are endemic to Turkey. Scorzonera L. species are consumed as a vegetable and the use of complementary medicine in the world and Turkey (1,2). Biological activity investigations have highlighted on the anti-inflammatory, diuretic, antimicrobial, antioxidant, analgesic, wound healing, anti-tumor activities, mucolytic, and stomachic (3-5). In the literature, flavonoids, phenolic acid derivatives, dihydroisocoumarins, lignans, neolignans, bibenzyl derivatives, benzyl phthalates, triterpenes, and sesquiterpenes were obtained in phytochemical studies from Scorzonera (1,3). As a result of ongoing investigations, we report the isolation and structure elucidation of three new natural compounds from the water extract of *S. aucheriana* species which is endemic to Turkey.

Materials and Methods:

S. aucheriana was collected in July 2018 from Sivas Province, Zara District, Yarağıl region in Turkey. The plant was identified by Prof. Kamil Çoşkunçelebi by using Flora of Turkey (2) and taxonomical conspectus of Turkish Scorzonera (1). Voucher (Makbul 244 & Coşkunçelebi) was deposited in the Herbarium of Biology (KTUB) at Karadeniz Technical University, Turkey. Optical rotations were measured on an Automatic AA-5 Series polarimetry. UV spectra were obtained with a Spectrostar nano BMG labtech spectrometer. Infrared spectra were obtained with a PerkinElmer 1600 FT-IR (ATR) (4000-400 cm^{-1}) spectrometer. The mass spectral analyses were carried out on a Agilent 6230A LC-Q-TOF-Q-MS. Shimadzu QP2010 ultra GC-FID/MS was used to identify the FAMEs. Melting points were determined using Thermo-var apparatus fitted with a microscope and are uncorrected. ^{1}H and ^{13}C NMR, along with 2D NMR spectra were obtained on a Bruker 400 MHz NMR spectrometer (400 MHz for ^{1}H, 100 MHz for ^{13}C), using TMS as an internal standard. CD_3OD and $CDCl_3$ were used as NMR solvent. ACD NMR program was used for the elucidation of isolated compounds. Chemical shifts were expressed in δ (ppm) and coupling constants (*J*) were reported in hertz (Hz). CC was carried out on silica gel (Kieselgel 60, 320-400 mesh), RP18 silica gel and PTLC (Silica gel HF_{254}, 20x20 cm, 0.5mm,). TLCs were carried on silica gel (Kieselgel 60 F_{254}, Merck) plates and the spots were visualized by UV lamp or spraying with 20% H_2SO_4 and heating. The method's extraction were made according to our previous study (3). Chromatographic purification on the water fraction yielded compounds **1** (23.9 mg), **2** (12.3 mg), and **3** (14.4 mg). All test microorganisms were obtained from the Hifzissihha Institute of Refik Saydam (Ankara, Turkey) and were as follows: *Escherichia coli* ATCC35218, *Yersinia pseudotuberculosis* ATCC911, *Pseudomonas aeruginosa* ATCC43288, *Enterococcus faecalis* ATCC29212, *Staphylococcus aureus* ATCC25923, *Lisssteria monositogenes NCTS11994, Bacillus cereus* 709 Roma, *Mycobacterium smegmatis* ATCC607, *Candida albicans* ATCC60193, and *Saccharomyces*

cerevisiae RSKK 251. The antimicrobial screening test using agar-well diffusion method as adapted was used earlier (6,7). Each microorganism was suspended in Brain Heart Infusion (BHI) (Difco, Detroit, MI) broth and diluted approximately 106 colony forming unit (cfu) per ml. They were “flood-inoculated” onto the surface of BHI agar and Sabouraud Dextrose Agar (SDA) (Difco, Detriot, MI) and then dried. For *C. albicans* SDA was used. Five-millimeter diameter wells were cut from the agar using a sterile cork-borer, and 50 µL of the extract substances were delivered into the wells. The plates were incubated for 18 h at 35°C. Antimicrobial activity was evaluated by measuring the zone of inhibition against the test organism. The antimicrobial properties of compounds **1**-**3** were investigated quantitatively in respective broth media by using double microdilution and the minimal inhibition concentration (MIC) values (µg/mL) were examined (6,7). The antibacterial and antifungal assays were carried out in Mueller-Hinton broth (MH) (Difco, Detroit, MI) at pH. 7.3 and buffered Yeast Nitrogen Base (Difco, Detroit, MI) at pH 7.0, respectively. The micro dilution test plates were incubated for 18 h at 35°C. Brain Heart Infusion broth (BHI) (Difco, Detriot, MI) was used for *M. smegmatis*, and incubated for 48-72 h at 35°C. The MIC was defined as the lowest concentration that showed no growth. Ampicillin (10 mg/mL), streptomycin 10 mg/mL and fluconazole (2 mg/mL) were used as standard antibacterial and antifungal drugs, respectively. The 1/10 dilution of each solvent was used as a control.

Results:

Chromatographic separation of water fraction of a crude methanol extract obtained from aerial parts of the *S. aucheriana* yielded three new compounds, scorzoaucherin A (**1**), scorzoaucherioside III (**2**), scorzoaucherioside IV (**3**). The structures of the isolated compounds (figure) were elucidated on the basis of NMR (^{1}H, ^{13}C, COSY, HMBC, HSQC, and TOCSY), UV, FT-IR, and LC-QTOF-MS spectrometric data. The antimicrobial properties of all isolates were investigated against ten microorganisms. Compound **1**, **2**, and **3** showed selective anti-tuberculosis activity in the concentration range of 30.9-47.5 µg/mL, respectively.

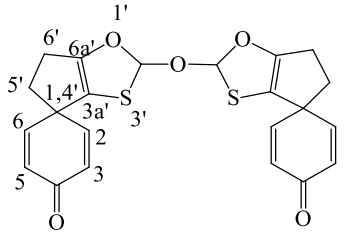

1

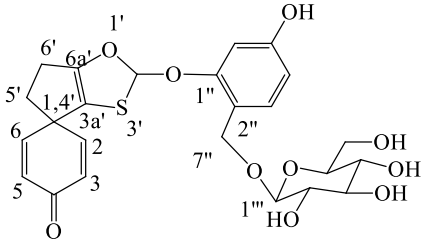

2

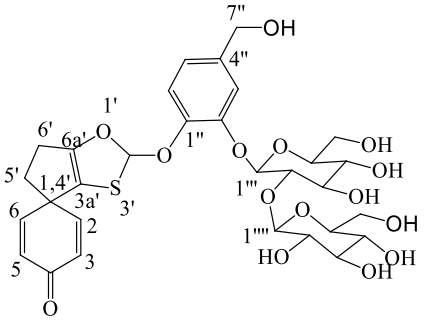

3

Figure. Chemical structure of isolated new compounds from *S. aucheriana.*

Conclusions:

Water fraction of a crude methanol extract of the *S. aucheriana* gave cannabispiradienone type natural compounds (scorzoaucherin A (**1**), scorzoaucherioside III (**2**), scorzoaucherioside IV (**3**)). All compounds were isolated and identified for the first time from this species. The antimicrobial properties of all isolates were investigated against ten microorganisms. Compounds **1**-**3** showed selective anti-tuberculosis activity within the range of 30.9-47.5 µg/ml (MIC), respectively.

Acknowledgements

The authors are thankful to Karadeniz Technical University for the financial support (KTÜ-BAP 8133).

References:

1. Coşkunçelebi K, Makbul S, Gültepe M, Okur S, Güzel ME (2015). A conspectus of *Scorzonera* L. in Turkey. Turkish Journal of Botany, 39:76-87.
2. Chamberlain DF. Scorzonera L. In: Davis PH (editors). Flora of Turkey and East Aegean Island. Edinburg, UK: Edinburg University Press, 1975, 632-657.
3. Erik I, Yaylı N, Coskunçelebi K, Makbul S, Karaoglu SA. (2021). Three new dihydroisocoumarin glycosides with antimicrobial activities from *S. aucheriana*. Phytochemistry Letters, 43:45-52.
4. Zidorn C, Ellmerer-Müller E, Stuppner H (2000). Sesquiterpenoids from Scorzonera hispanica L. Die Pharmazie, 55: 550.
5. Zidorn C, Ellmerer-Müller EP, Stuppner H (2000). Tyrolobibenzyls–novel secondary metabolites from Scorzonera humilis. Helvetica Chimica Acta, 83: 2920-2925.
6. Barry AL (1999). Standards NCfCL. Methods for determining bactericidal activity of antimicrobial agents: approved guideline. National Committee for Clinical Laboratory Standards Wayne, PA.
7. Woods GL (2011). Susceptibility testing of mycobacteria, nocardiae, and other aerobic actinomycetes. Approved Standard M24-A2 2011.

OP173: DETERMINATION OF CAFFEINE CONTENT IN WORLD COFFEES BY NEW VALIDATED HPLC METHOD AND INVESTIGATION OF THE RELATIONSHIP BETWEEN CAFFEINE CONTENT AND LIPASE INHIBITION

[1]Sener, S.O., [1]Ozgen, U.

[1] Karadeniz Technical University, Department of Pharmacognosy, Trabzon, Turkey, silashener@ktu.edu.tr, uozgen@ktu.edu.tr

Introduction:

1.9 billion people worldwide are overweight, and 650 million of them are obese (1). Obesity is accounted for between 2% and 8% of costs of total health-care in many countries (2). Obesity is evaluated as a serious risk for global health problems and economic burden (3). The combat obesity can be done through surgery, pharmacotherapy or lifestyle modification. Nowadays, natural products have been becomes popular because of their bioactive components potentially useful in pharmacotherapy of obesity. Natural products have anti-obesity effects based on their different mechanisms; such as lipase inhibitory effect, suppressive effect on food intake, stimulatory effects on energy expenditure, inhibitory effect on adipocyte differentiation, regulatory effect on lipid metabolism, anti-inflammatory effect (4,5). Pancreatic lipase plays a key role for the fat metabolism of human . It converts tyrigliserides into glycerol and fatty acids. Pancreatic lipas inhibitors control the fat metabolism to achieve decrasing effect of lipid levels (6). Coffee has proven to reduce risk for obesity based on caffein content (7). The range of caffeine contents reported for *C. arabica* L. growing different ranges vary in the literature between 7-17 mg/g dry material (8). The aim of the study is to determine caffeine content in world coffees by new HPLC technique and to uncover relationship between lipase inhibition and caffeine content.

Materials and Methods:

Coffees grown five different regions in the world were used as samples. Coffee samples were extracted with deionized water for a day by using incubator with shaker. After one day extraction, to obtain a completely dry extract, the extracts were evaporated using a rotary evaporator. Quantitative analysis was performed by new validated HPLC method using C18 column (ZORBAX Eclipse Plus, 4.6 × 150 mm, 5 µm) and gradient program with a two solvents system A: 100% methanol; B:2.5% acetic acid in deionized water at a constant solvent flow rate of 1.2 mL/min and UV 273 nm as the detector. Lipase inhibition effects of the world coffees were evaluated using spectroscopic method.

Results:

The method indicated good linearity (R^2 >0.999) over the assayed concentration range (10-100 µg/mL) (Figure 1). Relative standard deviation (RSD) values for intra-day and inter-day precision were detected as 0.14%, and 0.36%, respectively. Accuracy for quality controls was varied from 98.8% to 100.1% (RSD<0.88%) (Table 1). Quantitative analysis of caffeine in coffee samples was performed based on the peak areas of chromatograms of coffee samples using the calibration curve (Figure 1) .

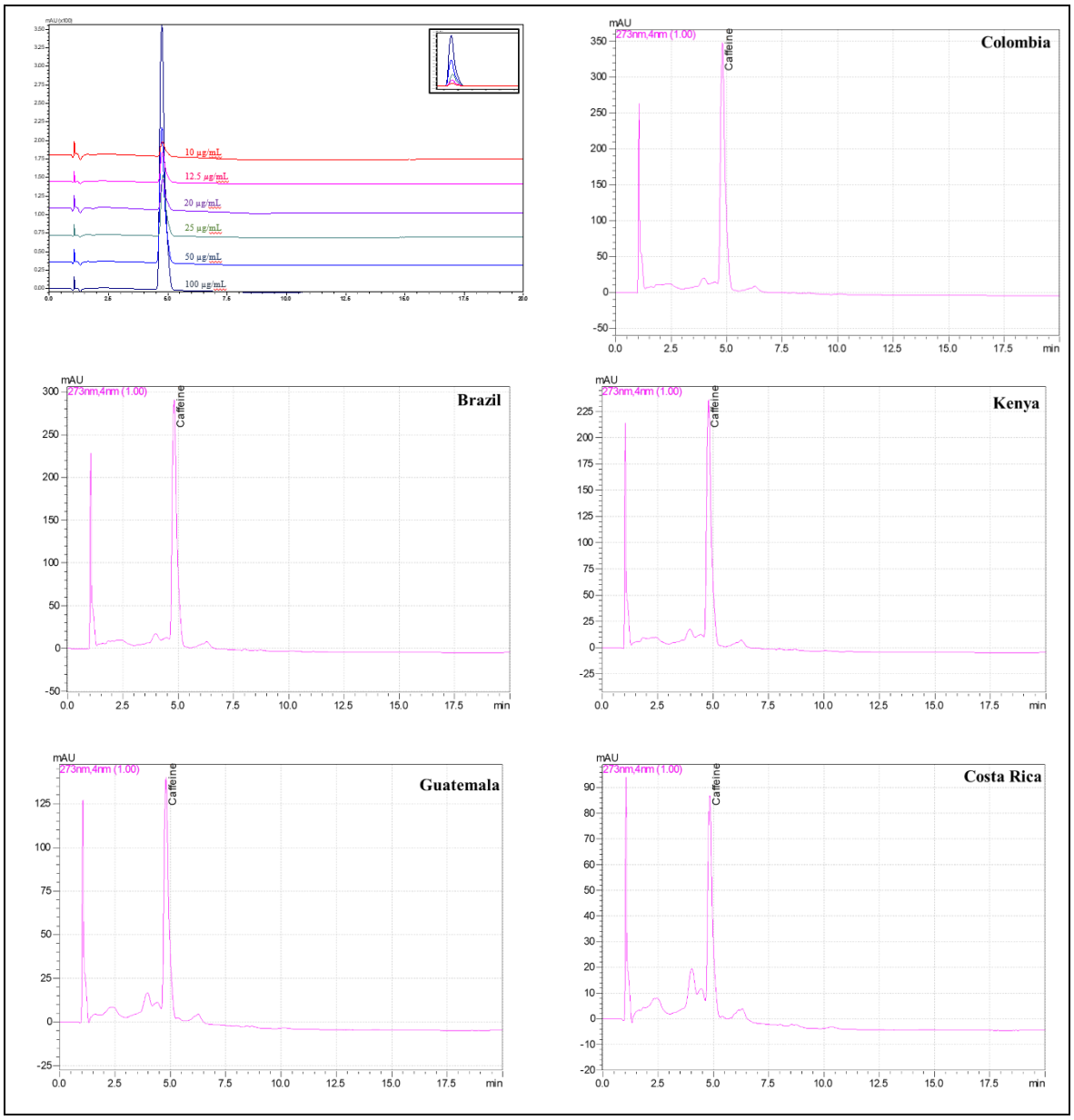

Figure 1. HPLC chomatograms for six different concentrations of caffeine and coffee samples

Table 1. Validation parameters of new HPLC method

Caffeine	**Retention Time (min.)**	**Regression coefficient (R^2)**	**LOD (µg/mL)**	**LOQ (µg/mL)**
	4.77	0.9997	1.8879	5.7211
	Retention Time (% RSD)		**Peak Area (% RSD)**	
	Intra-day	Inter-day	Intra-day	Inter-day
	0.14	0.36	0.42	0.48
	% Recovery (Mean ± SD)			
	10 µg/mL	**25 µg/mL**	**100 µg/mL**	
	98.8 ± 0,0577	99.40 ± 0,8888	100.1 ± 0,2645	

It was revealed that all samples have caffeine content and lipase inhibition for detection ranges while colombian coffee possesses the highest caffeine (86.44 mg/g) content and lipase inhibition (IC_{50}= 54.84 ± 0.9256) (Figure 2).

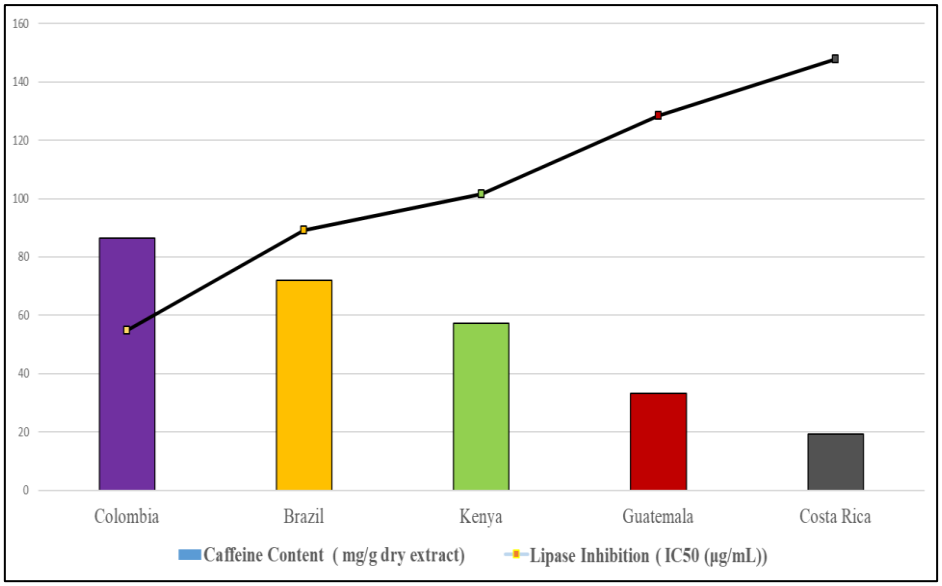

Figure 2. Comparative graph of the caffeine content and lipase inhibition of coffee samples

Conclusions:

All the parameters of new HPLC method were acceptable according to current recommendations for method validation. It has been proven to be positive correlation between the caffeine content and lipase inhibition. Colombian coffee is the most remarkable sample but all coffees have therapeutic potential for global health problem obesity.

References:

1. World Health Organization. Obesity and Overweight Fact Sheet (2016).
2. Ataey A, Jafarvand E, Adham D, Moradi-Asl E (2020). Journal of Preventive Medicine and Public Health, 53: 98-105.
3. Blüher M (2019). Nature Reviews Endocrinology, 15: 288-298.
4. López Ja, Remesar X, Foz M, Alemany M (2002). Drugs, 62: 915-944
5. Yun, JW (2010). Phytochemistry, 71: 1625-1641.
6. Liu TT, Liu XT, Chen QX, Shi Y (2020). Biomedicine & Pharmacotherapy, 128: 110314.
7. Martins, IJ (2017). Annals of Obesity & Disorders, 2: 1018-1020.
8. Paula J, Farah A (2019). Beverages, 5: 1-50.

OP174: ENZYME INHIBITORY AND PHYTOCHEMICAL STUDIES ON Pistacia terebinthus COLLECTED FROM DIFFERENT LOCATIONS

[1]Pekacar, S., [1]Deliorman Orhan, D.

[1]Gazi University, Department of Pharmacognosy, Ankara, Turkey

Introduction:

Pistacia terebinthus L., known as Menengiç, is a species belonging to the Anacardiaceae family that grows in Turkey. Numerous ethnobotanical uses of different *Pistacia* species have been reported in the literature (1). There are various ethnobotanical and traditional use based studies on *P. terebinthus*, including antidiabetic activity (2). In this study, *in vitro* antidiabetic (*α*-glucosidase and *α*-amylase enzyme inhibition) and antiobesity (pancreatic lipase enzyme inhibition) potentials of *P. terebintus* leaves collected from different locations were investigated in addition to the inhibition of pancreatic cholesterol esterase enzyme. The phytochemical contents of the extracts tested were examined by HPLC techniques.

Materials and Methods:

P. terebinthus samples were collected from different locations in 2019. The inhibitory effects of *α*-amylase and *α*-glucosidase, pancreatic lipase and pancreatic cholesterol esterase of extracts with 80% ethanol from leaf parts of the plant were evaluated. In experiments in which enzyme inhibition was evaluated *in vitro*, acarbose was the reference substance in *α*-amylase and *α*-glucosidase enzyme inhibition, orlistat was used in pancreatic lipase inhibition, and simvastatin was used as reference substance in pancreatic cholesterol esterase enzyme inhibition experiment. (3, 4). General chromatograms were obtained to elucidate the phytochemical content of the extracts. A more detailed phytochemical analysis was performed on naturally grown *P. terebinthus* leaves collected from Kilis province. In addition to the qualitative analysis of phenolic acid and flavonoids on leaves collected from Kilis performed by HPLC method, quantitative analysis of protocatechuic acid was conducted. In the HPLC analysis, a method using acetonitrile and water was preferred in the mobile phase system with gradient flow. In the analysis performed on the SPTK coded extract, analysis was performed at different wavelengths. The phenolic acid mixture used for qualitative analysis contains reference substances such as gallic acid, protocatechuic acid, chlorogenic acid, vanillic acid, syringic acid, p-coumaric acid, ferulic acid, sinapic acid, transcinnamic acid, rosmarinic acid, epicatechin, catechin. In the mixture with flavanoids, reference substances such as umbelliferone, rutin, naringenin, hesperidin, quercetin-3-O-glucoside, apigenin-7-O-glucoside, myrcetin, quercetin, luteolin, apigenin were present (5).

Results:

As a result, *in vitro* enzyme inhibitor activity experiments were performed on *P. terebinthus* extract collected from different locations. It was concluded that *α*-amylase and *α*-glucosidase inhibitory activities of all extracts were quite high when compared to the reference compound acarbose. All extracts showed excellent and dose dependent inhibitory effect on *α*-glucosidase enzyme. The highest α-amylase inhibitory activity at a dose of 2 mg/ml was found in leaves collected from Kilis (98.31±0.28%), and this inhibition was found at almost the same levels as the reference substance acarbose. The best pancreatic cholesterol esterase (38.82±1.20%)

and pancreatic lipase (59.06±2.09%) inhibitory activity were found in the SPTS coded extract at a dose of 2 mg/ml. When the yields of the extracts were evaluated, the highest yield was obtained from *P. terebinthus* collected from Siirt with a rate of 22.59%. According to the results of HPLC analysis, The SPTK coded extract was standardized over the protocatechuic acid using the HPLC method. Kilis *P. terebinthus* leaf ethanol extract was determined to have a content of 0.060±0.002 protocatecuic acid g/100 g.

Table 1. Table of extract codes, gathering places of plants

Extract Code	Collection sites
SPTK	Kilis
SPTS	Siirt

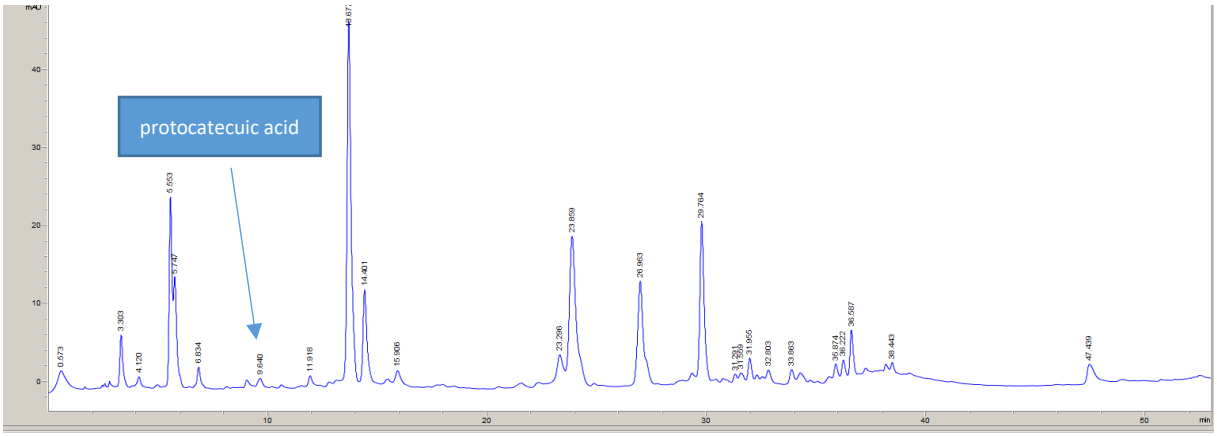

Figure 1. HPLC chromatogram of SPTK extract at 280 nm

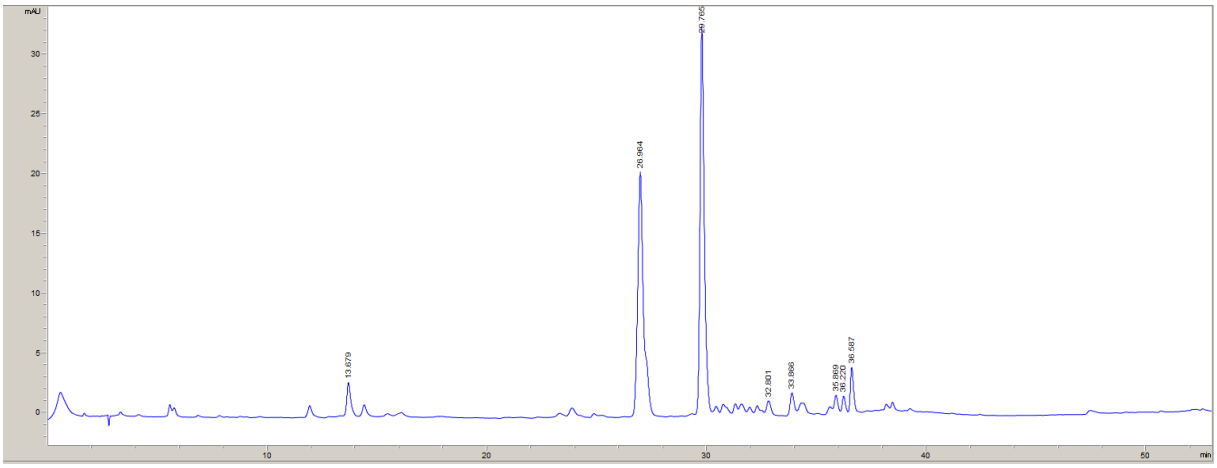

Figure 2. HPLC chromatogram of SPTK extract at 320 nm

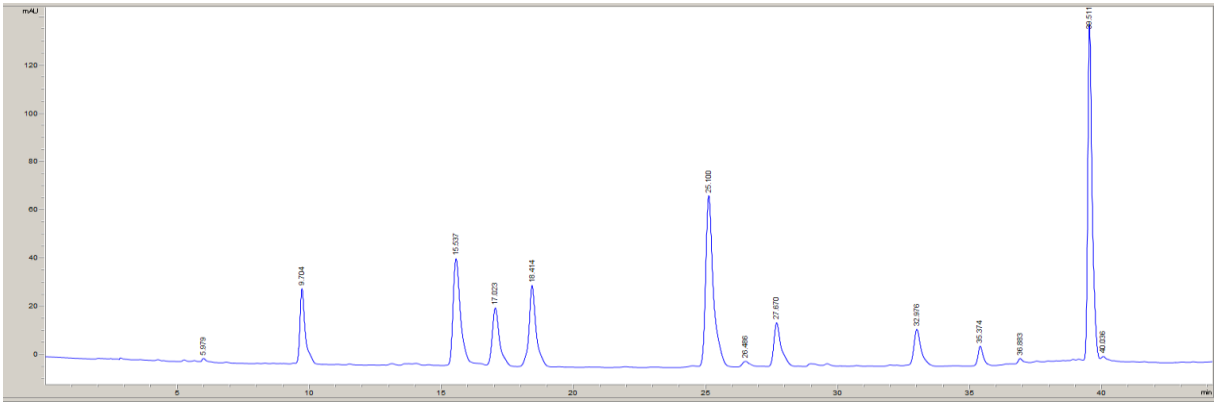

Figure 3. HPLC chromatogram of standard phenolic compounds at 280 nm

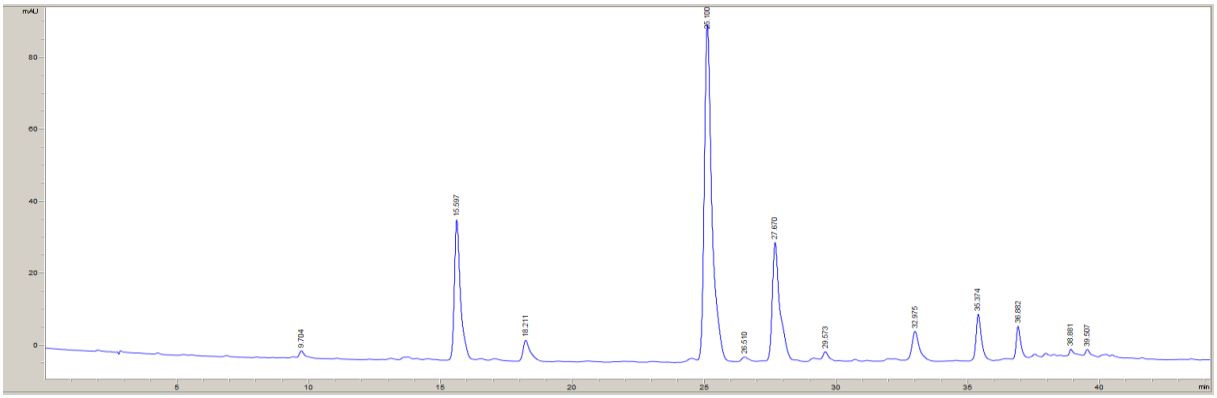

Figure 4. HPLC chromatogram of standard phenolic compounds at 320 nm

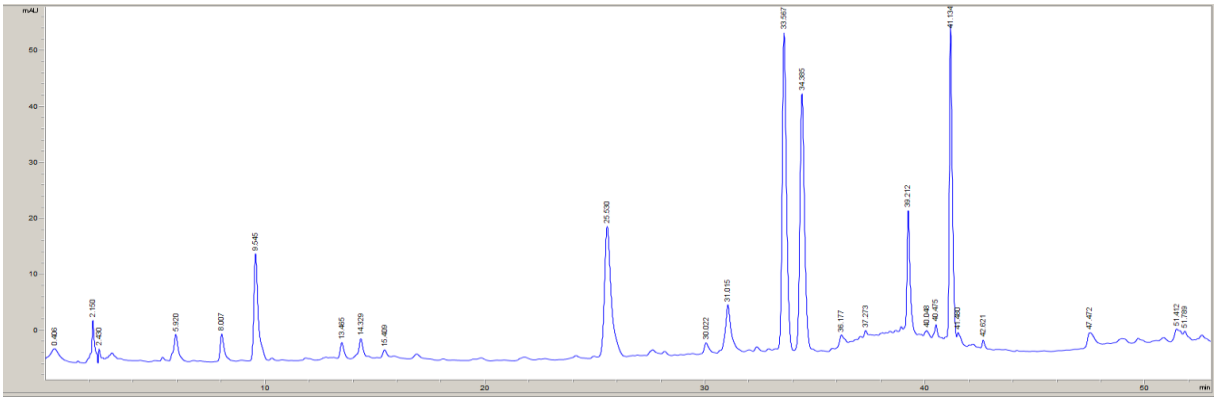

Figure 5. HPLC chromatogram of standard flavonoid compounds at 280 nm

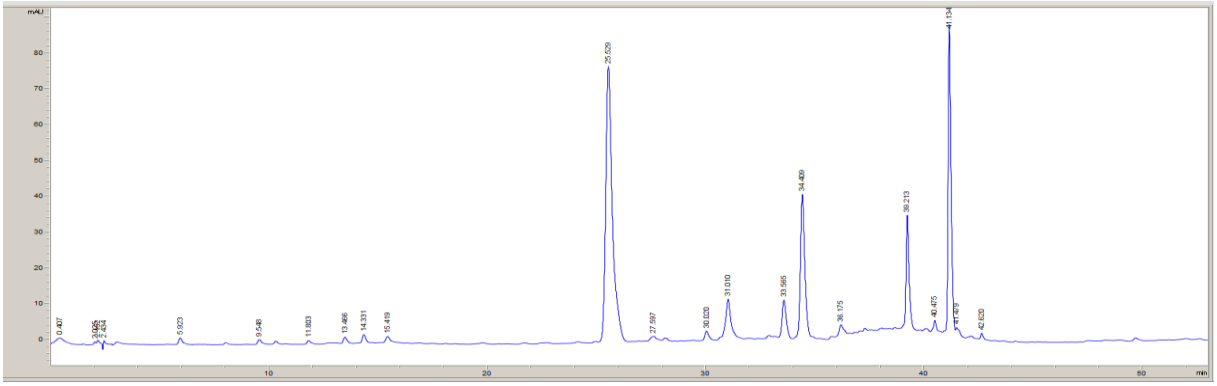

Figure 6. HPLC chromatogram of standard flavonoid compounds at 320nm

Conclusions:

The findings from the experiments revealed the potent antihyperglycemic and potential antiobesity activity of *P. terebinthus* leaves. In the light of literature data, it can be thought that the protocatechuic acid compound determined by HPLC method may be responsible for the antidiabetic activity. Within the scope of these results, Antihyperglycemic and antiobesity activity guided isolation studies should be carried on *P. terebintus* leaves. The aim of further study is to determine the effective compounds by isolation studies.

Acknowledgements

This study was supported by a grant of Gazi University-BAP (02/2019-32). Thanks to TUBITAK 2211/A National PhD Scholarship Program.

References:

1. Rauf, A., Patel, S. et al., (2017). Biomedicine&Pharmacotherapy, 86:393-404.
2. Bozorgi, M., Memariani, Z. et al., (2013). The Scientific World Journal, 2013:1-33.
3. Gökbulut, A., Orhan, N. et al., (2017). South African Journal of Botany, 108:387-392.
4. Ngamukote, S., Mäkynen, K. et al., (2011). Molecules, 16:5054-5061.
5. Gök, H. N., Deliorman Orhan, D. et al., (2020). Journal of Food Science, 85:3220-3228.

OP181: THE COMBINATORY ANTIFUNGAL ACTIVITY OF CURCUMIN AND QUERCETIN ON *CANDIDA SPP*.

[1,2]Simsek, D., [1]Altanlar, N.

[1] Ankara University, Department of Pharmaceutical Microbiology, Ankara, Turkey

[2] Turkish Medicines and Medical Devices Agency, Ankara, Turkey,

dsimsek@ankara.edu.tr, naltanlar@ankara.edu.tr

Introduction:

Candida species are an important group of opportunistic pathogenic fungi. *Candida albicans* is the most common species in the clinic, nearly 10 species are among the opportunistic agents of mycosis. A wide variety of treatment options include antifungal creams, ointments, instillation solutions or systemic treatment options (1). But the number of agents used is limited. Nowadays, treatment options including natural active ingredients are reconsidered for fungal pathogens as well as for all microbial infectious agents (2). Curcumin is the active compound of *Curcuma longa* and quercetin is a phenolic compound found in many plants in nature (3). For both compound, the most outstanding biological activities among the many detected to date are anti-inflammatory activity, antimicrobial activity, antioxidant activity, anti-tumor activity and hepatoprotective activity (4). In this study, we aimed to determine the combinatory antifungal activity of curcumin and quercetin on selected *Candida spp*.

Materials and Methods:

Antifungal activity experiments of curcumin and quercetin were carried against standard strains *Candida albicans* ATCC 10231, *Candida albicans* ATCC 90028, and *Candida parapsilosis* ATCC 22019 supplied from the culture collection of Ankara University, Faculty of Pharmacy, Department of Pharmaceutical Microbiology. Firstly, stocks in -80 °C were suspended in Sabouraud Dextrose Broth (SDB) medium and incubated in 35 ± 2 °C. Then, overnight cultures passaged to Sabouraud Dextrose Agar (SDA) medium. Colonies from these passages were used in experiments. Minimum Inhibition Concentration (MIC) tests were evaluated by micro broth dilution test according to current EUCAST guidelines (5). Briefly; RPMI 1640 (with l-glutamine, without bicarbonate) supplemented with glucose to yield final 2% concentration. Working dilutions of drugs and phytochemicals prepared according to ISO guides from stock solutions. Two-fold serial dilutions (1024-1 µg/ml) of solutions were dispensed to flat-bottom 96 well microdilution plates in 100 µL volume. Inoculums were prepared to obtain the final 0.5-2.5x10^5 CFU/mL concentration with distilled water. After inoculation to microplates in 100 µL volumes, incubated at 35 ± 2 ºC in ambient air for 24 hour. Results were read at 540 nm. Combinatory activity evaluated with checkerboard test (6) in flat bottom microplates. One agent diluted in X-axis and the other one in Y-axis. Doubling dilutions were determined according to MIC results (4xMIC to MIC/16). Both agents were distributed to wells in 50 µL volumes. Inoculums were prepared to yield the final 0.5-2.5x10^5 CFU/mL concentration with distilled water and inoculated to microplates in 100 µL volumes. Microplates incubated at 35 ± 2 ºC in ambient air for 24 hour. Experiments were carried duplicate. Results were read at 540 nm.

Fractional inhibition concentration indexes were determined via the formula:

$$FICI = (MIC_{\text{in combination}} / MIC_{\text{alone}})_{Quercetin} + (MIC_{\text{in combination}} / MIC_{\text{alone}})_{curcumin}.$$

Results:

Micro broth dilution test results showed that curcumin and quercetin has antifungal activity at 256 μg/ml concentration for *C. albicans*. MIC values of curcumin and quercetin were 8 μg/ml and 128 μg/ml, respectively for *C. parapsilosis*. Combinatory test results show that all the values decreased except quercetin for *C. parapsilosis*. Results were given in Table 1. According to checkerboard test FICI values were 0.75, 1, and 1.5 for *C. albicans* ATCC 10231, *C. albicans* ATCC 90028, and *C. parapsilosis* 22019, respectively.

Table 1. Combinatory Activity Test Results (in μg/ml)

Species	Curcumin		Quercetin	
	Alone	Combination	Alone	Combination
Candida albicans ATCC 10231	256	64	256	128
Candida albicans ATCC 90028	256	128	256	128
Candida parapsilosis ATCC 22019	8	4	128	128

If we interpret the obtained values, it should be noted that no synergistic effect was detected for any species. However, we must say that for *C. albicans* there is partial synergy or additive effect, whereas for *C. parapsilosis* this combination is ineffective.

Conclusions:

The MIC value for curcumin and quercetin in the literature review is comparable to the values found in our study. Naranyan *et al.* (7) found MIC value of curcumin as 500 μg/ml for *C. albicans* ATCC 90028 and Freitas *et al.* (8) 8 μg/ml for *C. parapsilosis*. In recent years, there have been many study investigating the combined effects of these two phytochemicals with various agents (9, 10). The results of the study in which curcumin and quercetin were combined their better activity than fluconazole were shown in co-encapsulated nanovesicles against Candida species (4). Güran *et al.* indicated that combination of these compounds reduces the minimum inhibitory concentration at the levels of additive to synergistic effects on methicillin-resistant *Staphylococcus aureus* (11). Evaluating the experimental results and recent literatures, we think that both curcumin and quercetin can be revaluated in treatment options after with formulations that will provide stability and increase bioavailability besides reducing activity concentration.

References:

1. Tümbay E (2016). In: Us AD, Başustaoğlu A (Çev. ed). Tıbbi Mikrobiyoloji. Pelikan Kitabevi, Ankara pp 675-696.
2. Negri M, Salci TP, Shinobu-Mesquita CS, Capoci IR, Svidzinski TI, Kioshima, ES (2014). Early state research on antifungal natural products, Molecules, 19(3):2925-2956.
3. Lund KC & Pantuso T (2014). Combination effects of quercetin, resveratrol and curcumin on in vitro intestinal absorption, Journal of Restorative Medicine, 3(1):112-120.

4. Sadeghi-Ghadi Z, Vaezi A, Ahangarkani F, Ilkit M, Ebrahimnejad P, Badali H (2020). Potent in vitro activity of curcumin and quercetin co-encapsulated in nanovesicles without hyaluronan against Aspergillus and Candida isolates, Journal de Mycologie Medicale, 30(4): 101014.
5. Arendrup MC et al. (2020). Method for the determination of broth dilution minimum inhibitory concentrations of antifungal agents for yeasts (EUCAST defnitive document E.Def 7.3.2)
6. Schwarz P, Bidaud AL, Dannaoui E (2020). In vitro synergy of isavuconazole in combination with colistin against *Candida auris*. Scientific Reports, 10(1):1-8.
7. Narayanan VS, Muddaiah S, Shashidara R, Sudheendra US, Deepthi NC, Samaranayake L (2020). Variable antifungal activity of curcumin against planktonic and biofilm phase of different candida species, Indian Journal of Dental Research, 31(1): 145.
8. Freitas DD, Silva CRD, Andrade Neto JBD, Campos RDS, Sampaio LS, Nascimento FBSAD, .. Nobre Júnior HV (2018). In vitro evaluation of the curcumin against fluconazole-resistant strains of Candida spp. and Cryptococcus neoformans, International Journal of Current Microbiology and Applied Sciences, 7(4): 1191-1202.
9. Rajasekharan SK, Ramesh S, Bakkiyaraj D (2015). Synergy of flavonoids with HDAC inhibitor: new approach to target Candida tropicalis biofilms, Journal of Chemotherapy, 27(4): 246-249.
10. Tan Y, Leonhard M, Moser D, Ma S, Schneider-Stickler B (2019). Antibiofilm efficacy of curcumin in combination with 2-aminobenzimidazole against single-and mixed-species biofilms of Candida albicans and Staphylococcus aureus, Colloids and Surfaces B: Biointerfaces, 174: 28-34.
11. Güran M, Şanlıtürk G, Kerküklü NR, Altundağ EM, Yalçın AS (2019). Combined effects of quercetin and curcumin on anti-inflammatory and antimicrobial parameters in vitro, European Journal of Pharmacology, 859:172486.

OP183: ANTIBIOFILM ACTIVITY OF TWO NEW GENERATION DISINFECTANTS

[1]Sad Eldin, E., [1]Gurpinar, S.S., [2]Kart, D., [1]Eryilmaz, M.

[1] Ankara University, Department of Pharmaceutical Microbiology, Ankara, Turkey, eslamsadeldin@gmail.com, ssgurpinar@ankara.edu.tr, meryilmaz@ankara.edu.tr

[2] Hacettepe University, Department of Pharmaceutical Microbiology, Ankara, Turkey, dturk@hacattepe.edu.tr

Introduction:

Biofilms are a populace of cells arising on a surface and encased in an exopolysaccharide lattice. They are remarkably known to be difficult to annihilate and are a reason for numerous refractory infections (1). 65% of the microbial infections and 80% of the chronic infections are caused by bacterial biofilms (2). A biofilm is a natural form of existence of both S. epidermidis and Pseudomonas aeruginosa responsible for their virulence (3). Pseudomonas aeruginosa, an opportunistic pathogen that is a reason for many chronic infections like nosocomial infections (4). Staphylococcus epidermidis is one of the human body's normal flora and it's one of the causative microorganisms of catheter-associated sepsis and implant infections (3). Disinfectants are chemical agents which are extensively used in hospitals and other healthcare settings, to inhibit or destroy microorganisms and consequently to prevent infections. New generation disinfectants are defined as products that are completely broken down in nature without harmful residues in the environment. They are also defined as non-carcinogenic products for users. Chlorine dioxide (ClO_2) and hypochlorous acid (HOCl) are powerful oxidizing agents. Both of them are used as new generation disinfectants. Their degradation products are safe for the environment (5,6). Scarce data of the effectiveness of disinfectants on bacterial biofilms at labeled-use concentrations are available. This study aimed to evaluate the antibiofilm activity of two new generation disinfectants against *Staphylococcus epidermidis* and *Pseudomonas aeruginosa*.

Materials and Methods:

In this study, Ar-Dez Sniper® (0.2 % chlorine dioxide) and Crystalin® (hypochlorous acid) were used as new generation disinfectants. *Pseudomonas aeruginosa* PAO1 and *Staphylococcus epidermidis* ATCC 35984 were used as biofilm-forming test bacteria. Both bacteria were firstly cultured in Brain Heart Infusion broth. Biofilms were formed on 96-well polystyrene rounded bottomed microliter plate, incubated for 24 h in ambient air at 35.8 °C. To determine the anti-biofilm effects of the two new generation disinfectants, 100 µl of each disinfectant was added to each well, except for the control wells. Each disinfectant was evaluated at two different contact times (Ar-Dez Sniper® (1 and 10 min) and Crystalin® (1 and 2 min)). Then, 100 µl of %5 crystal violet solution was added to each well for 30 min and washed with PBS 1x., after that, 100 µl of acetone alcohol was then added to each well for 15 min. Optical density values were measured at 620 nm. The percentage inhibition values of biofilms were calculated (4,7).

Results:

Chlorine dioxide-containing disinfectant showed antibiofilm activity against *S. epidermidis* at one and ten minutes (47,1% and 44,2%, respectively). However, no or relatively low activity was detected against *P. aeruginosa* at the tested contact times (Figure 1). Hypochlorous acid-containing disinfectant showed antibiofilm activity against both Gram-positive and Gram-negative bacteria at one and two minutes (41,8%-35,6% and 41,3%-60,7%, respectively) (Figure 2).

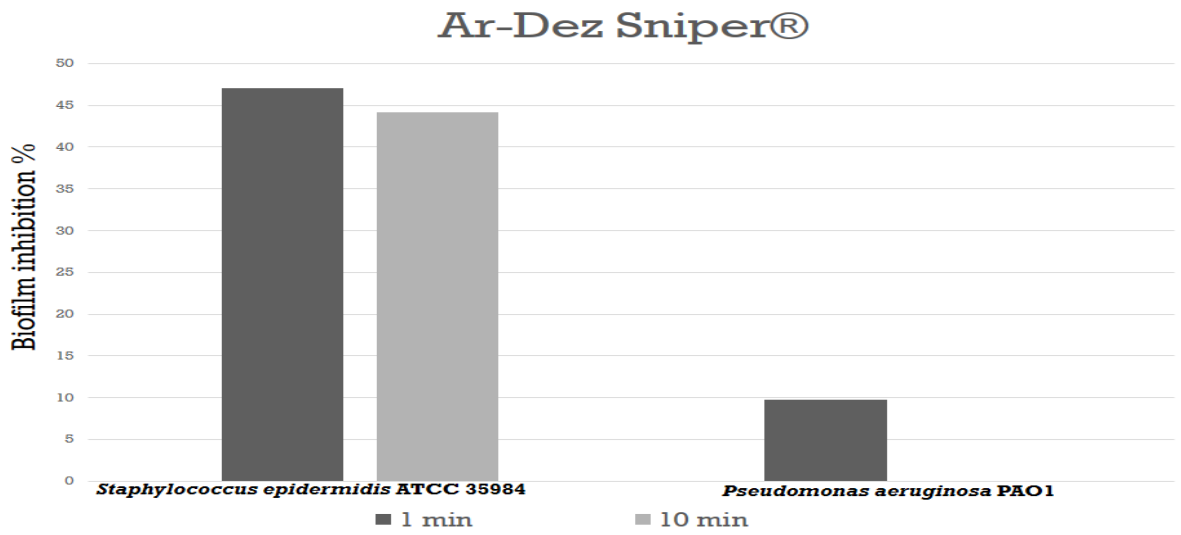

Figure 1. Antibiofilm activity of chlorine dioxide (Ar-Dez Sniper®) against the two tested bacteria in 1 min and 10 mins

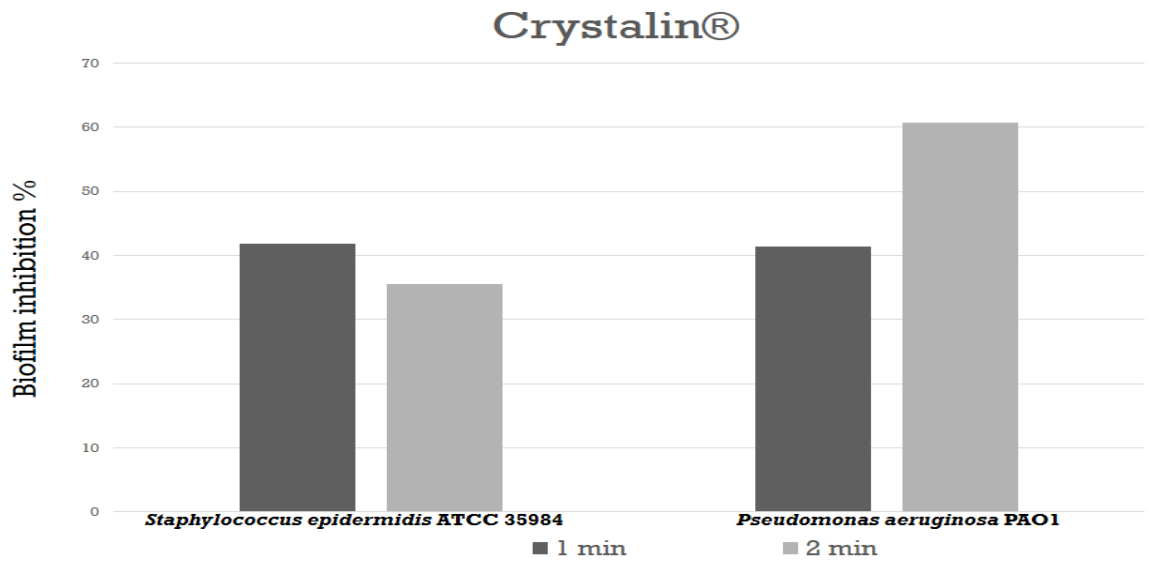

Figure 2. Antibiofilm activity of chlorine dioxide (Ar-Dez Sniper®) against the two tested bacteria in 1 min and 2 mins

Although no or relatively low activity was detected against *P. aeruginosa* at the tested contact times, this result opposes the findings obtained by Behnke and his colleague (8). The antimicrobial activity of Hypochlorous acid-containing disinfectants against Gram positive bacterial biofilms has been described previously (9).

Conclusions:

Appropriate disinfection practices are the most important part of preventing the spread of resistant microorganisms thus maintaining public health. The findings indicate that the tested new generation disinfectants may be used as antibiofilm agents. Hypochlorous acid-containing disinfectant showed a broad spectrum of antibiofilm activity against both Gram-positive and Gram-negative tested bacteria compared with chlorine dioxide-containing disinfectant.

References:

1. Lewis K. (2001). Riddle of Biofilm Resistance. Antimicrobial Agents and Chemotherapy, 45(4): 999–1007.
2. Lineback et al., (2018). Antimicrobial Resistance & Infection Control, 7(1).
3. Presterl et al., (2007). Journal of Antimicrobial Chemotherapy, 60(2):417–420.'
4. Kart et al., (2020). Turkish Bulletin of Hygiene and Experimental Biology, 77(3): 311-318.
5. Eryılmaz et al., (2016). Tropical Journal of Pharmaceutical Research, 15(10): 2191-2195.
6. Eryılmaz M & Palabıyık IM (2013). Tropical Journal of Pharmaceutical Research, 12(1): 123-126.
7. Jardak et al., (2021). LWT, 140: 110691.
8. Behnke S & Camper AK., (2012). Biofouling, 28(6), 635–647.
9. Ortega-Peña et al., (2016). International Wound Journal, 14(3), 470–479.

OP186: ANTIBACTERIAL ACTIVITY OF SOME ANTIDEPRESSANT ACTIVE SUBSTANCES AGAINST CLINICAL *ACINETOBACTER BAUMANNII* ISOLATES

[1]Gurpinar, S.S., [2]Kart, D., [1]Eryilmaz, M.

[1] Ankara University, Department of Pharmaceutical Microbiology, Ankara, Turkey, ssgurpinar@ankara.edu.tr, meryilmaz@ankara.edu.tr

[2] Hacettepe University, Department of Pharmaceutical Microbiology, Ankara, Turkey, dturk@hacattepe.edu.tr

Introduction:

Antibiotic resistance is one of the serious global health problems that spread despite the precautions taken all around the world. Infections caused by these resistant bacteria cause worse clinical outcomes and increase the risk of death, especially in intensive care units and in patients with weak immune system (1). These rapid resistance mechanisms that develop in microorganisms and the inadequacy in the treatment of infectious diseases force scientists to seek different solutions in the fight against resistant infectious agents. Scientific studies have shown that some drugs that are not used in the treatment of infections also have antimicrobial activity (2). These drugs, called non-antibiotic drugs, include neuroleptics, antihistamines, antidepressants, antiplatelets, and nonsteroidal anti-inflammatory drugs (3). Antidepressants are long-term used drugs that treat the symptoms of depressive disorders. Besides their main therapeutic effects, some of them demonstrate antimicrobial activity. Studies have shown that fluoxetine and sertraline which belong to selective serotonin reuptake inhibitors (SSRI) have antibiotic modulating activities as well as antimicrobial activities (4, 5).

Acinetobacter baumannii is one of the agents causing serious infections, especially in patients hospitalized in intensive care units. And also it is one of the primary causes of hospital infections. In recent years, it has been reported that *Acinetobacter* sp. has developed resistance to antibiotics at increasing rates. Therefore especially carbapenem-resistant *Acinetobacter* sp. is classified among the bacteria that need urgent action in the threat report prepared by the CDC (6). The aim of this study is to investigate the antibacterial activity of fluoxetine, sertraline, and amitriptyline against clinical *A. baumannii* isolates.

Materials and Methods:

In this study, ten ciprofloxacin, gentamicin, imipenem, and colistin susceptible and one resistant clinical *A. baumannii* isolates were used. *A. baumannii* ATCC 1709 and *A. baumannii* ATCC 1799 were used as standard strains. The antibacterial activity of fluoxetine, sertraline, and amitriptyline was determined by using the broth dilution method. The minimum inhibitory concentration test was performed in the concentration range of 25-0,195 µg/ml of active substances (7).

Results:

MIC values of fluoxetine, sertraline, and amitriptyline were given in Table 1.

Table 1. MIC values of test bacteria against fluoxetine, sertraline, amitriptyline (µg/ml). (1-10: Susceptible isolates 11: Resistant isolate 12: *A. baumannii* ATCC 1709 13: *A. baumannii* ATCC 1799)

Isolates number	MIC values (25-0.195 µg/ml)		
	Fluoxetine	**Sertraline**	**Amitriptyline**
1	25	12.5	-
2	25	12.5	-
3	12.5	12.5	-
4	12.5	12.5	-
5	25	12.5	-
6	12.5	12.5	-
7	12.5	12.5	-
8	6.25	6.25	25
9	25	12.5	-
10	12.5	12.5	-
11	25	12.5	-
12	12.5	12.5	25
13	25	25	-

Fluoxetine and sertraline possessed activity having MIC values of 6,25-12,5-25 µg/ml against all test bacteria. Amitriptyline possessed activity having MIC values of 25 µg/ml against only one susceptible isolate and *A. baumannii* ATCC 1709 strain.

Fluoxetine and sertraline (classified in SSRI) have shown better antibacterial activity than amitriptyline (classified in tricyclic antidepressant). In addition, the antidepressant active substance that has the best antibacterial effect on susceptible test bacteria was found to be sertraline.

Conclusions:

The findings indicate that SSRI antidepressants showed better antibacterial activity than tricyclic antidepressant. However, the mechanism of action of the active substances with antimicrobial effect is not yet clear. More comprehensive studies are needed to clarify the antimicrobial activity and mechanism of action of different antidepressant groups. In addition to the different usage purposes of these drugs, their effects on microflora should be considered.

Acknowledgments

This study was supported by a grant of TUBITAK (SBAG-119S907).

References:

1. Morehead, M. S., Scarbrough C. (2018). Primary Care: Clinics in Office Practice, 45, 467-484.
2. Tyski, S. (2003). *Acta poloniae pharmaceutica*, 60(5), 401-404.
3. Lagadinou, M. et al. Antibiotics 9.3 (2020): 107.
4. de Sousa et al. (2018). Microbial Pathogenesis, 123: 368-371.
5. Ayaz et al., (2015). Journal of Biological Research-Thessaloniki, 22 (1): 4.

6. Centers for Disease Control and Prevention. https://www.cdc.gov/drugresistance/pdf/threats-report/2019-ar-threats-report508.pdf, Accessed date: December 02, 2020.
7. Clinical and Laboratory Standards Institute. Methods for dilution antimicrobial susceptibility tests for bacteria that grow aerobically. M7-A8, CLSI; Wayne, PA, USA; 2009.

OP194: PRENATAL STRESS MAY INCREASE THE RISK OF DEVELOPING ALZHEIMER-LIKE NEUROPATHOLOGY IN THE HIPPOCAMPUS OF RATS

Turunc Ozoglu, E.

Izmir Katip Celebi University, Faculty of Pharmacy, Department of Biochemistry, Izmir, Turkey, ezgi.turunc@ikcu.edu.tr

Introduction:

The brain is the key organ of the response to stress. Because it determines what is threatening and, therefore, potentially stressful, as well as the physiological and behavioral responses which can be either adaptive or damaging. The hippocampus was the first brain region, besides the hypothalamus, to be recognized as a target of glucocorticoids. Neuroplasticity is the ability of central nervous system for adapting its structural and functional organization according to developmental and environmental influences. It has been revealed that prenatal stress is affecting brain functions in early life and underlies various diseases during adulthood (1).

Alzheimer's Disease (AD) is the most common form of dementia and characterized by progressive cognitive decline. The neuropathologic hallmarks of AD are amyloid plaques (AP) and neurofibrillary tangles (NFT) (2). Amyloid-β peptides are derived from differential proteolytic cleavage of the amyloid precursor protein (APP) by secretase enzymes. BACE1 is the major beta secretase for the amyloidogenic pathway. Aβ(1-40) is found more often but the toxic form is Aβ(1-42). Tau is the major microtubule-associated protein.The hyperphosphorylation of tau decreases its ability to bind to microtubules and affect the neuronal microtubule network. Neurofibrillary tangles are constituted of bundles of abnormal filaments called 'paired helical filaments' (PHF). The PHF are composed of hyperphosphorylated forms of tau. Glycogen synthase kinase-3β (GSK-3β) has been inolved in hyperphosphorylation of tau (3).

We searched the effects of prenatal stress on neuropathologic changes specific to AD through amyloid beta peptide generation and tau hyperphoshorylation in hippocampal tissues of rats. The mRNA levels of amyloid precursor protein (APP), beta-secretase 1 (BACE1), microtubule-associated protein tau (MAPT) and glycogen synthase kinase 3β (GSK-3β) were investigated by real-time PCR. The amyloid beta peptide (1-42) (Aβ(1-42)) and tau levels were measured with ELISA.

Materials and Methods:

Prenatal stress model: Prenatal stress were induced in rats with dexamethasone (Dex), a synthetic glucocorticoid (4). From GD 14 to GD 21, pregnant rats were injected daily with Dex at a dose of 200 µg/kg s.c. (Dex group) or saline (control group). After the birth, at the age of 3 months, male rats were decapitated (n=5) and hippocampuses were dissected on ice.

Gene expressions: Total RNA was extracted from the hippocampus by RNA/DNA isolation kit (Lucigen, Cat No. MC85200). Total RNA was used for first-strand cDNA synthesis (Thermo Fisher Scientific, Cat No. K1622). Real-time PCR amplifications were carried out using AriaMx Real-time PCR System (Agilent, USA). One microliter of cDNA (1:5 dilution) was amplified with 1 µl of 250 nM forward and reverse primers, 10 µl of Brilliant III Ultra-Fast QPCR Master Mix, 7 µl of nuclease-free water in a total volume of 20 µl. The relative mRNA levels were assessed

according to comparative CT method ($2^{-\Delta\Delta CT}$) with use of glyceraldehyde 3-phosphate dehydrogenase (GAPDH) as reference gene.

Aβ (1-42) and tau levels: Hippocampal samples were homogenized on ice and were centrifuged 20 min at 3.000 *g* at 4°C. Levels of Aβ(1-42) and tau were measured in triplicate using commercially available ELISA kits (Sunred Biotechnology, SRB-T-85491 and SRB-T-86822) following manufacturer's instructions. Absorbance was measured with in 60 min on a multimode microplate reader (BMG Labtech Clairostar plus) equipped with a 450 nm filter.

Statistical analyses: Data were analyzed using analysis of variance (ANOVA). In the case of a significiant ANOVA, post hoc analysis was performed using Tukey's test. Values were expressed as mean ± standard deviation (SD). Level of $p<0.05$ was considered to be statistically significiant. Statistical analysis were performed with SPSS (Version 25.0.0).

Results:

Prenatal Dex exposure caused significant increases in mRNA expressions of BACE1 (Fig. 2b) and GSK-3β (Fig. 3b) while decreased MAPT mRNA expression (Fig. 3a). No signficant differences were found in the mRNA level of APP gene between control and Dex groups (Fig. 2a). Aβ(1-42) and tau levels were significantly elevated in Dex group when compared to control (Fig. 1).

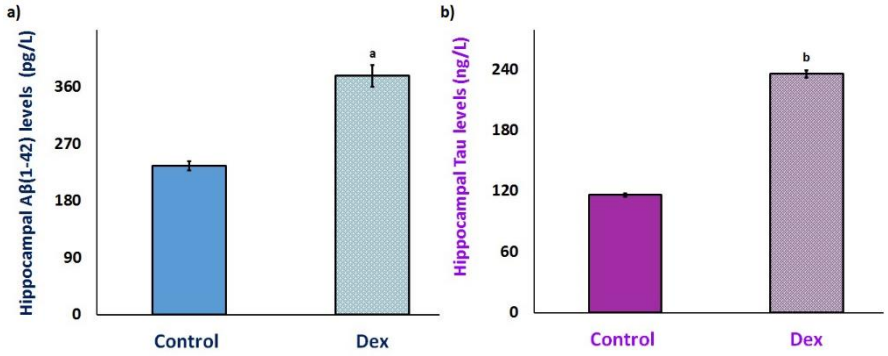

Figure 1. Hippoacampal Aβ(1-42) (pg/L) and Tau (ng/L) levels in control and Dex groups. The results were given mean ± S.D. (n=5, $^{a,b}p<0.05$ *vs control*).

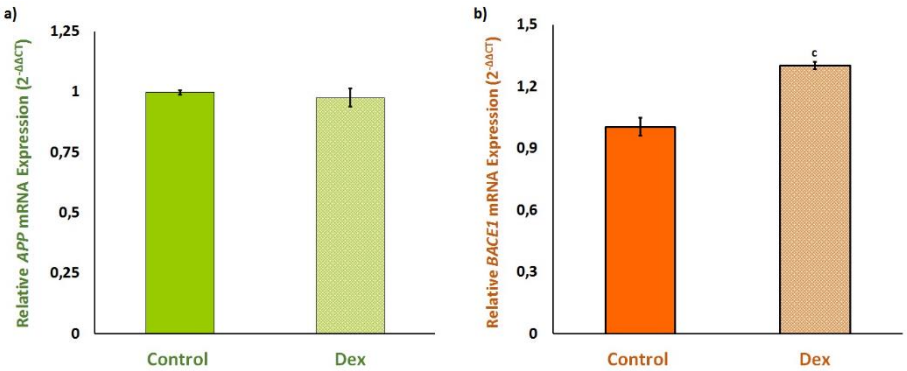

Figure 2. Relative expression of *APP* and *BACE1* mRNAs in control and Dex groups. The results were given mean ± S.D. (n=5, $^{c}p<0.05$ *vs* control).

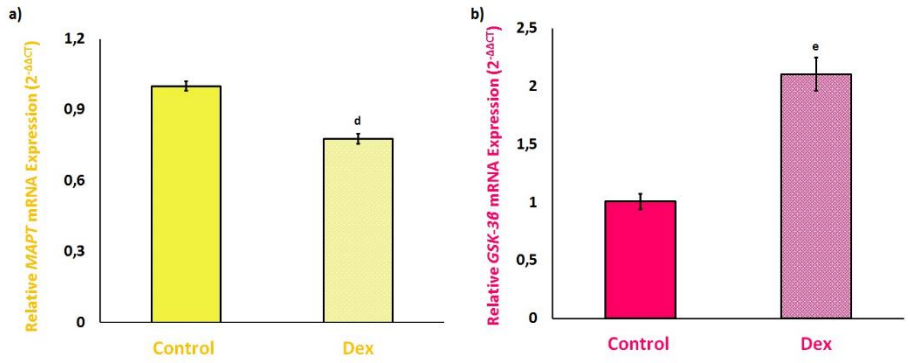

Figure 3. Relative expression of *MAPT* and *GSK-3β* mRNAs in control and Dex groups. The results were given mean ± S.D. (n=5, $^{d,e}p<0.05$ *vs* control).

Conclusions:

The results of this study showed that prenatal stress induced by Dex caused significant changes in hippocampal Aβ(1-42) and tau levels, and expression levels of genes that involved in APP processing, Aβ(1-42) generation and tau hyperphoshorylation. It was concluded that prenatal stress may trigger development of Alzheimer-like neuropathology in the hippocampus and represent a new therapeutic strategy against AD.

Acknowledgements

This study was supported by a grant of Izmir Katip Celebi University (2018-ONAP-ECZF-0001).

References:

1. Braun K et al., (2020). Neuroscience and Biobehavioral Reviews, 117:281-296.
2. Loera-Valencia R et al., (2018). Journal of Internal Medicine, 284(1):2-36.
3. Tiwari S et al., (2019). International Journal of Nanomedicine, 14:5541-5554.
4. Kjaer SL et al., (2011). Physiology and Behavior, 102(5):444-452.

OP198: INVESTIGATION OF IN VITRO ANTIOXIDANT, CYTOTOXIC AND MUTAGENIC ACTIVITIES OF ESSENTIAL OIL DERIVED FROM *Lavandula angustifolia* CULTIVATED in TURKEY

[1]Biltekin, S.N., [2]Omurtag Özgen, P.S., [3]İduğ, T.,[4]Macit, Ç., [5]Ayran, İ., [5]Çelik, S.A., [5]Kan, Y., [6]Omurtag G.Z.

[1] Istanbul Medipol University, Department of Pharmaceutical Microbiology, İstanbul, Turkey, snbiltekin@medipol.edu.tr
[2] Istanbul Medipol University, Department of Analytical Chemistry, Istanbul, Turkey, psozgen@medipol.edu.tr
[3] Istanbul Medipol University, Department of Pharmacognosy, Istanbul, Turkey, tidug@medipol.edu.tr
[4] Istanbul Medipol University, Department of Pharmacology, Istanbul, Turkey, cmacit@medipol.edu.tr
[5] Selçuk University, Department of Medicinal Plants, Konya, Turkey, kanyuksel@gmail.com
[6] Istanbul Medipol University, Department of Pharmaceutical Toxicology, Istanbul, Turkey, gzomurtag@medipol.edu.tr

Introduction:

Today, depression is one of the most common diseases and can be described as a reflection of worsening mental conditions on daily activities. Although there are many factors that cause depression, it is believed that the biochemical changes that conducted in the brain are the main reason for depression. Drugs that used for the treatment of depression have several adverse effects such as nausea, constipation. Thus, new treatment strategies must be developed.

Due to reasons like presence of adverse effects of drugs, usage of treatments with medicinal herbs (phytotherapy) and essential oils is increased in public-health. Quality of essential oil is important for showing its desirable effects. Main factors, which determine the quality of essential oils, are plant growth medium and storage conditions. Our country has the natural flora that necessary for the cultivation of plants.

Lavandula angustifolia, which is grown in many areas in our country and is produced efficient essential oil from its flowers, is important in traditional medicine because it is used for depression treatment and has no known adverse effects (1).

The aim of this study is to determine the chemical profile of lavender essential oil, investigating probable *in vitro* antioxidant, cytotoxic, mutagenic and antienflamatuar activities of oil.

In this project, our target is to evaluate the efficiency of *Lavandula angustifolia* essential oil, determination of chemical profile of essential oil, the possibility of being a synergistic/additive product that can be used in complementary medicine or being therapeutic medicine.

Unfortunately, patients can easily reach to herbal products such as bad-stored herbal teas, poor quality essential oils and they can not determine the useful dose of these products exactly.

Materials and Methods:

In this context, CCK-8 was used for cytotoxic effects (NIH/3T3) of *Lavandula angustifolia* essential oil (LA). For antioxidant activity both DPPH and TPC were used. In addition, the anti-inflammatory effect was also examined. The AMES test kits (TA98 and TA100) were used to determine the mutagenic activity.

Results:

As a result of the cytotoxicity analysis of LA, the IC_{50} value was found to be 0.372 mg/mL. DPPH and anti-inflammatory experiments IC_{50}'s were found to be 6.522 mg/mL and 1.238 mg/mL, respectively. TPC was determined as 1.220 mg/mL. No mutagenic effect of LA was detected even at a concentration of 0.290 mg/mL.

Lavandula angustifolia

CYTOTOXICITY	ANTIOXIDANT ACTIVITY		ANTI-INFLAMMATORY ACTIVITY
CCK-8 (IC_{50})	**DPPH (IC_{50})**	**TPC (IC_{50})**	**5-LOX (IC_{50})**
372.6 ± 5.03 µg/ml	6.522 ± 0.069 mg/ml	1.22 ± 0.04 mg/ml	1.238 ± 0.026 mg/ml

Mutagenic Activity

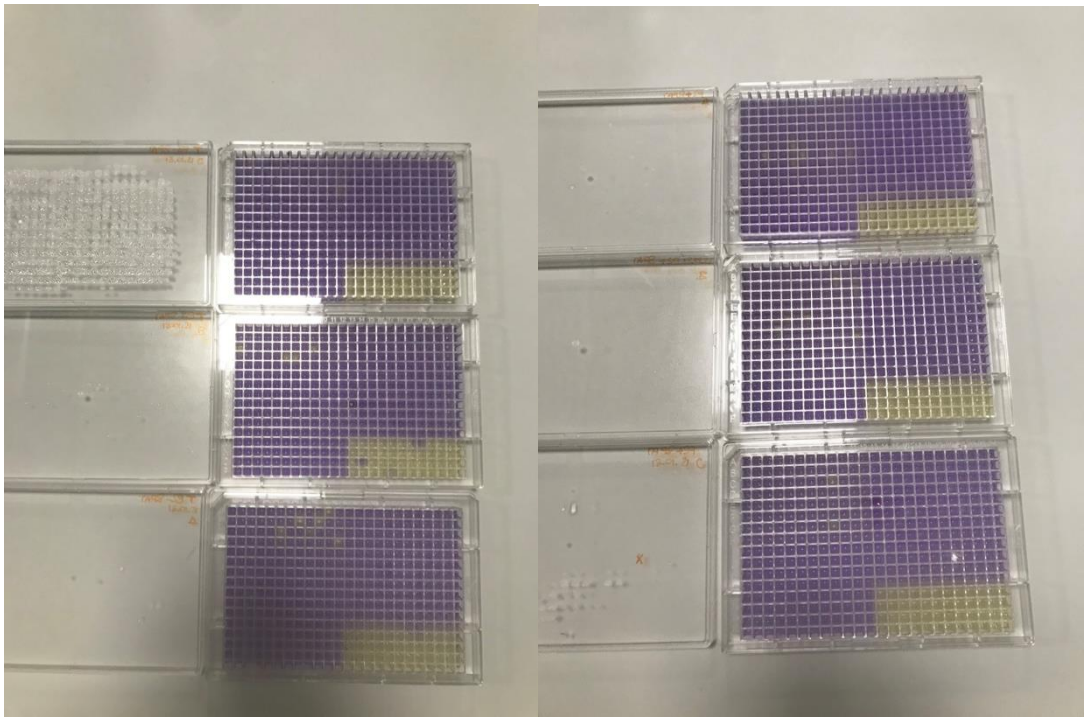

Conclusions:

This study provides an important contribution in terms of developing a medical product of standardized lavender essential oil, which is not present in Turkey at the moment.

Acknowledgements

This study was supported by the grants of Istanbul Medipol University (BAP-2020/15, BAP-2019/03).

References:

1. Nikfarjam, M., et al., (2013). The Effects of Lavandula Angustifolia Mill Infusion on Depression in Patients Using Citalopram: A comparison Study, Iranian Red Crescent Medical Journal,15(8): 734-9.

OP205: CINCHONA BARK AND ITS ALKALOIDS IN THE 4TH PORTUGUESE OFFICIAL PHARMACOPOEIA

[1,2]Semedo, M., [1,2]Pita, J.

[1] Group of History and Sociology of Science and Technology-CEIS20

[2] University of Coimbra, Faculty of Pharmacy, Portugal, maria.guilherme@gmail.com, jrpita@ci.uc.pt

Introduction:

Cinchona bark, obtained from a plant native to South America, is known for its antimalarial properties (1). Cinchona bark has four main alkaloids: quinine, quinidine, cinchonine and cinchonidine. Quinine and quinidine are used as therapeutic agents. Quinine is still being used as an antimalarial and was instrumental as a treatment for malaria since its isolation in 1820 (1, 2). Quinidine is a class 1A antiarrhythmic and has antimalarial activity. Pharmacopoeias are important barometers for current and past therapeutic options and remain a crucial source for the history of pharmacy.

This study aims at searching and presenting the references to cinchona bark and its alkaloids in the *Farmacopeia Portuguesa* IV, the fourth Portuguese official pharmacopoeia. The *Farmacopeia Portuguesa* IV had two editions (the first one published in 1935, and the second one published in 1946) and a supplement to the second edition (published in 1961). The *Farmacopeia Portuguesa* IV's two editions were written by a self-appointed commission of pharmacists. Two of them were Inspectors of the Pharmaceutical Exercise, two were from the Portuguese army and one was from the Portuguese navy (3,4). The *Farmacopeia Portuguesa* IV is one of the most important pharmacopoeias for the history of pharmacy in Portugal. The 1961 supplement to the second edition was produced by the *Permanent Commission of the Portuguese Pharmacopoeia*, created in 1955 to periodically revise the Portuguese official pharmacopoeia, and whose members were appointed in 1957 (5).

Materials and Methods:

The references to cinchona bark and its alkaloids in the fourth Portuguese official pharmacopoeia's 2 editions – the *Farmacopeia Portuguesa* IV published in 1935 and the *Farmacopeia Portuguesa* IV published in 1946 – plus the 1961 Supplement for the second edition were identified and analyzed. The data from the second edition (1946) and the data from the 1961 Supplement was combined since the supplement constitutes an addition to this pharmacopoeia's second edition. The total number of medicines in each edition was also quantified.

Results:

The *Farmacopeia Portuguesa* IV's first edition (1935) has one cinchona bark monograph, which characterizes yellow and red bark, indicating the species that belonged to each "type" of cinchona bark. The yellow cinchona bark was identified as the *Cinchona calisaya* Weddel and should have a minimum 2% quinine percentage content. The red cinchona bark was identified as *Cinchona succirubra* Pavon and should have a minimum 1,5% quinine percentage content. The cinchona bark monograph also includes a method for quantitative determination

of total alkaloid content and a method for quantitative determination of quinine content. The *Farmacopeia Portuguesa* IV's first edition has 10 medicines made with cinchona bark (1,37%), 17 medicines made with quinine (2,34%), and 1 medicine made with quinidine (0,14%), the quinidine sulfate. The medicines prepared with quinine included the quinine sulfate (also called "antiperiodic salt") and two injectable medicines. The medicines prepared with cinchona bark included the cinchona bark and aloe pills, the cinchona bark wine, and the cinchona bark extract. In the report that accompanied this pharmacopoeia's first edition, quinine was dubbed "the most important and precious medicament that is extracted from cinchona bark". The first edition has a total number of medicines of 728 (3).

The second edition of the *Farmacopeia Portuguesa* IV (1946) also has a cinchona bark monograph. This monograph is very similar to the first edition's cinchona bark monograph. The second edition's cinchona bark monograph also identifies the yellow and red cinchona bark species and its minimum quinine accepted content and contains the same method for quantitative determination of total alkaloid content. Notwithstanding, this cinchona bark monograph presents a different method for quantitative determination of quinine content. The cinchona bark monograph present in the second edition also adds information on where Cinchona trees were being cultivated – São Tomé Island (a Portuguese colony at the time), India and the Dutch colonies in the East. The second edition and its supplement have 10 medicines made with cinchona bark (1,20%), 19 medicines made with quinine (2,29%) and 1 medicine made with quinidine (0,12%). The medicines made with cinchona bark and quinidine are the same that were in the first edition. There are 2 additional medicines made with quinine, that weren't in the first edition, the quinine sulfate tablets (present in the 1961 supplement) and the *totaquina*, a mixture of cinchona bark alkaloids. In two of the quinine salts' monographs included in this pharmacopoeia, the brand names are also given: the "Aristoquina" was the quinine carbonate, and the "Euquinina" was the quinine ethyl carbonate. The combined number of medicines in the *Farmacopeia Portuguesa* IV's second edition and its 1961 supplement is 830 (4, 5).

Conclusions:

In the fourth Portuguese official pharmacopoeia's 2 editions and supplement to the second edition, there are several different medicines made with cinchona bark and quinine, as well as one medicine made with quinidine.

The cinchona bark monographs are detailed in both editions, with *Cinchona* species characterization, quantitative determination methods for total alkaloid content and quinine content, and a minimum accepted quinine content for each "type" of cinchona bark (yellow or red).

An interesting feature of both editions of the *Farmacopeia Portuguesa* IV (1935 and 1946) is the presence of 10 medicines prepared with cinchona bark, considering that quinine, which became the most important cinchona bark alkaloid for therapeutics, had been commercialized for more than 100 years. In theory, quinine should have mostly substituted the cinchona bark pharmaceutical preparations, since it is easier to predict the pharmacological effects of a medicine made with a single active substance such as quinine, as opposed to a medicine made with a part of a plant, such as cinchona bark, with multiple active substances in variable percentages. High quinine prices may have been a contributing factor for the longevity of cinchona bark medicines in Portuguese official pharmacopoeias. Another interesting feature

of both editions is the synonym presented for the quinine sulfate (antiperiodic salt) since usually in pharmacopoeias there isn't information on the therapeutic effects of the active substances. The name antiperiodic salt alludes to quinine sulfate's activity against "periodic" diseases, such as malaria, which can cause fever with an intermittent pattern.

References:

1. Costa AF (1944). O problema das quinas. Cosmos.
2. Al Khaja K, Sequeira RP (2021). Malaria journal, 20(1):62.
3. Fonseca JMP et al. (1935). Farmacopeia Portuguesa IV: edição oficial. Imprensa Nacional de Lisboa.
4. Fonseca JMP et al. (1946). Farmacopeia Portuguesa IV: edição oficial. Imprensa Nacional de Lisboa.
5. Comissão Permanente da Farmacopeia Portuguesa (1961). Farmacopeia portuguesa IV: suplemento. Imprensa Nacional de Lisboa.

OP207: COVID-19 ANXIETY OF THE STUDENTS AND ACADEMICIANS OF PHARMACY SCHOOLS IN TURKEY AND ITS EFFECTS ON THEIR PSYCHOLOGICAL WELL-BEING

[1]Çalıkuşu, M., [1]Özçelikay, G.

[1] Ankara University, Department of Pharmacy Management, Ankara, Turkey, mcalikusu@ankara.edu.tr, gulbin.ozcelikay@ankara.edu.tr

Introduction:

The state of anxiety seen during the Covid-19 pandemic needs to be evaluated and controlled. Studies show that high anxiety reduces students' academic performance (1). The productivity and scientific studies of academicians have also been negatively affected during the pandemic (2). Psychological conditions of students and academicians need to be improved as high anxiety levels can affect academic achievement. In this study, the effects on psychological well-being of the Covid-19 anxiety levels of students and academicians in Pharmacy Schools in Turkey have been determined.

Materials and Methods:

The research is quantitative. As a data collection tool in the research, a questionnaire consisting of three parts was applied to the academic staff and students of Pharmacy Schools. After the first part of the questionnaire aiming to determine general information, there are questions about the Pandemic Anxiety Scale (PA) developed by Çiçek and Almalı (2020) and the Psychological Well-Being Scale (PWB), which was translated into Turkish by the same researchers and whose validity and reliability studies were conducted (3, 4).

The universe of the study consists of 1563 academic staff working in Pharmacy Schools and 17101 students in these schools. Before starting the survey application, permission was obtained from the Ethics Committee of Ankara University (dated 12/04/2021, decision number 06/61) and the Scientific Research Platform of the Republic of Turkey Ministry of Health. Following the approval of the ethics committee, research data were collected between 12/04 - 02/05/2021. The level of significance (α) was determined as 0.05 in the analyzes made in the study.

Results:

247 academicians and 1698 students participated in the research. Data were analyzed by SPSS ver. 25.0 programme. 79% of the academic staff participating in the study were female, 21% were male; 77% of the students were female and 23% were male.

Findings of Academicians:

- ✓ Female academicians had a significantly higher (p=0.001) pandemic anxiety level than male academicians.
- ✓ Married academicians had a significantly higher (p=0.039) pandemic anxiety level than single academicians.
- ✓ Academicians with Covid-19 sight status in nearby had a significantly higher (p=0.006) psychological well-being level than those who did not.

- ✓ There was no significant difference between the parenting status of academicians of pandemic anxiety and psychological well-being levels.
- ✓ Correlation analysis was conducted to measure the effect of the pandemic anxiety of the academicians on their psychological well-being; a positive but very low correlation (Pearson Correlation coefficient: 0.027) was found.

Findings of Students:

- ✓ Female students had a significantly higher pandemic anxiety (p=0.000) and psychological well-being (p=0.027) levels compared to male students.
- ✓ There was no significant difference between the levels of pandemic anxiety and psychological well-being of the chronic disease status and Covid-19 sight status in nearby.
- ✓ There was no significant difference between the ages of the students and their pandemic anxiety and psychological well-being levels.
- ✓ While there was no significant relationship between students' years at the school and their pandemic anxiety levels, there was a significant difference between their psychological well-being levels. Students in the 1st year had a significantly higher level of psychological well-being than those in the 2nd year, and the students in the 5th year compared to the students in the 3rd and 4th years.
- ✓ Correlation analysis was conducted to measure the effect of pandemic anxiety of students on their psychological well-being; a very low and negative relationship (Pearson Correlation coefficient: -0.068) was found.

Conclusions:

Covid-19 pandemic has affected people of all age groups, although it has occurred to varying degrees. The possibility of getting sick and the uncertainty of the process can cause anxiety and thus a decrease in psychological well-being levels. In this study, it was found that academicians generally had lower pandemic anxiety and higher psychological well-being than students. This situation can be associated with the higher level of consciousness among the academicians. During the pandemic, it is recommended to take the necessary steps and precautions to make the academicians and students feel physiologically and psychologically healthy.

This pandemic will inevitably lead to redefining our relationship styles, which are no longer based on intimacy but on distance. The digitalization of lives is emerging, which begins with the emergence of social media, technology and virtual reality instead of physical contact. By emphasizing this reality and abandoning the idea of "things will return to normal" and being able to face the changes will alleviate the onset of possible psychopathological problems.

References:

1. Cong DD. (2021) The impact of fear and anxiety of Covid-19 on life satisfaction: Psychological distress and sleep disturbance as mediators. Personality and Individual Differences, 178/110869. https://doi.org/10.1016/j.paid.2021.110869
2. Gabster BP, van Daalen K, et al., (2020). Challenges for the female academic during the COVID-19 pandemic. The Lancet, 395(10242):1968-1970.

3. Çiçek B., Almalı V. (2020). COVID-19 Pandemisi Sürecinde Kaygı Öz-yeterlilik ve Psikolojik İyi Oluş Arasındaki İlişki: Özel Sektör ve Kamu Çalışanları Karşılaştırması. Electronic Turkish Studies, 15:4.
4. Diener E et al., (2009). New measures of well-being, in Assessing well-being. Springer. p. 247-266.

INDEX


ANKARA UNIVERSITY FACULTY OF PHARMACY
INTERNATIONAL SYMPOSIUM ON PHARMACEUTICAL SCIENCES
ISOPS 13